

2020

Development of an Activity-based Windowing Approach to Evaluate Real-World NO_x Emissions from Modern Medium and Heavy-Duty Diesel Trucks

Rasik Pondicherry
West Virginia University, prpondicherry@mix.wvu.edu

Follow this and additional works at: <https://researchrepository.wvu.edu/etd>

 Part of the [Energy Systems Commons](#), [Heat Transfer, Combustion Commons](#), and the [Other Mechanical Engineering Commons](#)

Recommended Citation

Pondicherry, Rasik, "Development of an Activity-based Windowing Approach to Evaluate Real-World NO_x Emissions from Modern Medium and Heavy-Duty Diesel Trucks" (2020). *Graduate Theses, Dissertations, and Problem Reports*. 7682.

<https://researchrepository.wvu.edu/etd/7682>


This Dissertation is protected by copyright and/or related rights. It has been brought to you by the The Research Repository @ WVU with permission from the rights-holder(s). You are free to use this Dissertation in any way that is permitted by the copyright and related rights legislation that applies to your use. For other uses you must obtain permission from the rights-holder(s) directly, unless additional rights are indicated by a Creative Commons license in the record and/ or on the work itself. This Dissertation has been accepted for inclusion in WVU Graduate Theses, Dissertations, and Problem Reports collection by an authorized administrator of The Research Repository @ WVU. For more information, please contact researchrepository@mail.wvu.edu.

2020

Development of an Activity-based Windowing Approach to Evaluate Real-World NO_x Emissions from Modern Medium and Heavy-Duty Diesel Trucks

Rasik Pondicherry

Follow this and additional works at: <https://researchrepository.wvu.edu/etd>

 Part of the [Energy Systems Commons](#), [Heat Transfer, Combustion Commons](#), and the [Other Mechanical Engineering Commons](#)

Development of an Activity-based Windowing Approach to Evaluate Real-World NO_x Emissions from Modern Medium and Heavy-Duty Diesel Trucks

Rasik Pondicherry

Dissertation submitted
to the Benjamin M. Statler College of Engineering and Mineral Resources
at West Virginia University

In partial fulfilment of the requirements
Of the degree of

Doctor of Philosophy
In
Mechanical Engineering

Marc C. Besch, Ph.D., Chair
Arvind Thiruvengadam, Ph.D.
Gregory Thompson, Ph.D.
Derek Johnson, Ph.D.
Alessandro Cozzolini, Ph.D.
Berk Demirgok, Ph.D.

Department of Mechanical and Aerospace Engineering

Morgantown, West Virginia
2020

Keywords: Real-world Emissions, Vehicle activity, SCR, PEMS, NTE, WBW,
NO_x sensor cross-sensitivity
Copyright: 2020 Rasik Pondicherry

Abstract

Development of an Activity-based Windowing Approach to Evaluate Real-World NO_x Emissions from Modern Medium and Heavy-Duty Diesel Trucks

The introduction of in-use emissions regulations by the United States Environmental Protection Agency (U.S.EPA) requires medium-duty (MD) and heavy-duty (HD) engine manufacturers to demonstrate emissions compliance during in-fleet operation. In the United States (U.S.), the Not-to-Exceed (NTE) method is used to evaluate real-world emissions compliance from on-highway MD and HD trucks. Regulatory agencies, engine manufacturers and research entities have identified that the NTE method incorporates numerous exclusions and evaluates emissions compliance only under selective operating conditions that are favorable for the selective catalytic reduction (SCR) system to reduce oxides of nitrogen (NO_x) emissions efficiently. Such operation is typically encountered only by vocations that experience sustained highway driving operation, which is not entirely representative of actual highly diverse real-world operation experienced by the engine/aftertreatment system.

Evaluation of real-world driving emissions (RDE) plays a critical role in monitoring and ensuring the performance of emissions control systems. Portable emissions measurement system (PEMS) serves as a robust tool to assess emissions levels during real-world operation. However, utilization of PEMS for large-scale deployment is time-consuming, labor-intensive, and expensive. As a vision of potential elements for a next-tier of in-use NO_x monitoring systems, there is an actively growing research and regulatory interest to evaluate the feasibility of using existing on-board NO_x sensors for HD on-board NO_x compliance. However, research studies have highlighted that NO_x sensor measurements are also subjected to cross-sensitivity from other species in the exhaust stream.

The global objective of the study was to develop an alternative approach that attempts to bridge the gap between current in-use certification procedures and highly diverse real-world operation for evaluation of in-use NO_x emissions. The study outlines a vehicle activity-based windowing (ABW) approach that provides an event-based bifurcation of the engine and aftertreatment operational conditions. The thermal boundary bin exhibits bin boundary conditions favorable for SCR catalytic activity. Results of the study show that the 90th percentile of ABW bin-1a bsNO_x emissions (i.e., on average of the individual vehicle datasets) was below the current NTE NO_x limit. In terms of data usage, the ABW approach provides a unique opportunity of utilizing ~95% and 83% (Phase-1 and Phase-2) of test activity acquired from valid ABW trips. In comparison, the current NTE approach evaluated over a diverse in-use test activity collected as part of the HDIUT program exhibits utilization of only a sparse amount (i.e., less than 10%) of in-use test activity for emissions compliance evaluation. In light of using existing on-board NO_x sensors for the screening of in-fleet activity, the study evaluates measurement thresholds of NO_x sensors under real-world operating conditions. In the absence of a substantial amount of ammonia (NH₃), it was observed that the average measurement deviation was within ±10% for NO_x concentration levels between 10 ppm and 200 ppm. However, statistical principal component analysis (PCA) indicates a hypothetical relation between NO_x sensor measurements and rapid changes in water (H₂O) concentrations.

Acknowledgements

The journey towards completion of an exciting academic adventure has been a collaborative endeavor, where I would like to thank a huge group of people who have supported me with guidance, motivation, and opportunities as stepping stones to achieve professional growth.

First and foremost, I would like to thank my parents Premnath and Ratnamala for providing me with their unconditional love, encouragement, endless support, and countless sacrifices in fulfilling every dream of mine since my childhood. This journey would not have been possible without the support of mom and dad, both emotionally and financially. Thank you for believing in me and always supporting me in my decisions, even through the most challenging times.

I would like to express my sincere appreciation to Dr. Marc Besch for serving as my academic advisor. Most importantly, thank you for your support and guidance all throughout my graduate school career. I am very grateful to have had the opportunity to work with you on several research programs and most importantly, thanks for ensuring the relation to be less of an advisor-student and more of a friend and colleague. Every time I had a conversation with you, I have always learnt something new, and exchanging ideas with you has helped me learn a lot both on the professional and personal front. Irrespective of the busy work-life in southern California and your busy travel schedule all throughout the year, you have always made sure to find time to discuss and exchange research ideas. Thank you for providing me with numerous opportunities to present our research work at International conferences and connecting me with experts from the industry. To me, Dr. Marc Besch a.k.a., Marc Sir! is one who sets an example of a perfect and complete engineer.

I would like to express my gratitude to my co-advisor and committee member, Dr. Arvind Thiruvengadam, for being a source of inspiration to all CAFEE graduate students and engineers. Your support and motivational guidance have helped me steer through this journey in the right direction. I truly admire your generosity towards graduate students, especially providing personal and professional support in one way or another. Thanks for inviting me over to your place for countless weekend dinners.

I would like to thank the Director Dan Carder for his mentorship and friendship. Thank you for providing me with your guidance as and whenever needed on a timely basis not only to me but to all CAFEE graduate students. Thank you for enduring your trust and believing in me, especially in working and handling industry

sponsored research projects. Thank you for always providing students with opportunities to connect with industry partners.

To the trio, Dr. Marc Besch, Dr. Arvind Thiruvengadam and Dan Carder, thank you for providing me with the opportunity to be part of this amazing research group “CAFEE”. It has been an exciting journey working with the HD engine and emissions experts.

I would like to thank my committee members Dr. Gregory Thompson and Dr. Derek Johnson, for their valuable feedback and comments both during my proposal and dissertation defense. Thank you very much for your time and efforts in reviewing this document and providing me with key insights that have helped me shape the document better.

I would like to thank my committee member and mentor (during my internship with Daimler Trucks North America (DTNA)), Dr. Alessandro Cozzolini for his support and valuable technical input with respect to my research work. It has been a great experience working with you on the 16L engine platform, and I have certainly learnt a lot from you with respect to engine controls and calibration strategies. Thanks are due to Dr. Igor Gruden and MDEG/DD-16 team at DTNA for providing me with opportunities to work on exciting projects during my 6-month tenure at DTNA.

Thanks are due to my committee member, Dr. Berk Demirgok, for his support, and valuable feedback with regards to my research activities at CAFEE. It has been a great pleasure collaborating and working with you on several research activities during your time at West Virginia University (as a senior Ph.D. student and also senior engineer). Thank you very much for imparting me with your knowledge and always being appreciative of my work. You have always valued my potential, which I genuinely appreciate.

A special thanks to Filiz Kazan and Batishahe Selimi for your support in several research tasks. It has been a pleasure working with you in accomplishing numerous tasks in a timely manner. Thanks for providing me with motivation and support in ensuring that I accomplish my dissertation writing on time. Thank you for always cooking special meals for me. No one can cook desserts as delicious as you guys do. Dr. Saroj Pradhan, thank you very much for your friendship and hosting me over for “momo” nights. You have always been a source of inspiration to graduate students and thank you for providing me with technical guidance whenever I reached out to you.

Christian Hushion, it has been a great experience working with you as a team on the cylinder deactivation research project which hopefully may be a future technology

moving forward for thermal management. Development of engine controls and the calibration experience on our “big beast” HD engine was one of the most fun-filled experiences that I have had during my time here at CAFEE. Thank you for your patience all throughout the calibration exercise, and I still remember the sigh of relief we had while we achieved impressive results with our collaborative efforts.

Thanks to CAFEE engineers and staff, Jason England, Aaron Leasor, Grover for their technical support and patience especially while supporting me in performing in-use testing with transportable emissions laboratory (TEMS).

In addition to the above-mentioned people, thanks are due to a large number of friends from CAFEE who have made this journey an exciting one. I must thank Dr. Ross Ryskamp, Jordan Leatherman, Diego Mejia, Cem Baki, Samuel Okeleye, Chakradhar Reddy, Dr. Vishnu Padmanaban, Renata Castiglioni, Ghadi Sadek, Adam Philips, Pavan Yadav, Koji Yanaga, Dr. Mahdi Darzi, Hemanth Bomisetty, Dr. Satish Guda, Sashank Jammalamadaga, Swathi Reddy, John Revercomb, and Sri Ram Challagala. I greatly apologize for anyone that I may have missed.

I consider myself fortunate indeed to have had the opportunity as part of the “CAFEE” journey to work with an amazing group of top-notch engineers who possess unique skill set and expertise in this challenging and exciting field of research. Thanks for teaching me valuable skills and most importantly, critically assessing my ideas and providing me with their critique and feedback in overcoming research challenges. Working with CAFEE as a graduate research assistant had led me as a student who joined WVU only to attain a master’s degree to continue his academic pursuit to complete a doctoral degree. Thanks are due to all CAFEE friends (i.e., current/former graduate students and engineers) and professors, for their help with various projects, without whose support this journey would not have been as exciting as it was in overcoming challenges.

I am very grateful to Dr.Nithi Sivaneri and family for their support since my very first day in the United States. Special thanks to my cousin Mona Sivaneri for your extended help all throughout my time in the United States. Thanks for inviting me over on numerous occasions to your place and hosting me with delicious delicacies.

Next to my family, thanks to Chitrangi Doshi for your friendship and being my biggest well-wisher for the last six and a half years. I really thank you from the bottom of my heart for the continuous support you have provided me during my academic career and especially during my final stages while I was working on finishing up this dissertation. You are the most humble person I have ever met, who always looks out to helping others than caring for yourself. Thank you for always being my travel partner, and it was a great fun-filled 6-month experience when I was

temporarily moved to Detroit for my internship. You have always helped me get through challenging and difficult phases in life, and most importantly supported me with the important decisions of my life. Thank you very much.

Special thanks to Ikttesh Chahal for your friendship since the time we met. Thanks for always offering me with your valuable advice whenever needed and believing in me that I had the potential to do more than I actually do and always told me to push my limits. I will never forget the delicious dinners that you have always cooked for me and all the fun activities that we have done together.

I have been very privileged to have known and collaborate with many other people who became close friends in the United States and back home in India. Special thanks to Anirudh Tirunahari, Abha Dwivedy, Garret Rinker, Chetan Pradhan, Srijana Pradhan, Akshay Gupte, Rahul, Utsav, Krishan Tulasi, Sai Charan, Dinesh Reddy, Arun Reddy, Shaik Farukh, Manish Reddy, Sirisha Lavu, Sreeja, Ajitesh Akula, Abhilash Reddy, Naresh Reddy, Arihanth Gunda, Soham Gokhale, Siddharth Jain, Karthik Natarajan, Zohaib Bashir, Bhavya Sugur, Arun Molhilyan, Kamlesh Sai Kumar, Kiran Reddy, Shiva, Sai Teja, Anmol Prabhu, Saif Ansari, Monika Roy, Neha Naaz, Shresta Vure, Deepak, Shashi Dharan, Tanveer Ahmed and Avinash. I sincerely apologize to anyone that I may have missed.

Table of Contents

Abstract	ii
Acknowledgements	iii
List of Figures	viii
List of Tables	xiii
1. Introduction	1
1.1. Problem Statement	3
1.2. Thesis Objective	5
2. Review of Literature	7
2.1. Exhaust Emissions from Diesel Engines	8
2.2. Legislative Requirements for Regulated Emissions	9
2.3. Emissions Control Technologies	14
2.4. Vocational Dependency on Vehicle Activity and NO _x Emissions	21
2.5. Advancements in On-board Emissions Measurement Systems	28
2.6. PEMS Measurement Allowance Program	32
2.7. In-use Emissions Quantification Protocol	37
2.8. Evaluation of In-use Emissions Compliance Protocols	44
2.9. Performance Evaluation of On-board NO _x Sensors	56
3. Experimental Setup and Procedures	64
3.1. Heavy-duty In-use Testing Program	65
3.2. Heavy-duty In-use Testing	67
3.3. In-use Testing using PAMS	77
4. Methodology	81
4.1. In-use Compliance Metric Evaluation	81
4.2. ABW Approach for In-use Emissions Assessment	84
4.3. Performance Evaluation of NO _x Sensors	90
5. Results and Discussion	94
5.1. Analysis of In-use Emissions Quantification Methods	95
5.2. Evaluation of ABW - Phase 1	106
5.3. Evaluation of ABW - Phase 2	146
5.4. Measurement Variability of On-board NO _x Sensors	169
6. Conclusions and Recommendations	180
6.1. Conclusions	187
6.2. Recommendations	191
6.3. Contributions	192
References	193
Appendix	204

List of Figures

Figure 1: U.S.EPA regulations for NO _x and PM emissions (Stanton, 2013)	11
Figure 2: Comparison of NO _x emissions and fuel consumption of an MY 2004 and 2007 certified engines with EGR technology (Stanton, 2013)	12
Figure 3: Effect of (a) Intake oxygen concentration on NO _x reduction; (b) EGR mass fraction on NO _x versus PM emissions (Stanton, 2013).....	15
Figure 4: NO _x conversion efficiency for vanadium-based and zeolite-based SCR systems (Kröcher, 2007)	17
Figure 5: Comparison of NH ₃ storage levels (i.e., grams per litre) as a function of catalyst temperature (Eijnden et al., 2009).....	19
Figure 6: Comparison of NO _x conversion efficiency of catalyst C (Vanadium-based) aged for 50hr at 600 °C and catalyst D (Cu-Ze) aged for 64hrs at 670 °C at 30k hr ⁻¹ (Ura et al., 2009)	19
Figure 7: Real-world SCR thermal profile of nine line-haul trucks (Stanton, 2013)	20
Figure 8: Comparison of NO _x emissions of diesel engines equipped with SCR technology operated over six distinct routes in California (Quiros et al., 2016).....	22
Figure 9: Comparison of distance-specific, brake-specific NO _x emissions, percentage of aftertreatment outlet temperature operation for test activity acquired four over chassis dynamometer test cycles (Thiruvengadam et al., 2015).....	23
Figure 10: Comparison of the cumulative NO _x mass from a MY 2010 engine operated under two scenarios: (Top chart) high load operation and (bottom chart) unloaded (Misra et al., 2013).....	24
Figure 11: Comparison of SCR temperature profiles of line-haul and drayage application trucks (Boriboonsomsin et al., 2018)	25
Figure 12: Comparison of average engine-out and tailpipe NO _x emissions of 68 HD trucks (Tan et al., 2019)	26
Figure 13: Generic representation of the NTE zone (Pondicherry, 2017)	38
Figure 14: Generic representation of WBW method (EU 582, 2011)	43
Figure 15: Percentage of valid NTE event duration (i.e., averaged and individual results for each manufacturer) (Badshah et al., 2019)	45
Figure 16: Comparison of route-averaged and NTE event-averaged NO _x emission rates separated based on engine manufacturer (Badshah et al., 2019)	46
Figure 17: Impact of reference work evaluated on a 9L diesel engine (Shade et al., 2008)	48
Figure 18: Comparison of average engine power and NO _x emissions of WBW's (Mendoza-Villafuerte et al., 2017).....	51
Figure 19: Vehicle-speed based distribution of NO _x emissions rates and post-SCR exhaust temperatures (Badshah et al., 2019)	54
Figure 20: Frequency distribution of (a) Engine power operation (i.e., left chart); (b) Normalized engine power (i.e., right chart) of vehicles from WLTP database	55
Figure 21: Example of an in-use test evaluated using CLEAR method (Hausberger and Lipp, 2014)	56
Figure 22: Schematic of electrochemical reactions in Zr-O ₂ NO _x sensor (Blanco-Rodriguez, 2013)	58

Figure 23: Relationship between the applied voltage and current of the NO _x sensor (Todo et al., 2018).....	59
Figure 24: Comparison of NO _x measurements (i.e., laboratory analyzer and sensor), NH ₃ sensor measurements, and urea injection at exhaust gas flow temperature: 300 °C, gas flow rate: 100 kg/hr, and SCR inlet gas NO _x concentration: 200-mole ppm (Bonfils et al., 2012).....	59
Figure 25: Evaluation of NO _x sensor accuracy in the presence of NO, NH ₃ , H ₂ O and O ₂ (Frobert et al., 2013)	60
Figure 26: Impact of changes in H ₂ O concentration on NO _x sensor measurements (Soltis et al., 2006)	61
Figure 27: Comparison of output error versus residual O ₂ concentration on the sensor electrode (Todo et al., 2018).....	62
Figure 28: General schematic representation of the experimental setup for on-road emissions testing (Rework of Besch et al., 2017).....	65
Figure 29: Distribution of HDIUT datasets as a function of engine displacement, MY and rated power	66
Figure 30: Schematic of the instrumentation setup of gaseous emissions sampling	68
Figure 31: Comparison of vehicle speed and Altitude for Highway-Hill Climb route	69
Figure 32: Operational segment-based classification of vehicle speed profile for ISC route	70
Figure 33: Generic representation of vehicle speed profile of port route	71
Figure 34: Generic representation of vehicle speed profile of grocery distribution route	72
Figure 35: Class 8 HD tractor hauling WVU TEMS near LA port harbour	73
Figure 36: Semtech-DS on-board emissions analyzer (Sensors, 2011).....	75
Figure 37: Schematic representation of FTIR interferometer (Sanchonx, 2017).....	77
Figure 38: Comparison of Engine MY and vehicle mileage at the beginning of the data logging phase	79
Figure 39: Schematic representation of an HD truck equipped with PAMS	80
Figure 40: Picture of data acquisition hardware (a) Left image: PAMS (control-tec) (left); (b) Right image: Continental Uni-NO _x 2.8 tailpipe NO _x sensor (right).....	80
Figure 41: Comparison of vehicle speed and cumulative engine work (i.e., for theoretical window generation) of an in-use test performed on vehicle-A	85
Figure 42: Categorization of events within each ABW	86
Figure 43: Time-weighted vehicle speed distribution of 75 HDIUT in-use datasets	96
Figure 44: Contribution of individual exclusions towards NTE event invalidation .	99
Figure 45: Comparison of (a) Top graph: Time-weighted NTE event duration and (b) Bottom graph: NTE NO _x mass fraction for three different NTE test cases	101
Figure 46: Time-weighted data utilization for (a) All WBW's generated, and (b) Valid WBW's generated as per of EU VI (c) and EU VI (d) power cut-off thresholds	103
Figure 47: WBW percentile comparison of bsNO _x emissions for valid work-windows generated as per (a) Top graph: EU VI (c) based power cut-off threshold, and (b) Bottom graph: EU VI (d) based power cut-off threshold.....	104

Figure 48: Comparison of window averaged $T_{SCR\ OUT}$ and bsNO _x emissions of valid WBW's	105
Figure 49: Time-weighted vehicle speed distribution of all in-use datasets sampled in section 3.2.....	107
Figure 50: Time-weighted $T_{SCR\ IN}$ distribution of all in-use datasets sampled in section 3.2.....	108
Figure 51: Description of theoretical window generation for Route-2 evaluated on vehicle A.....	111
Figure 52: Comparison of NO _x emissions during cold engine operating conditions for events generated in bin-1b and bin-2b	112
Figure 53: ABW summary of results for vehicle-A operated on route-2	113
Figure 54: Box and whisker distribution of all events generated in (a) Top graph: bsNO _x emissions and (b) Bottom graph: CO ₂ -specific NO _x emissions rates of vehicle-A operated on route-2	114
Figure 55: Comparison of time-weighted test activity distribution for minimum event time duration and engine power fraction (i.e., for bin-1)	117
Figure 56: Impact of ABW $T_{SCR\ IN}$ threshold on bsNO _x emissions	118
Figure 57: Distribution of test activity accumulated during transition mode.....	119
Figure 58: ABW bin-based summary of NO _x emissions for vehicle-D operated on route-4	121
Figure 59: Comparison of event averaged $T_{SCR\ IN}$ and bsNO _x emissions of all events generated in bin-1a and 1b for vehicle-D operated on route-4	123
Figure 60: Comparison of event averaged $T_{SCR\ IN}$ and bsNO _x emissions of all events generated in bin-1a and 1b for vehicle-C operated on route-4.....	126
Figure 61: Comparison of SCR inlet and outlet temperature profile, NO _x and CO ₂ emissions of an event generated in bin-1a (ABW-13)	127
Figure 62: ABW bin-based summary of NO _x emissions for vehicle-C operated on route-4	128
Figure 63: ABW bin-based summary of NO _x emissions for vehicle-D operated on route-3	131
Figure 64: Summary of ABW binning for NO _x emissions for vehicle-C operated on route-3	134
Figure 65: Comparison of event averaged $T_{SCR\ IN}$ and bsNO _x emissions of all events generated in bin-1a and 1b for vehicle-C operated on route-3.....	135
Figure 66: Comparison of vehicle speed, engine work, and $T_{SCR\ IN}$ of vehicle-3 operated on leg-2 of route-3	137
Figure 67: Cumulative frequency distribution of bsNO _x emissions of all events generated in ABW-bin-1a	138
Figure 68: Cumulative frequency distribution of bsNO _x emissions of all events generated in ABW bin 1b	142
Figure 69: Comparison of work-specific and CO ₂ -specific NO _x emissions of all events generated in bin-1a and 1b of each vehicle dataset	143

Figure 70: Comparison of duration-specific NO _x emissions for events generated in bin-2b divided into two categories: (a) Event-averaged T _{SCR IN} greater than 230 °C; (b) Event-averaged T _{SCR IN} less than 230 °C	145
Figure 71: CARB HD-OBD NO _x binning approach (Henderick, 2019).....	146
Figure 72: Time-weighted vehicle speed distribution of all in-use datasets sampled in section 3.3; (CAT-Vocational category).....	150
Figure 73: Time-weighted T _{SCR IN} distribution of all in-use datasets sampled in section 3.3; (CAT-Vocational category).....	153
Figure 74: Comparison of trip count and overall data utilization for ABW binning; (CAT-Vocational category).....	154
Figure 75: Trip-based distribution of engine work.....	155
Figure 76: Comparison of work-specific NO _x emissions of (a) Top graph: All events generated within each ABW in bin-1a, and (b) Bottom graph: All events generated within each ABW in bin-1b for each of the 18 vehicle datasets.....	156
Figure 77: Distribution of event-averaged T _{SCR IN} of bin-1a events.....	157
Figure 78: Cumulative frequency distribution of event averaged NH ₃ concentration in bin-1a	159
Figure 79: Proportion of event count for bin-1a (T _{SCR IN} < 230°C)	160
Figure 80: Distribution of NO _x emissions for bin-1b events	161
Figure 81: Comparison of CO ₂ -specific NO _x emissions of (a) Top graph: All events generated within each ABW in bin-1a, and (b) Bottom graph: All events generated within each ABW in bin-1b for each of the 18 vehicle datasets.....	163
Figure 82: (a) Top graph: Box and whisker distribution of events generated in bin-2b; (b) Bottom graph: Comparison of average and standard deviation of NO _x emissions rates as a function of average T _{SCR IN} ; (Avg: Average).....	165
Figure 83: Comparison of error propagation (Tailpipe measurements) of NO _x sensor with respect to PEMS measured under real-world operating conditions: (a) Top graph: Vehicle-D, and (b) Bottom graph: Vehicle-A.....	170
Figure 84: Cumulative frequency distribution of NH ₃ gas concentration.....	171
Figure 85: Comparison of measurement accuracy of reported NO _x sensor signal versus NH ₃ corrected (α=0.67) NO _x signal for data acquired from vehicle A.....	171
Figure 86: Bench-scale cross-interference evaluation of NH ₃ gas on NO _x sensor measurement (Demirgok et al., 2019).....	172
Figure 87: Influence of NH ₃ slip on tailpipe NO _x sensor response.....	173
Figure 88: Biplot for PCA analysis: Iteration-1.....	175
Figure 89: Biplot for PCA analysis: Iteration-2.....	176
Figure 90: Comparison of (a) NO _x measurements acquired from a PEMS and sensor, (b) T _{SCR OUT} , and (c) Rate of change of H ₂ O concentration	179
Figure 91: Comparison of (a): Top Chart: 90 th percentile distribution of bsNO _x emissions of each vehicle dataset, and (b) Bottom Chart: Total time-weighted data utilization for NTE, WBW and ABW approach; *: Duration-specific NO _x emissions rates (Right y-axis)	181
Figure 92: Thermal-based weighting scheme for bin-1a.....	191
Figure 93: Flow chart-based description of ABW approach.....	206

Figure 94: Comparison of NO _x versus CO ₂ emissions	207
Figure 95: Error propagation of ECU derived exhaust flow rate	208
Figure 96: Error propagation of ECU derived CO ₂ emissions	209
Figure 97: Distribution of T _{SCR IN} for in-fleet vocational activity	210

List of Tables

Table 1: U.S.EPA HD emissions standards (U.S. EPA, 2016a).....	11
Table 2: Current and proposed CO ₂ emissions standards for MHD and HHD engines (U.S. EPA, 2016b).....	13
Table 3: Audit tests for 40 CFR §1065 compliant laboratory and PEMS based measurements for Measurement allowance program (Feist et al., 2009)	28
Table 4: NTE limits used in measurement allowance program (Buckingham et al., 2009).....	35
Table 5: Measurement allowance determined by the MC method from percent of NTE threshold and final additive bsemissions measurement in-use limit (Buckingham et al., 2009).....	35
Table 6: Boundary conditions for vehicle speed and power bins (Badshah et al., 2019)	53
Table 7: Test vehicle specification for on-road PEMS testing	67
Table 8: Summary of test routes and vehicles tested.....	73
Table 9: Vehicle recruitment test matrix as a function of Vocation, and vehicle activity	78
Table 10: Boundary conditions for NTE evaluation.....	82
Table 11: Boundary conditions for WBW evaluation	83
Table 12: Range of boundary parameters selected for ABW sensitivity analysis.....	89
Table 13: DOE test design matrix for sensitivity analysis of ABW approach	89
Table 14: Time-weighted average and standard deviation for engine power and vehicle speed distribution of 75 HDIUT datasets	96
Table 15: Comparison of mean exclusion contribution (i.e., in percentage) towards NTE event invalidation	99
Table 16: Comparison of NTE event characteristics for the three different NTE test cases	100
Table 17: Average test duration and distance for each of the test routes	106
Table 18: Route-averaged engine power distribution for in-use datasets collected in section 3.2.....	107
Table 19: Overview of window start and end duration, and total engine work for all seven windows generated for route two evaluated on vehicle A.....	112
Table 20: Boundary parameter thresholds selected for evaluation of ABW binning approach.....	119
Table 21: Comparison of membership distribution within each event category of route-4 operated on vehicle D.....	125
Table 22: Comparison of NO _x mass distribution within each event category for grocery distribution route operated on vehicle D.....	125
Table 23: Comparison of data membership and NO _x mass distribution within each event category of route-4 operated on vehicle C.....	129
Table 24: Comparison of data membership and NO _x mass distribution within each event category of route-3 operated on vehicle-D	133

Table 25: Comparison of data membership and NO _x mass distribution within each event category of route-3 operated on vehicle-C.....	136
Table 26: Global comparison of time spent and NO _x mass distribution within each ABW bin categories.....	141
Table 27: Comparison of group average CO ₂ -specific NO _x emissions of all events generated in bin-1a and 1b.....	144
Table 28: Summary of vocation-specific vehicle/engine operational parameters ...	148
Table 29: Summary of vocational vehicle class, engine MY, and time-weighted fraction of active OBD MIL and DPF regeneration	149
Table 30: Time-weighted vehicle speed and engine power distribution segregated by vocational category	151
Table 31: T _{SCR IN} distribution as a function of three different temperature bandwidths	153
Table 32: Proportion of event count and duration for events generated above and below the NTE in-use limit for NO _x emissions for bin-1a and 1b.....	158
Table 33: Comparison of group mean CO ₂ -specific NO _x emissions of all events generated in bin-1a and 1b.....	163
Table 34: Distribution of bin-2b events separated as a function of event averaged T _{SCR IN}	166
Table 35: Event-duration based data distribution for each of the ABW bins	167
Table 36: Loading matrix for PC 1 and 2.....	177
Table 37: Percentage contribution of individual variables	177
Table 38: Summary of reference to the discussion of in-use emissions quantification methods	181
Table 39: Comparison of metric characteristics for NTE, WBW and ABW approach	184
Table 40: Specifications of Semtech-DS NDIR analyzer (Sensors, 2011).....	204
Table 41: Specifications of bench-scale evaluation for Semtech-DS NDUV analyzer (Sensors, 2011).....	205

1. Introduction

On-road medium-duty (MD) and heavy-duty (HD) diesel trucks are a significant workforce for the trucking industry and are deployed in a wide range of vocational applications such as refuse trucks, port delivery, transit buses, construction, local delivery and long haul goods movement (Cai et al., 2015; Scora et al., 2019). The variety of vocations include highly diverse engine operating conditions to meet the applicational objective. Diesel-fueled trucks are a preferred technology of choice by the HD trucking industry primarily due to their durability, fuel efficiency and torque output (MECA, 2007). However, the technology is often characterized as a significant source of oxides of nitrogen (NO_x) and particulate matter (PM) emissions in terms of emissions inventory. Increased awareness of health and environmental impact of these pollutants has led to the implementation of stringent control of HD diesel emissions over controlled environmental testing and also during in-use operation (Dallmann and Harley, 2010).

Traditionally, HD engine manufacturers were only required to certify engines in a controlled engine dynamometer testing environment on the Federal Test Procedure (FTP) test cycle to demonstrate compliance with the applicable emissions standard. As part of the 1998 consent decrees, a milestone settlement by Department of Justice (D.O.J) between the United States Environmental Protection Agency (U.S.EPA) and settling HD engine manufacturers led to augmentation of an additional 13-mode steady-state Supplementary Emissions Test (SET) cycle and in-use emissions measurement and verification using a portable emissions measurement system (PEMS) (He and Jin, 2017). The Not-to-Exceed (NTE) region emissions evaluation protocol was developed to verify emissions compliance under real-world driving conditions. Therefore, establishing a necessity to develop a laboratory-grade PEMS to quantify real-world driving emissions accurately. An academic research institute, West Virginia University (WVU) was contracted by the settling HD engine manufactures to develop a portable emissions analyzer capable of measuring tailpipe

emissions levels of criteria pollutants during real-world operating conditions (Gautam et al., 2001). Currently, PEMS comprising of individual gas detection analyzers serves as a robust laboratory-grade tool to evaluate in-use emissions. The United States (U.S.) regulations provide an extensive protocol to evaluate and calibrate the equipment's detection abilities based on periodic test protocols (CFR/40/1065/J).

With the promulgation of U.S.EPA 2010 emissions standards, majority of MD and HD diesel engine manufacturers adopted selective catalytic reduction (SCR) aftertreatment systems as a feasible pathway to reduce tailpipe NO_x emissions, combined with diesel particulate filter (DPF) for PM emissions reduction and diesel oxidation catalyst (DOC) for the oxidation of incomplete combustion products through chemical reaction kinetics. Since the introduction of 2004 emissions standards, external exhaust gas recirculation (EGR) technology is the most common hardware configuration used in modern HD trucks to reduce in-cylinder NO_x emissions (Johnson, 2008). The technological developments associated with emissions control hardware and reduction strategies are primarily aimed at ensuring real-world emissions compliance throughout the useful life of the engine without drastically affecting the engine's performance in terms of durability and fuel efficiency (Carder et al., 2017).

The introduction of DPF and SCR aftertreatment systems have significantly contributed to reducing tailpipe NO_x and PM emissions from MD and HD diesel engines. However, the SCR system requires a minimum exhaust gas temperature in the range of 200 to 250 °C to hydrolyze the injected urea to initiate NO_x reduction through catalytic chemical reactions. Urea injection is ceased to avoid any solid-deposit or nitrate formation on the SCR catalyst under modes of in-use operation where the exhaust gas temperature is below the catalyst light-off threshold (Boriboonsomsin et al., 2018). Numerous emissions measurement studies including on-road in-use, chassis dynamometer and road-side tunnel studies have highlighted upon deviations in brake-specific NO_x (bsNO_x) emissions compared to certification

standards from modern HD diesel trucks. Some of the observed and identified challenging modes of in-use operation for NO_x control are characterized as vehicle activity below SCR light-off temperatures, cold start, low-load and creep mode operation (Bishop et al., 2013; Dixit et al., 2017; Misra et al., 2013; Quiros et al., 2016). Specific vocations such as port-drillage operation, urban delivery (i.e., goods distribution) and refuse trucks are known to experience higher in-fleet operational time during low-vehicle operation (Boriboonsomsin et al., 2018; Sandhu et al., 2016). Furthermore, such vocations may experience most of the in-fleet operational time when the SCR is not functional. Such modes of in-use operation linked with relatively higher NO_x emissions rates are exempt from the emissions assessment as per the current NTE protocol.

1.1. Problem Statement

The U.S.EPA, in collaboration with HD engine manufacturers, introduced the HD in-use testing (HDIUT) program in 2004 to evaluate real-world emissions compliance. The program includes manufacturer-run, in-use emissions testing (i.e., typically based on measurements acquired from a PEMS in line with an exhaust flow meter (EFM)), reporting and verification of emissions compliance (i.e., using NTE protocol) from a sample of fleet operational trucks for each engine family. Regulatory agencies, manufacturers and research entities have identified that the current approach (NTE) incorporates numerous data-point exclusions, and only caters to modes of operation that are favorable for the SCR system to reduce NO_x emissions efficiently. Such operation is typically encountered only by vocations that experience sustained highway driving operation. Therefore, allowing only limited amount of the entire in-fleet activity data collected for compliance evaluation (Pondicherry et al., 2018; Shade et al., 2008; Tan et al., 2019). The NTE bin boundaries exempt assessment of real-world vocational activity such as extended engine idle, low-load operation and creep-mode operation that are linked to relatively higher NO_x emissions from in-use emissions assessment. In view of limitations associated with the current NTE protocol, California Air Resources Board (CARB) in their 2019 white paper proposed

to implement the moving average work-based window (WBW) approach that is used in Europe to evaluate in-service emissions conformity. The method generates moving average windows as a function of a predefined reference parameter as a function of engine work produced over the certification test cycle. Integrated emissions rates are calculated for each WBW, and the 90th percentile of window emissions results is used to determine emissions compliance. However, in the U.S. the regulatory agency's interest for evaluation of emissions compliance is based on test activity acquired from fleet operation, unlike European Union (EU) regulations that are comprised of a standardized predefined trip-based duty cycle requirement (CARB, 2019). Modern MD and HD diesel-fueled trucks are greatly dependent on the exhaust aftertreatment systems (EATS) to limit tailpipe NO_x and PM emissions. The performance of EATS is significantly dependent on the dynamics of the duty cycle. The non-uniform distribution of 1Hz emissions data (i.e., specifically for NO_x) across multiple windows may result in significant variability in compliance factor determination.

Evaluation of real-world driving emissions (RDE) plays a critical role in determining the performance of the emissions control systems. Currently, PEMS serves as a robust in-use emissions measurement device compared to other laboratory-grade emissions analyzers. However, utilization of PEMS for large scale deployment is complex, time-consuming, expensive, and labor-intensive. Therefore, potentially allowing only limited assessment of the entire fleet population. As a potential vision for the next tier of low-cost instrumentation for in-use NO_x assessment, there is an actively growing research and regulatory interest to evaluate the feasibility of utilizing existing zirconium dioxide (Zr-O₂) NO_x sensors (i.e., part of the current aftertreatment configuration) to monitor and report on-board NO_x compliance (CARB, 2019; Spears, 2019). However, research studies have highlighted upon measurement cross-interference due to ammonia (NH₃) gas and residual oxygen (O₂) ions on the reported NO_x sensor measurements (Frobert et al., 2013; Soltis et al., 2006; Todo et al., 2018).

Based on the background presented in this section, it is essential to highlight that there exists a critical need to develop a robust in-use emissions evaluation protocol that would serve as a viable tool in determining emissions characteristics (i.e., specifically of NO_x) from diverse real-world operation acquired from MD and HD on-road trucks.

Some of the characteristics of a “good” in-use emissions evaluation metric are:

- (a) Aids in a realistic representation of RDE, and therefore reduces the risk of a “false-positive” and “false-negative” results
- (b) Supports predictability of operational mode-based emissions characteristics
- (c) Implementation of minimum method-based exclusions to, therefore, evaluate a higher percentage of real-world operation
- (d) Separates the influence of diverse real-world engine/aftertreatment operating conditions

A successful implementation of a robust in-use emissions evaluation metric in conjunction with a robust on-board NO_x monitoring system would, therefore, reduce the complexity associated with in-use testing procedures and aid in the development of a cost-effective platform for large-scale deployment to evaluate real-world emissions (i.e., specifically of NO_x).

1.2. Dissertation Objective

The global objective of the study is to demonstrate the applicability of an alternative analytical approach that attempts bridges the gap between the current in-use certification procedures and highly diverse real-world operation for evaluation of in-use NO_x emissions. The goal of the approach was to demonstrate a robust assessment of tailpipe NO_x emissions from modern MD and HD diesel trucks across a wide range of real-world operating conditions. The following three specific aims have been investigated to address the global objective of the study.

Specific aim-1: Examine metric-based performance characteristics of current in-use emissions compliance evaluation protocols (i.e., U.S.EPA: NTE, and EU: WBW) to

assess tailpipe NO_x emissions levels and to evaluate the sensitivity of boundary parameters governing the two methods.

Specific aim-2: Develop a vehicle activity-based windowing (ABW) technique designed to categorize real-world engine and aftertreatment operation to explicitly characterize operational mode-specific NO_x emissions rates. Experimental on-road test activity collected using a 40 CFR §1065 compliant PEMS as well as Zr-O₂ based NO_x sensor technology from modern MD, and HD diesel trucks were used to evaluate the analytical approach.

Specific aim-3: In light of utilizing on-board NO_x sensors to evaluate the ABW approach (i.e., based on large-scale sampling of in-fleet vocational operation), this specific task evaluates the sensor's response in comparison to a laboratory-grade reference analyzer under real-world operating conditions. Furthermore, a statistical procedure, i.e., principal component analysis (PCA) was used to investigate the factors and modes of in-use operation that may contribute to cross-sensitive behavior of NO_x sensors.

2. Review of Literature

This chapter discusses an overview of primary combustion-derived exhaust emission from HD diesel engines in section 2.1. Section 2.2 illustrates the regulatory framework developed to evaluate HD emissions compliance. Section 2.3 discusses the current technologies used in modern diesel trucks to limit/reduce tailpipe emissions. Section 2.4 presents literature associated with vocational duty-cycle dependency on aftertreatment performance and its associated impact on tailpipe NO_x emission rates from modern HD diesel trucks. The evolution of on-board emissions measurement systems is discussed in section 2.5.

As a consequence of the 1998 consent decrees, an additional regulatory framework was introduced to evaluate real-world driving emissions using a PEMS. A measurement allowance program (i.e., discussed in section 2.6) was designed to quantify an error margin associated with measurements acquired from a PEMS. Section 2.7 provides a detailed overview of the regulatory framework used to evaluate real-world emissions compliance by the legislative agencies in the U.S. and Europe. Section 2.8 presents research studies that evaluated the regulatory framework for in-use emissions compliance. In light of utilizing on-board NO_x sensors as a potential tool for in-use NO_x monitoring, section 2.9 discusses the measurement principle of the NO_x sensor technology and presents a general overview of research studies that examined the performance of on-board Zr-O₂ NO_x sensor technology.

2.1. Exhaust Emissions from Diesel Engines

In-cylinder combustion derived pollutant formation is greatly dependent on the distribution and quantity of fuel injected, air mass management and in-cylinder thermal conditions. The primary and regulated exhaust species from diesel engine exhaust includes total hydrocarbons (HC), carbon monoxide (CO), carbon dioxide (CO₂), NO_x and PM emissions. The characteristic lean-burn combustion process poses a challenge in terms of controlling and limiting in-cylinder NO_x formation (Stanton, 2013). NO_x emissions in the atmosphere reacts with volatile organic fraction (VOC) in the presence of sunlight and forms ground-level ozone (O₃). Specific to PM emissions, research studies have demonstrated adverse effects on human health (i.e., respiratory and a potential source of carcinogenic) and deterioration of urban air quality due to long term exposure (Brook et al., 2010; Dahlmann et al., 2011; Jiang et al., 2018).

NO_x emissions species (i.e., a combination of nitric oxide (NO) and nitrogen dioxide (NO₂)) are formed due to exothermic and endothermic thermal reactions. The three main reactions causing NO emissions are based on the extended Zeldovich mechanism that occurs above 1800 K (i.e., equation 2.1, 2.2 and 2.3). The formation of NO_x emissions is temperature sensitive and predominantly occur after the start of the combustion phase. NO₂ is formed primarily during the expansion stroke where relatively cooler excess air is mixed with residual NO from the chemical reactions that occur during the combustion phase (i.e., equation 2.4). These reactions typically occur below 1200 K. With the increase in in-cylinder temperature, NO₂ can convert back into NO (i.e., equation 2.5) (Glarborg et al., 2018; Heywood, 1988; Iverach et al., 1973).



PM emissions is another major pollutant of diesel engine comprising of solid carbon material and ash combined with organic compounds (Kamimoto and Bae, 1988). PM emissions are formed from various sources such as incomplete combustion of hydrocarbons, wear of engine components, and combustion control strategies. The formation of solid carbon from in-cylinder combustion is greatly dependent on the equivalence ratio and is primarily formed during fuel-rich operation (Besch, 2016; Kittelson, 1998; Liati et al., 2013).

One of the significant limitations of in-cylinder combustion control strategies is the NO_x versus PM trade-off (Ishida et al., 2010; Zelenka et al., 1990). Often engine control strategies used to reduce NO_x emissions causes an impact on PM formation and vice versa. As NO_x formation is susceptible to in-cylinder temperatures, several transient combustion control and optimization strategies (i.e., related to air mass management and fuel injection) are used to control engine-out NO_x and PM emissions without significantly affecting engine performance and formation of other exhaust gas pollutants (Ardanese, 2008; Cozzolini et al., 2012; O'Connor and Musculus, 2013; Ravichettu et al., 2017).

2.2. Legislative Requirements for Regulated Emissions

In view of health and environmental effects of combustion derived products, the Clean Air Act (CAA) of 1974 by the U.S Congress led to the introduction of the first HD emissions standards for both compression and spark ignition engines to meet the allowable levels of regulated emissions over a standardized FTP engine dynamometer test cycle (CFR/40/1065, 2016; Environmental Policy Division, 1975; He and Jin, 2017). The FTP test cycle was developed as part of a sponsored research work funded jointly by the U.S.EPA and Coordinated Research Council (CRC) as a subset of the CAPE-21 program. The test cycle was generated based on Monte Carlo (MC) simulation and statistical analysis from real-world vehicle activity collected from HD trucks operating in two major cities in the U.S. – New York City (NYC) and Los Angeles (LA). The FTP cycle is illustrative of four different driving conditions, and

the sequence of operation is described as follows: (a) NYC non-freeway traffic, (b) LA non-freeway, (c) LA freeway and (d) NYC non-freeway (Smith, 1978). The procedure for emissions certification requires the engine to be evaluated over both cold and hot start conditions. A composite of 1/7th and 6/7th of the integrated emissions result is quantified for a cold and hot start test, respectively, to determine emissions compliance. There exists a 20-minute soak time in between the two tests (CFR/40/1065). Since the introduction of HD emissions regulations, there has been a significant periodic decrease in the allowable levels of NO_x and PM emissions over the standardized test cycle.

In light of standardization of emissions measurement protocol, U.S.EPA developed standards in association with national laboratories, academic institutions and the Engines Manufacturers Association (EMA). The emissions certification procedure requires the emissions to be measured from a constant volume sampling (CVS) system where the raw exhaust is diluted with ambient air to maintain a constant volumetric flow throughout the tunnel. The desired requirements for the measurement verification protocol as described in CFR 40 Part 1065 needs to be met to satisfy the regulatory requirements. Figure 1 shows the historical trends of HD diesel emissions standards of on-highway vehicles for NO_x and PM emissions set forth by the legislative agencies in the U.S. Table 1 presents an overview of the allowable emissions limits set forth by U.S.EPA for regulated pollutants. In the year 2007, NO_x and NMHC emissions standards were phased-in based on sales volume percentage. Most of the HD engine manufactures certified their engines sold for 2007-2009 to a NO_x limit of about 1.2 g/bhp-hr based on the fleet averaged calculation. Current regulations (i.e., U.S.EPA 2010) require the NO_x and PM emissions evaluated over the FTP test cycle to be at or below 0.20 g/bhp-hr and 0.01 g/bhp-hr, respectively.

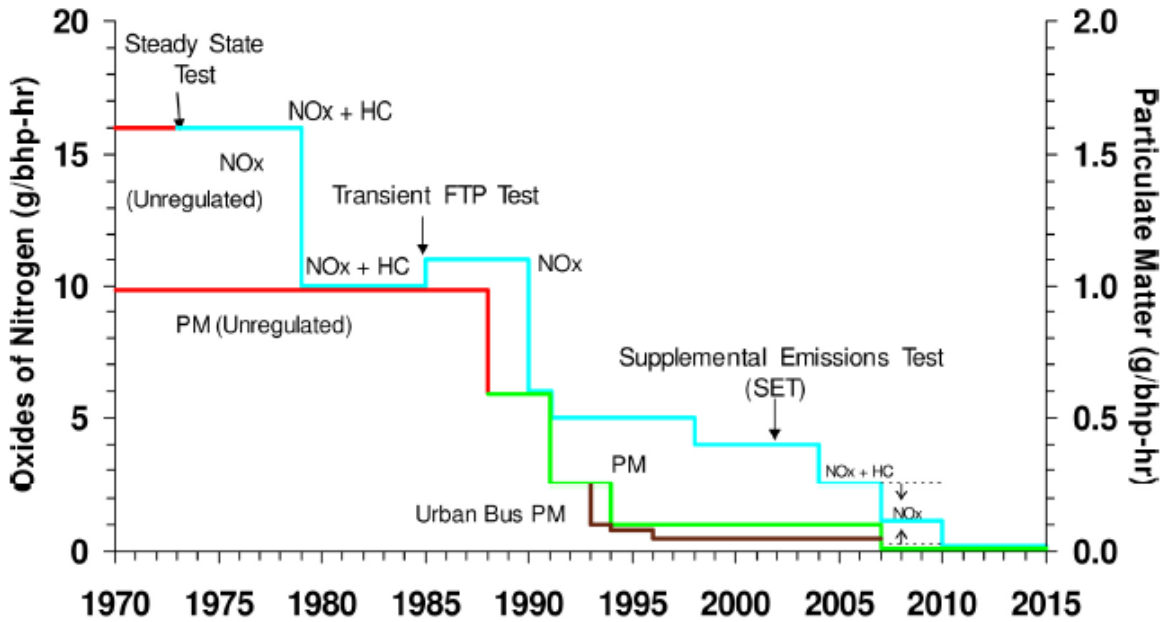


Figure 1: U.S.EPA regulations for NO_x and PM emissions (Stanton, 2013)

Table 1: U.S.EPA HD emissions standards (U.S. EPA, 2016a)

Engine Model Year [MY]	HC/NMHC	CO	NO _x	PM
[#]	[g/bhp-hr]			
1979-1984	1.5	25	-	-
1985-1987	1.3	15.5	10.7	-
1988-1989	1.3	15.5	10.7	0.6
1990	1.3	15.5	6	0.6
1991-1993	1.3	15.5	5	0.25
1994-1997	1.3	15.5	5	0.1
1998-2003	1.3	15.5	4	0.1
2004-2006	-	15.5	-	0.1
2007+	0.14*	15.5	0.2*	0.01

* Phase-in of NO_x and NMHC standards based on percent of sale-basis: 50% from 2007 to 2009 and 100 % in 2010

The 2007 emissions standards led to the introduction of DPF aftertreatment systems to trap PM. The use of DOC and DPF systems enabled HD engine manufacturers to meet the regulatory thresholds for PM, CO and non-methane hydrocarbons (NMHC) emissions. Stanton's systematic development of a commercial vehicle that will meet future regulations shows a comparison of NO_x emissions versus fuel consumption for

engines certified for two different emissions standards equipped with EGR technology (Figure 2). The engine certified for 2007 emissions standard was equipped with a DOC and DPF exhaust aftertreatment system. The study shows that even though the MY 2007 engine demonstrated a decrease in fuel consumption by 2.5% to achieve a NO_x target of 1.2 g/bhp-hr, the introduction of DPF caused an increase in backpressure, therefore, increasing fuel consumption. Additionally, HC metered dosing is also required for active DPF regeneration. The study also highlights that on a global comparison basis, trends in fuel efficiency did not change between the 2004 and 2007 certified engines (Stanton, 2013).

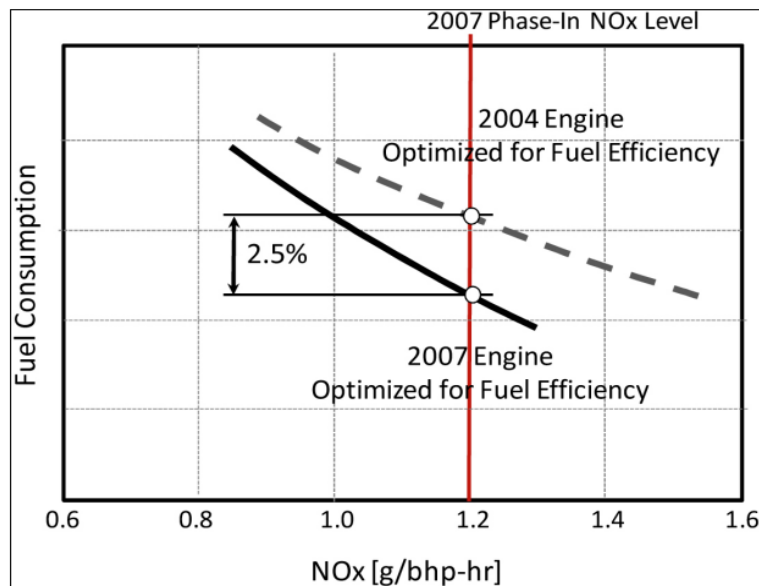


Figure 2: Comparison of NO_x emissions and fuel consumption of an MY 2004 and 2007 certified engines with EGR technology (Stanton, 2013)

In 2010, the majority of HD engine manufacturers selected the DOC-DPF-SCR aftertreatment package to comply with the U.S.EPA 2010 emissions standards. Introduction of the SCR system was identified as an optimal and balanced approach that created a robust pathway to control NO_x emissions. Introduction of aftertreatment technologies demonstrated a shift from NO_x versus PM tradeoff to NO_x versus fuel consumption/CO₂ emissions tradeoff. The primary driving force is the necessity of relatively higher exhaust temperatures for the catalyst to meet the light-off temperature thresholds (Fontaras et al., 2017; Stanton, 2013).

In the year 2014, GHG regulations addresses were introduced to control emissions levels of CO₂, nitrous oxide (N₂O) and methane (CH₄) emissions. Table 2 presents an overview of the current and proposed standards category based on medium-heavy (MH) and heavy-heavy (HH) duty engines. The engines installed for vocational and tractors applications are required to meet the desired GHG targets over the FTP and SET test cycle, respectively (U.S. EPA, 2016b).

Table 2: Current and proposed CO₂ emissions standards for MHD and HHD engines (U.S. EPA, 2016b)

		Vocational Application		Tractors	
		FTP Test Cycle		SET Test Cycle	
Category	Year	CO ₂ emissions	Fuel consumption	CO ₂ emissions	Fuel consumption
[-]	[#]	[g/bhp-hr]	[gallon/100 bhp-hr]	[g/bhp-hr]	[gallon/100 bhp-hr]
MHD	2014	600	5.89 ^a	502	4.93 ^a
	2017	576	5.66	487	4.78
	2021	545	5.35	473	4.64
	2024	538	5.28	461	4.52
	2027	535	5.25	457	4.48
HHD	2014	567	5.57 ^a	475	4.67 ^a
	2017	555	5.45	460	4.52
	2021	513	5.03	447	4.39
	2024	506	4.97	436	4.28
	2027	503	4.94	432	4.24

a) Voluntary in MY 2014 and 2015

The 1998 consent decrees led to the augmentation of a new discipline of regulatory requirements that comprised of evaluating real-world emissions performance while the vehicle was performing its regular in-fleet operational duty cycle. The in-use emissions regulations were introduced to verify compliance with the set forth allowable in-use pollutant limits throughout the useful life of the engine (DOJ and U.S.EPA,1998.). U.S.EPA, in collaboration with HD engine manufactures, introduced the HDIUT program that involved verification of emissions compliance from fleet-

based vocational operation (U.S.EPA, 2005). A detailed explanation of the in-use emissions compliance quantification protocol used in the U.S. is discussed in section 2.7. The continuous efforts in sophisticated developments associated with the diesel engine and aftertreatment technology are aimed at delivering efficient and cleaner engine technology.

2.3. Emissions Control Technologies

With the initiative of meeting stringent standards and reducing tailpipe emissions, HD engine manufacturers have introduced sophisticated emissions control technologies to limit tailpipe emissions of critical emissions species such as NO_x and PM, without significantly affecting fuel economy and engine/catalyst durability. Modern diesel engines are typically configured with advanced electronic high-pressure common rail fuel injection systems, turbochargers, EGR technology and an aftertreatment package that includes DOC-DPF-SCR technology.

In addition to oxidizing unburnt exhaust gases, the DOC also oxidizes engine-out NO emissions to NO₂ emissions. The DOC is typically composed of a honeycomb monolith structure that comprises of cordierite (i.e., a composition of platinum (pd), palladium (Pd) and ceria (C_eO₂)) which aids in achieving a NO/NO₂ ratio of 1:1.

DOC plays a significant role in:

- (a) Promoting oxidation of soot stored in the DPF
- (b) Utilization of NO₂ generated for SCR “fast reactions” to reduce NO₂ to nitrogen (N₂) and water (H₂O)

A study by Stanton showed the influence of NO₂ generation with respect to oxidation of soot. The chemical reaction kinetics observed show that during the passive regeneration process, NO₂ was converted into NO and CO₂. However, active operation of DOC is confined to catalyst light-off temperature that is dependent on the real-world duty cycle and thermal management incorporated for efficient catalytic

activity. EGR and SCR technology play a significant role in limit in-cylinder NO_x formation and tailpipe NO_x control (Stanton, 2013).

2.3.1. Exhaust Gas Recirculation

External EGR technology is one of the most effective and conventional technologies that is used to limit in-cylinder NO_x formation. As the name indicates, the basic working principle of the technology is to re-circulate a portion of the exhaust gas back into the engine air intake flow stream using a valve mechanism. In-cylinder NO_x formation is primarily attributed to peak cylinder combustion temperature; the addition of cooled exhaust gas increases the heat capacity of the charge air. Therefore, the reduction of NO_x formation is mainly due to the dilution effect (i.e., due to the presence of diluents such as CO₂ and H₂O), thermal effect, and additional mass effect, therefore leading to a reduction in the in-cylinder combustion temperature and intake oxygen concentration (Stanton, 2013).

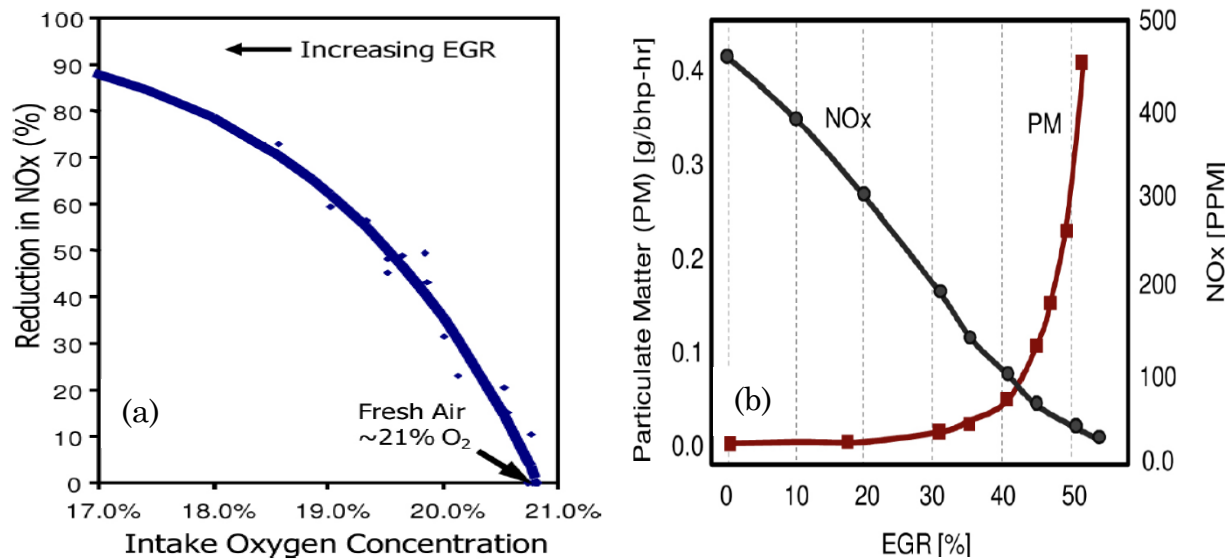


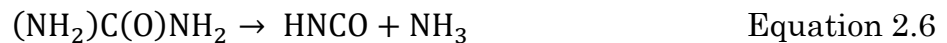
Figure 3: Effect of (a) Intake oxygen concentration on NO_x reduction; (b) EGR mass fraction on NO_x versus PM emissions (Stanton, 2013)

Figure 3a shows the effect of intake oxygen concentration as a function of the percent reduction in in-cylinder NO_x formation. Research studies have highlighted an increase in soot emissions due to the presence of unburnt fuel. Higher levels of EGR

mass rates exhibit an increase in CO and HC emissions (Idicheria and Pickett, 2005; Jacobs et al., 2003). Therefore, potentially decreasing the engine's thermal efficiency and fuel economy. Figure 3b shows the characteristic curve of NOx and PM emissions as a function of EGR fraction. Several robust traditional and model-based advanced EGR control strategies are implemented to reduce NOx emissions across various engine operational modes where the SCR technology is not active (Ardanese, 2008; Thiruvengadam, 2017).

2.3.2. Selective Catalytic Reduction

The urea-SCR technology is the most widely used aftertreatment technology in MD and HD diesel engine industry for NOx abatement. NOx reduction is primarily achieved by injecting diesel exhaust fluid (DEF) (i.e., 32.5% urea in H₂O) into the exhaust stream using an atomizing nozzle upstream of the SCR catalyst (i.e., Nobel metals varying from composition combination of Platinum (Pt), Copper (Cu) and zeolites with metal oxides) (Burch et al., 1994; Kang et al., 2006; Olsson and Fridell, 2002). The quantity of urea injected is based on the NH₃ demand that corresponds to the catalyst's NOx conversion efficiency. The quantity of urea injection is dependent on several factors such as NH₃ storage on the catalyst, catalyst material, NO-to-NO₂ ratio, and exhaust gas thermal conditions within the control volume of the SCR catalyst (Keuper et al., 2011). The injected urea decomposes into NH₃ (i.e., primary reaction agent) and CO₂ through hydrolysis and thermolysis. NH₃ is trapped in active sites of the SCR catalyst and is used to reduce NO/NO₂ emissions.



There exist three significant chemical reactions that play a critical role in achieving NOx reduction. Equation 2.8 (i.e., the standard SCR reaction) is an equimolar reaction between one mole of NH₃ and one mole of NO. Consequently, equation 2.9 uses NO₂ as a primary reagent to reduce NO₂ into elemental N₂. The equation plays its role when the ratio of NO₂ and NOx exceeds 50%. Equation 2.10 is often recognized

as the fast-SCR reaction (i.e., faster than standard SCR reaction) comprising of 1:1 composition of NO and NO₂. As the engine exhaust comprises of a dominant fraction of NO (i.e., for NO_x component), the oxidation catalyst plays a significant role for converting a portion of NO exhaust species to NO₂ to support SCR catalytic reactions (Stanton, 2013). One of the primary challenges for NO_x conversion efficiency at low-temperature operation is the catalyst light-off temperature. In a study by Smith et al., it was shown that vaporization of urea was slow at exhaust gas temperatures below 160 °C and increased injection rates at low-temperature operation generally led to deposit formation on the catalyst substrate (Smith et al., 2014).

Figure 4 shows a comparison of catalyst activity on NO_x conversion efficiency for iron-based (◆), copper-based (▲) and vanadium-based (●) coated catalysts. The optimum operating temperature window for effective NO_x reduction is between 250 and 450 °C for Copper Zeolite (CuZe) catalyst while for Iron Zeolite (FeZe), it is between 350 and 500 °C.

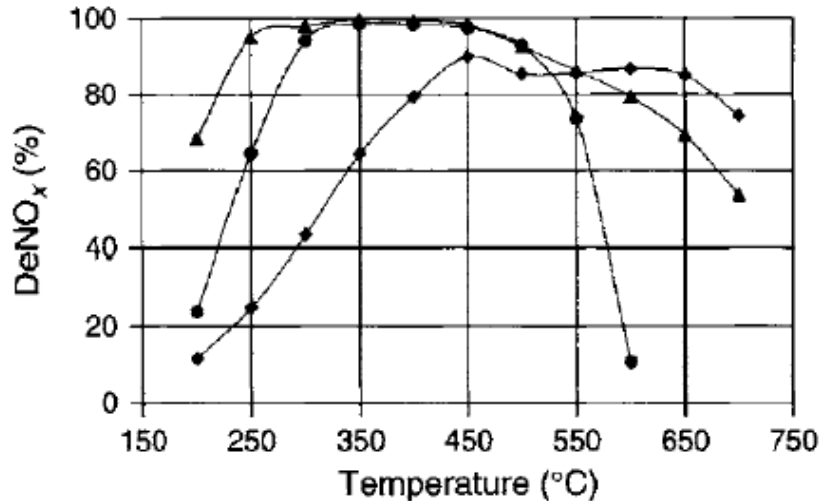


Figure 4: NO_x conversion efficiency for vanadium-based and zeolite-based SCR systems (Kröcher, 2007)

In a study by Girrard et al. it was identified that the performance of the CuZe SCR catalyst for NO_x conversion efficiency was sensitive to the presence of HC on the SCR catalyst. Research studies indicated that Vanadium-based catalysts were less sensitive to HC emissions and are thermally durable up to 550 °C compared to CuZe and FeZe catalysts (Girard et al., 2008; Nova and Tronconi, 2014; Ura et al., 2009).

Figure 5 shows that the NH₃ storage shows a non-linear behavior with respect to catalyst temperature. In a study by Eijnden et al., it was observed that zeolite-based catalysts exhibit the ability to store relatively higher NH₃ than vanadium-based catalyst at catalyst temperatures below 300 °C (Eijnden et al., 2009). Figure 6 shows that the vanadium-based catalyst demonstrated improved performance for NO_x conversion in comparison with CuZe SCR catalyst for a wide range of thermal boundary conditions. Although at low-temperature operation, vanadium-based catalyst demonstrated relatively lower NO_x conversion performance compared to CuZe catalyst. At 200 °C, the vanadium-based catalyst achieved ~80% conversion, compared to CuZe technology that achieves nearly 90% reduction in NO_x emissions. Although Vanadium-based catalyst demonstrates superior performance across a wider thermal operating bandwidth compared to CuZe, the catalyst compound thermally deteriorates faster in time. A study by Cavataio et al. evaluated the effect of thermal ageing on various SCR catalysts. In this study, after 64 hours of thermal exposure to gas temperatures around 670 °C, it was observed that the NO_x conversion efficiency of Vanadium-based catalyst significantly decreased when compared to CuZe and FeZe catalyst which demonstrated a de-NO_x efficiency that was above 90% (Cavataio et al., 2007; Nova and Tronconi, 2014). Due to limitation associated with the ageing impact of vanadium-based catalyst, CuZe catalysts are widely used in modern HD diesel trucks because of the superior NO_x conversion efficiency attained at relatively lower temperatures as compared to FeZe (Kamasamudram et al., 2010).

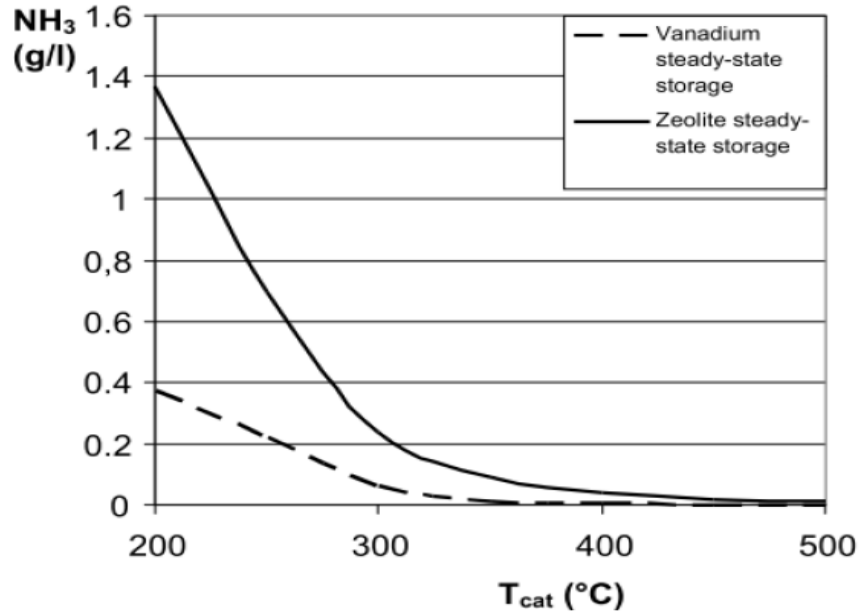


Figure 5: Comparison of NH₃ storage levels (i.e., grams per litre) as a function of catalyst temperature (Eijnden et al., 2009)

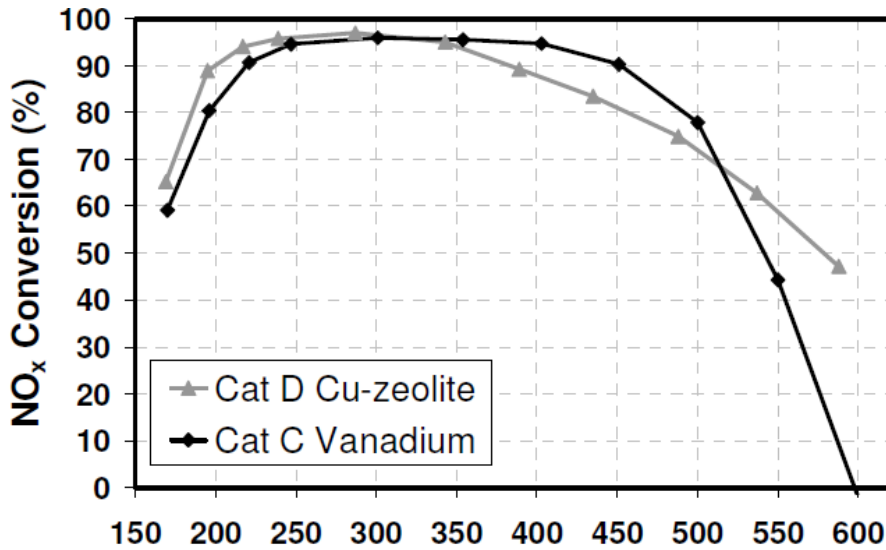


Figure 6: Comparison of NO_x conversion efficiency of catalyst C (Vanadium-based) aged for 50hr at 600 °C and catalyst D (Cu-Ze) aged for 64hrs at 670 °C at 30k hr⁻¹ (Ura et al., 2009)

A study by Stanton shows the influence of in-use activity associated with SCR temperature distribution and NO_x conversion efficiency of nine line-haul HD trucks equipped with CuZe SCR catalysts. The bar chart presented in Figure 7 shows that

a majority of real-world operation for the data collected from line-haul trucks was between 250 and 400 °C. The quantified SCR NO_x conversion efficiency was above 80% for in-use activity that exhibited SCR gas temperature between 250 and 500 °C (Stanton, 2013). Therefore, exhibiting the impact of exhaust gas thermal boundary conditions for real-world tailpipe NO_x abatement.

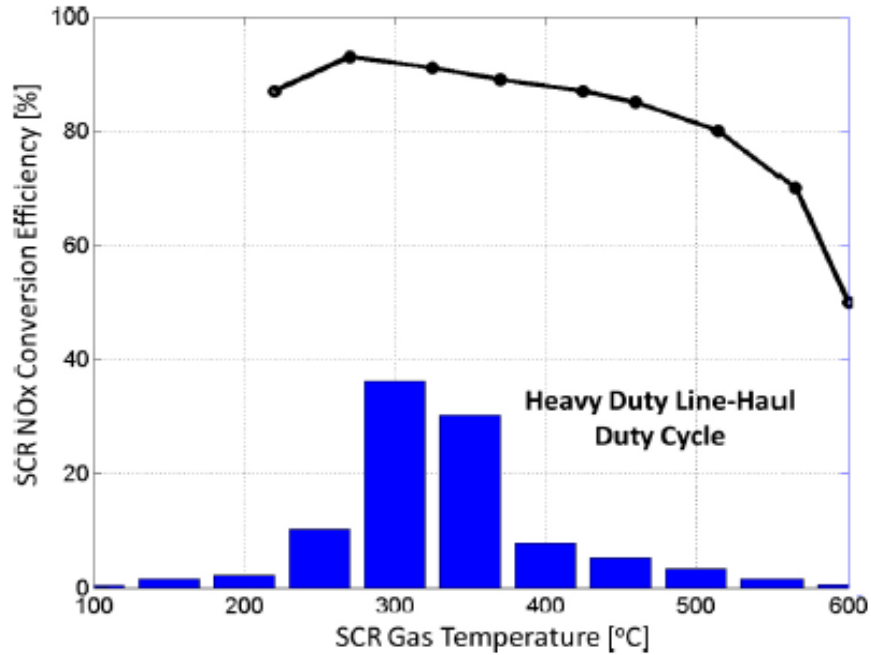


Figure 7: Real-world SCR thermal profile of nine line-haul trucks (Stanton, 2013)

2.4. Vocational Dependency on Vehicle Activity and NO_x Emissions

The SCR catalyst technology is widely investigated and has proven to be an effective solution for NO_x reduction and also to meet the stringent U.S.EPA 2010 emissions regulations. Currently, the MD and HD diesel trucking industry in the U.S. are greatly dependent on the SCR system to demonstrate real-world NO_x reductions. Several engine manufacturers use advanced combustion control strategies in addition to EGR and SCR system to effectively reduce tailpipe NO_x emissions during real-world operating conditions (Stanton et al., 2013). Research studies have highlighted upon elevated levels of NO_x emissions from in-use vehicle activity that is characterized by cold start activity, low-load engine operation, extended idle operation, urban driving operation with frequent stop-and-go activity (Boriboonsomsin et al., 2018; Misra et al., 2013; Quiros et al., 2016; Thiruvengadam et al., 2015).

In a real-world emissions assessment study, Quiros et al. evaluated NO_x emissions rates from modern trucks equipped with SCR technology using WVU's transportable CVS laboratory operated across major freight corridors in California. Figure 8 shows a route-based comparison of averaged NO_x emissions rates from two MY 2013 and two MY 2014 diesel trucks with SCR technology. One of the vehicles was certified for a higher standard than the U.S.EPA 2010 emissions standards. The results of the study show that on average NO_x emissions emitted from the Near-Dock route were in the range of 0.50 to 1.62 g/bhp-hr, i.e., one and a half to seven times higher than the certification standard. However, the study suggests that the observed NO_x emissions are lower (i.e., in the range of 73-92%) than trip-averaged NO_x emissions rates observed from a MY 2007 diesel engine. The Near-Dock drayage route represents activity at the port comprising of frequent stop-and-go activity associated with low-vehicle speed driving conditions. The Hill-climb and interstate route comprise of dominant time fraction of operational time during highway driving operation. The route-averaged NO_x emissions were observed to be below the

certification standard. The vehicle activity of such driving conditions results in exhaust gas thermal conditions that were favorable for the SCR system to actively reduce NO_x emissions (Mendoza-Villafuerte et al., 2017; Quiros et al., 2016).

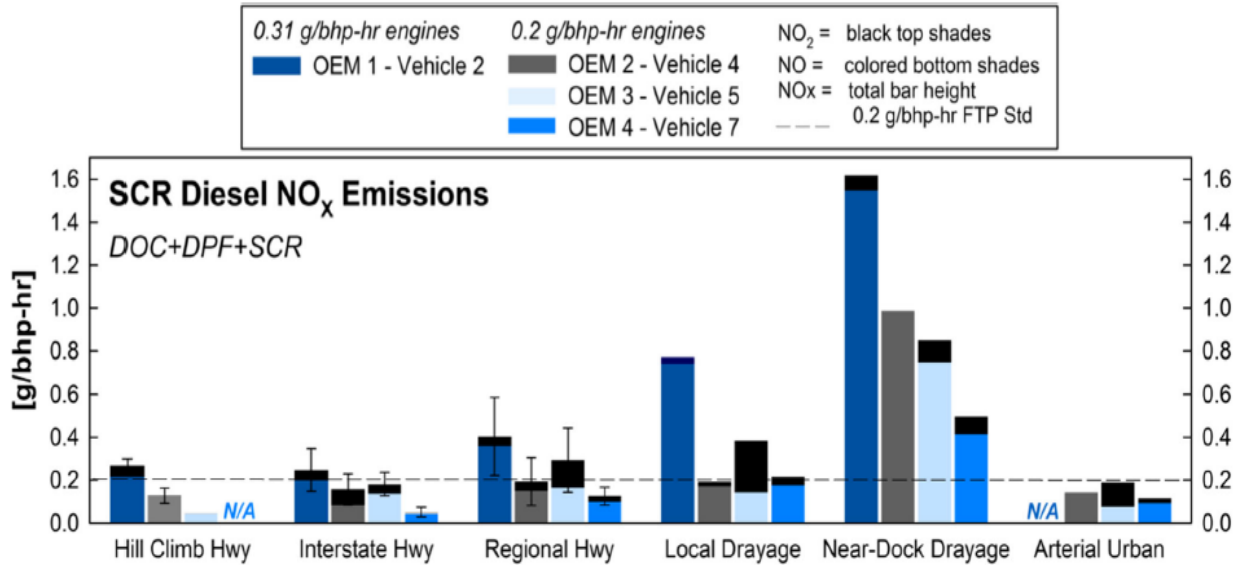


Figure 8: Comparison of NO_x emissions of diesel engines equipped with SCR technology operated over six distinct routes in California (Quiros et al., 2016)

In a study by Thiruvengadam et al., it was observed that NO_x emissions from 2010 and later MY engines with SCR technology were six to nine times higher than the certification limit for chassis dynamometer testing cycles such as local and near-dock (i.e., presented in Figure 9). The higher NO_x emissions rates observed were primarily from test activity where the SCR catalyst temperatures were below the catalyst light-off temperature. Vocational duty cycles demonstrated bsNO_x emissions levels to be relatively higher than that of the UDDS cycle (i.e., nearly representative of the FTP engine certification cycle) (Thiruvengadam et al., 2015). The research, as mentioned earlier, highlights the necessity of developing innovative and cost-effective emissions control technologies to reduce NO_x emissions rates from off-cycle vocational operation. Similarly, Dixit et al. performed chassis dynamometer experiments to evaluate the feasibility of attainment of vehicle activity for emissions compliance assessment using the NTE protocol. The study highlighted that more than 90% of the

test activity lies outside the NTE control area for vocational drive cycles representative of goods delivery operation (Dixit et al., 2017).

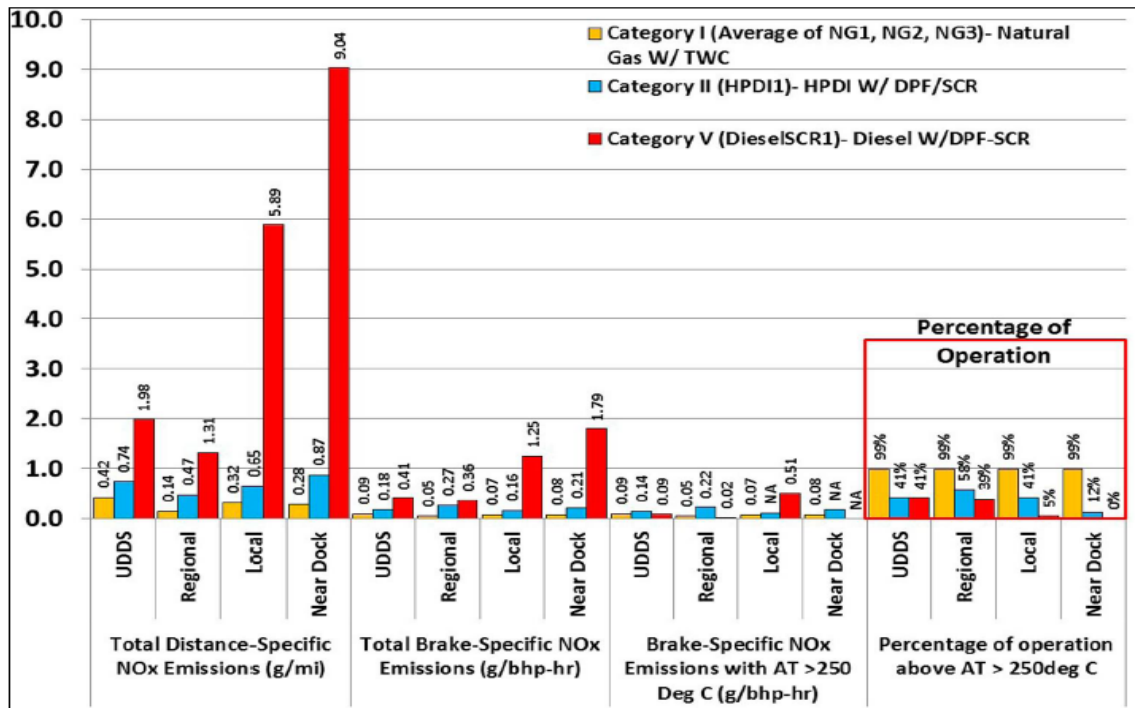


Figure 9: Comparison of distance-specific, brake-specific NOx emissions, percentage of aftertreatment outlet temperature operation for test activity acquired four over chassis dynamometer test cycles (Thiruvengadam et al., 2015)

A study by Misra et al. shows a comparison of NOx emissions profiles in Figure 10 for a test route comprising of approximately 15% of time fraction of urban/rural driving conditions and the remainder of the test route comprising of highway driving operation. A cold start emissions test was performed for two scenarios: (a) High load (i.e., test weight: 90% of allowable GVWR) and (b) Unloaded (i.e., test weight: 40% of allowable GVWR). The first 2 miles of test activity was considered as cold start operation. In both test case scenarios, NOx emissions evaluated from cold start operation were 27 and 45 times higher than that of highway driving segment of the same test. The authors highlight that the elevated levels of NOx emissions can be attributed to the nonfunctional EGR and SCR system during cold temperature operation (Misra et al., 2013).

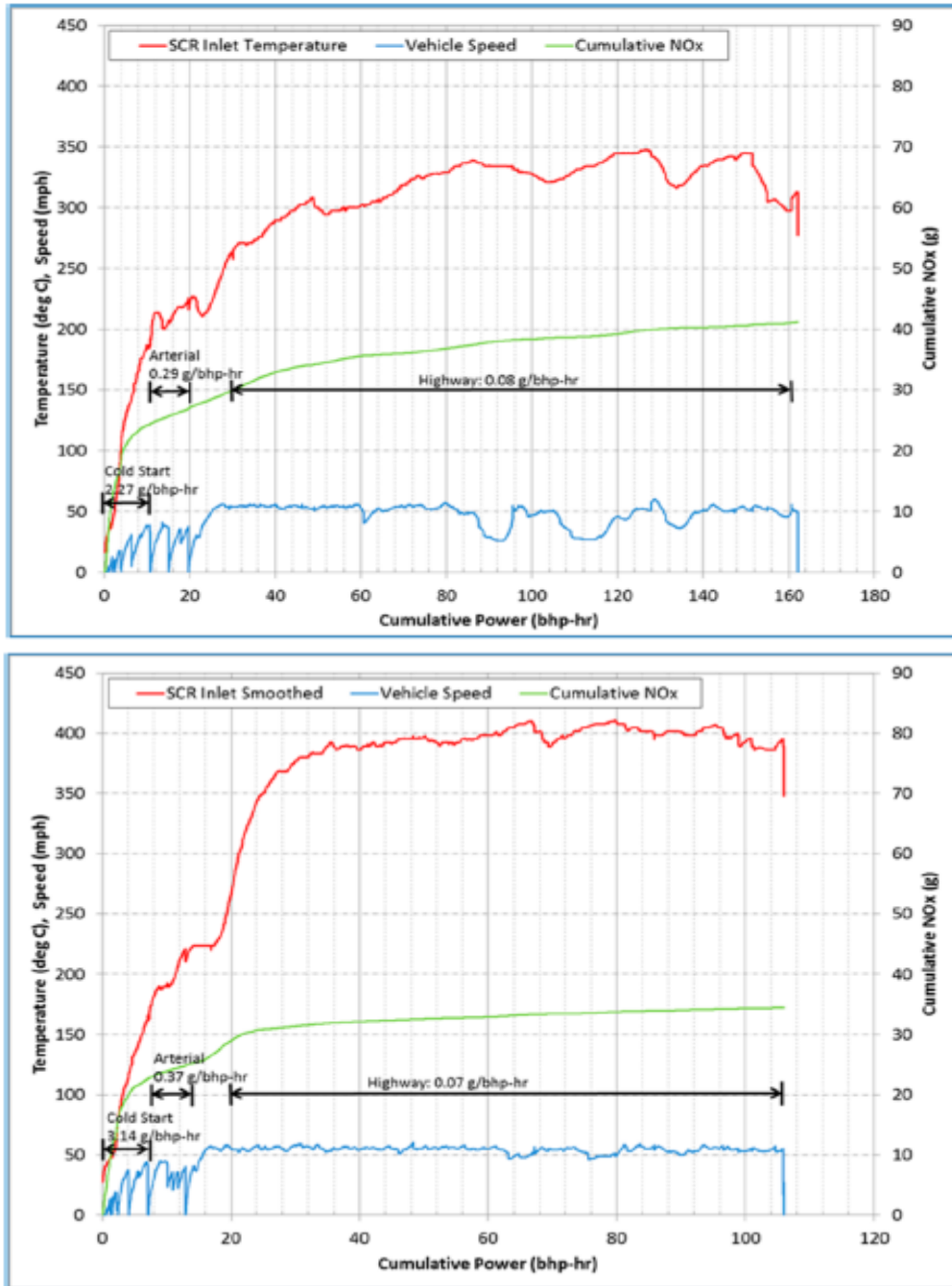


Figure 10: Comparison of the cumulative NOx mass from a MY 2010 engine operated under two scenarios: (Top chart) high load operation and (bottom chart) unloaded (Misra et al., 2013)

A study by Boriboonsomsin et al. evaluated fleet-based vehicle activity acquired from 90 trucks operating in the state of California. The study showed that depending on the vocational activity approximately 42 to 89% of operating time of in-fleet activity

comprised of SCR operation below 250 °C. Figure 11 shows that approximately 70% of the test activity collected in the study for drayage application was below 200 °C. This is primarily due to operation acquired from activity acquired at the port harbour which comprises of extended idle operation followed by low vehicle speed activity near the port. Majority of operation acquired from line-haul trucks exhibits SCR gas temperature between 250 and 300 °C, i.e., above the SCR light-off temperature threshold (Boriboonsomsin et al., 2018).

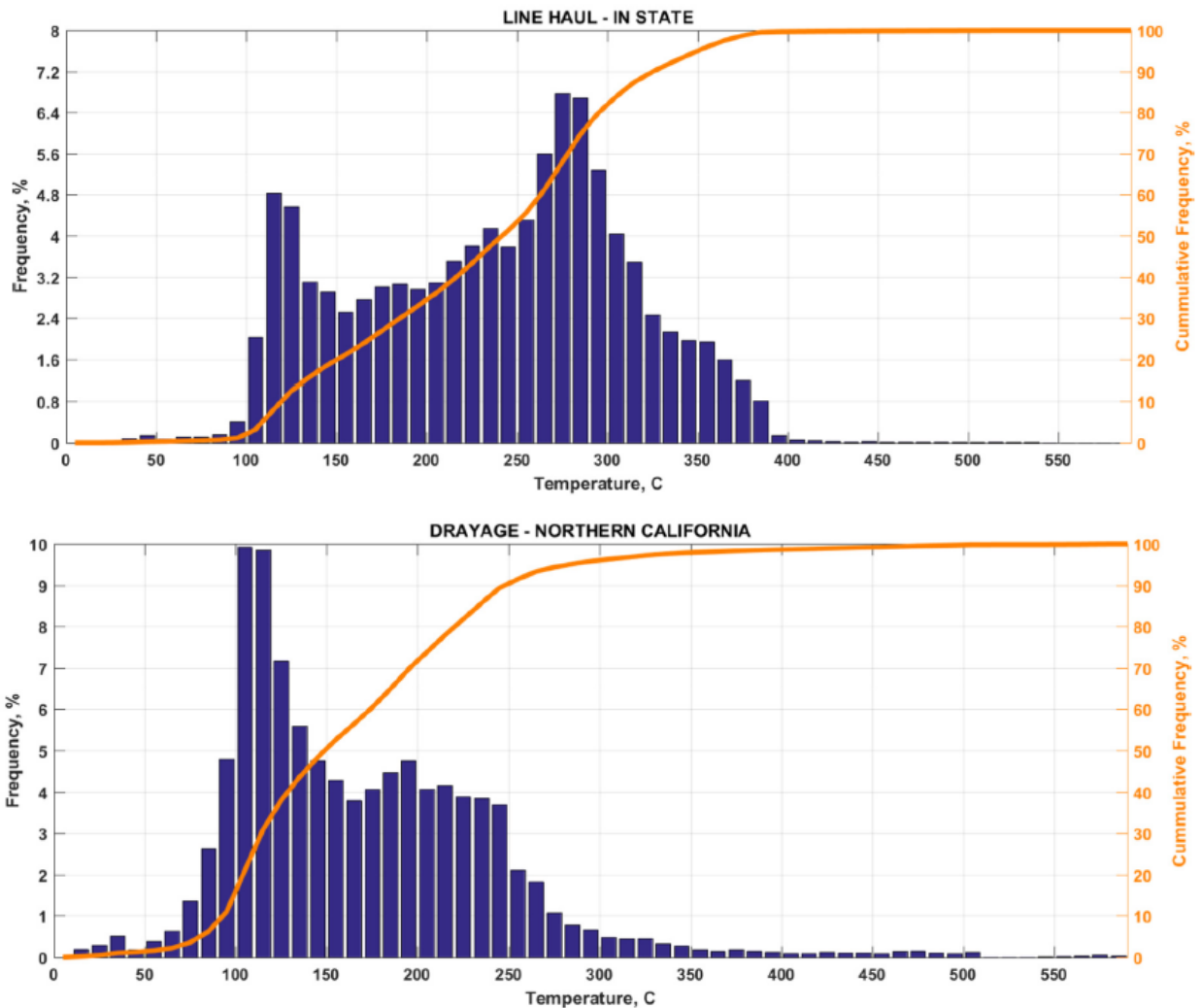


Figure 11: Comparison of SCR temperature profiles of line-haul and drayage application trucks (Boriboonsomsin et al., 2018)

Tan et al. evaluated in-fleet vehicle activity and on-board NO_x sensor data collected using ECU data loggers from 68 HD diesel trucks. Figure 12 shows a comparison of average NO_x emissions levels from test activity procured using original equipment manufacturer (OEM) broadcasted NO_x sensors. The chart segregates the collected data based on average NO_x conversion efficiency levels during real-world operation. The NO_x conversion efficiencies were lower than 70% for 21 vehicles, therefore resulting in bsNO_x emissions rates to be 1.60 g/bhp-hr on average. Similarly, vehicles that exhibited NO_x conversion efficiencies above 90% resulted in average bsNO_x emissions of 0.25 g/bhp-hr. Data presented is skewed to operating conditions only when the on-board NO_x sensor is active. This is because on-board NO_x sensors (i.e., part of the aftertreatment package) are inactive under certain exhaust gas thermal conditions to avoid any structural damage. (Tan et al., 2019).

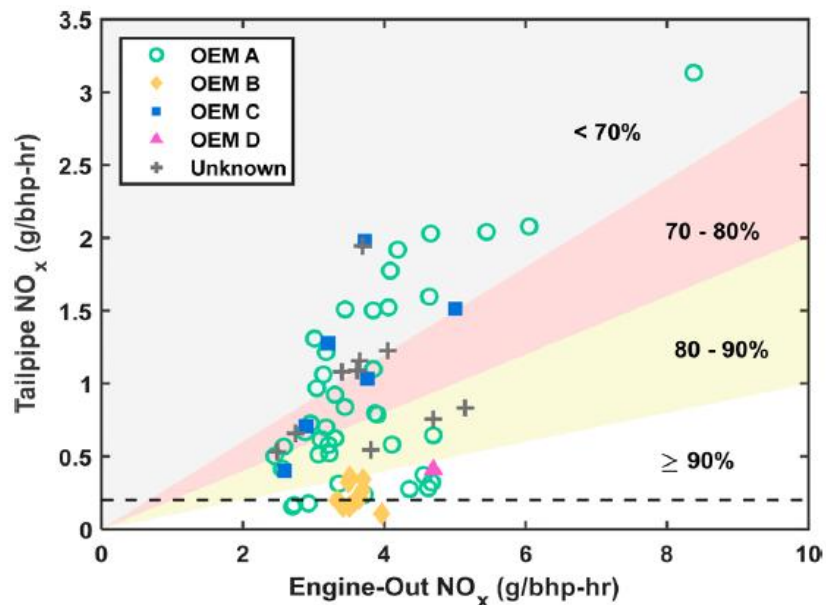


Figure 12: Comparison of average engine-out and tailpipe NO_x emissions of 68 HD trucks (Tan et al., 2019)

In summary, variability in vocational duty cycle plays an integral role in SCR performance of modern on-highway HD diesel trucks. Scora et al. characterized real-world vehicle activity profiles from 90 MD and HD trucks, i.e., comprising of a range

of vehicle vocations such as urban buses, airport shuttle, refuse haulers, food and beverage distribution, concrete mixers, line-haul in-state and out of state goods distribution. The results of the study show that the average vehicle speed for line-haul (out-of-state) trucks is the highest as expected at 41.1 mph, whereas drayage trucks operating in Northern California are at 8.9 mph. Similar results of relatively lower average vehicle speed were observed from vocations such as airport shuttle, refuse trucks and urban buses. Beverage distribution trucks exhibited an average vehicle speed of 11.6 mph and 39.3% of operational time was acquired while the engine was idling. This is solely due to the majority of in-fleet operation occurring within the LA metropolitan area, where the traffic is congested. As anticipated the concrete mixers spent most of the in-fleet operation (i.e., 59.3% of test activity) while the vehicle was idling (i.e., because of PTO activity) (Scora et al., 2019).

A conference presentation by Besch et al. showed a comparison of daily-averaged bsNO_x emission rates from 159 pre-2010 MY and 100 non-credit post-2010 MY HDIUT diesel vehicle datasets. An average of 81% reduction in bsNO_x emissions was observed from post-2010 MY vehicle datasets with SCR technology compared to pre-2010 MY vehicle datasets. In relation, the engine certification limit for U.S.EPA 2010 emissions standards demanded a reduction of 84.6%. It must be highlighted that the certification value pertains to engine dynamometer testing over a predefined test cycle with only a limited contribution of cold-start emissions (i.e. 1/7 of cold-start FTP). In contrast, the 81.8% reduction in NO_x emissions was obtained over a wide range of real-world engine operation comprising of a diverse mixture of driving and ambient conditions (Besch et al., 2018).

2.5. Advancements in On-board Emissions Measurement Systems

The 1998 consent decrees devised the official development of a PEMS that was capable of robust measurements of tailpipe pollutant constituents (i.e., specifically of CO, CO₂, NO_x, and THC) under real-world driving conditions. The portable device needed to be robust in terms of data acquisition to capture the transient response, meet the linearity, accuracy and repeatability thresholds comparable to a laboratory-grade measurement device for calibration gas and engine exhaust, and also withstand a range of ambient conditions. Additionally, the device was required to meet a range of validation protocols set forth by the regulatory agencies. A detailed overview of the extensive periodic examination per the 40 CFR §1065 testing procedures for PEMS is outlined in Table 3 (Feist et al., 2009).

Table 3: Audit tests for 40 CFR §1065 compliant laboratory and PEMS based measurements for Measurement allowance program (Feist et al., 2009)

Description	CFR Reference	Lab Raw	Lab Dilute	PEMS
Linearity	1065.307	x ¹	x ¹	x ²
Torque Meter	1065.310	x	x	
Fuel Flow	1065.320	x		
Intake Flow	1065.325	x		
Exhaust Flow	1065.330			x
CVS Verification	1065.341		x	
H ₂ O Interference on CO ₂	1065.350	x	x	x
H ₂ O and CO ₂ Interference on CO	1065.355	x	x	x
FID Optimization	1065.360	x ³	x ³	x ³
Non-stoichiometric raw FID O ₂ Interference	1065.362	x		x
Nonmethane cutter penetration fractions	1065.365	x	x	
CLD H ₂ O and CO ₂ quench	1065.370	x	x	
NDUV HC and H ₂ O Interference	1065.372			x
Chiller NO ₂ penetration	1065.376			x
NO ₂ -to-NO converter check	1065.378	x	x	
¹ Linearity for lab on gas analyzers, flow meters, torque meter, pressures, temperatures ² Linearity for PEMS on gas analyzers, exhaust flow meters ³ Verify methane response factors only, THC instruments				

Before the official development of PEMS, several research and commercial entities had developed portable and transportable systems to measure PM and gaseous emissions for inspections and maintenance (I/M) and research activities. In 1982, Englund developed a bag-based in-field measurement system to measure NO_x emissions. The test apparatus was evaluated over full-load operating conditions, and the results indicated that the approach demonstrated the measurement error to be within $\pm 10\%$ compared to laboratory-based instruments on a concentration basis (Englund, 1982). Similarly, Southwest Research Institute (SWRI) developed an advanced integrated bag-based emissions collection system to measure undiluted regulated exhaust emissions species individually and separately using a mini-wind tunnel. The bagging approach provided the ability to monitor integrated emissions rates, but its inability to monitor continuous emissions rates was one of the significant limitations for such an approach (Shade, 2006).

To evaluate transient emissions measurements, Flemish Institute of Technological research developed a system to measure diluted exhaust emissions from both gasoline and diesel-fueled vehicles. The system used a non-dispersive infrared (NDIR) detection principle for CO and CO₂ emissions, a chemiluminescent (CLD) detection principle for NO_x and a heated flame ionization detector (HFID) for HC emissions. Vojtisek-Lom and Cobb reported the measurements for NO_x and CO₂ to be within $\pm 10\%$ compared to a laboratory-grade analyzer (Vojtisek-Lom and Cobb, 1998). In 1999, the U.S.EPA developed a mobile device: Real-time On-road Emissions Recorder (ROVER). The system incorporated measurement for HC, CO, CO₂, and NO_x species using a Snap-On MT3505 emissions analyzer. An Annubar-based differential pressure device determined transient exhaust flow measurements to quantify mass rates. The developed unit was lightweight and portable, which provided ease in terms of instrumentation; however, the absence of a NO_x converter, unheated filter and sampling line caused limitations in accurately quantifying the emissions measurements. Similar to ROVER, Ford Motor Company in collaboration with WPI-Microprocessor Systems, Inc. developed a fully integrated on-board system capable of measuring up to 40 engine operational parameters and exhaust emissions of HC, CO,

CO₂, and NO_x. The system used an infrared-based analyzer to measure HC, CO and CO₂, and NO_x was measured using an ultraviolet (UV) analyzer (Gautam et al., 2001). Specific to NO_x emissions measurement, Horiba, Ltd and NGK, Ltd developed an on-board NO_x monitoring system using Zr-O₂ sensors. Kihara et al. evaluated the developed technology on a chassis dynamometer testing environment to simulate on-road test conditions. Correlations with laboratory compliance tests demonstrated a 4% error for NO_x mass emissions (Kihara et al., 2000).

As part of the 1998 consent decrees, Gautam et al. were contracted by the settling HD engine manufacturers to develop a compact portable device capable of measuring the pollutants (i.e., such as CO, CO₂, HC, and NO_x) and validate the developed system with laboratory-grade analyzers. The research group at WVU developed a portable system called Mobile Emissions Measurement System (MEMS) that used individual gas detection analyzers to measure the pollutant concentration levels. An NDIR analyzer was used to detect CO, CO₂ and HC emissions, and NO_x emissions were detected using a solid-state Zr-O₂ sensor. A conference proceeding presented by Gautam et al. comprised of a detailed description of the fundamental working principle of the MEMS device and the emissions sampling setup (i.e., including a thermoelectric chiller, heated filter, and heated pump). ECU broadcasted parameters were used to determine the engine speed and reported torque to determine the work-specific emissions rates. A cross-sectional annubar flow meter was used to measure and quantify the exhaust flow measurements. Engine dynamometer evaluation of the MEMS device compared to a laboratory-grade instrument showed that the device was capable of accurately reporting only NO_x and CO₂ measurements (i.e., within 5%). The developed MEMS set a benchmark as a PEMS to accurately quantify exhaust emissions rates for regulated pollutant species. Researchers performed an experimental evaluation of the MEMS device developed by WVU, ROVER developed by U.S.EPA and compared the measurement variability with respect to a laboratory-grade instrument. The results demonstrated that NO_x concentrations measured by MEMS were within 0.5% compared to a laboratory instrument, while ROVER reported a deviation of 7.9% (Gautam et al., 2001).

In 2002, Horiba Inc., developed an on-board system for real-time emissions measurement using heated NDIR for HC, CO and CO₂, Zr-O₂ sensor for NO_x measurement, and dual pressure pitot tube transducer for exhaust flow rate measurement. Oestergaard et al. compared measurements reported from Horiba 1000 series and WVU developed MEMS over on-road test routes. The study concluded that the Horiba device demonstrated error deviations of 11% for NO_x, 7% for HC and 3% for CO₂ emissions compared to the MEMS device (Oestergaard et al., 2004). The use of heated NDIR (h-NDIR) provided the ability to measure H₂O concentration in the exhaust gas to determine the interference factors with other gaseous analyzers (Akard et al., 2005). In a study by Nakamura et al., it was identified that the h-NDIR showed H₂O cross-interference to be within $\pm 1\%$ and $\pm 2\%$ for supply gas span concentration for CO₂ and CO analyzers under experimental conditions of 12% volume of H₂O. Horiba further developed a next-generation PEMS (i.e., OBS 2200) comprising of partial vacuum FID, h-NDIR and CLD analyzers in compliance with CFR requirements. A study by SWRI concluded that the device met CFR requirements for a uniform response, time alignment verification. Statistical analysis such as F and t hypothesis tests showed that the emissions constituents measured over various test cycles demonstrated results to be less than the 90% and 95%, respectively (Nakamura et al., 2007).

Another emissions instrument manufacturer, SEMTECH, developed two instrument variants-D and G in a cooperative agreement with Ford Motor Company. The primary difference between the two commercial variants was detection principle for HC emissions. SEMTECH-G used NDIR principle to measure HC emissions while SEMTECH-D used an HFID (Gierczak et al., 2006; Sensors, 2011). Similarly, AVL developed a system (i.e., MOVE-493) that used an HFID for HC emissions measurement, NO and NO₂ were measured simultaneously using UV analyzer without requiring a NO_x converter, and CO and CO₂ were measured using an NDIR analyzer (AVL, 2010). Likewise, Horiba designed a next-generation portable analyzer in 2014 (i.e., Horiba-OBS-ONE) for measuring regulated emissions for both LD and HD vehicles (Horiba, 2014).

With technological advancements and research developments in emissions measurement technologies, the current PEMS typically include a non-dispersive ultraviolet analyzer (NDUV) (or) CLD, NDIR and h-FID analyzer for NO_x, CO/CO₂, and HC emissions measurement, respectively. The current protocol for in-use emissions measurement includes a 1065 compliant PEMS along with EFM for exhaust flow rate measurement and data acquisition system capable of capturing on-board engine operational parameters.

2.6. PEMS Measurement Allowance Program

The 1998 consent decrees led to the introduction of real-world emissions measurement for compliance evaluation using a PEMS. As part of the consent decrees program, the settling HD engine manufacturers sponsored research activities associated with the development and evaluation of a portable emissions analyzer to accurately measure and quantify emissions constituents under the real-world operation of HD trucks. During the consent decree program, it was identified that ambient test conditions influenced emissions measurements collected using a PEMS. This led to the introduction of a measurement allowance program (i.e., a joint effort by U.S.EPA, CARB and EMA) to better understand deviations associated with measurements from a PEMS. The primary objective of the measurement allowance program was to determine the error margin for emissions measurement using a PEMS and to determine an additive accuracy margin for in-use emissions compliance testing. The study was evaluated in three phases, as described below.

2.6.1. Laboratory Experimental Evaluation of PEMS

The specific task of the study discussed in this section involved evaluation and comparison of emissions measurements from a PEMS that met the U.S.EPA requirements and compared the measurements with a 40 CFR §1065 compliant laboratory-grade dilute emissions analyzers. Experimental evaluation was performed simultaneously on three different engines comprising of MHD, HHD and light heavy-duty (LHD) engine segments on steady-state and transient test cycles to evaluate the

measurement variability. A 3-dimensional surface error was developed from paired points of measurement errors to demonstrate the associated error factor as a function of test conditions. Furthermore, the study also evaluated the influence of ambient test conditions on the PEMS measurement in an environmental test chamber. A total of 37 error surfaces were developed as part of the specific task were categorized into six different categories: (i) Steady-state tests; (ii) Transient tests (i.e., operating within 30-second NTE events); (iii) Torque and brake-specific fuel consumption (bsfc); (iv) Exhaust flow measurement; (v) Environmental testing; and (vi) Miscellaneous errors.

The error surfaces for categories (i), (ii), and (iv) were generated as a function of an extensive evaluation of the PEMS and EFM compared to traditional laboratory-grade measurement equipment (i.e., dilute laboratory measurement for emissions) over an engine dynamometer testing environment. The ECU broadcast of torque and fuel consumption were used to generate the error surfaces for category (iii). The environmental error surface (Category v) was generated by evaluating the PEMS in an environmental chamber to understand the influence of the various environmental conditions such as temperature, pressure and humidity. Category (vi) generated error surface explicitly for PEMS unit to unit variability and time alignment of emissions measurement signals.

The results from Phase-1 of the study indicated that the PEMS measurement errors were inconclusive and did not follow a significant trend for most of the critical measurement parameters at similar reference levels. In addition, the measurements performed in the environmental chamber resulted in inconclusive data due to functional failure (Feist et al., 2009).

2.6.2. Statistical Modelling to Determine Error Propagation

A simulation-based MC approach was performed to determine the measurement error associated with a PEMS in comparison with a laboratory-based reference instrument. The MC approach provides the opportunity for random selection of error

sources in a normal distribution for the delta in bs emissions between the measurements from a PEMS and the reference laboratory-grade analyzer. Three different methods were used to quantify bs emissions rates for measurements collected using a PEMS (i.e., emissions measurement from individual gas detection analyzers, fuel and torque measurements from in-line sensors (or) ECU broadcast, exhaust flow rate measurement using an EFM).

Method 1: This method uses exhaust flow rate measurement from the EFM and ECU broadcast of torque for quantifying brake-specific (bs) emissions rates. This method was referred to as Torque-Speed approach.

$$e_{\text{emissions}} = \frac{\sum(\text{concentration}_{\text{pollutant}} \cdot \text{exhaust flow})}{\sum(\text{engine speed} \cdot \text{engine torque})} \quad \text{Equation 2.11}$$

Method 2: This method uses bsfc in-line with the carbon balance from fuel consumption to determine the engine work produced.

$$e_{\text{emissions}} = \frac{\sum(\text{concentration}_{\text{pollutant}} \cdot \text{exhaust flow})}{\sum \frac{\text{exhaust flow} \cdot \text{concentration}_{\text{carbon}}(\text{HC} + \text{CO} + \text{CO}_2)}{\text{bsfc}}} \quad \text{Equation 2.12}$$

Method 3: This method is dependent on the ECU broadcasted parameters and was referred to as the fuel-specific approach.

$$e_{\text{emissions}} = \frac{\sum \frac{\text{concentration}_{\text{pollutant}} \cdot \text{fuel flow}}{\text{concentration}_{\text{carbon}}(\text{HC} + \text{CO} + \text{CO}_2)}}{\sum(\text{engine speed} \cdot \text{engine torque})} \quad \text{Equation 2.13}$$

The MC simulation was evaluated on test activity that was collected from transient laboratory-based experiments performed at SWRI, pre-pilot in-use emissions measurement data and also experimental data provided by the settling HD engine manufacturers. The simulations were primarily focused on engine operation captured within the reference NTE events. The simulations were performed up to 30,000 times for data acquired from each of the NTE windows while applying the error value to the bs emissions determined from the laboratory-based measurement. The analysis

generated nine different distribution of the 95th percentile of delta error between measurements obtained from a PEMS and a reference laboratory instrument. The error propagation resulted in nine different measurement allowance values for each pollutant and quantification method. The final additive measurement allowance was determined by multiplying the maximum error (i.e., in percent) and the allowable pollutant limit. Table 4 presents an overview of the emissions threshold values for the corresponding pollutants that were fixed based on MY 2007 HD diesel emissions certification standards.

Table 5 outlines the measurement allowance specific to each method and pollutant based on the percent of the NTE threshold (i.e., values presented in Table 4) and the final additive measurement allowance (Buckingham et al., 2009).

Table 4: NTE limits used in measurement allowance program (Buckingham et al., 2009)

Pollutant	NTE Threshold
	[g/bhp-hr]
bsNMHC	0.21
bsNO _x	2.00
bsCO	19.40

Table 5: Measurement allowance determined by the MC method from percent of NTE threshold and final additive bsemissions measurement in-use limit (Buckingham et al., 2009)

Pollutant	Method 1	Method 2	Method 3	Final Measurement Allowance
	[% Threshold]	[% Threshold]	[% Threshold]	[g/bhp-hr]
bsNMHC	10.08	8.03	8.44	0.02
bsNO _x	22.30	4.45	6.61	0.45
bsCO	2.58	1.99	2.11	0.5

2.6.3. Validation of Measurement Allowance Statistical Simulation Results

The third phase of the study involved real-world experimental evaluation of the measurement allowance thresholds determined in Phase-2. The goal of the specific task was to experimentally verify the errors associated with in-use emissions measurement using a PEMS compared to a mobile full-scale CVS emissions measurement system. To this aim, the University of California’s mobile laboratory was used to validate the measurement allowance determined from simulation-based results. The measurement deviations were observed to be within 2% for NO_x emissions based on an inter-laboratory study that was performed between the mobile laboratory and SWRI’s laboratory.

On-road validation of the model was determined from test activity collected from a test truck coupled with CE-CERT’s mobile CVS laboratory and one of the PEMS units that were used in the preliminary phase of the study for laboratory evaluation. The in-use testing included diverse real-world driving conditions and was operated over a period of nine days. A total of 429 valid NTE events were generated from the data collected, out of which only 100 NTE events were utilized in the model validation process. The limited evaluation of NTE events was performed to weigh the NTE events evenly across various ambient operating conditions. The error surfaces determined from Category (iii) in Phase-1 of the study were excluded from the MC model validation. The emissions quantified by the model disregarded ECU versus laboratory measurement error surface. The bs emissions were quantified from the model generated results and data procured using a PEMS, as described in Equation 2.14 and 2.15.

$$\text{bs emissions} = \text{bs emissions with validation error} - \text{Reference bs emissions} \quad \text{Equation 2.14}$$

$$\text{bs emissions} = \text{bs emissions from PEMS} - \text{Reference bs emissions} \quad \text{Equation 2.15}$$

An empirical distribution function (EDF) of the 195 valid NTE events was used as a validation criterion. The EDF serves as a reference dataset for validation of the results obtained from the MC model and real-world operation. The delta error in measurement of bs emissions is valid only if 90% of the measurement error from on-road experimental data is between 5th and 95th percentile of the error derived from the MC model and its associated quantification approach. The final measurement allowance was determined from data evaluated using method-1 described in Phase-2 of the study and is outlined in

Table 5 (Sharp et al., 2009).

2.7. In-use Emissions Quantification Protocol

2.7.1. Not-To-Exceed Region Method

The NTE method was developed as a consequence of 1998 consent decrees to verify real-world emissions compliance from MD and HD trucks in the U.S. The approach evaluates for real-world emissions compliance while the engine is operating within the NTE control area beneath the maximum torque curve of the engine during real-world operation.

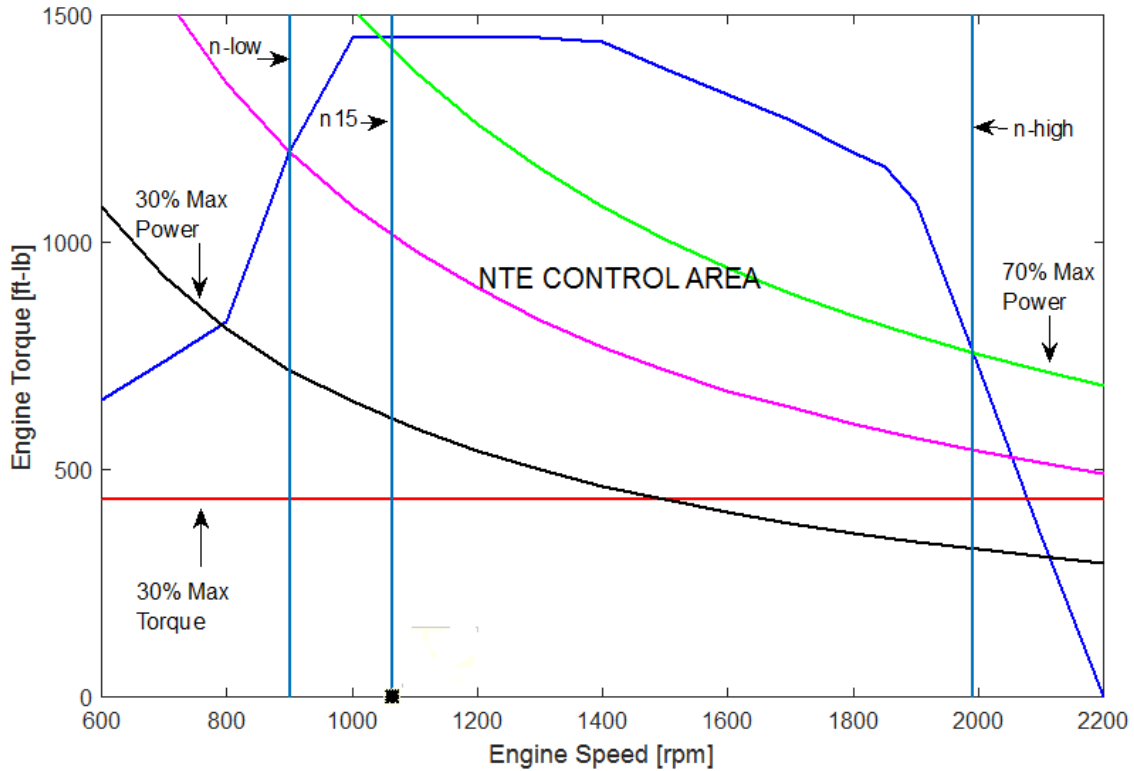


Figure 13: Generic representation of the NTE zone (Pondicherry, 2017)

2.7.1.1. NTE Control Area

The NTE control area is defined based on setpoints of engine speed, torque, and power to evaluate engine work producing activity. Figure 13 presents an overview of the associated boundary conditions defining the NTE control area.

- (1) Engine Speed (ES): The instantaneous test engine speed requires to be higher than the desired engine speed threshold (i.e., a function of engine speed at 50% and 70% of the rated power of the engine).

$$n_{NTE} > n_{15} \quad \text{Equation 2.16}$$

$$n_{15} = 0.15 (n_{high} - n_{low}) + n_{low} \quad \text{Equation 2.17}$$

(2) Engine Torque (ET): The instantaneous test engine torque must be equal or greater than 30% of rated torque (T_{max}).

$$T_{NTE} \geq T_{30} \quad \text{Equation 2.18}$$

$$T_{30} = 0.30(T_{max}) \quad \text{Equation 2.19}$$

Where:

T_{max} is the maximum engine brake torque

(3) Engine Power (EP): The instantaneous test engine power must be equal or greater than 30% of rated power (P_{max}).

The instantaneous engine power is derived as a function of engine speed and torque as reported by the broadcasted parameters as per SAE J1939 protocol.

$$\text{Engine Power} = \frac{\text{Engine Speed (rpm)} \cdot \text{Engine Torque (lb - ft)}}{5252} \quad \text{Equation 2.20}$$

$$P_{NTE} \geq P_{30} \quad \text{Equation 2.21}$$

$$P_{30} = 0.30(P_{max}) \quad \text{Equation 2.22}$$

Where:

P_{max} is the rated/maximum engine power

2.7.1.2. NTE Exclusions

The NTE method incorporates a range of method-defined exclusions that are required to be satisfied while the engine is operating within the NTE region to generate a valid NTE event.

(1) Altitude(Alt): The instantaneous test altitude requires to be less than or equal to 5500 ft. Due to the lower density of ambient air (i.e., engine air intake), U.S.EPA approved the Altitude exclusion as it would be challenging to meet the emissions requirements at high altitude. The altitude is determined based on the GPS or barometric pressure data recorded.

$$\text{Alt}_{\text{NTE}} \leq 5500 \quad \text{Equation 2.23}$$

(2) Ambient Temperature (T_{Amb}): The instantaneous measured ambient temperature is required to be below the desired threshold $T_{\text{Amb-Alt}}$ [°F] that is dependent on the altitude.

$$T_{\text{NTE}} \leq T_{\text{Amb-Alt}} \quad \text{Equation 2.24}$$

$$T_{\text{Amb-Alt}} = -0.00254(\text{Alt}) + 100 \quad \text{Equation 2.25}$$

Where:

Alt: Altitude [ft] of the test location (i.e., above the sea level)

The exclusion was also incorporated to exclude emissions assessment for compliance evaluation at relatively lower ambient temperatures since it is difficult for engine and emissions control devices to meet the set forth requirements at higher altitudes.

(3) Intake Manifold Temperature (IMT): The instantaneous measured engine intake manifold temperature needs to be above the desired threshold intake manifold temperature $(\text{IMT})_{\text{Limit}}$ [°F] (i.e., a function of engine intake manifold pressure). The IMT exclusion was incorporated to avoid emissions compliance evaluation under cold EGR operating conditions. In the following document, IMT is also referred to as T_{IMT} .

$$\text{IMT}_{\text{NTE}} \geq \text{IMT}_{\text{Limit}} \quad \text{Equation 2.26}$$

$$\text{IMT}_{\text{Limit}} = 11.428(\text{IMP}_{\text{Abs}}) + 88.571 \quad \text{Equation 2.27}$$

Where:

IMP_{Abs} is the absolute intake manifold pressure [bar]

(4) Engine Coolant Temperature (ECT): The instantaneous measured ECT needs to be above the desired threshold $\text{ECT}_{\text{Limit}}$ [°F] (i.e., a function of engine intake manifold pressure). The exclusion was incorporated as part of the regulatory requirement to avoid compliance evaluation during cold engine operating conditions. In the following document, ECT is also referred to as T_{ECT} .

$$ECT_{NTE} > ECT_{Limit} \quad \text{Equation 2.28}$$

$$ECT_{Limit} = 12.853(IMP_{Abs}) + 127.11 \quad \text{Equation 2.29}$$

Where:

IMP_{Abs} is the absolute intake manifold pressure [bar]

A valid NTE event is generated while the engine is operating within the NTE zone and has met the NTE instantaneous data point exclusion criteria for a minimum continuous consecutive period of 30 seconds. For engines equipped with aftertreatment technology, the measured aftertreatment outlet temperature ($T_{AT\ OUT}$) within the entire NTE event requires to be above or equal to 250 °C to be considered as a valid event. Additionally, a correction factor called the regeneration fraction (RF) exists for test operation that occurs during an active DPF regeneration event. A detailed overview of RF is discussed in 40 CFR 86.1370. Furthermore, if any instantaneous data point within an NTE event includes a PEMS hourly periodic zero-check activity, the entire NTE event is discarded from compliance evaluation. To determine emissions rates within an NTE event, the total integrated mass of emissions is scaled by the total engine work produced within the NTE event. Equation 2.34 in section 2.7.2 shows the quantification procedure of bs emissions rates.

The verification of in-use emissions compliance is evaluated on a time-weighted vehicle pass ratio (VPR) as defined in 40 CFR 86.1912. The VPR is defined as a duration metric, i.e., the total duration of time spent within all valid NTE events that are below the applicable NTE emissions threshold (i.e., in g/bhp-hr) and the total duration of all valid NTE events generated during the in-use test. The applicable NTE threshold is a function of certification limit, NTE multiplier (1.5) and the measurement allowance (i.e., 0.15 g/bhp-hr for NO_x) (CFR/40/86/1912).

$$\begin{aligned} \text{NTE Limit} = & (\text{Certification Limit} \times \text{NTE multiplier}) \\ & + \text{Instrument measurement allowance} \end{aligned} \quad \text{Equation 2.30}$$

To meet the in-use emissions compliance requirements, the VPR requires to be above 0.90 for each of the emissions species (CFR/40/86/1370).

2.7.2. Work-based Window Method

The WBW is a continuous moving average windowing (MAW) approach used to evaluate real-world emissions compliance of HD trucks in Europe. The test requirements include predefined route-based characteristics (i.e., dependent on the vehicle class) comprising of a certain specific time fraction (i.e., percentage of the operational time) and sequence of test activity comprising of urban, rural and highway driving. The window generation is based on a predefined reference quantity (i.e., total engine work generated over a certification test cycle for HD trucks).

The WBW approach also incorporates a range of data point exclusions as defined by EU 582 regulatory guidelines to exclude engine operation that potentially challenges emissions control strategies. The window generation process starts once the method-defined exclusions are satisfied.

- (1) ECT: The instantaneous test data point has reached 343 K for the first time during the test or after the ECT has stabilized within ± 2 K over a period of 5 minutes, whichever condition is first met depending on the duty cycle no later than 20 minutes after the engine has started.
- (2) Ambient Pressure (P_{Amb}): The instantaneous test data point requires to be above greater than or equal to 82.5 KPa.

$$P_{Amb} \geq 82.5 \text{ Kpa} \quad \text{Equation 2.31}$$

- (3) Ambient Temperature (T_{Amb}): The measured ambient temperature needs to be greater than or equal to 266 K and less than or equal to the desired threshold (i.e., a function of barometric pressure).

$$T_{Amb} \geq 266 \text{ K} \quad \text{Equation 2.32}$$

$$T_{\text{Amb}} \leq -0.4514 \cdot (101.3 - P_{\text{Baro}}[\text{Kpa}]) + 311$$

Equation 2.33

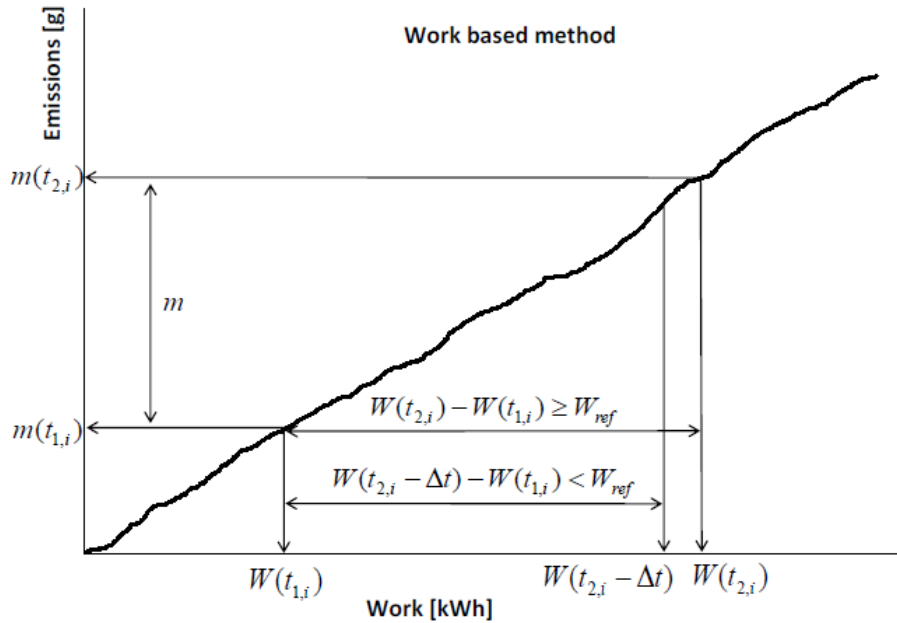


Figure 14: Generic representation of WBW method (EU 582, 2011)

A window is generated from the first valid data point, satisfying the method-defined exclusion criteria and continuous until the predefined reference work is met, and the window generation process is repeated from the next data point. Equation 2.34 is used to quantify the bs emissions [g/bhp-hr], where the mass of each pollutant is scaled over the difference in cumulative engine work produced for each MAW.

$$\text{bs emissions} = \frac{\text{mass of the pollutant [g]}}{W(t_{2,i}) - W(t_{1,i})} \quad \text{Equation 2.34}$$

The European (EU VI (c)) regulations states that work-windows comprising of average window power equal or less than 20% maximum power are excluded from the in-service compliance evaluation. The total number of windows generated above 20% of rated power (i.e., valid windows) requires to be equal or greater than 50% of the total windows generated. If the condition is not satisfied by the in-use test dataset, the regulation allows a stepwise (1%) reduction of the average power threshold until the overall percentage of valid windows is greater than 50% of all windows generated. The stepwise reduction is permissible only until 15% of rated

power if the condition is not satisfied, the in-use test dataset is void, and the test needs to be repeated. A conformity factor (i.e., the ratio of bs emissions for all valid windows scaled to its applicable emissions limit) is quantified to determine in-service compliance. The 90th cumulative percentile of the conformity factor of the valid work-windows should not exceed 1.5 for the vehicle to pass an in-use compliance test (EU 582,2011).

$$CF = \frac{\text{brake – specific emissions of the pollutant}}{\text{Applicable certification limit}} \quad \text{Equation 2.35}$$

2.8. Evaluation of In-use Emissions Compliance Protocols

In-use emissions compliance is determined by a range of regulatory testing and data evaluation protocols. Limited research entities have evaluated the performance of the compliance evaluation methodology over a range of diverse real-world driving scenarios. A study by International Council on Clean Transportation (ICCT) evaluated NO_x emissions performance from 160 in-use non-credit vehicle datasets (i.e., post-2010 MY) from eight different engine manufactures comprising of 26 engine families. The data evaluated in this study was collected as part of the manufacturer-run HDIUT program. Each of the HDIUT dataset comprised of no prescribed/predefined drive cycle and test activity was collected while the vehicle was performing its regular in-fleet operation as per the NTE regulatory requirement. Figure 15 shows the percentage of the total duration of time spent in valid NTE events for each of the individual PEMS datasets. The average time spent in valid NTE events varied for each PEMS dataset depending on the in-fleet activity, route and ambient conditions, and engine size/manufacturer. The data evaluated in the study shows that on average, only 9.8% (i.e., excluding test data comprising of zero NTE events) of the total test time used for NTE evaluation. Overall, the average time spent in NTE events based on average results from each engine manufacturer ranged from 3 to 22%.

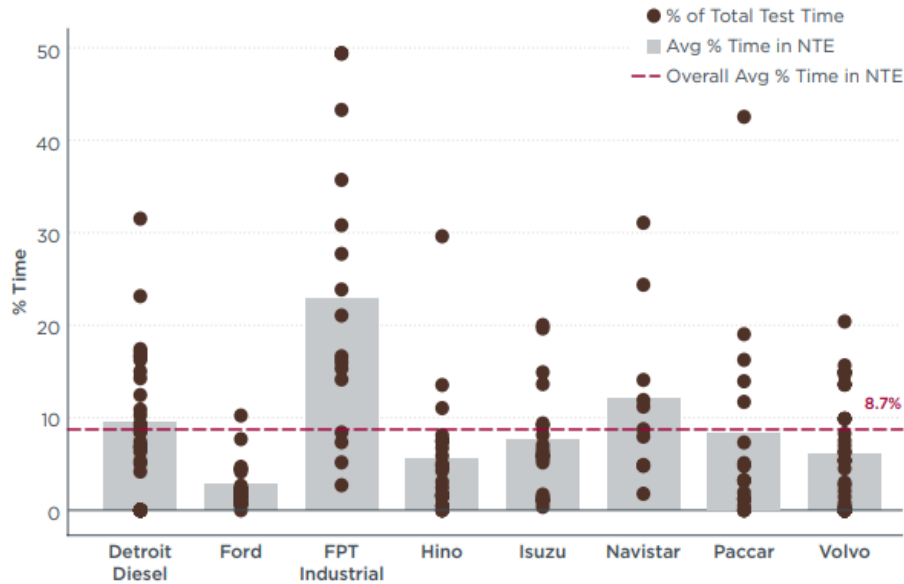


Figure 15: Percentage of valid NTE event duration (i.e., averaged and individual results for each manufacturer) (Badshah et al., 2019)

A report by Joint Research Center (JRC) shows that on average only a small fraction of the in-use data, i.e., 10 to 20% of entire activity collected was used to evaluate real-world emissions compliance using the NTE method (Bonnell et al., 2011). Figure 16 summarizes a comparison of route averaged (i.e., without engine idle operation) and NTE NO_x emissions results for data analyzed from each of the engine manufacturers. The results indicate that the average route-averaged (i.e., excluding engine idle operation) NO_x emissions rates for these datasets were 0.34 g/bhp-hr (i.e., approximately 1.9 higher than that of average NTE NO_x emissions, i.e., 0.18 g/bhp-hr) (Badshah et al., 2019).

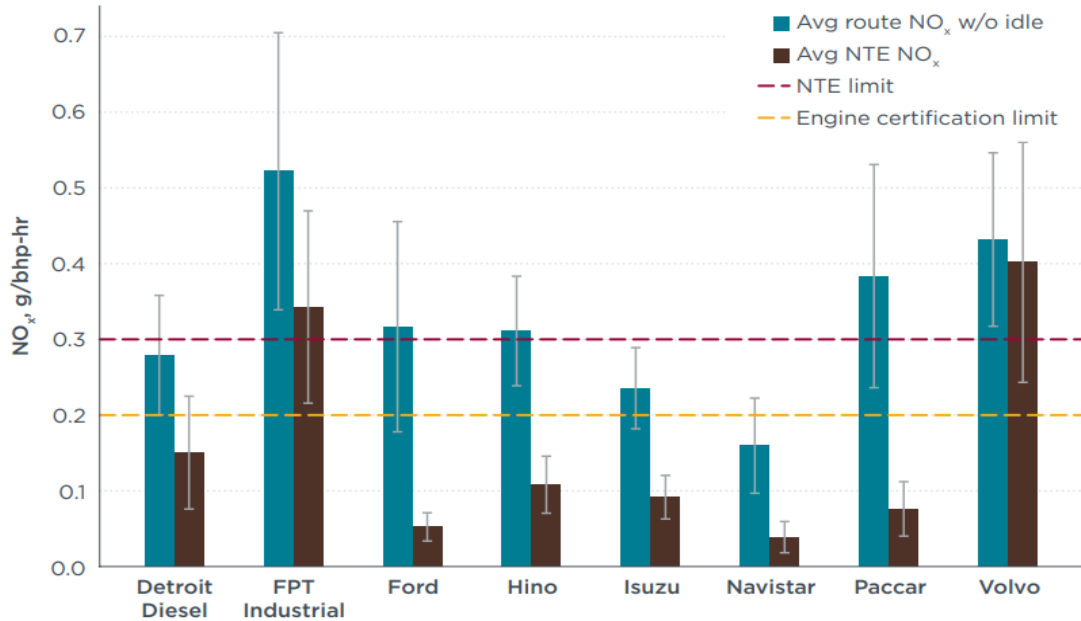


Figure 16: Comparison of route-averaged and NTE event-averaged NO_x emission rates separated based on engine manufacturer (Badshah et al., 2019)

A data-driven study by Besch et al. evaluated HDIUT datasets comprising of both pre-and post-2010 MY vehicle datasets using NTE in-use emissions compliance protocol. A total of 159 pre-2010 MY and 165 post-2010 MY (i.e., including credit engines) in-use datasets were analyzed as part of the study. The results of the study showed that on average only 5.3%, 5.1%, and 6.6% (i.e., pre-2010, post-2010 and post-2010 MY non-credit vehicle datasets) of the entire test activity was used for NTE compliance evaluation. The overall event-averaged bsNO_x emissions were 1.66, 0.27, 0.16 g/bhp-hr for the three subsets of vehicle datasets described above respectively. A sensitivity analysis was also performed by modifying engine torque, power and exhaust gas aftertreatment temperature on the post-2010 MY vehicle datasets. The results show the engine power threshold and the exhaust aftertreatment temperature exclusion demonstrate the most substantial impact on the generation of NTE events and the event-averaged bsNO_x emissions (Besch et al., 2018).

In summary, the NTE in-use emissions compliance metric excludes evaluation of low-load engine operation. Such modes of in-service operation linked with relatively higher bsNO_x emissions rates are often experienced by vocational applications such

as port drayage and urban delivery with frequent stop-and-go activity. The relatively lower NTE NO_x emissions rate for post-2010 MY datasets presented in Badshah et al. and Besch et al. are primarily due to test activity acquired from valid NTE events, i.e., comprising entirely of test activity where the exhaust gas thermal conditions are favorable for active SCR operation.

A doctoral dissertation by Shade resulted in the development of a continuous MAW approach to evaluate real-world emissions compliance. The study focused on the generation of windows as a function of a predefined reference parameter such as engine work produced in a certification cycle. A range of reference parameter thresholds were altered and evaluated on in-use test activity collected using MEMS on 9L and 12L engines. The study showed that the smaller size of the work-windows resulted in higher bsNO_x emissions, and as the size of the work-windows increased the bsNO_x emissions gradually decreased and reached a constant level. This level was typically observed to be approximately less or equal to that of the engine work produced over the certification cycle. Figure 17 shows that an increase in reference work of the WBW method resulted in a decrease in the average bsNO_x emissions. The error bars demonstrate the variance in bsNO_x emissions to be lower while the reference work was at or above the FTP work. Furthermore, it was also observed that the results from the WBW approach could result in relatively higher bsNO_x emissions depending on the type of engine operation the window captured. Therefore, a short period of higher NO_x emissions rate during in-use operation may demonstrate variable characteristics depending on the overall window activity due to the time-based increment of the continuous MAW. In order to exclude accumulation of low power engine activity as part of the evaluation criterion, a test failure methodology was developed that required average window power to be higher than that generated over an FTP test cycle (Shade et al., 2008).

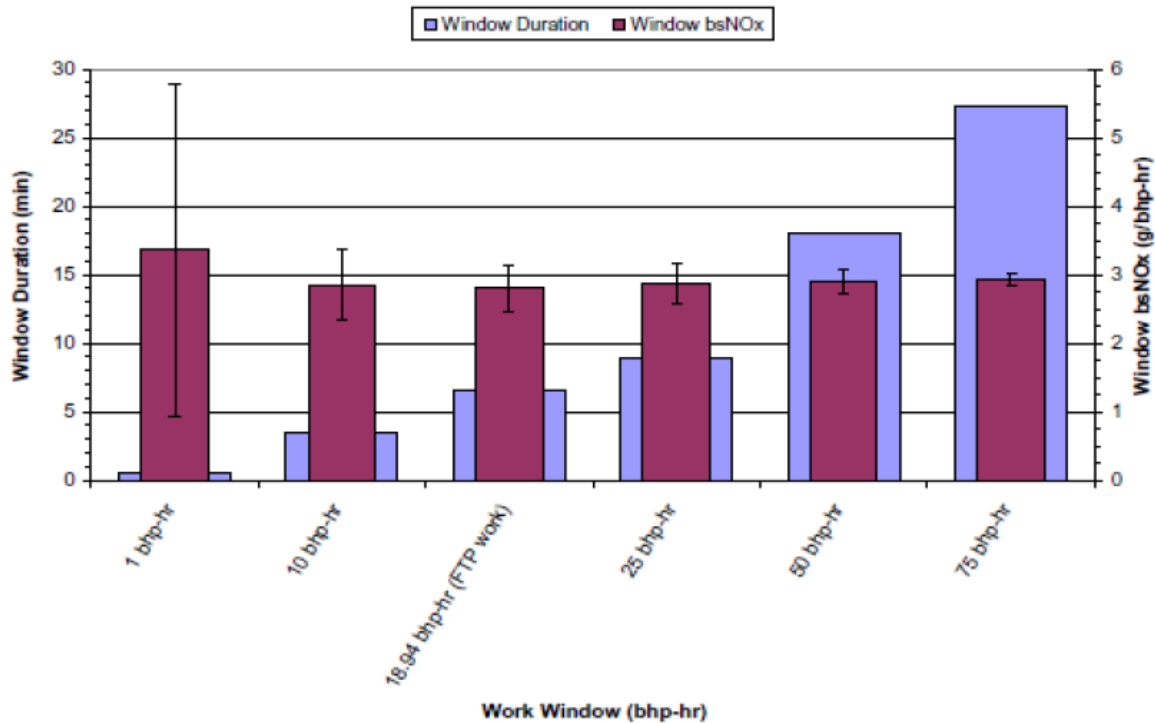


Figure 17: Impact of reference work evaluated on a 9L diesel engine (Shade et al., 2008)

A Master's thesis by Pondicherry also outlined a similar effect on the window averaged bsNOx emissions while altering the reference work. The study evaluated two pre-2010 MY and four post-2010 MY HDIUT datasets. The results of the study show that an increase in reference engine work using the WBW method led to a continuous decrease in the overall number of work-windows (i.e., due to large segments of continuous in-use test activity accumulated in each window) and simultaneously also led to a gradual decrease in the window-averaged bsNOx emissions. Furthermore, similar results were obtained by evaluating the minimum average window power threshold from 0 to 30% of rated power. Higher bsNOx emissions were observed from windows comprising of lower power threshold (i.e., below 16% of rated power). This is primarily due to the accumulation of segments of test activity comprising of a combination of low and medium/high power engine operation that is linked to relatively higher NOx emissions rates. Additionally, the study also evaluated the sensitiveness of the exhaust aftertreatment temperature for

post-2010 MY vehicle datasets equipped with SCR technology. The results indicate that the window-averaged bsNO_x emissions were below 0.20 g/bhp-hr for valid windows whose SCR outlet temperature ($T_{SCR\ OUT}$) were above 190 °C (Pondicherry, 2017).

In 2011, JRC performed extensive research in the evaluation of the WBW metric to be implemented as a regulatory protocol for verification of real-world emissions compliance in Europe. The metric demonstrated variability in emissions rates as a function of engine operating conditions to compare emissions rates from different engine sizes. To minimize the variability in emissions results, the WBW compliance metric evaluates work-windows whose average engine power is above 20% of rated power. A percentile-based ranking criterion was determined to quantify the in-use emissions compliance. However, the study also highlights potential case scenarios that may cause window emissions to exceed an applicable threshold. Such case scenarios comprise of test activity with extended engine idle operation, lower average vehicle speed operation and test activity with low payloads (or) vocations that use an oversized engine for their application (Bonnell et al., 2011). This led to the introduction of a predefined route-based drive cycle characteristics and a minimum window power threshold criterion which therefore indirectly induces thermal boundary guardrails for emissions compliance assessment in Europe. The EU in-use regulations require the vehicle to be tested on a test route comprising of a certain percentage of operational time spent in urban, rural and highway driving conditions to suffice the in-use testing requirements dependent on the vehicle type and application.

Another study by JRC evaluated the WBW metric on in-use PEMS collected data on 20 vehicles that were compliant with EU No. 582. The study analyzed the impact of varying the reference work threshold for the window generation, minimum power threshold cut-off and cold start activity. The in-depth data analysis shows that the current threshold of window generation (1 x Certification cycle work) is deemed as a plausible and logical approach. The analysis indicates that the minimum window

power threshold eliminates the opportunity to evaluate emissions generated during the urban segment of the test activity. In order to assess emissions generated from the urban segment, the study suggests reducing the minimum power threshold from 20% (i.e., EU VI (c) regulations) to 10% of rated power (Perujo Mateos del Parque and Mendoza Villafuerte, 2015).

Mendoza-Villafuerte et al. performed on-road test experiments on a Euro VI HD diesel vehicle equipped with DOC-DPF-SCR and ammonia oxidation catalyst (AMOX) using EU in-service conformity (ISC) EU test guidelines. The test article discussed here was a cold start in-use test that included a trip duration share of 48%, 17%, and 35% for urban, rural and highway driving operation respectively. As prescribed in the EU regulation, the emissions compliance for the test article was evaluated using the WBW method. Four different case scenarios were evaluated in the presented study that includes (a) Baseline: Evaluation as per legislative requirements, i.e., exclude cold start activity and evaluate windows whose average power is equal or greater than 20% of rated power, (b) Method-1: Include cold start activity and evaluate windows whose average power is equal or greater than 20% of rated power, (c) Method-2: Include cold start activity and implement no power threshold, (d) Method-3: Include entire test activity collected for compliance factor evaluation. For (a), (b) and (c), a 90th cumulative percentile approach, and for (d) a 100th cumulative percentile approach was used to determine emissions factors. Figure 18 shows the MAW average engine power versus NO_x emissions distribution of NO_x emissions of each of the windows. The analysis shows that windows that are associated with relatively higher bsNO_x emissions are not considered for compliance evaluation with the EU VI (c) legislative requirement. The NO_x emissions factors for each of the evaluated methods i.e., (a), (b), (c) and (d) are 0.30, 0.30, 0.45, and 1.60 g/KWh, respectively. Method (c) demonstrated 1.5 times higher emissions rates compared to emissions factors developed using the baseline EU VI (c) requirements. The increase is primarily attributed due to the inclusion of low power engine operation. The emissions values reported for NO_x emissions shows that when no WBW boundary conditions were applied, the results were five times higher than the

baseline results. The study concludes that using the EU VI (c) MAW window approach 85% of NO_x emissions that are emitted during in-use operation are excluded for in-use compliance evaluation. Similar to conclusions presented by Perujo Mateos del Parque and Mendoza Villafuerte, the study suggests that there is a necessity to lower the engine power threshold in order to implement stringency in emissions control from windows pertaining to low power engine operation primarily generated during urban driving operation (Perujo Mateos del Parque and Mendoza Villafuerte, 2015).

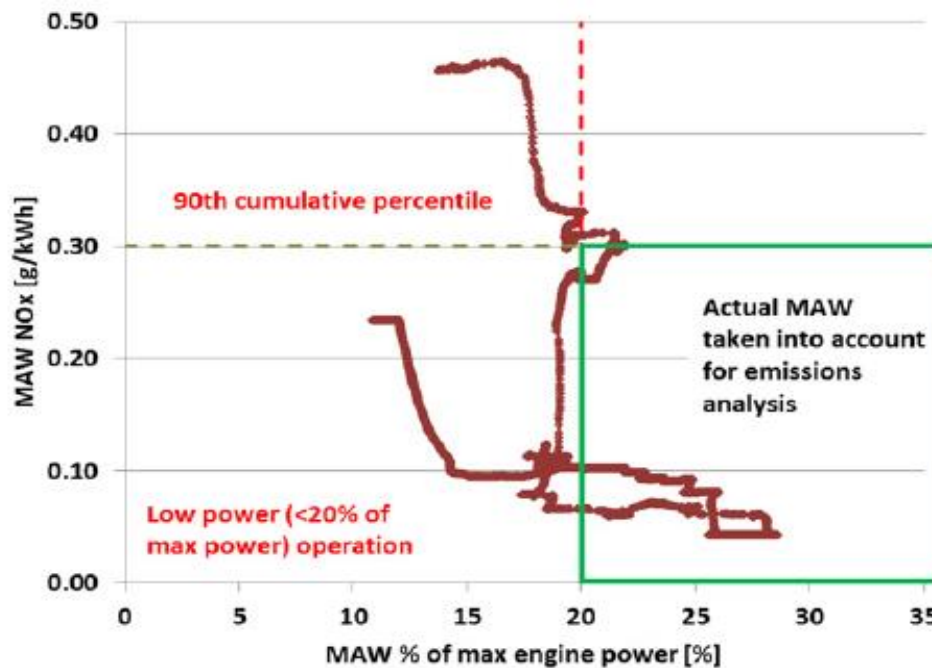


Figure 18: Comparison of average engine power and NO_x emissions of WBW's (Mendoza-Villafuerte et al., 2017)

With respect to the comparison of in-use emissions quantification methods (i.e., NTE and WBW), a data-driven study performed by Besch et al. on test activity collected by the manufacturer-run HDIUT program addressed limitations associated with the current NTE protocol. It was identified that the time-weighted data utilization for NTE as opposed to the WBW was 5.3% versus 91.1% and 5.1% versus 91.7% for a total of 159 pre-2010 and 165 post-2010 MY in-use vehicle datasets. The findings highlight that the boundary conditions of the NTE zone cause a potential challenge

for the engine to operate in the NTE zone under real-world driving operation continuously. As a direct comparison of NTE and WBW evaluation methodologies, the WBW approach allows an in-depth analysis of in-use vehicle activity for emissions compliance as opposed to NTE. Also, modes of operation comprising of low-power operation experienced by drayage activity are not evaluated using the NTE approach (Besch et al., 2018). A similar comparison study performed by CARB highlighted upon a 55.2% increase in data utilization for in-service evaluation by adapting to the WBW approach (CARB, 2019). Both the studies pre-dominantly demonstrated the reduction in pass-ratio with the WBW approach. As the performance of the advanced NO_x emissions control devices is greatly dependent on real-world duty cycle, the combination of diverse modes of in-use operation from the regular in-fleet operation can potentially cause significant variation in the NO_x emissions while determining the emissions compliance using the WBW approach.

2.8.1. Alternative Methods for Evaluation of In-use Emissions

To better understand real-world driving emissions, several research entities have developed methods to characterize emissions rates as a function of engine operational characteristics. The developed methods are aimed to minimize the influence of drive-cycle characteristics and varying driving patterns.

2.8.1.1. Vehicle Speed Binning (VESBIN)

The Netherlands Organization for Applied Scientific Research (TNO) developed a binning structure based on the vehicle speed to characterize in-use emissions performance. The quantified average vehicle speed for each of the bins allows comparison of emissions rates based on the binned vehicle speed. The entire in-use data is split into different speed bins (i.e., 5 km/hr in width) and the average emissions (i.e., NO_x over CO₂) are quantified for each bin. To avoid evaluation of cold start test activity, the metric only evaluates test data comprising of ECT above 70 °C.

$$\frac{\text{NOx [g]}}{\text{CO2 [kg]}} = \frac{\sum_{v=v_i}^{v=v_i+5} \text{NOx} \left[\frac{\text{g}}{\text{sec}}\right]}{\sum_{v=v_i}^{v=v_i+5} \text{CO2} \left[\frac{\text{kg}}{\text{sec}}\right]} \quad \text{Equation 2.36}$$

Where:

v_i is the vehicle speed in km/hr

Like the VESBIN approach, ICCT also developed a binning metric, i.e., a combination of vehicle speed and engine power boundary conditions and evaluated 160 HDIUT datasets. The boundary conditions of the vehicle speed bins used are described in Table 6.

Table 6: Boundary conditions for vehicle speed and power bins (Badshah et al., 2019)

Vehicle Speed Bin	Boundary Conditions	
	Vehicle Speed	Engine Power Fraction
[-]	[mph]	[percent of max. power]
Engine Idle	< 1	< 10
Urban	1 – 25	5 – 25
Suburban	25 – 50	10 – 45
Highway	≥ 50	≥ 25

Figure 19 shows a characteristic trend of NOx emissions and exhaust gas aftertreatment temperature for three transient operational bins (i.e., urban, suburban and highway), and route averaged emissions rates. The average post-SCR exhaust gas temperature for activity in highway driving operation is approximately 290 °C that is favorable for the SCR system to reduce NOx emissions, therefore resulting in averaging bsNOx emissions approximately close to the certification standard. However, urban driving operation results in the highest bsNOx emissions (i.e., 1.05 g/bhp-hr). This is primarily due to the majority of transient activity in this specific vehicle speed bin comprising of operation where the SCR was not active. Therefore, resulting in elevated levels of NOx emissions levels (Badshah et al., 2019).

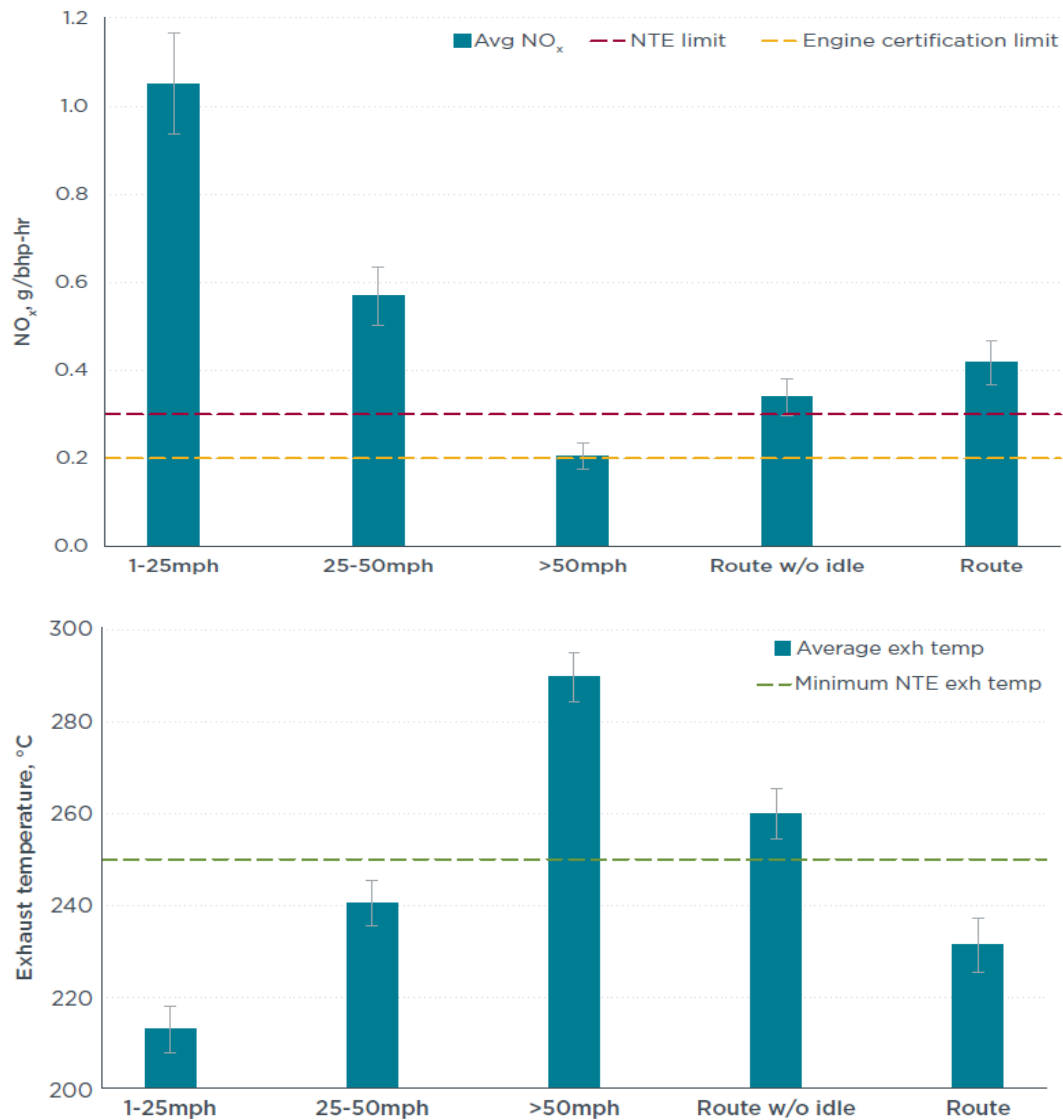


Figure 19: Vehicle-speed based distribution of NO_x emissions rates and post-SCR exhaust temperatures (Badshah et al., 2019)

2.8.1.2. Classification of Emissions from Automobiles in Real Driving

Technical University of Graz (TUG) developed an analytical approach to quantify emissions as a function of engine operational power. The in-use operation is binned into normalized engine power profiles to eliminate variations in driving patterns. The normalized engine power patterns are dependent on the road load coefficients such as vehicle-specific mass, air, and rolling resistance. TUG evaluated the CLEAR

analytical approach using data from WLTP-short-trips using different vehicle datasets. Figure 20 shows the distribution of instantaneous data into specific target power bins dependent on the real-world engine power demand.

$$P_{\text{drive}} = v_{\text{ref}} * [m_{\text{ref}} * a_{\text{ref}} + R_0 + R_1 * v_{\text{ref}} + R_2 * v_{\text{ref}}^2] \quad \text{Equation 2.37}$$

$$P_{\text{norm}} = \frac{\text{Instantaneous Power}}{P_{\text{drive}}} \quad \text{Equation 2.38}$$

Where:

R_0 , R_1 and R_2 are the road load coefficients in [N], [Ns/m] and [Ns²/m²]

m_{ref} is the test mass of the vehicle in kg

a_{ref} is the reference acceleration in m/s²

v_{ref} is the reference velocity in m/s

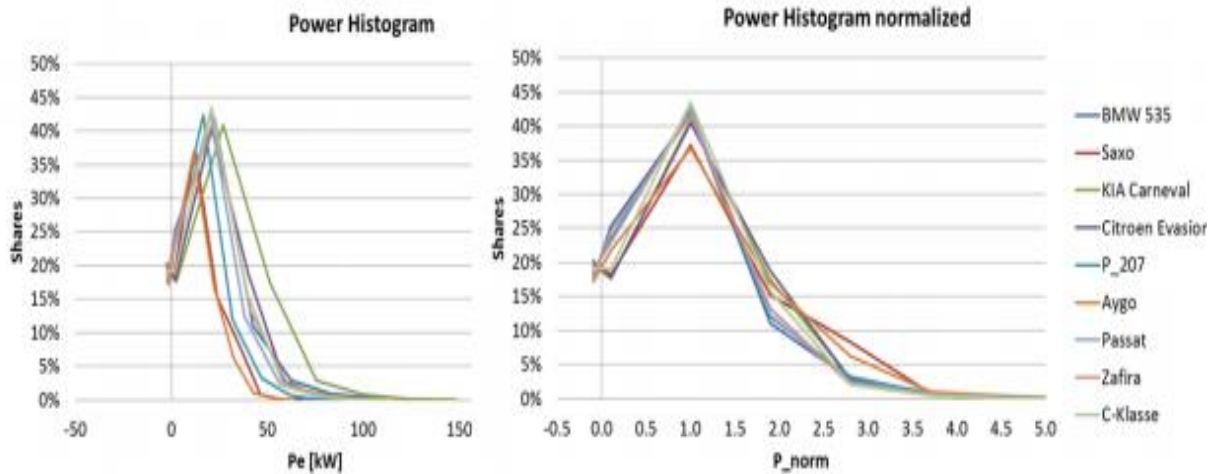


Figure 20: Frequency distribution of (a) Engine power operation (i.e., left chart); (b) Normalized engine power (i.e., right chart) of vehicles from WLTP database

The analysis indicates that using the normalized version of classification shows that under “normal” driving conditions, all trips demonstrate similar behavior in the normalized power bins. The aggressive driving, i.e., translating to high power engine operation shows that less than 1% of the test time is spent in power bins that comprise of P_{norm} to be higher than 3.5. The approach uses a 3-second moving averaging filter to sort the engine operational and emissions data into respective normalized power bins. The corresponding emissions results are weighted depending

on the frequency of the bin in the target power pattern. The test-based emissions evaluation is quantified as a sum of the weighted emissions calculated per bin.

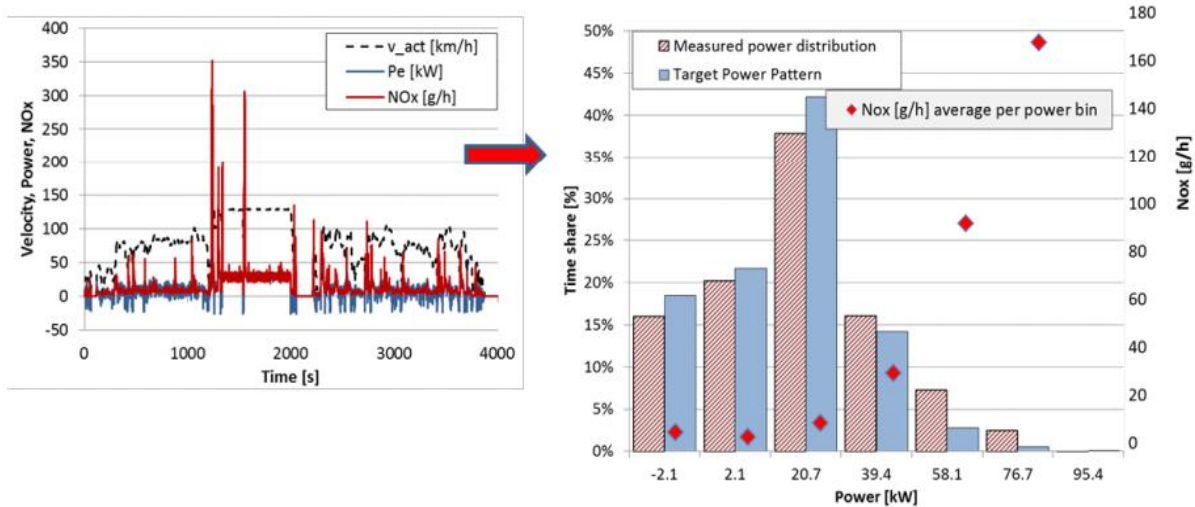


Figure 21: Example of an in-use test evaluated using CLEAR method (Hausberger and Lipp, 2014)

Figure 21 demonstrates the translation of an in-use test into different engine power bins using the CLEAR method. The study shows that the weighting of emissions rates as a function of engine power demand provides an opportunity to ensure stringent emissions control independent of the driving behavior (Hausberger and Lipp, 2014).

2.9. Performance Evaluation of On-board NOx Sensors

Substantial developments in stringent emissions regulations and advancements in MD and HD diesel engine/aftertreatment technology are the primary driving force for improvements in accuracy and sensitivity/selectivity of NOx sensor technology. Zr-O₂ based NOx sensors comprise of porous zirconia electrolyte and are the preferred technology of choice for on-board (OB) and SCR aftertreatment control strategies (Yong-Wha and Van Nieuwstadt, 2006). Several researchers have outlined the necessity of development of a cost-effective on-board NOx monitoring system to better understand trends associated with real-world vocational driving emissions from a large sample of fleet operational on-highway trucks (Pondicherry et al., 2019; Spears, 2019; Tan et al., 2019). This can be addressed by the development of a miniature

sensor-based platform that is capable of being instrumented in the vehicle to collect and quantify emissions rates associated with driving performance over a long period of time. Current on-board Zr-O₂ NO_x sensors are compact, comprise of reduced warm-up time, and demonstrate improved accuracy (Blanco-Rodriguez, 2013; Hofmann et al., 2004). Utilization of tailpipe NO_x sensor in conjunction with an ECU data logger can potentially serve as a complementing or alternative cost-effective medium to monitor real-world NO_x emissions rates. However, the detection ability of the NO_x sensors is affected due to cross-sensitivity to other interfering exhaust gas species due to electrochemical reactions (or) accumulation of molecules on the electrolyte surface (Frobert et al., 2013; Murray et al., 2017; Sakai et al., 2003; Soltis et al., 2006; Todo et al., 2018). Therefore, to be implemented as a feasible, cost-effective alternative for NO_x monitoring, it is essential to gain an in-depth understanding of the impact of cross-sensitivity on sensor-based measurements.

Figure 22 shows the schematic representation and description of the chemical reactions within a Zr-O₂ based NO_x sensor technology. The on-board NO_x sensors are manufactured using planar porous Zr multilayer technology (Moos, 2005; Murray et al., 2017). The sensor includes a heater that is used to keep the sensor element at high temperatures (i.e., above 600 °C) to collect measurements with high resolution. The sensor element is split into two cavities, where the first cavity includes an electrochemical pump that modulates the available oxygen (O₂) concentration in the exhaust gas to a predefined value by reducing O₂ to O²⁻. This conversion typically occurs in the presence of an electrolyte (i.e., usually Platinum (Pt)). Therefore, providing a linear measurement of lambda (λ). Additionally, NO is converted to NO₂, and NO₂ diffuses into the second cavity where an electrochemical pump is used to dissociate NO₂ into N₂ and O₂. The output of the electrochemical pump is the sensor reported measurements of NO_x concentration in the exhaust gas (Blanco-Rodriguez, 2013; Riegel et al., 2002).

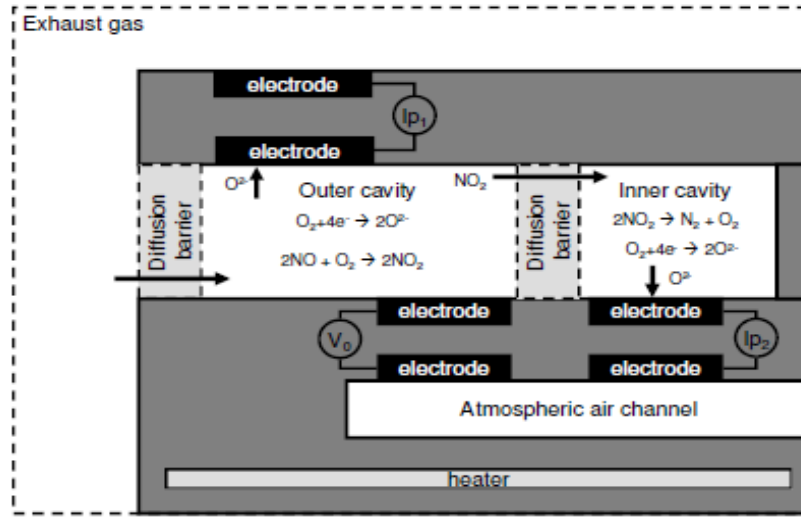
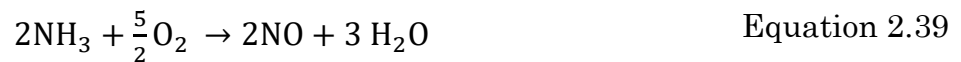


Figure 22: Schematic of electrochemical reactions in Zr-O₂ NO_x sensor (Blanco-Rodriguez, 2013)

The characteristic relationship of the electric current to NO_x measurement is depicted in Figure 23. Several research studies were performed on Zr-O₂ NO_x sensors to evaluate the accuracy and cross-interference to other species in the exhaust gas. The cross-sensitivity to NH₃ gas is one of the primary interfering components that is described in the literature and is often used as a feedback command in SCR control to limit NH₃ slip (Bonfils et al., 2012; Chih-Cheng et al., 2014; Frobert et al., 2013; Wang et al., 2016). As the sensor element is preheated to a higher temperature for better resolution and to reduce the time delay in measurement, it is observed that at higher sensor temperatures a part of NH₃ gas is oxidized to NO and H₂O, therefore resulting overestimation of NO (Moos, 2009). For research and applicational purposes, a cross-sensitivity factor (α) was introduced to compensate for the additional NH₃ gas interference (Frobert et al., 2013).



$$\text{NO}_{x\text{sensor}} = \text{NO}_x + \alpha \cdot \text{NH}_3 \quad \text{Equation 2.40}$$

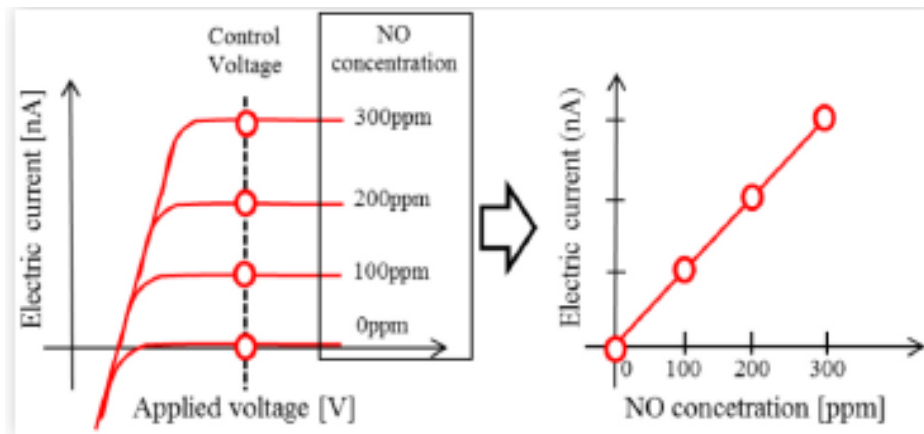


Figure 23: Relationship between the applied voltage and current of the NOx sensor (Todo et al., 2018)

Bonfils et al. performed a bench-scale experimental evaluation of the NOx sensor using a DOC-SCR-DPF EATS setup. The study evaluated changes in NOx sensor response with respect to a rise in NH₃ gas in the post-SCR exhaust stream. Figure 24 summarizes the results obtained from exhaust gas test conditions such as 300 °C, 100 kg/hr, and 200 ppm for exhaust temperature, flow rate, and SCR inlet NOx concentration, respectively.

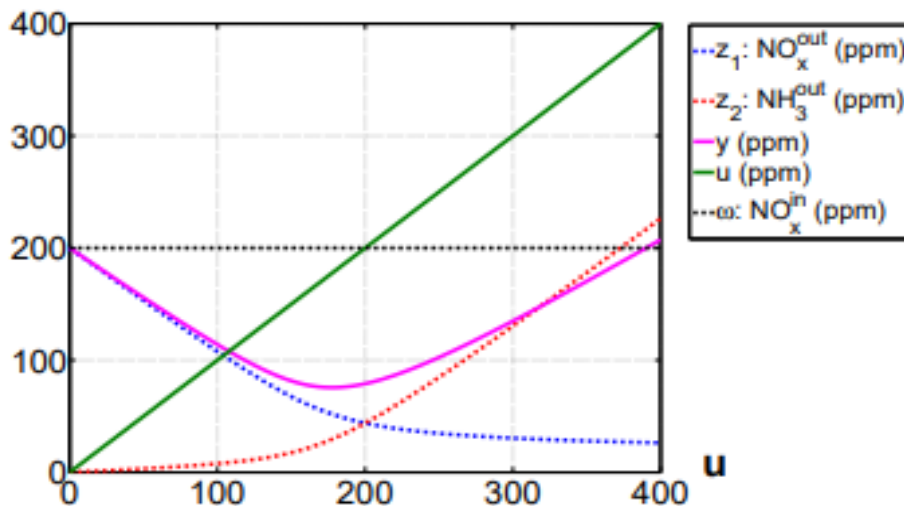


Figure 24: Comparison of NOx measurements (i.e., laboratory analyzer and sensor), NH₃ sensor measurements, and urea injection at exhaust gas flow temperature: 300 °C, gas flow rate: 100 kg/hr, and SCR inlet gas NOx concentration: 200-mole ppm (Bonfils et al., 2012)

The steady-state experimental measurements presented in Figure 24 are aftertreatment outlet laboratory-grade NO_x analyzer measurements (i.e., z1), aftertreatment outlet laboratory-grade NH₃ analyzer measurements (i.e., z2), aftertreatment outlet NO_x sensor measurements (i.e., y), the urea injection rate (i.e., u) and aftertreatment inlet NO_x concentration (i.e., w). The results show that as urea injection rate increases, NO_x concentration decreases due to the SCR catalyst chemical reactions. It is to be noted that the NO_x sensor measurements demonstrate a linear correlation with the laboratory-grade measurements, but with the urea injection rate and an increase in NH₃ slip, the sensor-based measurements report an increase in concentration levels due to interference observed from NH₃ gas (Bonfils et al., 2012).

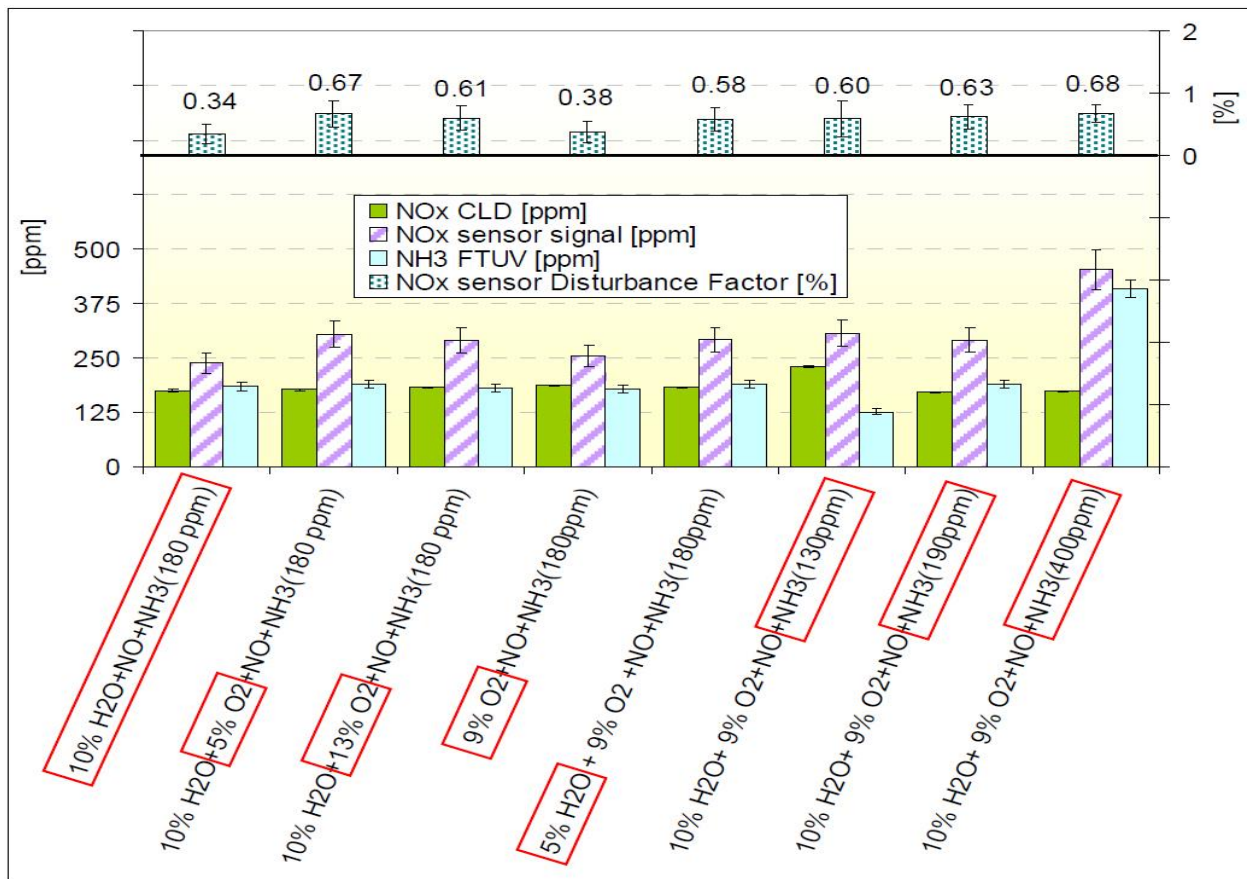


Figure 25: Evaluation of NO_x sensor accuracy in the presence of NO, NH₃, H₂O and O₂ (Frobert et al., 2013)

Frobert et al. that performed bench scale evaluation of NO_x sensors using a synthetic gas blend. The study compared variations in NO_x sensor-based measurements with respect to CLD-based measurements in the presence of NO, H₂O, O₂ and NH₃. Figure 25 shows that the presence of NO and NH₃ gas (i.e., between 180 and 400 ppm) in the presence of H₂O (i.e., in the range of 5 to 10%) and O₂ (i.e., in the range of 5 to 13%) depict a variability in the NH₃ cross-interference factor on the sensor-based measurements in the range of 0.58 and 0.68. The study indicates that the presence of H₂O and O₂ concentration in the exhaust stream can cause a significant impact on Zr-O₂ NO_x sensor-based measurements (Frobert et al., 2013).

Woo et al., and Soltis et al. have highlighted upon the deviations in NO_x sensor output as a function of rapid fluctuations/changes in the H₂O content present in the exhaust stream (Woo and Glass, 2012). The study by Soltis et al. shows that the rate of change of H₂O concentration can potentially impact NO_x sensor measurements. Figure 26 shows the transient impact of NO_x sensor response in the presence of 0 ppm NO_x, O₂, and CO₂ concentration, while the H₂O concentration changes from 2% to 8%.

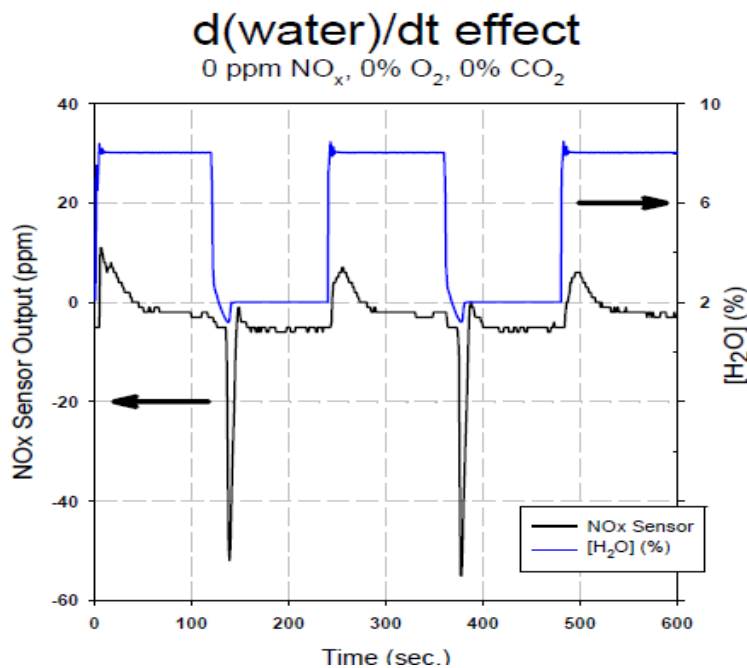


Figure 26: Impact of changes in H₂O concentration on NO_x sensor measurements (Soltis et al., 2006)

Results show an increase in the NO_x sensor measurements due to the rapid change in H₂O, and then further slowly reduce back a steady-state response. It is to be noted that the presented results outline potential scenarios where the NO_x sensor response is affected due to a rapid increase and decrease in H₂O concentration (Soltis et al., 2006). In light of developing a quick light-off and highly accurate NO_x sensor, Todo et al. identified that residual O₂ on the sensor electrode can cause an error in the reported measurements. To address the issue, the authors instrumented a monitoring electrode (i.e., Pt-Au) in addition to pumping and sensor electrode within the element to detect/monitor the residual O₂ on the sensor electrode. Figure 27 shows a linear correlation between the residual O₂ on the sensor electrode and reported output error in concentration. Correction of sensor response signal using the measurements from the monitoring electrode demonstrated an 80% reduction in output error due to the residual O₂.

Additionally, the authors also addressed the impact of output error due to the effect of electron conduction and Rh oxidation on the sensor electrode. The study also presents a protocol where hydrogen (H₂) gas is generated by increasing the applied voltage to the electrochemical pump. This resulted reducing the sensor light-off time from 70 seconds to 30 seconds (Todo et al., 2018). A detailed overview of the sensor development research is discussed in the technical paper presented by Todo et al.

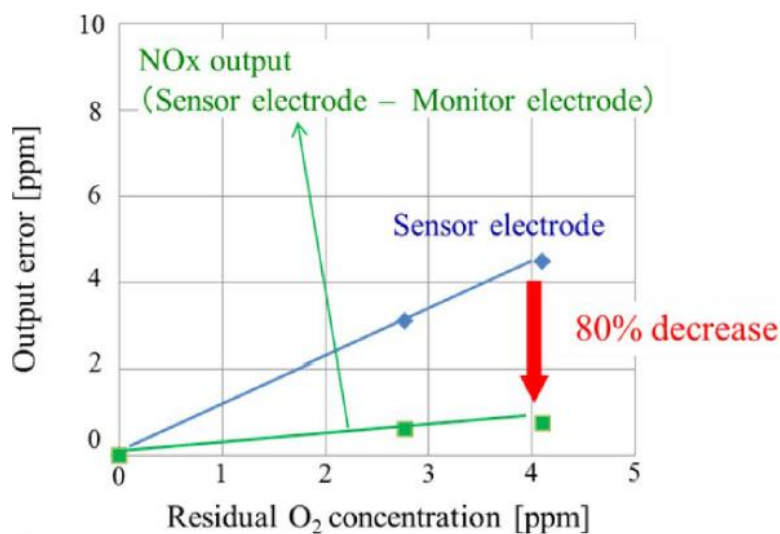


Figure 27: Comparison of output error versus residual O₂ concentration on the sensor electrode (Todo et al., 2018)

2.10. Summary

The literature survey discussed in this study presents an overview of vocational dependency on the performance of SCR systems for NO_x reduction, and metric-based performance evaluation of in-use emissions quantification methods. Exhaust gas thermal conditions is a primary challenge associated with limiting SCR performance for NO_x abatement across all modes of driving conditions. Research studies presented in section 2.4 highlight the dependency of vehicle activity/duty-cycle patterns on NO_x emissions rates. Literature presented in section 2.8 highlights the gap between the current NTE in-use emissions quantification protocol and actual real-world operation. As observed modes of real-world operating conditions linked with elevated levels of NO_x emissions are not considered for evaluation using the NTE protocol. While NTE approach was developed to cater a different objective (i.e., part of the 1998 consent decrees), with technological changes and advancements in emissions control technologies, there exists a need to identify a viable metric that depicts a realistic representation of RDE. The study further reviewed different approaches used to characterize real-world tailpipe NO_x emissions as a function of vehicle/engine operational characteristics.

Finally, with regards to measurement technology, due to cost and complexity associated with data acquisition using a PEMS and in view of identifying a cost-effective alternative pathway for monitoring of in-use NO_x emissions, literature discussed in this study has highlighted upon the detection ability of Zr-O₂ NO_x sensors. In terms of cross-sensitive behavior, the research articles presented in section 2.9 show that the sensor response may be impacted due to the presence of NH₃ gas, and also due to the rate of change of H₂O.

3. Experimental Setup and Procedures

This chapter summarizes a general overview of the experimental setup, test vehicle specification, instrumentation and data collection procedures used in this study. The study includes evaluation of real-world emissions testing activity collected as part of three different research projects comprised of a variety of vehicle/engine platforms and vocations. The diverse dataset allows for evaluation of test activity collected over a range of ambient and engine operating conditions. All test articles used in the study were in-fleet operational diesel-fueled trucks certified to U.S.EPA 2010 emissions standards. During the course of this study, in-use emissions activity was acquired from multiple sources such as PEMS, FTIR and Portable Activity Monitoring System (PAMS), i.e., DAQ for ECU broadcasted signals in conjunction with tailpipe NO_x and NH₃ sensors.

Since the goal of the study was to develop and demonstrate the applicability of a metric for evaluation of real-world emissions, this study does not discuss the influence of measurement uncertainties on the metric-based results. However, it is crucial to keep in mind that all experimental analysis have errors associated with them that may cause a reported reading to vary (i.e., dependent on system response, accuracy, and cross-sensitivity). A report by JRC presents a detailed review of sources of uncertainty and the corresponding factors associated with the calculation of emissions rates from test activity procured from a PEMS (Giechaskiel et al., 2018). Another study by (Rohrer et al., 2018) examined the deviations associated with ECU engine speed and torque reporting (i.e., SAE J1939 protocol) versus engine dynamometer based measurements on a 4.5 L John Deere engine. For experimental data discussed in section 3.2 and 3.3, test protocols were followed during the data collection phase to ensure data integrity and quality.

3.1. Heavy-duty In-use Testing Program

The subset of in-use test activity collected as part of manufacturer-run HDIUT program was used to examine the influence of boundary parameter thresholds on in-use emissions compliance protocols. A total of 75 different in-use test data files collected from five different HD engine manufacturers were used for the above-mentioned specific task of this study. Test data comprises of in-fleet vocational vehicle activity and tailpipe emissions collected using a PEMS compliant with requirements set forth by CFR, Title 40, Part 86 and 1065. The device simultaneously sampled ECU parameters (i.e., necessary for NTE in-use compliance quantification), emissions constituents measured from the analyzer, exhaust flow rate measured using an exhaust flow meter, ambient measurements (i.e., such as temperature, pressure, humidity) and GPS measurements (i.e., such as vehicle speed, altitude, latitude and longitude). Figure 28 provides a schematic representation of the experimental setup that is typically used for raw exhaust emission sampling during on-road testing using an on-board emissions measurement system.

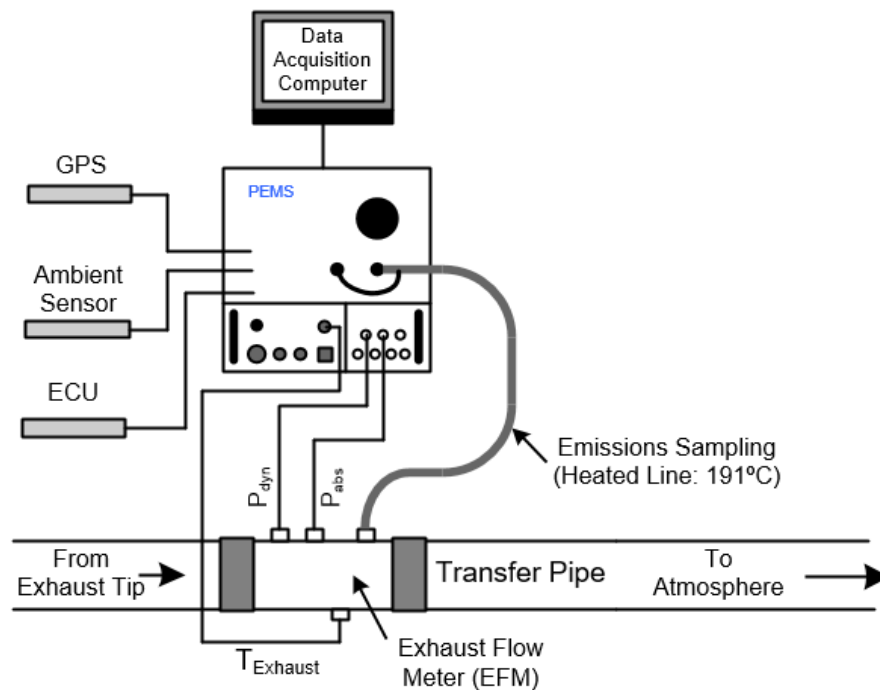


Figure 28: General schematic representation of the experimental setup for on-road emissions testing (Rework of Besch et al., 2017)

All vehicle datasets collected in this phase of the study were non-credit engines equipped with a DOC-DPF-SCR aftertreatment technology. Figure 29 shows the distribution of engine displacement, MY and power rating, respectively of all 75 vehicles datasets. Engine sizes ranged between 6.7 L to 16 L, Engine MY ranged between 2010 and 2014, and the engine's rated power ranged between 240 and 580 bhp. The majority of in-use datasets were from engine MY 2010 and engine rated power between 400 and 450 bhp. The reported vehicle odometer reading at the beginning of the in-use testing of all in-use test datasets ranged from 13,932 and 404,329 miles. Based on the categorization of MD and HD vehicles as a function of gross vehicle weight rating showed that in-use datasets as a subset of MD category ranged from vehicle mileage of 13,932 to 166,697 miles, and HD category ranged from 30,540 to 404,329 miles. The vehicles datasets sampled from the HDIUT program were within the useful life set forth by the regulatory agencies (i.e., 185,000 miles for MD and 435,000 miles for HD vehicle category).

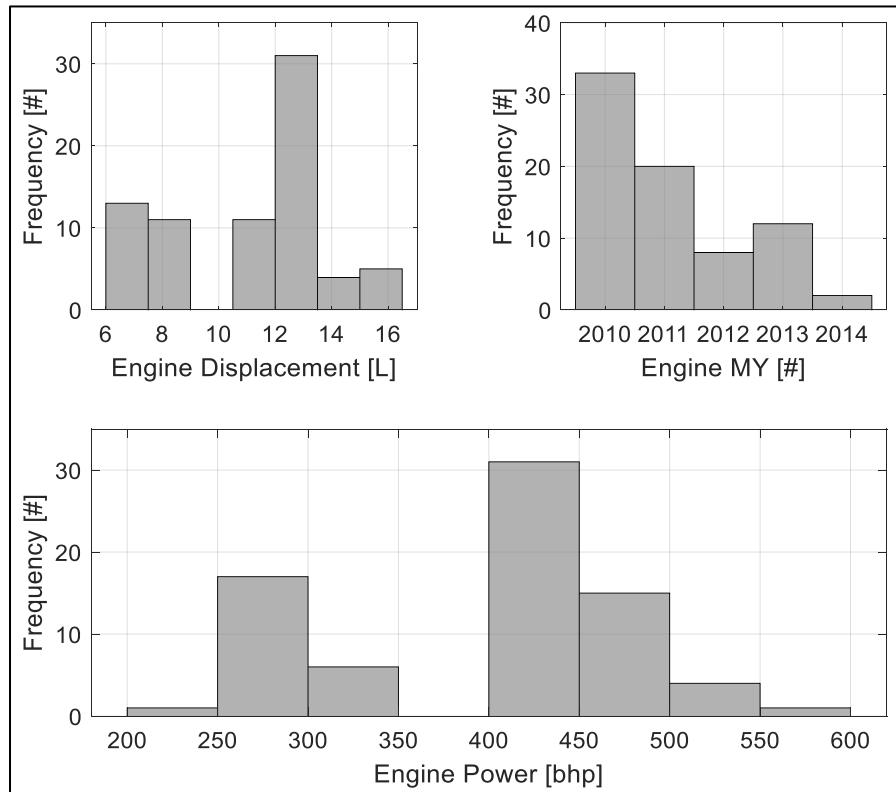


Figure 29: Distribution of HDIUT datasets as a function of engine displacement, MY and rated power

3.2. Heavy-duty In-use Testing

On-road PEMS evaluation of four class 8 HD tractors was performed to evaluate the impact of vocational drive cycles on in-use emissions rates. The data for this phase of the study were collected with WVU TEMS's coupled to the HD truck operated over custom real-world duty cycles representing vocational activity across major freight corridors in LA. Table 7 provides a general overview of the vehicle specifications, aftertreatment technology, and composite NO_x emissions result from a cold and hot FTP certification cycle.

Table 7: Test vehicle specification for on-road PEMS testing

Engine Manufacturer	A	B	C	D
Vehicle	A	B	C	D
Test Category [-]	(a)	(a)	(b)	(b)
Engine MY [#]	2018	2017	2013	2015
Test Weight [lbs]	74,620	66,780	65,120	65,920
Mileage ¹ [miles]	85,969	150,262	529,894	119,209
Vehicle Class [#]	8			
Aftertreatment Configuration [-]	DOC-DPF-SCR			
FTP Cert. NO _x [g/bhp-hr]	0.16	0.12	0.17	0.06
Simulated FTP Engine Work [bhp-hr]	37.22	31.16	27.20	32.35

¹ Vehicle mileage at the onset of in-use emissions testing

Figure 30 depicts a general overview of the schematic of the experimental setup used for data collection during this phase of the study. Tailpipe gaseous emissions measurement system included a 1065 compliant PEMS (i.e., Semtech-DS), FTIR device (i.e., MKS Multigas™ 2030) and Zr-O₂ NO_x sensors. In the current study, the truck's exhaust was routed using a 5-inches stainless steel transfer pipes which included a high-temperature flexible insulation hose into the CVS dilution tunnel

inside TEMS. An EFM (Semtech EFM-HS) was instrumented in the exhaust stream between the flexible hose and CVS tunnel inlet to measure the exhaust gas flow rate, temperature and pressure. Additionally, emissions sampling probes were instrumented next to the EFM to extract and direct exhaust sample to the emissions measurement system using temperature-controlled (i.e., maintained at 191 °C) sampling lines, filters and probes. An ECU data logger was used to capture engine and aftertreatment operational parameters broadcasted using the SAE J1939 protocol from the controller area network (CAN). The PEMS and FTIR systems were instrumented in WVU's TEMS, while the Zr-O₂ NO_x sensors were instrumented in-line with the gaseous emissions sampling probes. The portable HD laboratory (i.e., TEMS) was built inside a 30ft long cargo container and was designed by WVU personnel in the 2007-2008 time frame as per CFR 40/1065 requirements (Wu, 2010). The portable laboratory provides the ability to measure gaseous and particulate emissions using a range of raw and dilute emissions analyzers. Additionally, the laboratory also comprises of a gravimetric PM measurement system using filter media. A detailed overview of the experimental setup of TEMS laboratory that is typically used for measuring a range of gaseous and particulate emissions measurement is described in (Besch, 2016 and Quiros et al., 2016).

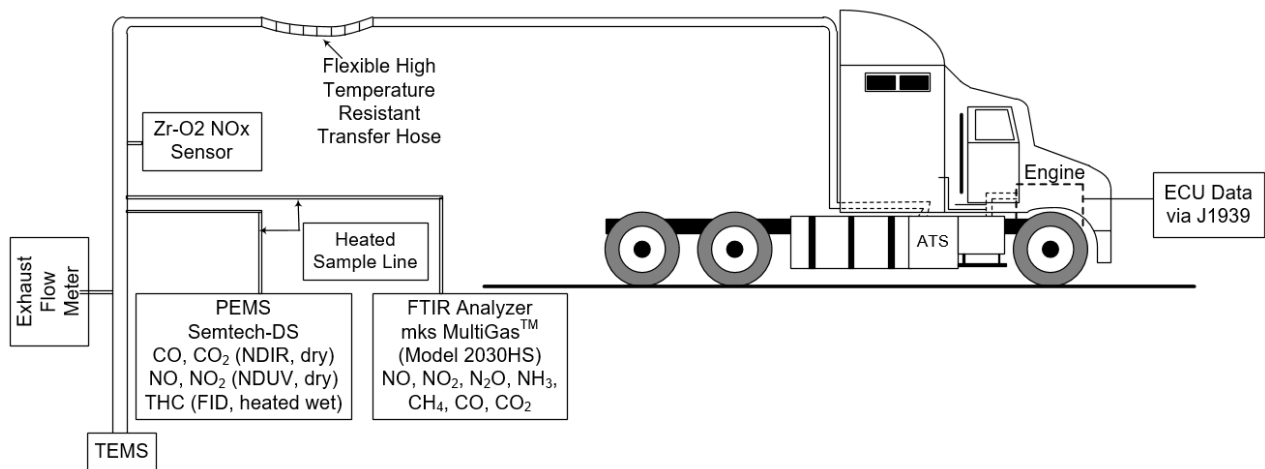


Figure 30: Schematic of the instrumentation setup of gaseous emissions sampling

3.2.1. Test Routes

In-use test activity collected from vehicles recruited in test category (a) as described in Table 7 were operated on two test routes representative of driving conditions namely: 1) Highway-Hill Climb, and 2) ISC. The routes were driven over four test days covering a total distance of approximately 339 miles per vehicle. The selected test routes comprised includes a combination of both urban and highway driving operation. Figure 31 shows the vehicle speed and altitude profile of the highway-hill climb test route, which includes both up-hill and down-hill driving conditions. The test is divided into three segments, and the route description of each test segment is described as follows: Segment-1 begins at Riverside, California to 215S, then heads onto I-15N until Exit 153B in Victorville, California. Segment-2 continues from exit 153B to I-15S, and then onto 215S, I-10E until exit 144 in Indio, California. Segment-3 continues from exit 144 to I-10W to 215S and back to Riverside, California.

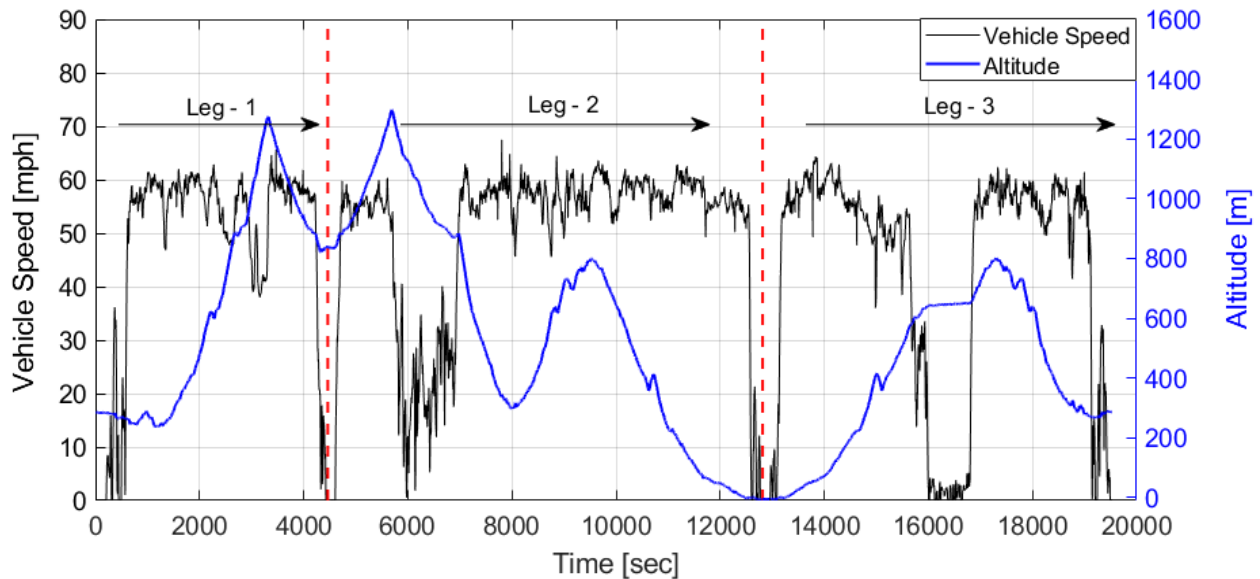


Figure 31: Comparison of vehicle speed and Altitude for Highway-Hill Climb route

The second test route (ISC) is a custom test route that was developed to replicate in-use test requirements as prescribed by EU VI (c) regulations for ISC verification of Class 8 HD trucks. As shown in Figure 32, the test route comprises of a sequence of

urban, rural and highway driving operation. The EU regulations require the ISC test requirements to include a share of 30%, 25% and 45% for urban, rural and highway driving segments, respectively, characterized by vehicle speed. The boundary conditions for the different driving operations are vehicle speeds between 0 to 50 kmph for urban operation, vehicle speeds between 50 to 75 kmph for rural operation and vehicle speeds above 75 kmph for highway driving operation. The regulations permit the target value for each of the operational segment to be within $\pm 5\%$ (EU 582, 2011). The developed test route was operated near Riverside, CA. Test activity acquired from vehicle-A did meet the route-based statistics requirements as per EU regulations. Data acquired from vehicle-B on this route did not comply with the EU route statistic requirements but included a similar sequence of activity as per the EU guidelines is treated as a valid dataset for this study.

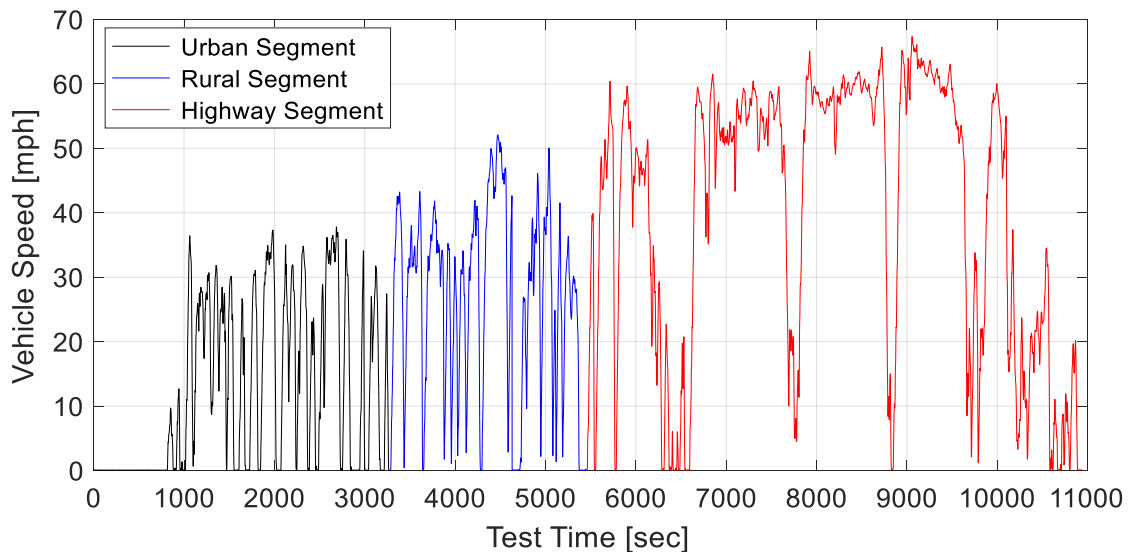


Figure 32: Operational segment-based classification of vehicle speed profile for ISC route

In-use test activity collected from vehicles recruited in test category (b) as described in Table 7 were collected on two vocational routes representing port delivery and urban grocery distribution. The port delivery route simulates the vocational truck operation entering and exiting the port of long beach. The test is divided into three different segments. The first leg of the route operates from Riverside, CA to Long

Beach, CA that includes a dominant fraction of time spent during highway driving operation. The route simulates LA freeway traffic approaching port of Long Beach. Leg-2 of the route includes simulation of drayage activity, i.e., the extended engine idle activity and creep operation, therefore representing frequent stop-and-go activity in the port. This leg simulates vehicle activity while the truck is waiting at the port terminals to receive shipping containers from the ocean vessels. The second leg was evaluated on publicly accessible Nimitz Pier inside the harbour of Long Beach, CA. The third leg of the route includes a return trip from port harbour to Riverside, CA simulating LA freeway driving. Figure 33 shows the continuous-time trace of vehicle speed for the port route comprising of the dominant amount of rural and highway driving operation in leg-1 and 3 of the test routes simulating LA freeway traffic.

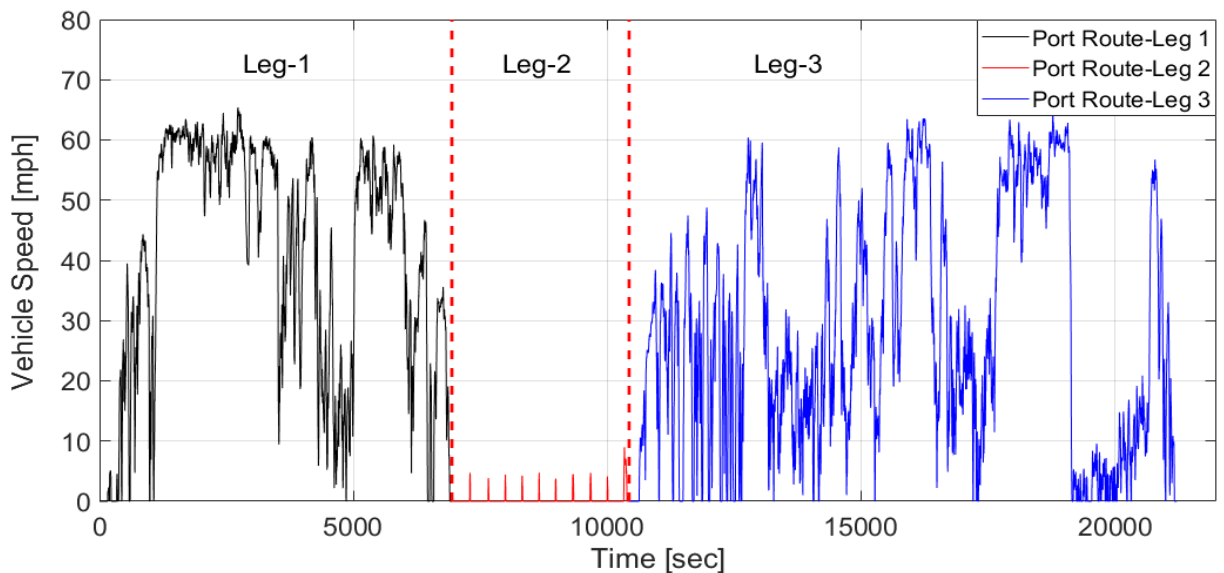


Figure 33: Generic representation of vehicle speed profile of port route

The grocery distribution route simulates the truck operation of goods delivery to grocery stores in LA. Figure 34 shows the vehicle speed profile of the entire test route, i.e., divided into five different segments. The entire route includes four stops at LA grocery stores to simulate unloading of goods at truck docks. The first leg of the route operates from Riverside, CA to central LA. This segment of the test simulates freeway traffic entering metropolis of LA. The second leg of the test operates from central LA

to the ramp entering US 110S near downtown LA. The third leg operates on US 110 S and ends near the vicinity of LA International airport. The second and third leg of this test includes test activity comprising of a dominant fraction of test activity at low vehicle speed operation (i.e., < 20 mph). The fourth leg of the test operates from a vicinity near LA International airport to Santa Ana representing LA freeway operation on US 405 S. The final leg of the test is from Santa Ana to Riverside, CA.

The port delivery and grocery distribution route were developed based on vehicle activity data collected using PAMS based on analyzing actual in-fleet operation. For both the test routes, the engine was shut down for 30 minutes after each operational segment of the test, except for leg-3 of the grocery distribution route where the engine was shut down for 60 minutes after the test. The post-test soak times were calculated from fleet-based activity data collected to simulate cool-down of the aftertreatment system during unloading of goods.

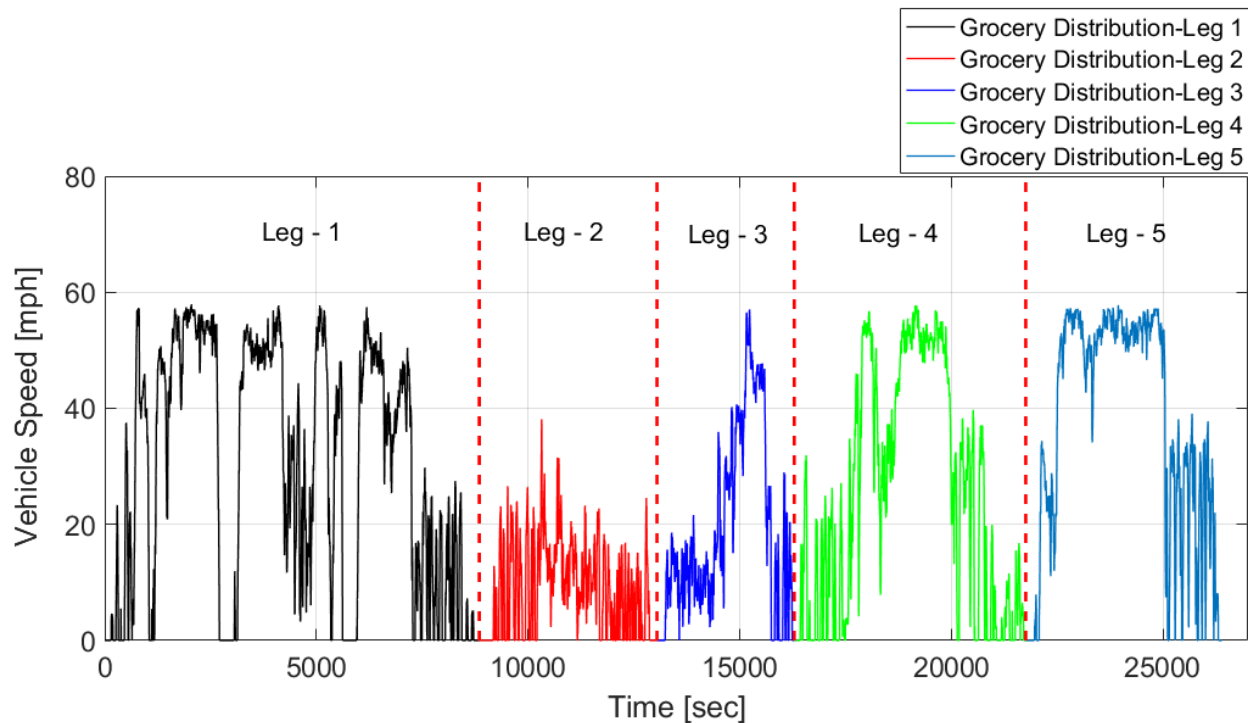


Figure 34: Generic representation of vehicle speed profile of grocery distribution route

Table 8: Summary of test routes and vehicles tested

Route Name	Route ID	Vehicle
Highway Hill Climb	1	A, B
ISC	2	A, B
Port Delivery	3	C, D
Grocery Distribution	4	C, D

Considering that this section comprises of multiple test trucks evaluated on different test routes, Table 8 outlines a summary of the test vehicles and its respective test routes and ID for further discussion. Figure 35 illustrates a picture of a test truck coupled with WVU TEMS laboratory near the LA port harbour.



Figure 35: Class 8 HD tractor hauling WVU TEMS near LA port harbour

3.2.2. Experimental Instrument

This section presents an overview of instruments used for sampling raw exhaust gas emissions in the current study. In addition to the two emissions instruments presented in this section, tailpipe NO_x sensors were instrumented in the exhaust

stream (i.e., post-SCR). A detailed outline of the working principle of the NO_x sensor technology was presented in section 2.9.

3.2.2.1. Semtech-DS

Semtech-DS designed by Sensors Inc. is the PEMS (i.e., as shown in Figure 36) that was employed during this course of the study to measure real-world gaseous emissions. The instrument is compliant with regulatory requirements set forth by 40 CFR §86 and §1065 for U.S.EPA in-use emissions compliance evaluation. A heated sample line (i.e., maintained at 191 °C) extracts the sample using an extraction pump from the exhaust stream and routes it to the PEMS. A thermoelectric chiller is used to dry the exhaust gas and remove water vapour before routing the exhaust to the individual gas detection analyzer to measure the exhaust gas concentrations. The instrument comprises an automotive micro-bench II (AMB II) NDIR spectrometer for measurement of CO and CO₂ exhaust gas species. The analyzer consists of a heated sample cell, light source, light chopper, solid filter and detector. The sample gas enters the cell and absorbs the infrared radiation, and the detected light intensity is proportional to the concentration levels. NDUV analyzer is used for independent measurement of NO and NO₂ exhaust species. The analyzer comprises of two filters (i.e., active and reference), and two detectors. The ultraviolet light source comprising of shorter wavelength but higher energy than IR is passed through the beam splitter into the sample cell where one of the detectors measures the absorbed energy while the other measures the non-absorbed energy. In parallel, a reference beam is also sampled, and the ratio of the detected wavelength and the reference beam is used to quantify the real-time pollutant concentration levels (Johnson, 2012). A compact high precision h-FID is used for measurement of THC. Hydrogen flame in the burner is produced by combustion of FID fuel (i.e., a blend of 40% of hydrogen and 60% helium) and air. HC present in the exhaust gas stream are ionized as the sample gas is introduced to the flame. The ion current is directly proportional to the carbon atoms that are introduced into the flame as HC's, therefore correlating to the total HC concentration. Individual analyzer specifications are presented in Appendix A.

The PEMS also collects ECU broadcasted signals, data broadcasted from a GPS device, and ambient measurements using an external probe. A high-speed exhaust flow meter comprising of a differential pressure flow meter that operates on Bernoulli's principle is used to measure exhaust flow rate accurately. The EFM is verified in a flow bench environment against a laminar flow element (LFE) that is calibrated as per NIST guidelines to evaluate for linearity and repeatability in measurements as per (CFR/40/1065/307).

The post-processing software of the device accounts for drift correction as per 40 CFR §1065.672, dry to wet correction as per 40 CFR §1065.659 and NO_x humidity correction factors to generate instantaneous duration-specific emissions mass rates. The test protocol includes a pre/post-test and periodic (i.e., every one hour) drift verification of the analyzer (Sensors, 2011).



Figure 36: Semtech-DS on-board emissions analyzer (Sensors, 2011)

3.2.2.2. Multigas™ 2030 FTIR

Multigas™ 2030 FTIR was used to analyze emissions constituents in the exhaust gas. The principle of spectroscopy is used to measure the high resolution of spectral data over a range of spectral gases. The salient feature of FTIR is the ability to measure more than 20 different exhaust species at the same time. The FTIR device consists of two infrared beams that originate from the same light source and are transmitted to two different optical paths that are reflected on i) fixed mirror, and ii) vibrating/moving mirror respectively as shown in Figure 37. The combined beams are then transmitted through the gas chamber where the molecules in the exhaust gas absorb energy depending on the spectral distribution of the molecules. The beam leaving the gas chamber is transmitted onto a detector which generates an interferogram. Depending on the intensity distribution detected based on the infrared absorption spectra, a mathematical Fourier transform is performed to translate the intensity distribution into representative gas concentrations for the exhaust gas species such as NO, NO₂, H₂O CO, CO₂, NH₃, etc. The manufacturer provides a pre-calibrated method. The calibration typically comprises of the exhaust gas species and calibrated ranges observed in the exhaust gas. As prescribed by MKS, the sampling setup comprising of dual-head diaphragm pump was used to extract part of the exhaust gas at a flow rate of 10 litres per minute. The instrument was operated by maintaining the cell pressure slightly under 1 atm for high-speed fast response of the measurement. The sampling setup includes a heated line and filter that are maintained at 191 °C. The filter is used to restrict any in-flow of solid particles into the FTIR gas chamber. Additionally, the spectrometer and optics components are purged with dry air prior and after a test run to remove any moisture (i.e., water vapour) and NH₃.

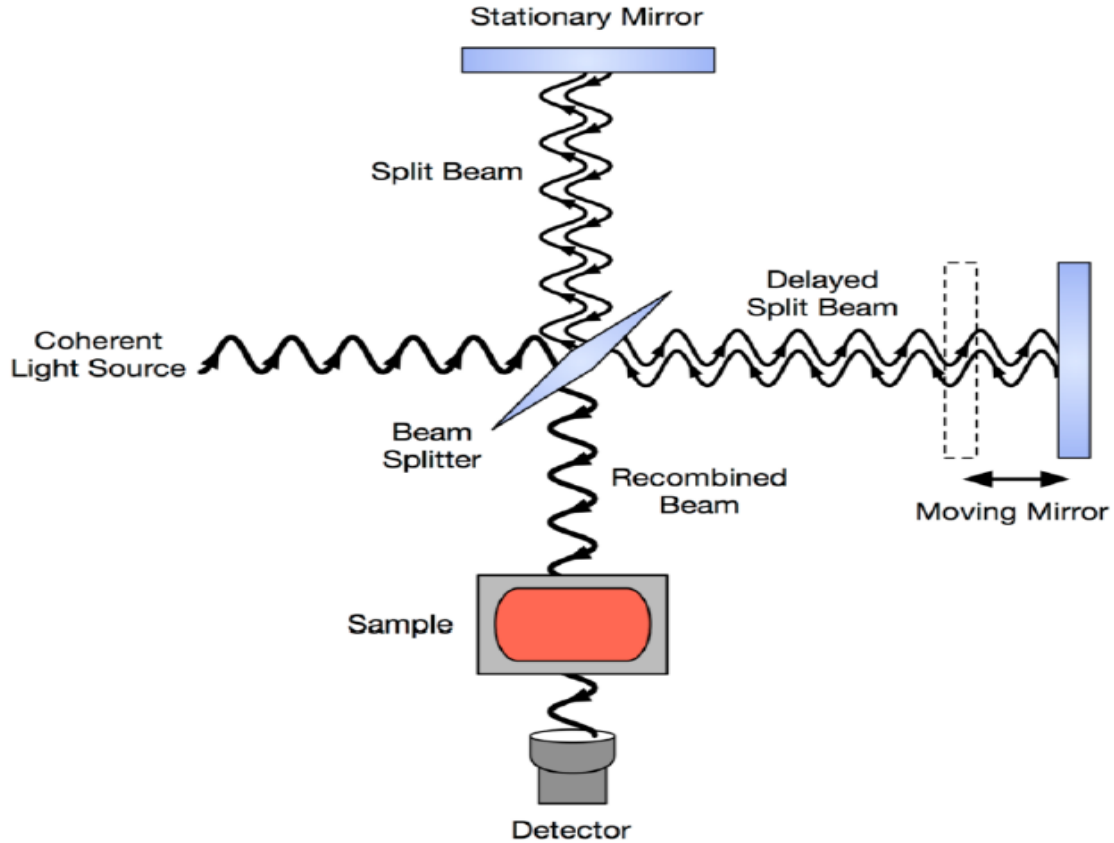


Figure 37: Schematic representation of FTIR interferometer (Sanchox, 2017)

3.3. In-use Testing using PAMS

In-use test activity was collected using PAMS (i.e., an on-board NO_x monitoring system) to evaluate actual fleet operational vehicle activity and its associated impact on in-use NO_x emissions rates. The vehicles recruited in the current study were on-road diesel-fueled MD and HD trucks equipped with MY 2014 or later engines and specifically operating in southern California. The vehicle class categories sampled in the current study was based on the EMFAC 2014 emissions inventory results. The test matrix includes vocational vehicle categories that contribute to a total of 81.8% or more daily NO_x emissions within the South Coast Air Basin. A telematics-based DAQ was used to simultaneously sample real-time publicly broadcasted J1939 ECU signals, GPS information and measurements from an additional tailpipe NO_x and NH₃ sensors installed in the exhaust stack. The advantage of using such a system is

the feasibility of low-cost data logging and measurement. Such a system provides an advantage of acquiring a longer duration of test activity while the truck is performing its in-use fleet operation.

Table 9 shows the summary of vehicles sampled in this study as a function of vocational activity. The sampled vehicles were deployed in a range of vocational application such as short/long haul goods distribution, urban delivery, cement mixers, food and beverage distribution, and drayage application. A total of 18 vehicles ranging from engine MY 2014 to 2018, and approximate vehicle mileage from 10,786 to 281,407 miles were recruited in this phase of the study (i.e., depicted in Figure 38).

Table 9: Vehicle recruitment test matrix as a function of Vocation, and vehicle activity

Category	Vocation	Activity	Count
[-]			[#]
A	Distribution	Short/Long haul	3
B	Southern Port	Short haul	3
C	Cement Mixer	Short haul	3
D	Food/Beverage	Delivery/Pick-up ¹	3
E	Food/Beverage	Delivery/Pick-up	3
F	Distribution	Short haul	3

¹ Power rating less than 300 hp

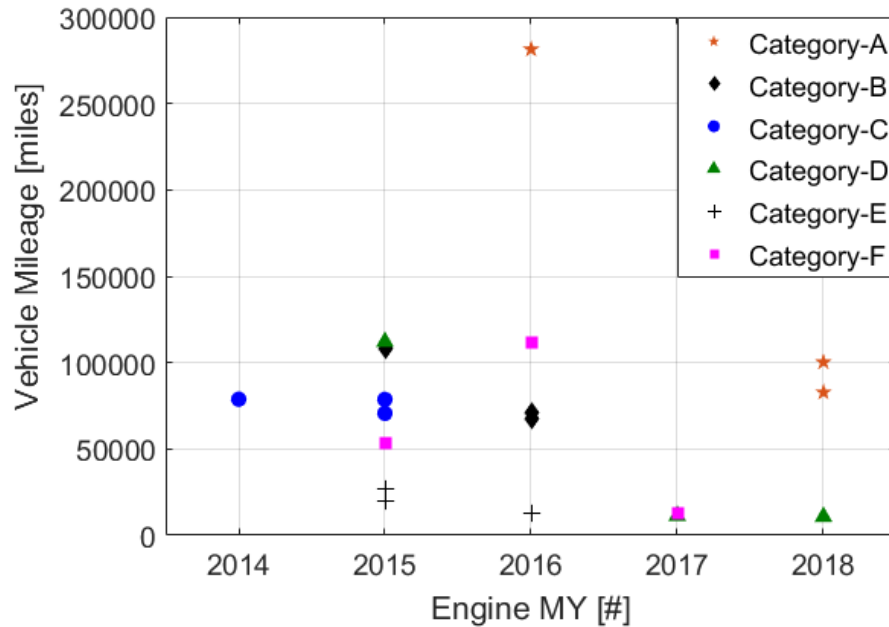


Figure 38: Comparison of Engine MY and vehicle mileage at the beginning of the data logging phase

3.3.1. Experimental Instrument

CT 1000 designed by ControlTec was used as the DAQ to continuously sample ECU broadcasted signals over the SAE J1939 CAN protocol in conjunction with additional tailpipe NO_x (i.e., Continental) and NH₃ (i.e., Delphi) sensors instrumented in the exhaust stack as shown in Figure 39. Figure 40 shows the pictures of the ControlTec DAQ and NO_x sensor used in this study. The open-source hardware can connect to multiple input-output options which provide an overarching advantage of connecting additional auxiliary sensors and sync with the global data stream platform. In addition to the telematics data stream, the data logger also houses the capability of on-board storage on a supported SSD with a capacity of up to 1TB (ControlTec, 2014). NO_x sensors instrumented in this study were configured to bypass the minimum dew-point temperature threshold to reduce the sensor-warmup time. A CAN wake-up signal was used to initiate the sensor warm-up procedure before the engine key-on event. Therefore, allowing maximum utilization of sensor reported measurements for NO_x emissions assessment. The external sensor was mounted perpendicular to the reference plane/flow direction. The current on-board NO_x sensors (i.e., part of the

aftertreatment package) are not in-use at exhaust gas conditions below a dew-point temperature threshold to avoid structural damage to the sensor cavities due to the presence of condensed water vapour droplets during low-temperature activity.

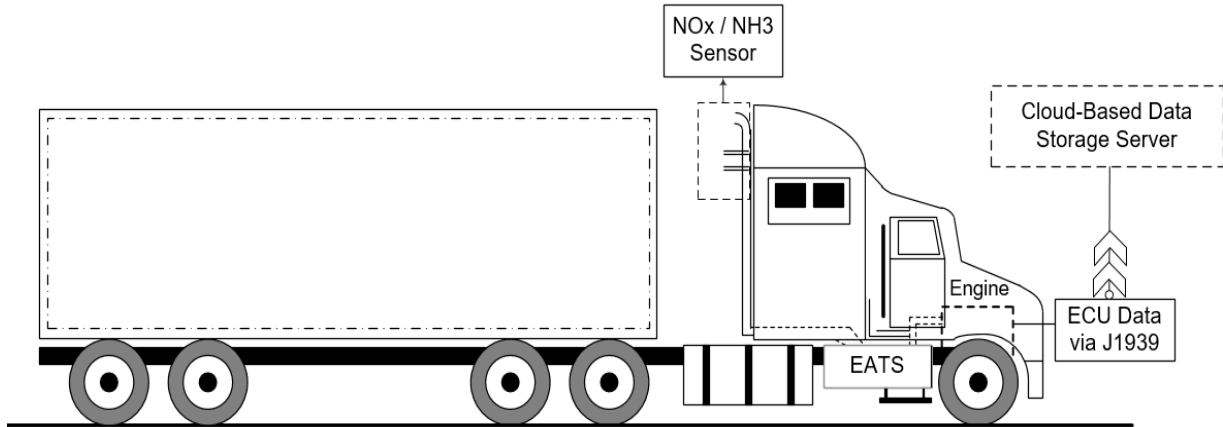


Figure 39: Schematic representation of an HD truck equipped with PAMS



Figure 40: Picture of data acquisition hardware (a) Left image: PAMS (controltec) (left); (b) Right image: Continental Uni-NOx 2.8 tailpipe NOx sensor (right)

4. Methodology

This chapter presents an overview of the approach used to meet the global objective of the study. Section 4.1 discusses different case scenarios implemented on the current in-use compliance evaluation metrics to identify the impact and influence of the governing boundary parameters on the method-based results. Section 4.2 outlines the design architecture of the novel activity-based windowing approach. Additionally, this section also discusses the statistical procedures used to generate governing boundary thresholds for variable parameters of the ABW approach. Section 4.3 explains the statistical methods used to evaluate the performance and measurement variability of NO_x sensors. Matlab (The MathWorks Inc.) environment was used for the data analysis discussed in this study.

4.1. In-use Compliance Metric Evaluation

4.1.1. NTE Method

The NTE method-defined thresholds were used to evaluate the current level of NO_x emissions compliance. In comparison to the current NTE thresholds, the study presents a general overview of two different combinations of NTE boundary conditions to characterize the impact on the amount of in-use data utilization for emissions compliance evaluation and its impact on NO_x emissions. The selected boundary conditions for evaluation are IMT, aftertreatment outlet gas temperature, engine torque, and power threshold. A parametric study performed by Pondicherry on the governing NTE boundary conditions indicates that a combination of reducing NTE engine power threshold in conjunction with post-SCR exhaust temperature threshold demonstrates an increase in the overall time-weighted data utilization for compliance evaluation without drastically affecting the event-averaged bsNO_x emissions (Pondicherry, 2017).

Table 10 lists the details of the different NTE case scenarios that were analyzed using 75 HDIUT datasets. The default NTE test case incorporates the thresholds as per the current regulatory requirements for the NTE method. ‘Modified NTE case-1’

comprises of lowering the $T_{AT\ OUT}$ from 250 °C to 200 °C and modifying the ambient temperature threshold to a fixed minimum threshold of 7 °C. ‘Modified NTE case-2’ includes lowering the engine torque and power threshold from 30% of maximum torque and rated power to 15%. With respect to the catalyst to achieve a NO_x conversion efficiency of 90% or higher (i.e., from Figure 4 and Figure 6), the test case scenario incorporates a 230 °C threshold for NTE $T_{AT\ OUT}$ limit. In both the test case scenarios (i.e., Modified NTE case-1 and 2), the IMT threshold was not implemented in the analysis.

Table 10: Boundary conditions for NTE evaluation

	Default NTE	Modified NTE Case	
		1	2
Minimum event duration [sec]	30		
Engine speed [rpm]	Per Current Regulations (n ₁₅)		
Engine torque [%]	30% ¹⁾	15% ¹⁾	
Engine power [%]	30% ²⁾	15% ²⁾	
Ambient temperature [°C]	C.R ³	7	C.R ³
Engine coolant temperature [°C]	C.R ⁴	C.R ⁴	C.R ⁴
Intake manifold temperature[°C]	C.R ⁵	N/A	N/A
Aftertreatment outlet temperature [°C]	250	200	230

- 1) Fraction of maximum engine torque from the torque curve
- 2) Fraction of maximum engine power from the torque curve
- 3) As per current regulations (C.R): 40 CFR Part 86.1370 (a)(4)(ii)(A)
- 4) As per current regulations (C.R): 40 CFR Part 86.1370 (f)(1)(i)
- 5) As per current regulations (C.R): 40 CFR Part 86.1370 (f)(1)(ii)

For all the three NTE experimental tests, the engine speed and ECT thresholds were implemented as per the current regulatory requirements. Due to lack of sufficient data to determine active and pending DPF regeneration events, the DPF regeneration exclusion was not implemented, and any data point that encountered an active DPF regeneration trigger was excluded from the analysis. It is to be noted that the boundary conditions for the exclusions used in ‘Modified NTE case-1’ are in-line with

the thresholds proposed by the regulatory agency to be implemented from MY 2022 (i.e., CARB) in their 2019 white paper (CARB, 2019). The NTE control area thresholds for ‘Modified NTE case-2’ were derived from sensitivity analysis performed on the NTE approach using limited HDIUT datasets by (Pondicherry, 2017).

4.1.2. Work-based Window Method

To better understand the impact of the entire duty cycle, method-defined thresholds as per EU VI (c) and (d) regulations were used to evaluate compliance factors (i.e., specifically for NO_x emissions) as per the WBW approach. The WBW generates MAW’s as a function of the total engine work produced in a certification test cycle. The reference work for each engine was generated by simulating the normalized engine speed and torque setpoints of the certification test cycle (i.e., FTP) using the engine torque curve to de-normalize the test cycle (CFR/40/1065.610). However, the EU regulations evaluate in-service compliance using the WBW approach on test data collected that is collected over a predefined route-based characteristic comprising of certain specific time fraction of urban, rural and highway driving segments. The WBW approach was performed on 75 HDIUT test datasets (i.e., collected based on regular in-fleet operation). Table 11 outlines the boundary parameters governing the WBW method.

Table 11: Boundary conditions for WBW evaluation

Parameter	EU VI (c)	EU VI (d)
Window reference work [bhp-hr]	1 x FTP Work	
Minimum window power threshold ¹ [%]	20 ²	10

1) Percent of maximum power

2) Step-by-step reduction from 20% to 15% of P_{max} until the ratio of valid WBW over total WBW generated is above 0.50

4.2. ABW Approach for In-use Emissions Assessment

The ABW approach comprises of a multistage integration and evaluation of an in-use test. The approach is divided into two segments where stage-1 includes generation of the duty-cycle/vehicle activity-based windows (i.e., named as theoretical window generation), and stage-2 generates events (i.e., consecutive sequence of test activity) within the windows generated in stage-1 and allocates the consecutive segments of activity into respective bins as a function of engine and aftertreatment operational boundary conditions. In-use data collected in section 3.2 from vehicles A and B will be used to develop the method-based boundary thresholds for ABW binning approach. Test activity collected from vocational and in-fleet operational data collected using PEMS and PAMS, as discussed in section 3.2 and 3.3 is used to present results of the ABW approach.

4.2.1. Theoretical Window Generation

The ABW approach splits the entire in-use test into multiple windows. The generation of each window is determined based on a predefined reference threshold, i.e., total engine work (W_{Ref}) generated over a certification test cycle as a minimum threshold. However, if the reference threshold is met during a transient duty cycle, the window continues data-point aggregation until the engine/vehicle reaches a steady-state idle mode (i.e., defined based on vehicle speed equal to 0 mph). The process is repeated beginning at the next in-use test data point post t_{end} until a new window is generated. The window generation process continues until the accumulating reference parameter is less than W_{Ref} . However, under test conditions where W_{Ref} is not met, the entire segment of test activity is incorporated as an additional window subjected to a minimum in-use trip requirement, i.e., generation of at least 1 ABW. The primary purpose of windowing is to isolate and evaluate individual segments of test activity to determine the performance of the emissions control aftertreatment system based on the duty-cycle experienced. Therefore, allowing a dynamic evaluation of each segment of in-use activity. The window

generation process in ABW is not a continuous MAW analysis, like the EU based compliance approach. Figure 41 presents a comparison of vehicle speed and cumulative engine work for an in-use test performed on ISC test route. It is to be noted that based on the theoretical window generation, the entire in-use test was split into seven different windows (i.e., where ‘W’ represents window count) to allow discrete evaluation of various segments of the in-use test activity.

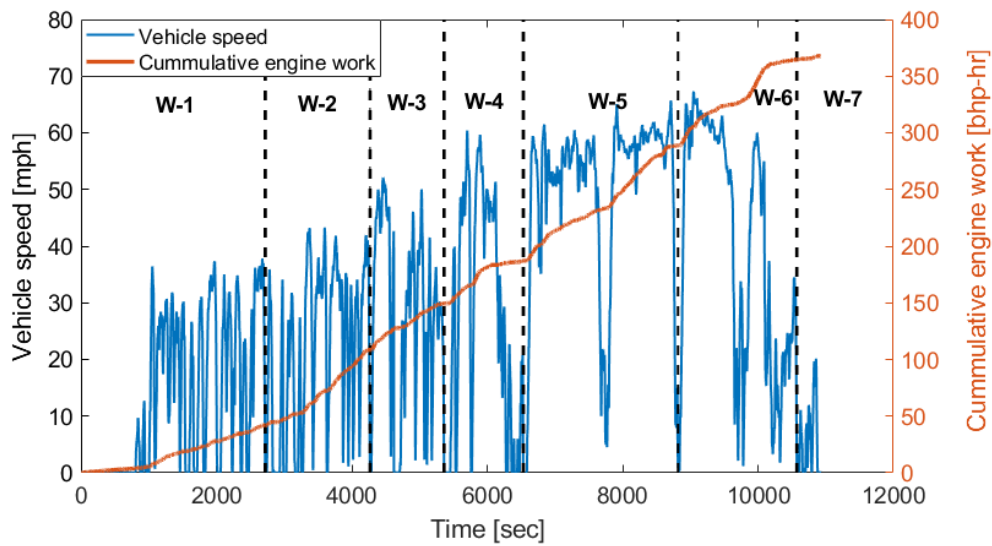


Figure 41: Comparison of vehicle speed and cumulative engine work (i.e., for theoretical window generation) of an in-use test performed on vehicle-A

4.2.2. Event Generation

Consecutive segments of test activity accumulated within each ABW is separated into two different bin categories (i.e., bin-1 and 2), i.e., engine work producing and non-work/low power operational bin. Figure 42 outlines a general overview of the four different subcategories that segregate in-use activity within each ABW. The coefficients for x, y and z described in Figure 42 are derived from analysis discussed in section 4.2.3.

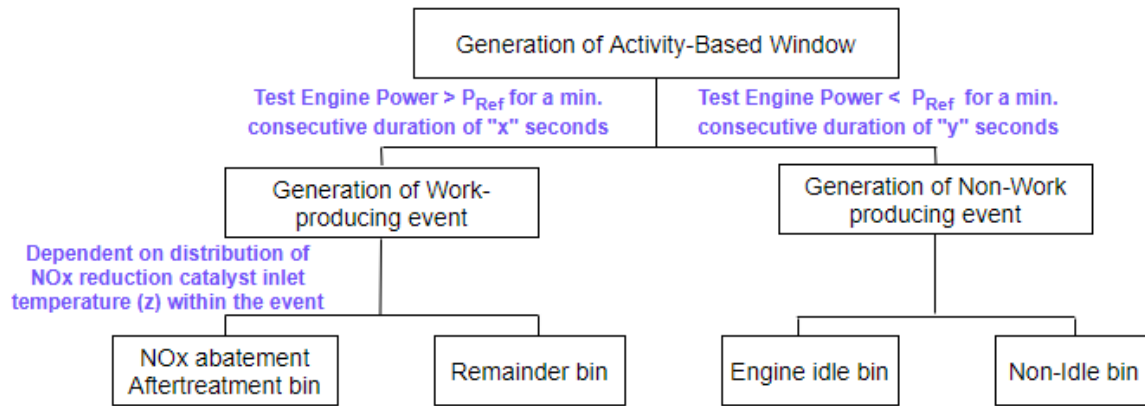


Figure 42: Categorization of events within each ABW

An instantaneous power-based filter (Operational power: Op) categorizes test activity into two different engine operational regimes (i.e., $Op-1$ and $Op-2$). $Op-1$ and 2 are defined as test activity above and below a certain engine power-based threshold (i.e., P_{Ref}). To account for test operation that experiences a short transition from $Op-1$ to $Op-2$ and back to $Op-1$, a transition mode with a maximum allowable time threshold (i.e., drop-out time) is incorporated to weight the associated bin allocation for data accumulated in the transition mode. The rapid transient operation acquired in the transition mode is captured into tractive work-producing operation (i.e., $Op-1$).

Engine work producing events (i.e., Bin-1) was defined as continuous segments of test activity meeting test conditions based on $Op-1$ comprising of a minimum time threshold of “x” seconds (Bin-1 minimum duration). Consecutive segments of test activity that does not meet the minimum time-based requirements are treated as activity in $Op-2$. Non-work producing events (i.e., Bin-2) are defined as a continuous segment of test activity categorized in $Op-2$ for a minimum time threshold of “y” seconds (Bin-2 minimum duration). The non-work producing events (i.e., Bin-2) is divided into two subcategories: (i) Bin-2a: Stationary engine idle bin (i.e., test activity where the vehicle speed is equal to 0), and (ii) Bin-2b: Non-idle bin (i.e., test activity that experiences a low power engine operation). Additionally, for engine-work producing events (i.e., bin-1), a thermal boundary-based condition is used to sort events into thermally favorable NOx reduction aftertreatment bin (i.e., Bin-1a) and

remainder bin (i.e., Bin-1b) that is dependent on the distribution of SCR inlet temperature ($T_{\text{SCR IN}}$) within each engine work producing event. Since the inlet temperature indicates sufficient gas temperature entering the catalyst, the parameter is selected to separate engine work-producing that may exhibit test activity that is favorable for the SCR system to reduce NO_x emissions (U.S. EPA, 2002). The measurements for $T_{\text{SCR IN}}$ are obtained from J1939 ECU broadcast (i.e., SPN: 4360). If the parameter is not broadcast from the CAN network, temperature measurements broadcasted from SPN: 3246 (i.e., DPF outlet temperature) are used for the data analysis presented in the study. The separation of events into Bin-1a (i.e., thermally stable SCR bin) is primarily based on the assumption that majority of event-based NO_x emissions rates (i.e., discussed in section 5.2.3) are below the current NTE in-use threshold (i.e., 0.45 g/bhp-hr for NO_x). The segregation of in-use activity based on SCR inlet temperature threshold provide an opportunity to specifically highlight a comparative discussion of NO_x emissions rates under test conditions that lead to active and non-active SCR operation. Specific to aftertreatment thermal conditions, the current NTE approach evaluates in-use test data only above 250 °C for EATS outlet temperature.

The ABW approach is significant as it allows categorization of various modes of in-use test activity (i.e., presented in Figure 42). The approach includes a dual-metric based emissions assessment comprising of conventional bs emissions units (i.e., g/bhp-hr) for all engine work producing activity (i.e., events produced in bin-1) and a duration-specific metric (i.e., g/hr) for all non-work/low power activity (i.e., Bin-2). The duration-specific metric is used for bin-2 primarily to avoid any asymptotic trend in bs emission rates while the engine experiences near-zero brake torque test activity.

Events that occur during an active DPF regeneration event (i.e., ECU data is equal to 2 for spn code: 3700) or an active on-board diagnostic malfunction indicator Lamp (i.e., ECU data is equal to 1 for spn code: 5096) are not evaluated for emissions and are shifted into a 'Report-only' bin. For test activity with respect to cold engine operating conditions, instantaneous data is weighted as a function of test activity

below 343 K(i.e., in-line with European in-use regulations). If any event experience test activity where ECT is below the desired threshold for more than 50% of the event-based duration, such events are not used for emissions assessment. For events that encounter a drift verification check of the analyzer, only valid data acquired while the periodic drift check is not active is used for emissions quantification.

4.2.3. Sensitivity Analysis

A parametric analysis is performed on the boundary parameters governing the ABW emissions binning approach to examine the influence of modifying the boundary thresholds on the distribution of NO_x emissions rates and time-weighted data utilization. JMP statistical software package was used to generate a design of experiments (DOE) based screening design test evaluation matrix. A screening response design generation approach was used to identify the principal elements influencing the process output. The software uses an iterative coordinate exchange algorithm to generate an optimized test design matrix.

The primary boundary conditions for the sensitivity analysis include minimum time duration for event generation (i.e., for Bin-1), T_{SCR IN} threshold to evaluate separation of dominantly active SCR operation versus non-active SCR operation (i.e., for Bin-1), and a minimum power threshold (i.e., for Bin-1) to separate tractive engine work producing operation versus low-power operational activity. One of the significant limitations associated with the NTE method is the minimum time threshold of valid engine operation in the NTE zone and associated exclusions. For example, in-use operation leading to frequent gear changes can potentially lead to activity drop-out of the NTE zone for a short period. Such drop-out events can result in terminating the NTE event early or discard the data accumulated if the minimum time is not met. The current ABW approach also incorporates a maximum drop-out duration threshold (i.e., to account for any rapid transition operation between Bin-1 and Bin-2 or vice versa). Table 12 shows the overall range of boundary parameters selected

for optimization of governing boundary parameter thresholds of the ABW binning structure.

Table 13 shows the out of the DOE test design matrix developed using JMP software. The primary goal of the parametric analysis was to examine the influence of $T_{SCR IN}$ (i.e., for a range of bin boundary conditions for minimum event-duration and power threshold for bin-1) on NO_x emissions rates for activity in bin-1a. Additionally, variation of bin-boundaries for event duration and power threshold were altered to determine the impact on bin membership-based data distribution.

Table 12: Range of boundary parameters selected for ABW sensitivity analysis

Boundary Parameter	Range of Boundary Parameter Thresholds
Bin-1 Minimum duration threshold [sec]	20, 30, and 40
Bin-1a Minimum $T_{SCR IN}$ threshold [°C]	190, 210, 230, and 250
Bin-1 Minimum power threshold [percent of engine maximum power]	10, 15, and 20

Table 13: DOE test design matrix for sensitivity analysis of ABW approach

DOE Iteration	Bin-1 Minimum Duration Limit	Bin-1 Minimum $T_{SCR IN}$ Limit	Bin-1 Minimum Power Threshold
1	40	230	20
2	20	230	15
3	30	190	15
4	40	210	15
5	20	250	15
6	40	250	10
7	30	250	20
8	30	210	20
9	20	190	20
10	30	230	10

11	20	210	10
12	40	190	10

Results from ABW binning approach are discussed in two separate phases, where phase-1 (i.e., discussion in section 5.2) will present the results of the parametric analysis and evaluation of the desired thresholds using in-use data collected in section 3.2 and phase-2 (i.e., discussion in section 5.3) will discuss results of data collected in section 3.3 using PAMS (i.e., in-fleet vocational activity collected using telemetry units in conjunction with additional tailpipe NO_x sensor).

4.3. Performance Evaluation of NO_x Sensors

While serving as an integral part for SCR control and on-board diagnostics (OBD), it is, therefore, essential to understand errors associated with the NO_x sensor reported measurements. Statistical techniques such as error propagation are used to interpret sensitivity of the measurement technique, associated errors and variability in the measurement compared to a conventional PEMS as a function of NO_x concentration. Furthermore, as outlined in the literature, it is inferred that the Zr-O₂ NO_x sensors are potentially cross-sensitive to other species in the exhaust gas. A statistical PCA analysis was used to identify potential elements in the exhaust gas that may interfere with the accuracy of the sensor measurement. In-use data collected from Vehicle-A and D in section 3.2 is used to evaluate the performance of the on-board NO_x sensor.

4.3.1. Principal Component Analysis

PCA is a non-parametric statistical approach (i.e., a least-squares method) used to analyze multi-dimensional data. The fundamental concept of the approach is to reduce the dimensionality of quantitative variables while retaining variation associated with the respective parameter by a linear transformation of the original data into a set of principal components. The method projects observations from a p-dimensional space with p variables to a k-dimensional space (where $k < p$). The data mining approach provides ease in gathering information from a large dataset. The observations from PCA summarize in identifying uniform or a typical group of

observations and provide an analogy of correlated and uncorrelated components (Abdi and Williams, 2010).

The primary step of PCA is to identify parameters of interest for evaluation and to create a data matrix, i.e., corresponding to an $n \times k$ matrix where n is the number of the samples and k is the coefficient associated with each parameter of interest.

$$X = \begin{bmatrix} x_{11} & \cdots & x_{1k} \\ \vdots & \ddots & \vdots \\ x_{n1} & \cdots & x_{nk} \end{bmatrix} \quad \text{Equation 4.41}$$

A deviation matrix (D) is generated by subtracting each data point in the matrix from the mean of the associated parameter. Furthermore, since each of parameter (i.e., column vector) comprises of an individual unit of measure, the entire matrix D is normalized such that each parameter has a cumulative variance equal to 1. The normalized covariance matrix is generated as follow:

$$P = \frac{D.D^T}{n} \quad \text{Equation 4.42}$$

$$P = \begin{bmatrix} c_{11} & \cdots & c_{1k} \\ \vdots & \ddots & \vdots \\ c_{n1} & \cdots & c_{nk} \end{bmatrix} \quad \text{Equation 4.43}$$

$$c_{ij} = \frac{1}{n \{(x_i - \bar{X}_i).(x_i - \bar{X}_j)\}} \quad \text{Equation 4.44}$$

$$c_{ij} = \frac{c_{ij}}{\sqrt{(\text{Var}(i)).(\text{Var}(j))}} \quad \text{Equation 4.45}$$

Where, T represents transpose,

i is the row element,

j is the column element

The normalized correlation matrix defines both the spread (i.e., variance) and the position/orientation of the entire dataset. Further, the matrix is converted into a diagonal set of elements that is used to identify the eigenvectors representing the direction and magnitude of each parameter and is presented in the following equations.

$$P \cdot \vec{v}_1 = \lambda_1 \vec{v}_1 \quad \text{Equation 4.46}$$

$$(P - \lambda_1 I) \cdot \vec{v}_1 = 0 \quad \text{Equation 4.47}$$

$$\text{Det. } (P - \lambda_1 I) = 0 \quad \text{Equation 4.48}$$

Where, λ_i is the eigenvalue

I is the identity matrix

\vec{v}_1 is the corresponding eigenvector

Quantifying parameters from the resultant matrix in equation 4.8 transforms into a set of eigenvalues and orthogonal eigenvectors. The approach generates a correlation matrix, and the matrix undergoes eigen decomposition using a singular value decomposition algorithm. Therefore, resulting in a sequence of rotational and scaling operations on the original dataset. The eigenvalue represents the associated variance, and the eigenvector represents the direction of the variance. The steps mentioned above are presented in equations 4.9 to 4.12.

$$PV = LV \quad \text{Equation 4.49}$$

$$PV - LV = 0 \quad \text{Equation 4.50}$$

$$PV - VL = 0 \quad \text{Equation 4.51}$$

$$P = VL V^{-1} \quad \text{Equation 4.52}$$

Where V represents the rotational matrix,

L represents the scaling matrix

To identify the principal component (PC), the original dataset, i.e., X is transformed into a new matrix Z (i.e., corresponding principal components). The PC_i corresponds to a mean value of 0 and variance of λ_i (i.e., the eigenvalue).

$$Z = V^T(x - \bar{X}) \quad \text{Equation 4.53}$$

$$z_{ni} = v_{ni}(x_{1i} - \bar{X}_1) + \dots + v_{nk}(x_{ki} - \bar{X}_k) \quad \text{Equation 4.54}$$

Where x is the column vector of the individual parameter in X

\bar{X} is the mean of the corresponding variable parameter

z_{ni} is the estimated score for i^{th} variable on the n^{th} principal component

The projected z_{ni} score for each variable represents the direction and length of the associated vector, therefore indicating the contribution of each variable to the corresponding principal component in matrix “ Z ” (Jolliffe, 2002).

5. Results and Discussion

This chapter discusses the results obtained of the specific tasks performed to achieve the global objective of the study. The data-driven analysis discussed in section 5.1 presents an overview of NTE and WBW in-use emissions evaluation approaches. The latter is of specific importance with regards to regulatory interest in evaluating the feasibility of MAW approach to determine in-use emissions compliance. Evaluation of ABW binning approach is divided into two sections, i.e., Phase-1 (discussed in section 5.2) provides a detailed overview of the binning procedure, sensitivity analysis of the method-based boundary parameters and evaluation of the approach on real-world test activity on custom vocational duty cycles using a 1065 compliant PEMS. Phase-2 of the ABW results discussed in section 5.3 demonstrates the application of ABW approach on in-fleet vocational activity collected using on-board telemetry-based ECU data logging systems in conjunction with additional tailpipe NO_x sensors. In light of potential elements of utilizing on-board NO_x sensors as a cost-effective alternative for in-fleet acquisition, section 5.4 investigates measurement thresholds associated with sensor reported measurements in comparison with a laboratory-grade PEMS during real-world driving conditions.

5.1. Analysis of In-use Emissions Quantification Methods

This section will discuss analysis with respect to in-use emissions quantification approaches used in the U.S. and Europe to determine in-service emissions compliance (i.e., NTE and WBW). This specific task was performed to gain an in-depth understanding of the metric performance on NO_x emissions characteristics. With respect to the NTE approach, this task examines the influence of expanding boundary conditions. The analysis was performed on test activity collected using a PEMS as part of the engine manufacturer-run HDIUT program to evaluate the effectiveness of the metric-based boundary conditions.

5.1.1. Vehicle Activity Characteristics

Figure 43 summarizes the time-weighted instantaneous vehicle speed distribution of all 75 HDIUT datasets used in this study. The instantaneous bins were classified into four different vehicle speed bins to understand the spread of vehicle activity. The test activity was characterized into (i) Idle (i.e., no vehicle movement), (ii) ‘Urban driving’ characterized by vehicle speeds up to 50 kmph (i.e., ~31.1 mph); (iii) ‘Rural driving’ characterized by vehicle speeds between 50 kmph and 75 kmph (i.e., ~46.6 mph); and ‘Highway driving’ characterized by vehicle speeds above 75 kmph. The three-vehicle speed bins selected for the herein presented analysis were selected based on requirements prescribed by EU 582 guidelines for in-service conformity testing. Two additional bins were selected to quantify the overall percentage of test activity spent during engine-off conditions and PEMS periodic analyzer zero/span events. Table 14 summarizes the mean and standard deviations of the time-weighted in-use test activity as a function of engine power and vehicle speed-based distribution for the entire dataset and test activity specific to tractive engine work producing activity. The engine power operation is divided into three different operational bins, (i) Low power operation characterized by engine power distribution below 30% of P_{max}, (ii)

Medium power operation characterized by engine power distribution between 30% and 60% of Pmax, and (iii) High power operation characterized by engine power distribution above 60% of Pmax.

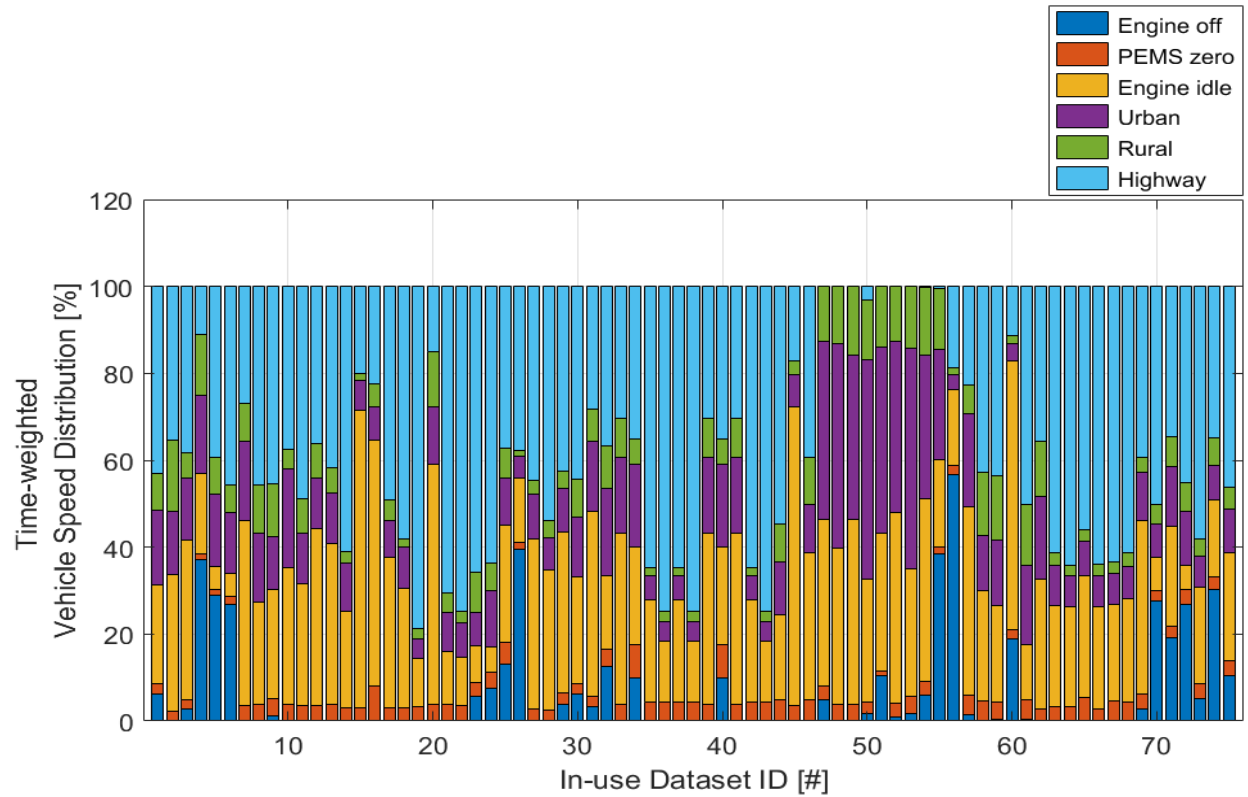


Figure 43: Time-weighted vehicle speed distribution of 75 HDIUT in-use datasets

Table 14: Time-weighted average and standard deviation for engine power and vehicle speed distribution of 75 HDIUT datasets

	Mean: μ [%]		Standard Deviation: σ [%]	
	Entire Dataset	Only TW ¹	Entire Dataset	Only TW ¹
Engine off	6.40		11.88	
PEMS Zero check	3.51		1.28	
Engine idle	28.03		14.0	
Vehicle Speed Binning				
Urban driving	14.93	25.68	11.09	19.83
Rural driving	7.17	12.23	4.49	8.28
Highway driving	39.96	62.09	21.72	26.70
Engine Power Binning				
Low power	29.48	48.34	10.15	14.62
Medium power	21.43	33.83	12.63	16.15

High power	11.15	17.84	8.14	11.51
------------	-------	-------	------	-------

1) TW-tractive engine work

The time-weighted (TW) vehicle speed and engine power binning depict a general overview of the vehicle activity patterns of the entire dataset. While considering all vehicle operational modes, the idle bin accounts for ~28% of the entire test activity collected. It is evident that highway driving operation accounts for the most significant amount of time spent during in-use operation (i.e., on average 39.96% considering all vehicle operational modes and 62.09% while considering only TW producing activity). Out of the 75 in-use datasets, nine datasets were from transit buses application, therefore specific to these in-use datasets, the time-weighted average distribution resulted in 73.41%, 25.89%, and 0.70% for urban, rural, and highway driving operation, respectively, during tractive engine work producing activity. Additionally, these vehicle datasets spent 66.98% of TW producing activity experiencing operation below 30% of rated power. On average for all the in-use datasets combined, low power operational bin accounts for the majority of test activity captured (i.e., ~48.34% for TW activity). This is particularly of great importance with regards to NTE compliance evaluation because one of the parameters governing NTE control area is the engine power threshold (i.e., engine operating conditions at or above 30% of Pmax) (CFR/40/86/1370). Additionally, WBW method also excludes windows whose average power threshold is less than 20% of Pmax as per EU VI (c) regulatory guidelines (EU/582,2011).

5.1.2. NTE Analysis

This section of the results discusses a detailed overview of the analysis performed on the HDIUT in-use datasets using NTE methodology as required and outlined in (CFR/40/86/1370). In addition to the default NTE boundary parameter settings, two additional test case scenarios as described in Table 10 were also analyzed. The experimental boundary conditions were evaluated to identify the potential impact of modifying boundary parameter settings on time-weighted event averaged data acquired for emissions assessment and its associated impact on NO_x emissions.

Before evaluating the test case scenarios, each parameter associated with the NTE exclusion criteria as outlined in section 2.7.1.2 was examined to understand the overall impact of the contribution of individual method-based boundary parameters towards invalidation of the NTE event. Figure 44 displays the box and whisker distribution of NTE event invalidation due to individual method-based boundary parameters as per current NTE exclusion boundary thresholds. The box represents the 25th and 75th percentile (i.e., blue box), and the whiskers represent the 10th and 90th percentile of the entire data distribution. The percentile distribution is based on the assumption that the data presented is normally distributed. Also, symbols (+) and (-) depict the mean and median of the distribution. For the data presented further in this study, the definitions mentioned above are valid for all box and whisker distribution charts.

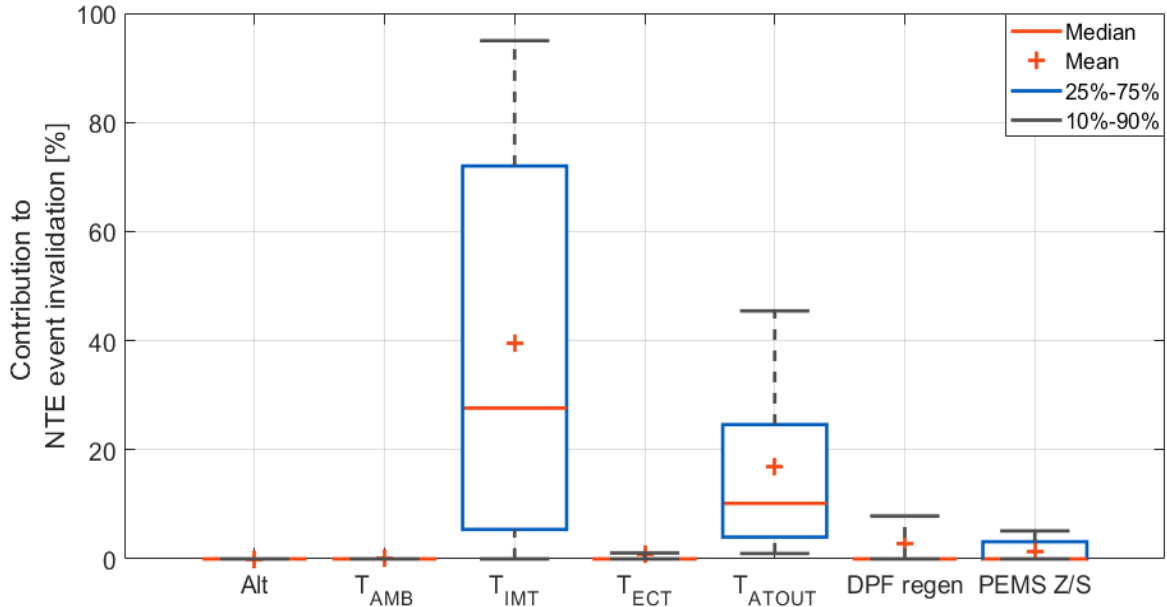


Figure 44: Contribution of individual exclusions towards NTE event invalidation

Table 15: Comparison of mean exclusion contribution (i.e., in percentage) towards NTE event invalidation

Alt	T _{AMB}	T _{IMT}	T _{ECT}	T _{ATOUT}	DPF regen	PEMS Z/S
0.0	0.03	39.63	0.77	16.98	2.72	1.46

The results of the analysis show that IMT and T_{ATOUT} exclusions are the most dominant NTE exclusions. An average of 39.63% and 16.98% of NTE events were invalidated due to the exclusions mentioned above, respectively. The IMT exclusion was initially incorporated in the NTE metric to avoid evaluation of test activity under cold EGR operating conditions that potentially limits the EGR performance (Kappanna, 2015; Warey et al., 2013). It is to be noted that this exclusion was introduced for engines prior to SCR technology (i.e., pre-2010 MY engines) and was carried forward for modern diesel engines as well. Since the introduction of U.S.EPA 2010 emissions standards, an additional exclusion based on T_{AT-OUT} was introduced. It is quite evident that NTE evaluation for in-service compliance is dependent on T_{ATOUT} threshold, therefore resulting in evaluation of in-use emissions compliance only under test conditions that are significantly favorable for the SCR system to reduce NO_x emissions efficiently.

Table 16 and Figure 45 present the results of the three different NTE case scenarios evaluated. The analysis indicates that evaluation of current NTE boundary conditions resulted in an overall average of 8.45% and 6.61% of test data utilization and NO_x mass fraction, respectively. The modification of boundary parameter thresholds as per ‘Modified NTE case-1’ results in an average increase of 88.13% for time-weighted data utilization compared to the default NTE boundary thresholds. Simultaneously, total NO_x mass coverage increased by 132.60%, and the overall VPR decreased from an average of 0.95 to 0.90 for default NTE boundary conditions and Modified NTE case-1, respectively.

Table 16: Comparison of NTE event characteristics for the three different NTE test cases

Parameter	Default NTE	Modified NTE	
		Case-1	Case-2
Number of events [#]	45 ± 52	81 ± 66	92 ± 54
NTE event duration [%]	8.45 ± 9.22	15.90 ± 13.37	26.67 ± 16.50
NTE NO _x mass fraction [%]	6.61 ± 8.80	15.37 ± 13.91	21.22 ± 15.66
Event-averaged bsNO _x emissions [g/bhp-hr]	0.16 ± 0.24	0.19 ± 0.26	0.19 ± 0.25
VPR [-]	0.95 ± 0.16	0.90 ± 0.24	0.91 ± 0.19

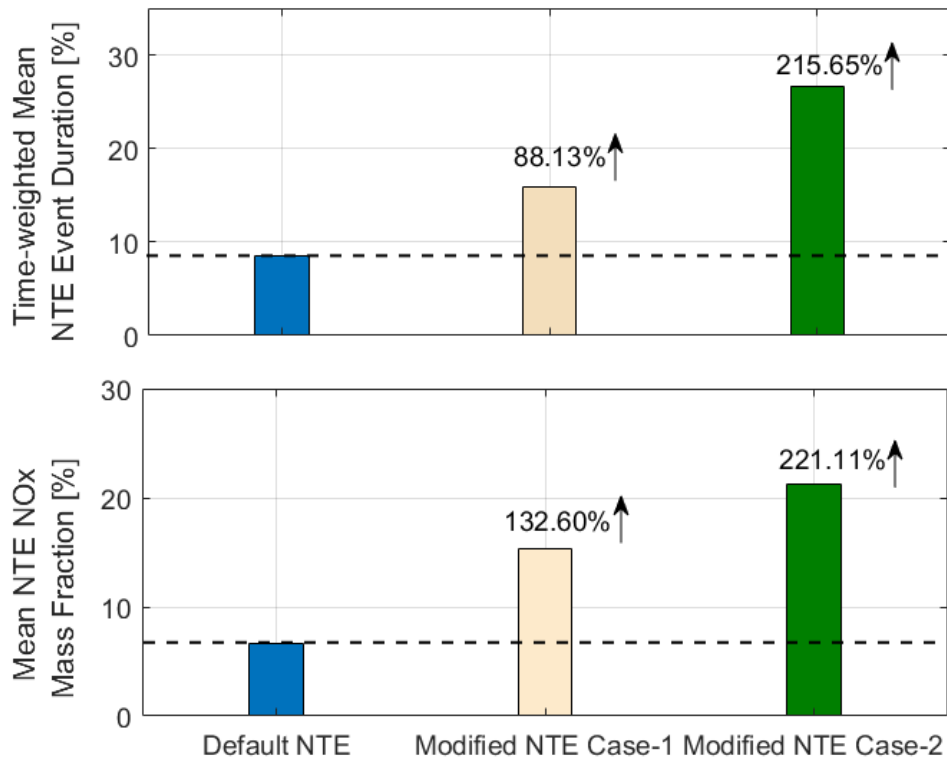


Figure 45: Comparison of (a) Top graph: Time-weighted NTE event duration and (b) Bottom graph: NTE NOx mass fraction for three different NTE test cases

As anticipated, results from ‘Modified NTE case-2’ exhibited the highest increase in the overall average number of NTE events, event duration, and NOx mass fraction. The results show an average increase of 215.65% and 221.11% for the overall average time spent in the NTE events and NOx mass fraction, respectively, compared to default NTE thresholds. This is primarily due to expansion of the NTE control area and elimination/lowering governing NTE exclusions. The test case scenario mentioned above, therefore, exhibits a potential of achieving an increase in the time-weighted utilization of test activity while demonstrating event average bsNOx emissions levels and VPR similar to that of Modified NTE case 1. The significant increase in the overall event averaged duration is primarily due to the elimination of the IMT threshold. The analysis shows that elimination of IMT threshold in conjunction with the modification of boundary conditions (i.e., as per Modified NTE case-1 and 2) results in an overall average increase in bsNOx emission of 0.03 g/bhp-

hr for NO_x emissions. The experimental evaluation on modifying the boundary conditions shows that expansion of NTE control area and modifying boundary thresholds results in an increase in data utilization compared to the current boundary thresholds, a substantial amount of test activity is still not considered for in-service compliance verification. The most significant increase in time-weighted data utilization was observed from Modified NTE case 2, but on average, 73.33% of entire test activity was not utilized for emissions compliance assessment using the NTE protocol.

5.1.3. WBW Analysis

This section outlines the analysis of HDIUT datasets performed using WBW emissions evaluation protocol, as discussed in section 2.7.2. The WBW method uses a continuous moving-average window approach to evaluate real-world emissions within each segment of the test activity. The reference engine work for each vehicle dataset was quantified by simulating the engine lug curve over the certification test cycle (i.e., FTP). The simulated FTP engine work for the 75 HDIUT datasets ranges from 15.12 bhp-hr to 40.97 bhp-hr. Figure 46 shows a comparison of time-weighted in-use data utilization using the WBW metric on the HDIUT datasets. On average, 79.26% of the entire test activity was utilized to generate WBW across the entire test activity. Emissions compliance is explicitly evaluated for windows that satisfy the minimum average window power requirements. Table 11 in section 4.1.2 outlines the minimum window averaged power thresholds implemented on the test datasets as per EU VI (c) and EU VI (d) regulations (i.e., 10% of P_{max} and step by step reduction from 20 to 15% of P_{max} until the ratio of valid WBW's over total WBW's is greater than 0.50, respectively). The low power operational windows are excluded from in-service compliance evaluation to avoid evaluation of windows that that experience challenging NO_x control operational modes (Bonnell et al., 2011). Implementing the minimum power threshold to generate valid WBW's resulted in an average data utilization of 61.76% and 75.55% for EU VI (c) and EU VI (d) thresholds, respectively. This resulted in an averaged increase of 53.31%, and 67.1% of time-weighted data

utilization compared to the NTE methodology as per the current regulatory boundary conditions (i.e., discussed in section 5.1.2) for the 75 HDIUT datasets.

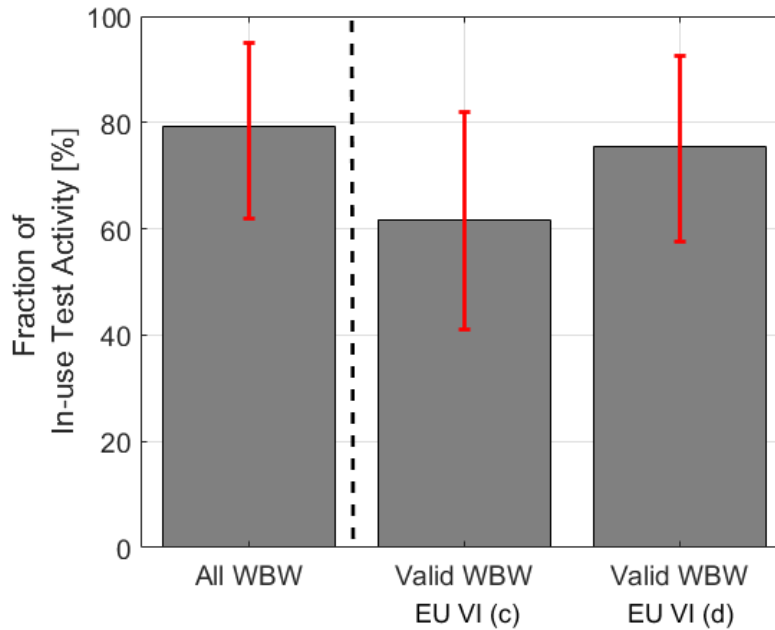


Figure 46: Time-weighted data utilization for (a) All WBW’s generated, and (b) Valid WBW’s generated as per of EU VI (c) and EU VI (d) power cut-off thresholds

Figure 47 illustrates a box and whisker comparison of bsNO_x emissions for all valid WBW’s generated as per EU VI (c) and EU VI (d) power thresholds (i.e., top graph and bottom graph respectively) for the 75 HDIUT datasets as a function of window percentile. It has to be emphasized that the European regulations implement the WBW emissions evaluation procedure for verification of in-service compliance on test activity collected on a predefined route-based statistic requirement comprising of a sequence and vehicle activity operation of urban, rural and highway driving conditions. In addition to the HDIUT datasets, the 90th percentile of WBW results for test activity acquired on the ISC route is presented to provide a comparison of emissions results of in-fleet operation versus predefined route operation. A detailed overview of the test route, dataset characteristics and vehicle specification is discussed in section 3.2.1 and 5.2.1.

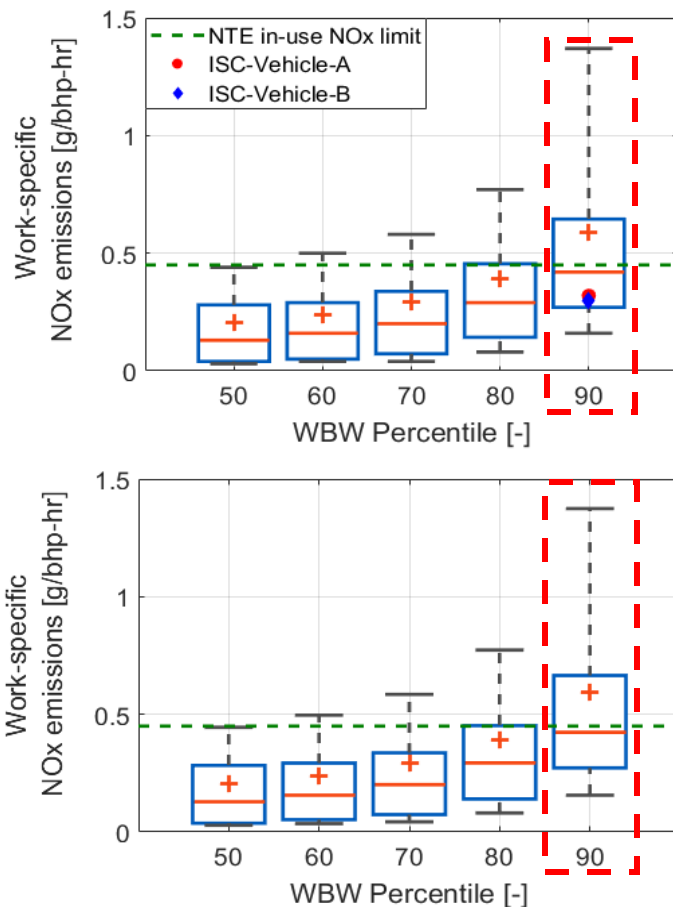


Figure 47: WBW percentile comparison of bsNOx emissions for valid work-windows generated as per (a) Top graph: EU VI (c) based power cut-off threshold, and (b) Bottom graph: EU VI (d) based power cut-off threshold

Emissions compliance assessment in Europe is determined by evaluating the 90th percentile of the valid WBW results (i.e., the ratio of bsNOx emissions results of the of valid WBW corresponding to the 90th percentile scaled over the certification limit to be below 1.5 to pass compliance) (EU 582,2011). The CARB white paper expressed interest in the implementation of a similar evaluation approach as EU regulations on emissions test activity acquired from the actual in-fleet operation. Results from the analysis presented in Figure 47 shows that the 90th percentile of bsNOx emissions demonstrates significant variability (i.e., dependent on vocational route-based activity). The emissions results vary from 0.15 to 1.30 g/bhp-hr, and 0.22 to 1.58 g/bhp-hr for the 10th and 90th percentile of the distribution for valid WBW's generated as per EU VI (c) and EU VI (d) power cut-off threshold respectively for the 75 HDIUT

datasets. Since modern diesel engines are dependent on the SCR technology for NOx reduction, windows comprising of a combination of operation of both active and non-active SCR operation, therefore, results in relatively higher bsNOx emissions depending on the duty cycle performance and in-cylinder NOx emissions reduction strategies.

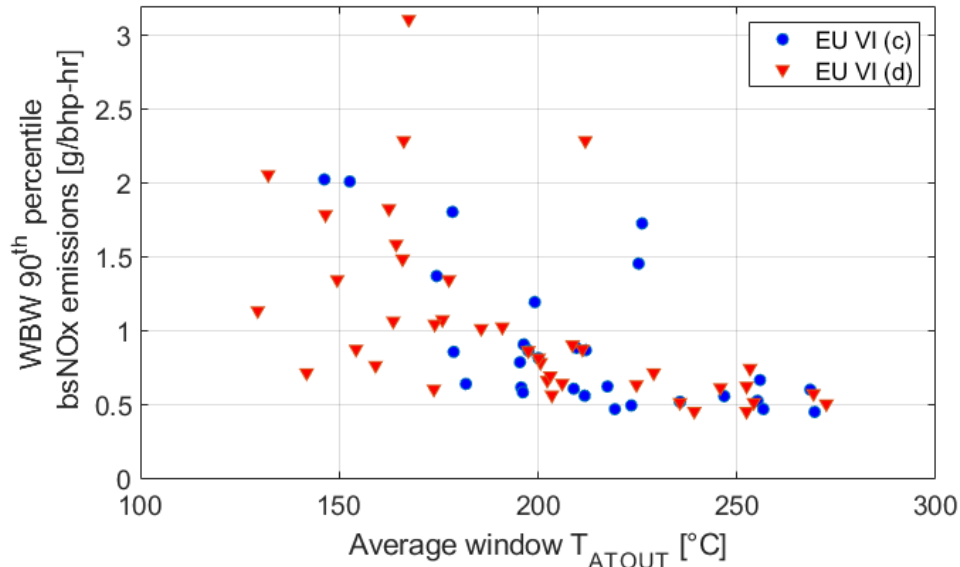


Figure 48: Comparison of window averaged $T_{SCR\ OUT}$ and bsNOx emissions of valid WBW's

Figure 48 depicts a comparison of window averaged bsNOx emissions and $T_{AT\ OUT}$ of the 90th percentile of valid WBW's whose bsNOx emissions were above 0.45 g/bhp-hr (i.e., current in-use limit) for NOx emissions. The overall trend of the results presented is as expected with reference to SCR performance and activation (i.e., catalyst light-off temperature) which is dependent on the exhaust gas thermal conditions.

5.2. Evaluation of ABW - Phase 1

This section describes the development and validation of the analytical ABW approach to characterize real-world emissions levels from modern HD diesel trucks. This subset of results presents the data analysis performed using the ABW binning approach. Furthermore, in-use emissions data collected from multiple HD trucks on vocational test routes (i.e., discussed in section 3.2) will be used to develop and evaluate the data-driven thresholds for the ABW approach.

5.2.1. Vehicle Activity Characteristics

This section will briefly discuss vehicle activity characteristics of the four distinctive test routes used to develop and validate the thresholds of the ABW binning approach. Details of the test vehicles and routes are presented in section 3.2.1. Table 17 shows a general overview of the average test duration and distance for each of the test route.

Table 17: Average test duration and distance for each of the test routes

Route ID	Test Duration	Test Distance
[#]	[hr]	[miles]
1	5.37	251.70
2	2.87	84.56
3	5.89	160.52
4	6.43	180.12

Figure 49 presents a time-weighted overview of the vehicle speed distribution for all of the datasets used for evaluation of the ABW binning approach. In Figure 49 and Figure 50, ‘R’ represents the route identification number (ID) and ‘L’ represents the operational leg/segment ID. The instantaneous data was sorted into four different vehicle speed bins, i.e., (i) ‘Idle’ characterized by vehicle speed less than 1.5 kmph, (ii) ‘Urban driving’ characterized by vehicle speed between 1.5 kmph up to 50 kmph (i.e. ~31.1mph); (iii) ‘Rural driving’ characterized by vehicle speed between 50 kmph up to 75 kmph (i.e., ~ 46.6 mph); (iv) ‘Highway driving’ characterized by vehicle speed above 75kmph.

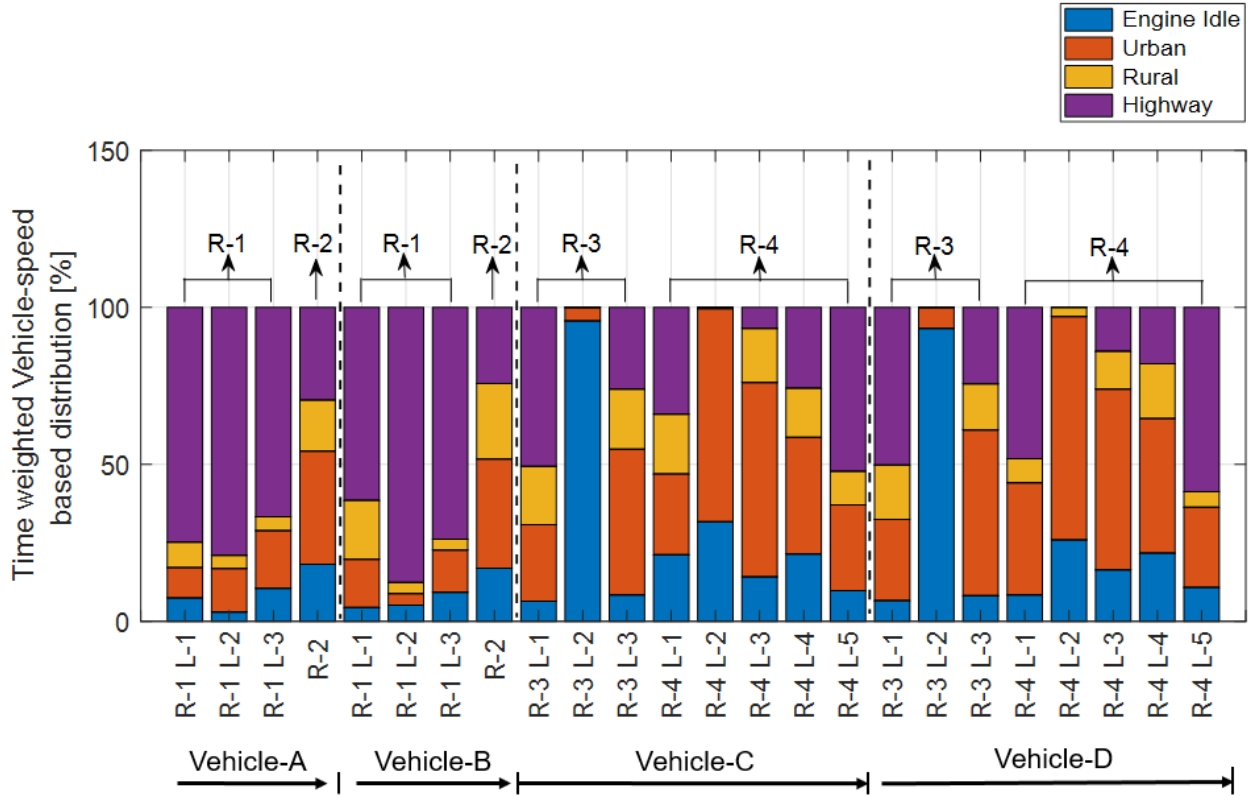


Figure 49: Time-weighted vehicle speed distribution of all in-use datasets sampled in section 3.2

Table 18: Route-averaged engine power distribution for in-use datasets collected in section 3.2

Route ID	Low Power	Medium Power	High Power
[-]	[%]		
1	51.51	15.41	33.08
2	65.79	15.46	18.75
3	76.41	11.31	12.28
4	72.45	12.49	15.05

Table 18 summarizes average time-weighted engine power distribution for each of the entire test routes that are split into three different engine operational power bins as defined in section 5.1.1. Similarly, Figure 50 presents a time-weighted distribution of SCR inlet temperature for all the datasets in this section. The SCR inlet temperature was distributed into five different temperature bins (i) $T_{SCR\ IN}$ is below 100 °C, (ii) $T_{SCR\ IN}$ is between 100 and 180°C, (iii) $T_{SCR\ IN}$ is between 180 and 250 °C, (iv) $T_{SCR\ IN}$ is between 250 and 400 °C, and (v) $T_{SCR\ IN}$ is above 450 °C. Although, not

a direct comparison with vehicle speed/engine power distribution, $T_{SCR IN}$ based distribution provides a general understanding of the thermal conditions experienced by the EATS for each of the unique set of test routes.

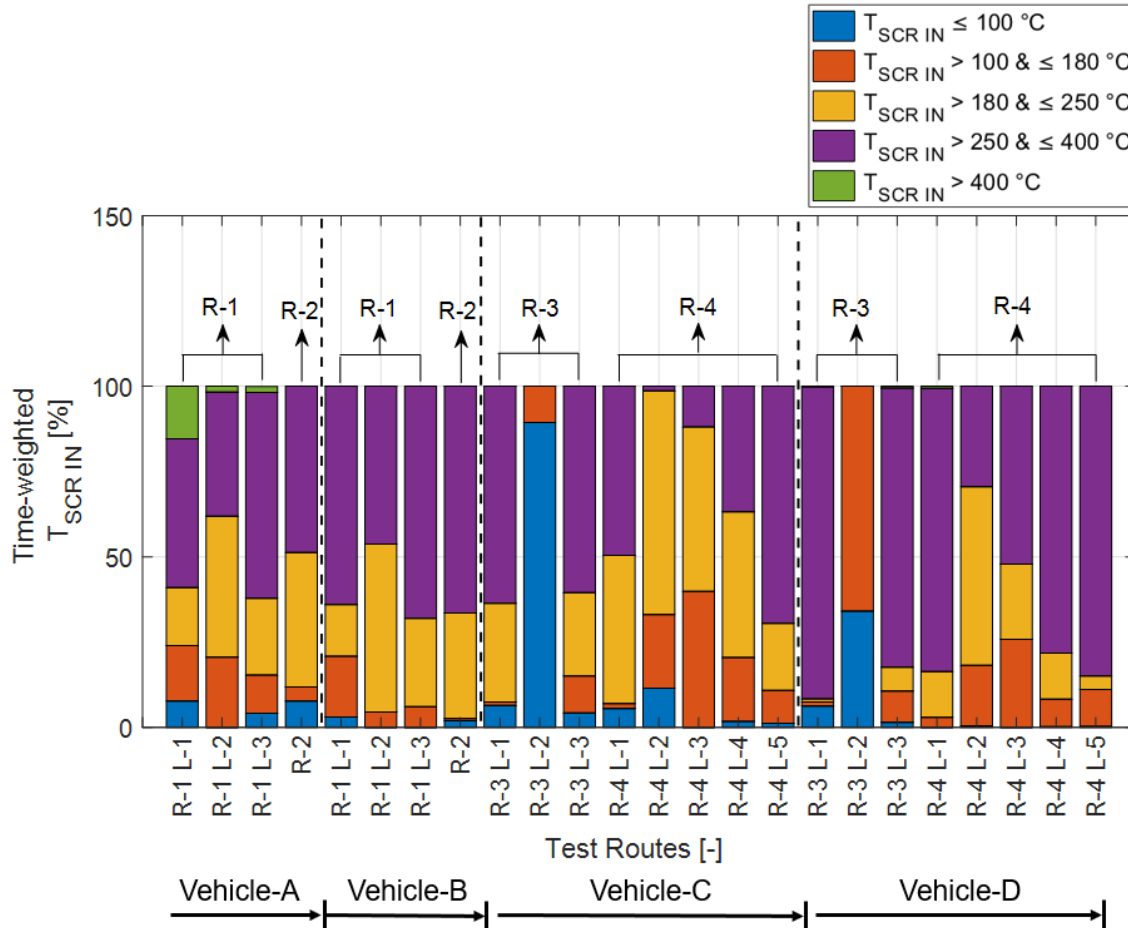


Figure 50: Time-weighted $T_{SCR IN}$ distribution of all in-use datasets sampled in section 3.2

'Route-1,' i.e., highway hill climb route operated on vehicle A, and B shows that on average, 74% operational time comprised of highway driving operation. In conjunction with engine power distribution, the test route experienced 33.08% of the operational time during high power engine operation, therefore resulting in vehicle operation for this specific test route with dominant time fraction of highway driving operation with notable changes in road grade. 'Route-2' (i.e., ISC test route) comprised of a sequence of vehicle speed-based operation, i.e., urban, rural and highway driving operation. The instantaneous vehicle speed-based binning shows

that the test route on average spent 17.58%, 35.39%, 20.15% and 26.88% of the entire operational time in idle, rural, urban, and highway driving operation, respectively. Although, this specific test includes a time-weighted distribution of test activity as a function of the sequence of route-based operation. The regulatory requirements as per EU 582 for the ISC test requires the in-use test to include 30%, 25% and 45% for urban, rural and highway driving segments characterized by vehicle speed (EU 582,2011). Vehicle-A met the requirements of the ISC test requirements, and the corresponding route-based statistics of route-2 are 30%, 20% and 50% of the time-weighted activity for urban, rural and highway driving segments of the in-use test, respectively. The ISC test presented in this study for vehicle-B was aborted in the highway operational segment due to technical issues. It, therefore, did not meet the route-based statistic requirement as per EU VI (d) route-statistic requirements. The test route statistics for vehicle-B of the ISC route is 27.3%, 36.57%, and 36.10% for the sequence of urban, rural and highway driving operation, respectively.

'Route-3' included vocational operation replicating vehicle activity of trucks operating to and from the port of Long Beach. Leg-1 and 3 represent vehicle activity operating along the freeway to and from the port harbour. On average, Leg-1 of route-3 included dominant amount of highway driving operation, i.e., 50.36% of the total operational time, while segment-3 experienced dominant amount of vehicle activity in urban driving operation (i.e., 49.60%). This is primarily due to dense traffic on the freeway near Long Beach, CA. Leg-2 of the test included simulation of vehicle activity in the port harbour. As the route/test cycle included extended engine idle operation followed by creep operation, the total test resulted in 94.53% of the test time where the vehicle speed was below 1.5 kmph (0.93 mph).

'Route-4,' i.e., the grocery distribution route is split into five different operational segments. Leg-1 and 5 exhibit a significant amount of highway driving operation, i.e., 41.09% and 55% of the operational time. Leg-2 and 3 operate along US 110S and demonstrates a significant amount of operational time spent in low vehicle speed operation, i.e., urban driving segments (i.e., on average 69.42% and 59.75%

respectively) due to traffic encountered on the freeway. It is essential to highlight that these test routes also experienced frequent stop and go activity. In summary, both route-3 and 4 depict significant amount of operational time fraction (i.e., 76.4% and 72.45% respectively) in low power operational mode (i.e., less than 30% of Pmax). Although not a direct comparison of data presented in Figure 49 and Figure 50 , in general, test activity that experienced a significant amount of time fraction of rural and highway driving operation exhibit relatively higher operational activity where $T_{SCR IN}$ was above 180 °C.

5.2.2. Explanation of ABW Approach

This section presents a detailed explanation of the calculation procedures and bin-specific emissions results associated with the ABW approach. This section is discussed before the sensitivity analysis to provide the reader with a step-by-step overview of the ABW emissions assessment protocol. This is completed a step earlier to better interpret the results associated with sensitivity analysis discussed in section 5.2.3. Additionally, results presented in this section will discuss the metric-based comparison between NTE, WBW and ABW binning approach. Test activity acquired from vehicle-A operated on route-2 is presented in this section of the results. Details regarding test vehicle, experimental setup and test route are discussed in section 3.2, as well as route-based characteristics are discussed in section 5.2.1.

The reference parameter (i.e., total engine work generated over a certification cycle) for window generation was quantified by de-normalizing the FTP cycle using data obtained from the engine torque curve. The denormalization procedure as prescribed in (CFR/40/1065/610) was used to generate a simulated version of the engine speed and torque setpoints of the FTP test cycle. The engine work derived from the quantified engine power for the entire test cycle and the summation of engine work represents the reference parameter for the ABW binning approach. Equation 5.1 depicts the quantification of instantaneous engine work derived from engine power (i.e., in equation 2.20).

$$\text{Engine work [bhp - hr]} = \frac{\text{Engine power [bhp]} \cdot 1[\text{hr}]}{3600}$$

Equation 5.55

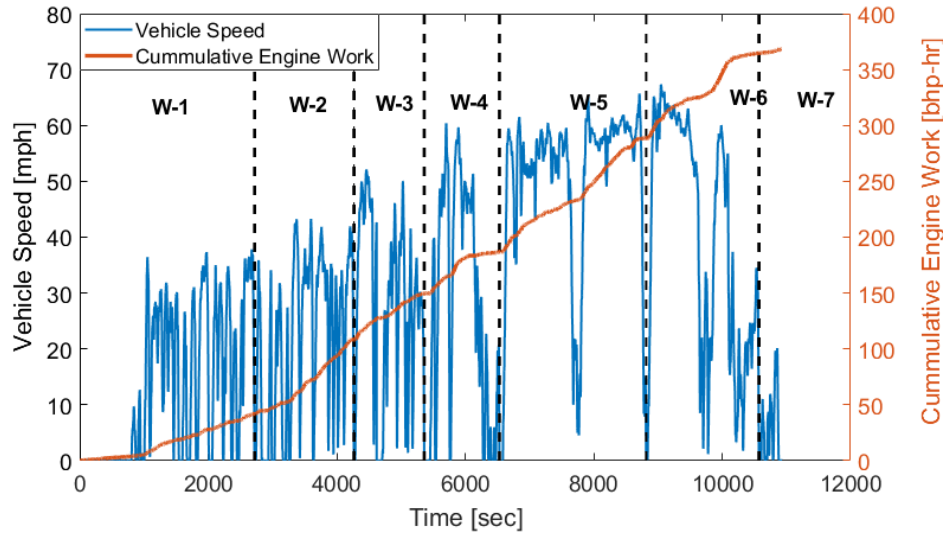


Figure 51: Description of theoretical window generation for Route-2 evaluated on vehicle A

Figure 51 presents a comparison of vehicle speed profile and cumulative engine work for the entire in-use test (i.e., route-2) used to generate the ABW's. In the figure, 'W' represents the ABW sequential ID. For this particular test, seven ABW's were generated as a function of the cumulative engine work. As described in section 4.2.1, the window generation process is not a continuous MAW. If the reference threshold was met while the vehicle is experiencing a transient activity, data point aggregation continues until vehicle speed reaches "0" mph. Therefore, each window may comprise a non-uniform distribution of engine work, as described in Table 19. The window generation process provides a unique opportunity to evaluate individual segments of test activity (i.e., treated as an individual duty cycle). All windows generated for route-2 exhibit total window engine work to be above the desired reference threshold, except for window-7. The ABW binning approach allows the generation of a window that is less than the reference threshold only under circumstances where the in-use test has already generated at least 1 ABW satisfying the theoretical window generation requirements. Since, the purpose of window generation is solely to isolate and evaluate individual segments of test activity, case scenarios such as generation

of W-7 are captured to evaluate in-use emissions from the final segment of test activity.

Table 19: Overview of window start and end duration, and total engine work for all seven windows generated for route two evaluated on vehicle A

ABW	Window T _{Start}	Window T _{End}	Engine Work
[-]	[sec]	[sec]	[bhp-hr]
1	1	2722	41.99
2	2723	4269	66.40
3	4270	5363	41.08
4	5364	6534	37.60
5	6535	8818	101.62
6	8819	10,574	75.41
7	10,575	10,931	3.27

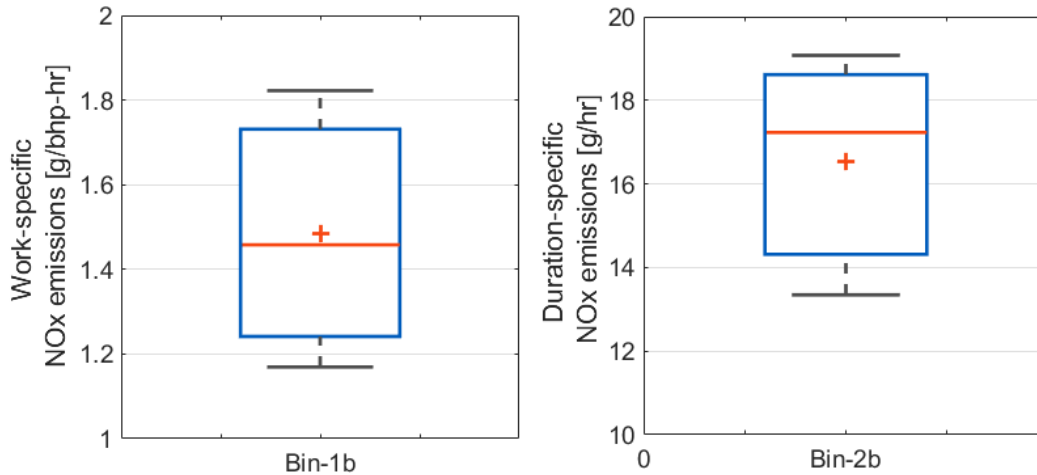


Figure 52: Comparison of NOx emissions during cold engine operating conditions for events generated in bin-1b and bin-2b

The ABW binning approach generates events as a function of continuous segments of in-use test activity within each window. For the analysis presented in this section of the results, the thresholds used for event generation and segregation are 20 seconds, 10 seconds, 230 °C and 10% of rated power for minimum event duration for bin-1, drop-out time and minimum event duration for bin-2, T_{SCR IN} threshold for separation

of events generated under bin-1 into bin-1a and bin-1b, and engine power threshold used to separate events into bin-1 and bin-2, respectively. The thresholds are procured from a data-driven analysis that is discussed in section 5.2.3.

Window-1 includes six events (i.e., Bin-1b (3 events) and Bin-2b (3 events) that experienced test activity under cold engine operating conditions. Due to the cold engine operating conditions, such events are excluded from global ABW emissions analysis. This is because it is difficult for the engine to control emissions rates under cold operating conditions due to combustion instability, i.e., due to the combination of cold intake air and incomplete atomization of fuel molecules (Ramadhas et al., 2017). Figure 52 illustrates the box and whisker distribution of the events generated under cold operating conditions in window 1. On average, bsNO_x emissions during cold engine operating conditions resulted in 1.48 g/bhp-hr and 16.55 g/hr for events generated in bin-1b and bin-2b, respectively. For events generated in bin-1b, the spread of the distribution varies from 1.16 to 1.82 g/bhp-hr respectively for the 10th and 90th percentile of the distribution.

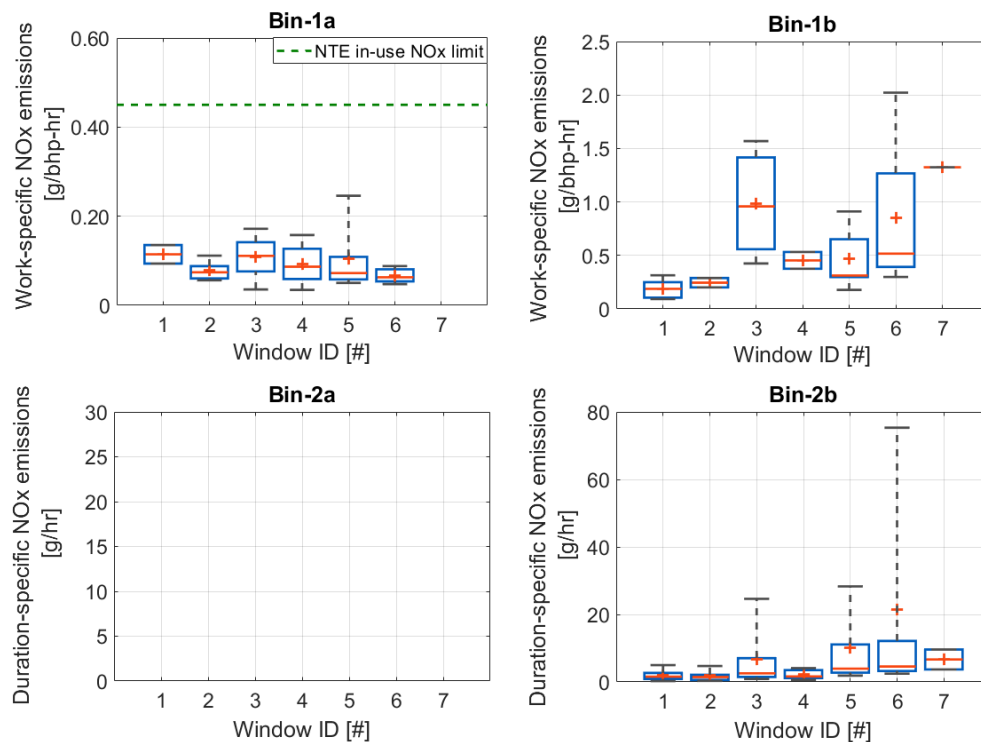


Figure 53: ABW summary of results for vehicle-A operated on route-2

Figure 53 presents the distribution of events generated within each ABW for the four different bin categories. Specific to bin-1a, i.e., all events generated in the 7 ABW's are below the current in-use bsNOx limit (i.e., 0.45 g/bhp-hr). The average bsNOx emissions of the 75th percentile of events generated in each ABW is 0.11 g/bhp-hr. This is because the events generated in bin-1a experienced favourable exhaust gas thermal conditions, therefore translating to a substantial decrease in tailpipe NOx emissions rates (i.e., primarily due to active SCR operation). For events generated in bin-1b whose bsNOx emissions are below 0.45g/bhp-hr, these events comprise of test activity where $T_{SCR IN}$ was below bin-1a threshold only for a fraction of test activity accumulated within the event. The majority of events generated in ABW-3, 5 and 6 exhibit elevated levels of NOx emissions rates because the average $T_{SCR IN}$ of these events was below 215 °C.

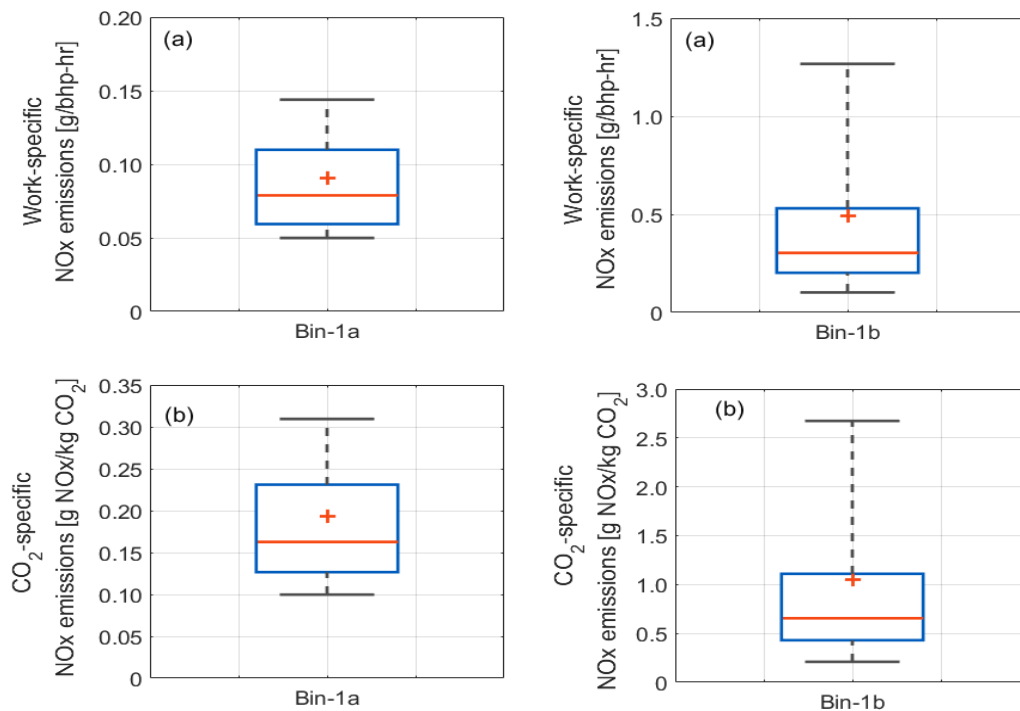


Figure 54: Box and whisker distribution of all events generated in (a) Top graph: bsNOx emissions and (b) Bottom graph: CO₂-specific NOx emissions rates of vehicle-A operated on route-2

Figure 54 shows a comparison of NOx emissions results of all events generated in bin-1a and 1b as a function of engine work-specific and CO₂ specific metrics. The

average bsNO_x results of all events generated in bin-1a were 0.09 g/bhp-hr and for bin-1b was 0.49 g/bhp-hr. Since bin-1a evaluates events only when T_{SCR IN} is above 230 °C for the entire event, any events comprising of test activity where T_{SCR IN} is below 230°C for a time fraction of event duration is captured in bin-1b. Additionally, CO₂-specific NO_x emissions rates were quantified for each of these events. The bottom chart of Figure 54 shows a comparison of NO_x emissions rates as a function of CO₂ emissions for the two data bin categories. For bin-1a, the CO₂ specific NO_x emissions ranged from 0.09 to 0.31 gNO_x/kgCO₂, while for bin-1b the values ranged from 0.20 to 2.67 gNO_x/kgCO₂. The spread of the distribution in the bottom charts of Figure 54 shows the trade-off associated with NO_x and CO₂ emissions, where bin-1a demonstrates an average of 0.19 gNO_x/kgCO₂ emissions, while bin-1b results in an average of 1.05 gNO_x/kgCO₂ emissions. Results from bin-1a in comparison with bin-1b show the increase in CO₂ emissions/fuel consumption that is needed to support thermal conditions required by the EATS to reduce NO_x emissions efficiently.

In summary, implementation of the ABW binning approach resulted in utilization of a 52.31% of the test activity in bin-1 (i.e., split into 25.79% in bin-1a and 26.52% in bin-1b), 36.80% of the data in bin-2b. Since the test type was a cold start, 9.74% of test activity was captured in the reported bin due to the cold start exclusion. The membership distribution of the ABW binning approach resulted in utilization of 89.1% and 88.93% of test activity and NO_x mass sampled, respectively.

To provide a metric-based comparison, NTE analysis was also performed on the same in-use test dataset. Due to the method-based thresholds, only 7.8% and 6.91% of test activity and NO_x mass sampled were utilized for evaluation of in-use compliance evaluation. The approach resulted in the generation of 16 NTE events, and bsNO_x emissions of all events generated were below the current in-use limit for bsNO_x emissions (i.e., 0.45 g/bhp-hr). Similarly, WBW analysis as per EU VI (c) thresholds was performed on the in-use dataset. The 90th percentile of the valid WBW (i.e., windows above 20% of P_{max}) bsNO_x emissions was ~0.33 g/bhp-hr and the approach resulted in utilizing 85.9% of the entire in-use test activity for generation of all

WBW's. Excluding the low-power windows resulted in the utilization of only 53.9% of the test activity.

5.2.3. Sensitivity Analysis

A parametric analysis (i.e., based on a DOE test matrix presented in Table 13) was performed on the ABW binning structure to evaluate the impact of the method-defined governing boundary parameters. In-use test activity collected from route-1 and 2 (i.e., comprising of city and highway driving operation) from vehicle-A and B were used for this task. The boundary parameters of interest were (i) Minimum engine power threshold for engine work producing events (i.e., bin-1), (ii) Minimum time threshold for bin-1 event generation, and (iii) $T_{SCR\ IN}$ threshold to separate engine work producing events between bin-1a and bin-1b. The primary goal of the DOE analysis was to assess thresholds for (i) and (ii) that adheres to maximum utilization of in-use data for evaluation in bin-1 and to identify an optimum range of $T_{SCR\ IN}$ threshold to characterizes active SCR operation for NO_x reduction.

Statistical software JMP was used to assess the influence of the boundary parameters of interest (i.e., minimum event time duration and minimum engine power threshold for bin-1) on the influence of the time-weighted average test duration for bin-1. A screening report was generated that lists the estimate of the factor (i.e., estimated in a linear model), length t-ratio (i.e., contrast scaled over the pseudo standard error), individual p-value and simultaneous p-value. Typically, the parameter that exhibits the most substantial influence is often characterized by relatively high absolute value for length t-ratio and contrast. At the same time, individual p-value and simultaneous p-value less than 0.01 indicates that a small variation in the threshold results in a notable significance. The values are computed based on MC simulation of length t-ratio based on the null hypothesis to generate an empirical sampling of the statistical distribution (JMP, 2018). The results indicate that the minimum power threshold demonstrates the most substantial influence for the time-weighted test duration for bin-1, followed by the minimum time duration. The contrast value quantified was -1.95 and -1.84 while the length t-ratio was -27.66 and -26.04 for minimum power

threshold and time duration for bin-1, respectively. The individual p-value was less than 0.001 for both the parameters of interest. Figure 55 shows a comparison of the time-weighted test activity acquired versus the thresholds of interest for minimum time duration and percentage of maximum power for bin-1. The comparative analysis shows that the minimum threshold of the selected parameters results in the utilization of more than 60% of test activity in bin 1.

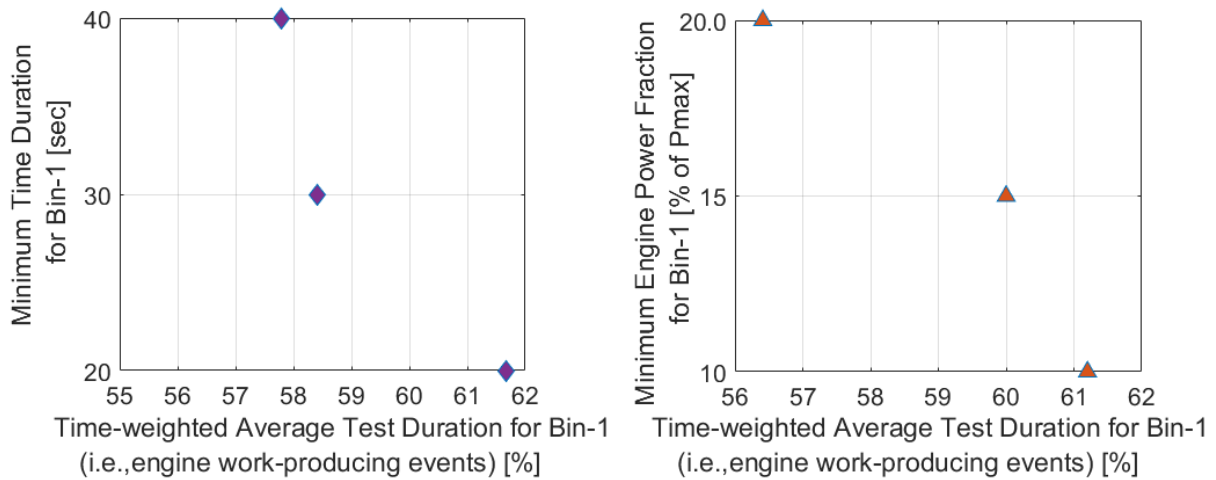


Figure 55: Comparison of time-weighted test activity distribution for minimum event time duration and engine power fraction (i.e., for bin-1)

To identify an optimum bandwidth for separation of SCR activity, bsNO_x emissions results were compared for the results obtained from the DOE analysis. Since the DOE analysis was performed on events generated within each ABW across multiple segments of test activity procured from each of the two vehicles, the results are outlined in a percentile distribution basis to ensure that the two rank categories are representative of values at and above the upper quartile of the data distribution. In Figure 56 window percentile rank Category-A represents the bsNO_x value, i.e., 75th percentile of the distribution among the 90th percentile bsNO_x results acquired from each ABW, whereas window percentile Category-B represents the bsNO_x value, i.e., 90th percentile of the distribution among the 75th percentile results from each ABW. The mean bsNO_x emissions rates for bin-1a showed a gradual decrease in the trend with the increase in T_{SCR IN} threshold. The data-driven evaluation shows that at T_{SCR}

$T_{SCR IN}$ threshold above 230 °C bsNO_x emissions results for bin-1a are below the current NTE in-use limit for bsNO_x emissions (i.e., 0.45 g/bhp-hr).

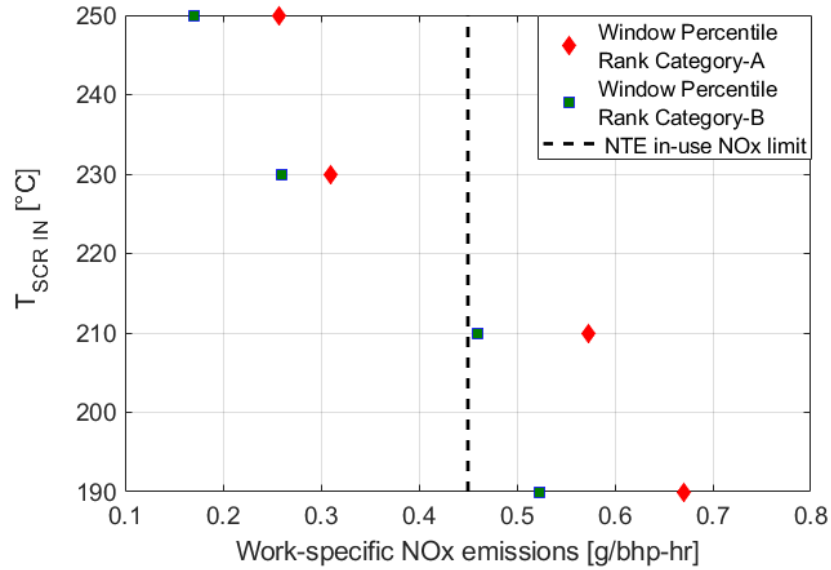


Figure 56: Impact of ABW $T_{SCR IN}$ threshold on bsNO_x emissions

One of the primary limitations associated with the NTE approach was acquiring continuous engine operation within the NTE zone. For example, if the engine operation (i.e., engine speed/torque/power) dropped out of the NTE zone, this, therefore, resulted in invalidation of the entire NTE event if the engine was operating within the NTE zone and met all the event-based exclusion criteria except the minimum event duration time (or) terminating the event. To address this limitation, a drop-out time was introduced in the ABW binning approach. The maximum allowable drop out time (i.e., transition mode) was determined based on evaluating the entire set of test activity from data collected from vehicle-A, and B. Figure 57 shows the time-weighted data distribution of entire test activity that results in drop out of bin-1 to bin-2 and back into bin-1. The distribution shows that the majority of test activity captured during transient operation from the limited test datasets evaluated exhibited test conditions as defined for transition mode to be less than 10 seconds. The remainder activity (i.e., greater than 10 second threshold) was primarily captured with a combination of coasting and transient low-power engine operation. Since the drop-out time plays a significant role in the allocation of test activity in

either bin-1 (or) bin-2, the maximum allowable drop-out time for test activity in bin-1 is considered as the minimum event generation duration for test activity in bin-2 (i.e., to avoid overlapping of data in either of the bins). Table 20 presents an overview of desired thresholds opted for evaluation of ABW binning approach on vocational in-use test activity presented in section 0, and 5.3.2. It is to be noted that these thresholds were derived from analyzing limited amount of in-use activity and may not necessarily be deemed valid for all vehicle datasets.

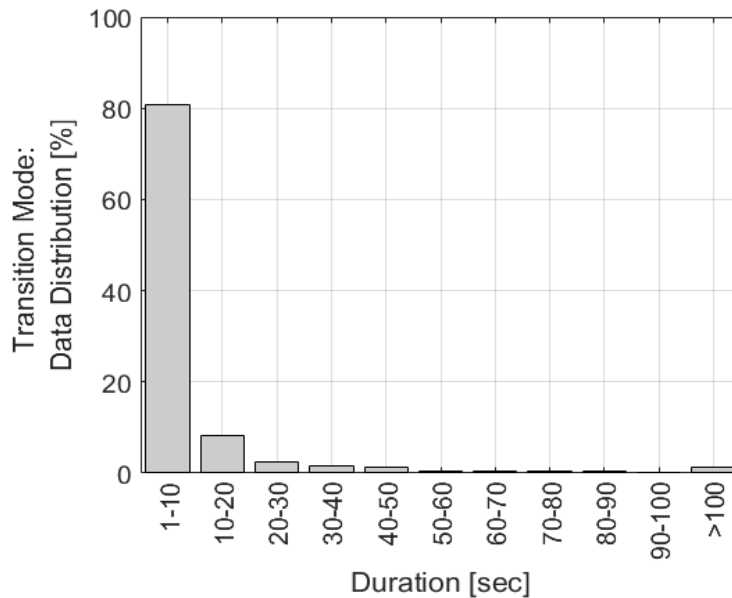


Figure 57: Distribution of test activity accumulated during transition mode

Table 20: Boundary parameter thresholds selected for evaluation of ABW binning approach

Boundary Parameter	Threshold
Bin-1: Minimum duration limit [sec]	20
Bin-1: Minimum $T_{SCR IN}$ limit [°C]	230
Bin-1: Minimum power threshold [% of Pmax]	10
Bin-1: Drop-out time/ Bin-2 Minimum duration limit [sec]	10

5.2.4. Application of Activity-based Windowing Approach

The ABW binning approach was evaluated on experimental emissions test activity collected from real-world operation representative of vocational freight operation (i.e., data collected in section 3.2). The thresholds for the ABW approach were developed from test activity collected from later MY engines (i.e., Engine MY 2017 and 2018) and were used to evaluate vocational vehicle and emissions activity collected from relatively older engines (i.e., Engine MY 2014 and 2015). Section 5.2.4.1 and 5.2.4.2 presents the application of ABW binning structure evaluated on grocery distribution (i.e., delivery operation) and port-drayage test routes. A global comparison of the metric-based results is discussed in section 5.2.4.3.

5.2.4.1. Grocery Distribution Route

Figure 58 presents a summary of ABW NO_x emissions results (i.e., bin-1a, 1b and 2b) for test activity collected from Vehicle-D on Route-4. The events generated within each ABW are presented in the form of a box and whisker distribution. A total of 12 ABW's were generated for the entire test route.

The NTE in-use limit for NO_x emissions is used as a reference to classify trends in bsNO_x emissions explicitly for events generated in bin-1a. All events generated in bin-1a (i.e., thermal SCR bin) demonstrate bsNO_x emissions levels to be below the current NTE limit for NO_x emissions except for ABW- 4, 5 and 6 that included few events among the total events generated (i.e., one, four and two events, respectively) in which bsNO_x emissions were above 0.45 g/bhp-hr. The window-averaged T_{SCR IN} was above 300 °C for ABW's whose 90th percentile of the distribution was observed to be below 0.20 g/bhp-hr (i.e., the certification standard). Therefore, indicative of efficient SCR NO_x conversion activity for the above-mentioned mode of in-use operation captured in bin-1a. Specific to events generated in ABW-4, 5 and 6, an in-depth evaluation of these specific segments of test activity showed that these events were generated during the warm-up phase of the SCR system and event averaged T_{SCR IN} for these events was between 230 and 260 °C, while T_{SCR OUT} was below 230 °C

for the entire event. Therefore, influencing the NOx emissions rates due to insufficient thermal energy to suffice SCR high NOx conversion. The window average and median average bsNOx emissions of all events generated in individual ABW's in bin-1a was 0.12 g/bhp-hr and 0.06 g/bhp-hr, respectively.

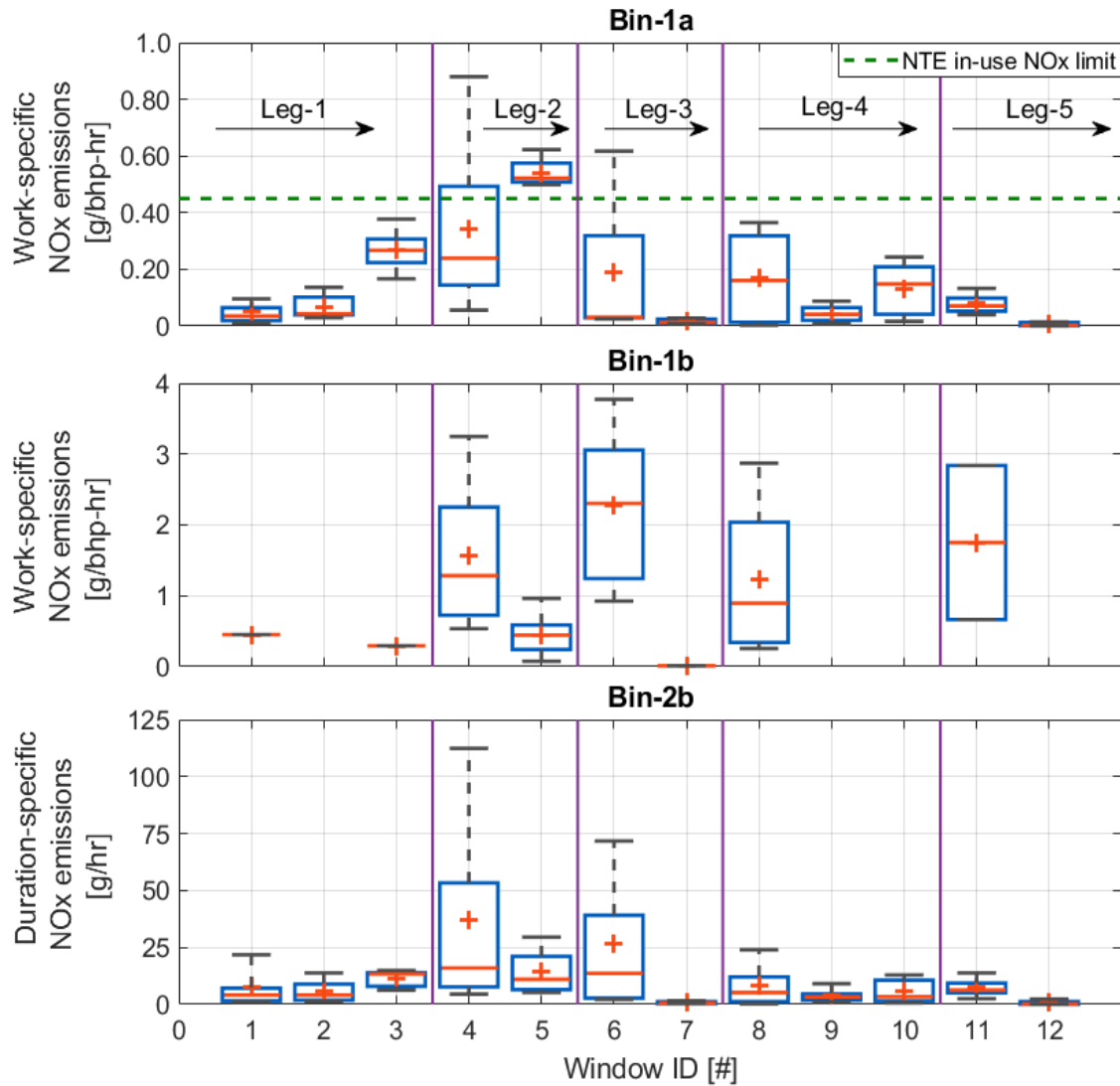


Figure 58: A summary bin-based summary of NOx emissions for vehicle-D operated on route-4

Typically, three types of events are generated in event category bin-1a and are representative of (i) Low-NOx and high-CO₂ emissions: These events are indicative of engine control or active thermal management strategies associated with an influence on fuel consumption to raise exhaust energy to suffice thermal requirements for SCR activity, (ii) Low-NOx and low-CO₂ emissions: These events are indicative of catalyst

favourable thermal conditions for SCR activity, therefore leading to the implementation of in-cylinder combustion control strategies to reduce fuel consumption, and (iii) High-NO_x and high/low CO₂: These events are indicative of relatively higher NO_x emissions generated either due to insufficient exhaust energy for efficient NO_x conversion (or) a potential failure/defect in the emissions control aftertreatment system. A comparative summary of event-averaged NO_x versus CO₂ emissions for activity collected from vehicle-C and D is presented in Appendix C. Although T_{SCR IN} was used as an indicator in the ABW approach to segregate SCR operational engine work producing events, several other factors impact SCR performance such as dynamics of exhaust gas thermal conditions, catalyst substrate design, i.e., cells per square inch (cps), thermal inertia across the SCR catalyst bed, NH₃ storage, urea deposits on the catalyst and SCR control strategies.

With regards to events generated in bin-1b, average T_{SCR IN} of all events generated in ABW-4, 6, 8, and 11 were observed to be below 230 °C. There were 20 out of 24 events generated in these four ABW's demonstrate engine-out bsNO_x emissions levels (i.e., ranging from 0.66 g/bhp-hr to 4.03 g/bhp-hr). Leg-2 and 3 of the test route experienced a significant time fraction (i.e., 97% and 74% of test time) of operational time during urban driving operation (i.e., low vehicle speed operation) due to traffic on US 110S. Therefore, resulting in 70.56% and 47.89% of the test time that experienced T_{SCR IN} below 250 °C. Since, bin-1b acts as a remainder event bin category, all events generated in ABW-1, 3, and 7 experienced a certain time fraction of event duration to be below ABW T_{SCR IN} threshold, while the dominant percentage of operation within the event was above the threshold. Therefore, resulting in relatively lower bsNO_x emissions levels for compared to other events acquired in bin-1b.

Figure 59 shows a quadrant comparison of average T_{SCR IN} and bsNO_x emissions of all events generated in bin-1a and 1b. The results highlight the characteristic dependency of the exhaust gas thermal conditions for SCR operation (i.e., highlighted particularly for events in bin-1a) under real-world driving conditions. Quadrant-2 (i.e., the top left portion of the graph) is indicative of test activity where the SCR

system has not attained thermal conditions to reduce NO_x emissions efficiently. A combination of in-cylinder combustion control strategies, use of EGR and turbocharger, are often used in such modes of in-use operation to limit in-cylinder NO_x formation. Data presented in Quadrant-3 (i.e., the bottom left portion of the graph) is representative of events that include thermal conditions (i.e., $T_{SCR IN}$) to be below 230 °C for a fraction of event activity. Quadrant-4 (i.e., the bottom right portion of the graph) is representative of test activity that exhibit thermally conducive exhaust gas conditions that are favorable for the SCR catalyst reactions to reduce NO_x emissions. A comparative discussion of NO_x versus CO₂ emissions for each of the event categories is presented in section 5.2.4.3 and appendix C.

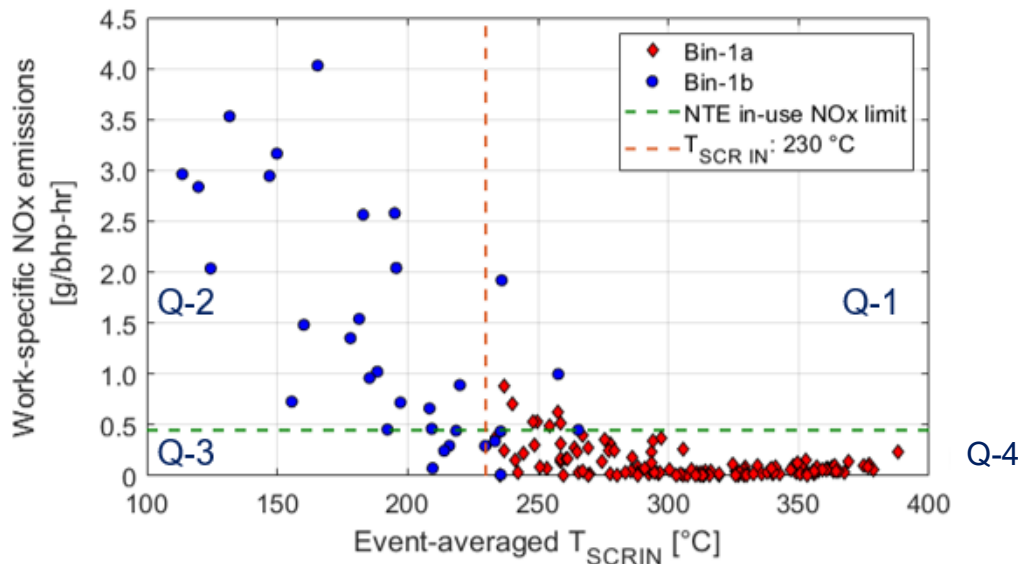


Figure 59: Comparison of event averaged $T_{SCR IN}$ and bsNO_x emissions of all events generated in bin-1a and 1b for vehicle-D operated on route-4

Event-activity captured in quadrant-4 is composed of a combination of both low-NO_x and low-CO₂, and low-NO_x and high CO₂ emissions (i.e., depicted in appendix-C). The trade-off between NO_x and CO₂ emissions from events captured in bin-1a is presented in Figure 94. The efficient NO_x reduction activity in quadrant-4 (~200 to 400 °C in Figure 59) is a function of the regulatory demand (i.e., performance over the FTP test cycle) that drives the engine calibration in a way to meet the thermal requirements favorable for SCR catalytic activity and simultaneously meeting the

NO_x and CO₂ requirements. Technical limitations for efficient and effective SCR catalytic activity at low-temperature exhaust gas conditions (i.e., due to limitations of catalyst light-off temperature, lower NO_x conversion efficiency and prevention of solid urea-deposit formation) therefore, results in the relatively higher bsNO_x emissions with the transition of the event captured from quadrant-4 to quadrant-2. While engine manufacturers use various in-cylinder combustion control strategies to limit NO_x formation, the next generation of emissions regulations would, therefore, mandate a reduction in NO_x emissions from modes of operating conditions captured in bin-1b. Therefore, potentially resulting in technical developments that support exhaust gas thermal conditions that aids in a reduction in the magnitude of difference between NO_x emissions characteristics captured in quadrant-2 in comparison with trends observed in quadrant-4. Several research and commercial entities are examining the potential of different technologies both from engine and aftertreatment design standpoint to unleash the potential of SCR catalyst using a viable technical pathway that does not cause a drastic impact on fuel consumption while supporting the expansion real-world thermal operational bandwidth.

Specifically, for events generated in bin-2a and 2b, NO_x emissions rates are presented using a time-specific metric (i.e., g/hr). This is primarily because a bs metric will lead to an asymptotic trend due to test activity that is captured during near-zero brake torque conditions. The average time-specific NO_x (tsNO_x) emissions of all events generated in event category-2b were 10.86 g/hr. Vehicle activity captured in ABW-4 and 6 (i.e., for bin-2b) included test operational segments comprising of low-vehicle speed operation due to frequent stop-and-go activity in dense traffic operation. Therefore, resulting in exhaust gas thermal conditions at or below the SCR light-off temperature. The average tsNO_x of events in ABW-4 and 6 whose T_{SCR IN} was below the 230 °C was 48.68 g/hr. It is evident from the literature that low load/power engine operation is one of the challenging NO_x control operational modes under real-world driving conditions (Quiros et al., 2016; Thiruvengadam et al., 2015). With respect to low-load engine operation, SWRI developed low-load engine dynamometer test cycle that is representative of vocational vehicle activity comprising of low power engine

operation. A CARB white paper has expressed interest in the implementation of the low-load test cycle as part of the certification process for MD and HD from engines MY 2024 onwards (CARB, 2019).

Table 21 and Table 22 present an overview of time-weighted data distribution and NOx mass distribution of each segment of test activity into four different bin categories. Specific to leg-2 and 3 of the test route that experienced a significant amount of test activity during urban driving operation. It is observed that data captured in bin-1b and bin-2b emitted the most significant amount of NOx mass fraction. On average, 96% of the entire data acquired across all segments was utilized for emissions assessment, and 4.25% of the test activity acquired in leg-1 of the test resulted in cold engine operating conditions (i.e., ECT < 343 K).

Table 21: Comparison of membership distribution within each event category of route-4 operated on vehicle D

Dataset Membership Distribution [%]					
	Leg-1	Leg-2	Leg-3	Leg-4	Leg-5
Bin-1a	61.58	21.75	29.63	49.93	62.12
Bin-1b	2.26	13.52	21.15	4.08	4.8
Bin-2a		5.14	5.84	3.71	
Bin-2b	29.4	59.59	43.39	37.77	27.36

Table 22: Comparison of NOx mass distribution within each event category for grocery distribution route operated on vehicle D

NOx Mass Distribution [%]					
	Leg-1	Leg-2	Leg-3	Leg-4	Leg-5
Bin-1a	47.9	28	11.6	39.1	50.7
Bin-1b	11.7	24.6	68.4	48.5	41.5
Bin-2a		0.05	0.70	0.02	
Bin-2b	16.9	47.4	19.3	12.4	7.9

Similar to the analysis presented earlier in this sub-section of results, test activity collected from vehicle-C operated on route-4 was evaluated using ABW binning

approach. The quantified simulated W_{Ref} for window generation was 27.20 bhp-hr. Figure 60 presents an overview of the distribution of events generated in bin-1a and 1b as a function of event-averaged SCR inlet temperature (i.e., a total of 88 and 84 events, respectively).

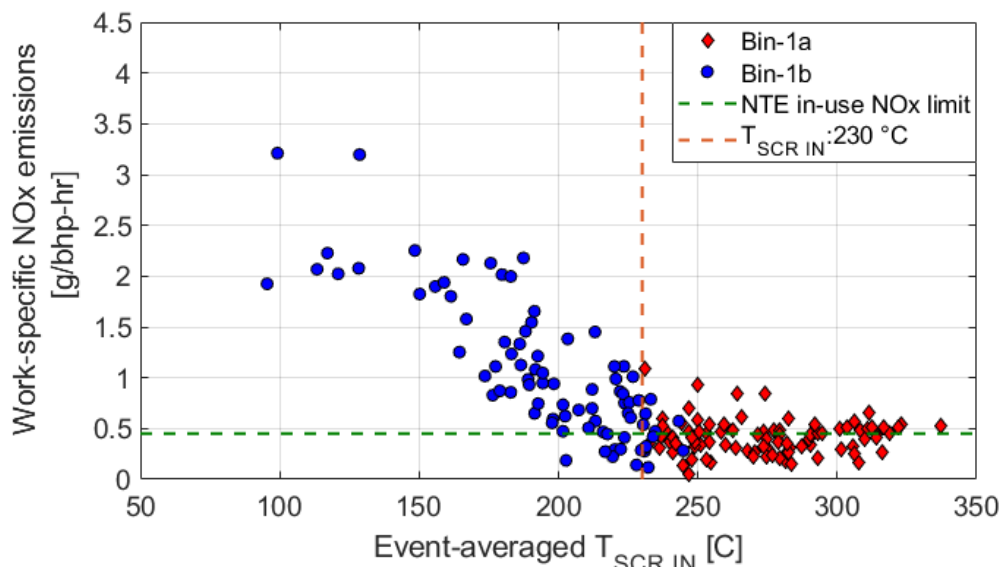


Figure 60: Comparison of event averaged $T_{SCR IN}$ and bsNOx emissions of all events generated in bin-1a and 1b for vehicle-C operated on route-4

Event-averaged bsNOx emissions rates of all events generated in bin-1a and 1b resulted in an average of 0.43 and 1.06 g/bhp-hr, respectively. For events generated in bin-1a, a total of 48.86% and 42.04% of the events generated demonstrated bsNOx emissions to be between 0.20 and 0.45 g/bhp-hr, and above 0.45g/bhp-hr, respectively. The data-driven analysis is inconclusive of the observed phenomena related to deviations observed in bin-1a NOx emissions results, i.e., data presented in quadrant-1. It is important to mention that during the emissions testing phase, the engine was beyond the useful compliance life based on vehicle mileage (i.e., above 435000 miles). In-depth analysis of specific events demonstrated that despite attaining $T_{SCR IN}$ and $T_{SCR OUT}$ to be above 250 °C under real-world driving conditions, tailpipe NOx emissions rates were observed to be above 0.45 g/bhp-hr.

Figure 61 presents a comparison of NOx and CO₂ emissions of one event (i.e., example test case) generated in ABW-13 that emitted bsNOx emissions of 0.84 g/bhp-hr.

During the first 30 seconds of the event even though $T_{SCR\ IN}$ and $T_{SCR\ OUT}$ were above 250 °C, the NO_x concentrations were above 150 ppm. Since, leg-5 of the test route comprised of a dominant time fraction of sustained highway driving operation, $T_{SCR\ IN}$ for 3041 seconds before the event presented in Figure 61 was observed to be above 250 °C. Similar break-through of NO_x emissions were observed from multiple events generated in bin-1a that exhibited bsNO_x emissions to be above 0.45 g/bhp-hr.

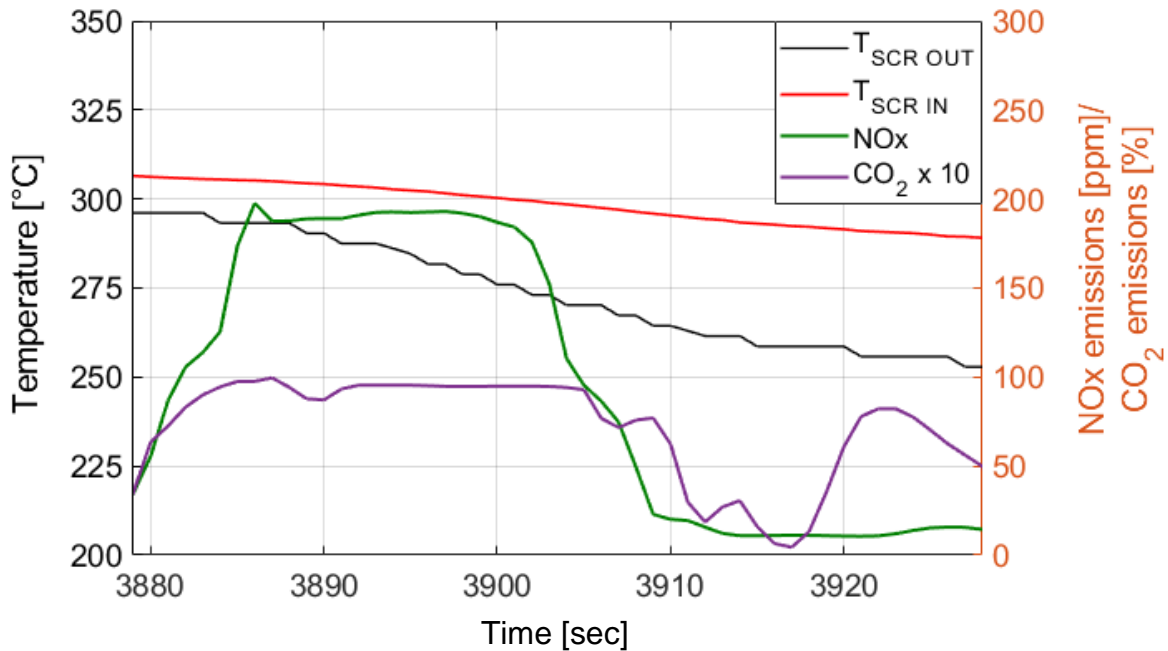


Figure 61: Comparison of SCR inlet and outlet temperature profile, NO_x and CO₂ emissions of an event generated in bin-1a (ABW-13)

Figure 62 illustrate the box and whisker distribution of event-averaged NO_x emissions rates for each ABW bin category into the four different bin categories, respectively. Specific to discussion with regards to events generated in bin-1b, all events generated in leg-1 $T_{SCR\ IN}$ to be above 180 °C. Therefore, average bsNO_x emissions of each ABW generated in leg-1 ranged from 0.47 to 0.70 g/bhp-hr. Leg-2 and Leg-3 of the test route exhibited low-vehicle speed operation due to dense traffic experienced on US 110 S. For test activity acquired in ABW-6 (i.e., leg-2 of the test route), 82.8% of test activity resulted from engine-work producing events generated in bin-1b. The event-averaged $T_{SCR\ IN}$ for 52 out of 54 events generated in ABW-6, 7,

8, 10 and 12 was below 230 °C. Therefore, resulting in bsNO_x levels of 1.30 ± 0.66 g/bhp-hr due to minimal SCR activity.

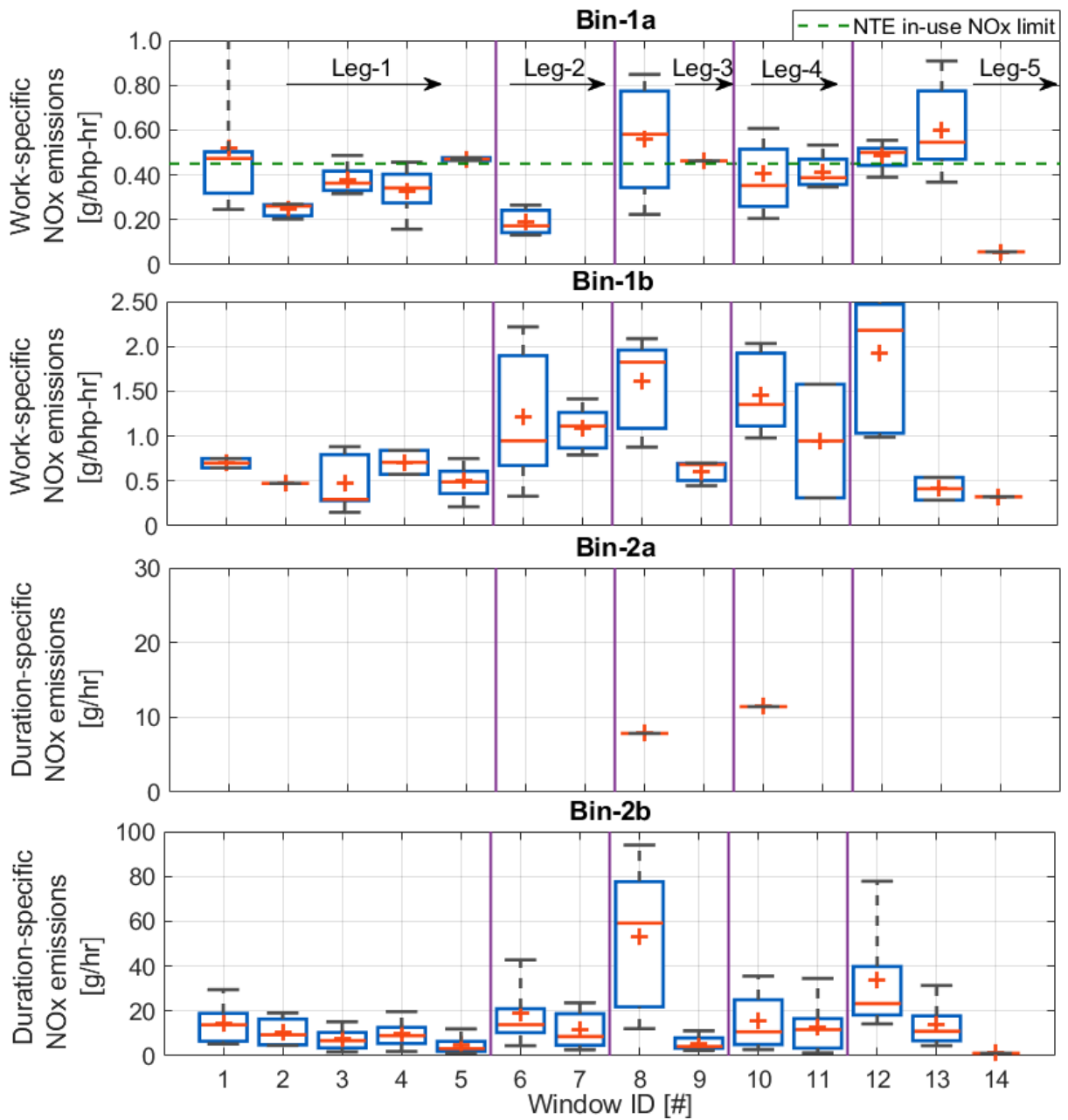


Figure 62: ABW bin-based summary of NO_x emissions for vehicle-C operated on route-4

For this specific test route, two low-power operational events were generated in bin-2a, i.e., engine idle operation that was captured during the initial segment of test activity in leg-3 and 4. The tsNO_x emissions of these two events were 7.85 and 11.43 g/hr. Therefore, based on the ABW binning definitions described in section 4.2, test

activity that includes a combination of stationary engine idle operation and low-power transient activity is captured in bin-2b. The average, median and 75th percentile of the distribution of all low-power events generated in bin-2b except for events generated in ABW-8 and 12 are below 30 g/hr. The relatively lower tsNO_x emissions from these events are because a majority test activity captured in this category was between transient tractive engine work producing events, therefore, resulting in an average T_{SCR IN} of 232.82 °C. There were 11 out of 13 events generated in ABW-8 and 12 were captured from test activity comprising of a combination of low-vehicle speed operation and low-power engine operation. The tsNO_x and CO₂-specific NO_x emissions of these specific events captured in ABW-8 and 12 were 48.00 ± 27.79 g/hr and 4.31 ± 3.82 gNO_x/kgCO₂.

Table 23: Comparison of data membership and NO_x mass distribution within each event category of route-4 operated on vehicle C

Dataset Membership Distribution [%]					
	Leg-1	Leg-2	Leg-3	Leg-4	Leg-5
Bin-1a	30.29	4.07	16.66	39.93	58.37
Bin-1b	19.28	25.83	19.5	8.73	11.18
Bin-2a			5.99	2.6	
Bin-2b	42.68	66.48	57.14	46.72	29.62
NO _x Mass Distribution [%]					
	Leg-1	Leg-2	Leg-3	Leg-4	Leg-5
Bin-1a	38.62	1.38	22.50	50.09	68.34
Bin-1b	37.30	65.35	37.60	31.40	23.23
Bin-2a			0.67	0.77	
Bin-2b	7.46	33.24	39.22	17.74	8.43

Table 23 illustrates a comparison of time-weighted data distribution and NO_x mass distribution of test activity acquired in each of the four different ABW bin categories. Dependent on vehicle activity within each segment of the test route, a majority of test activity was captured in a combination of bin-1b, 2a and 2b for all legs of the test

route except leg-5. This is because $T_{SCR\ IN}$ was above 250 °C for approximately 69.48% of test activity in leg-5 (data presented in Figure 50). Based on test activity collected from the five different test segments, on average (i.e., group average), 97.01 % and 96.68% of data acquired and NO_x mass emitted was utilized for emissions assessment using the ABW binning approach. There was 7.75% of test activity acquired in leg-1 of the test that was not evaluated for emissions because of the cold start exclusion criteria. During this segment of the in-use test, a total of 16.62% of NO_x mass was emitted.

5.2.4.2. Port Route

This section will discuss ABW bin results for in-use test activity collected from vehicle-C and D operated on route-3 (i.e., port route). The ABW binning approach generated windows only for leg-1 and leg-3 of the test route. Leg-2 of the test route included simulation of port activity comprising of extended engine idle and creep operation for approximately one hour, therefore, resulting in the total trip engine work to be less than W_{Ref} . The example scenario of leg-2 of this route highlights the sensitivity of the window generation with regards to a key-off event. Although ABW binning approach did not capture any test activity from a critical and challenging test operational segment, a summary of emissions results with respect to leg-2 is discussed towards the end of this section.

Figure 63 presents a summary of ABW bin results (i.e., for bin-1a,1b, and 2b) for in-use test activity collected from vehicle-D operated on route-4. The results indicate that event-averaged bsNO_x emissions for 89.7% of events generated in bin-1a were below 0.20 g/bhp-hr (i.e., certification standard for NO_x emissions). The event averaged $T_{SCR\ IN}$ of these events was 325.47 °C. Leg-1 and leg-3 of the test route comprised of a significant time-weighted operation where the vehicle was operating in rural and highway driving conditions. Therefore, resulting in favorable exhaust gas thermal conditions for SCR operation. The $T_{SCR\ IN}$ was above 250 °C for approximately 63.6% and 60.54% of the operational time for leg-1 and 3, respectively. The CO₂-specific NO_x emissions for these events was 0.12 ± 0.09 gNO_x/kgCO₂. Out

of 107 events generated in bin-1a, only two consecutive events generated in ABW-4 exhibited bsNO_x levels to be above 0.45 g/bhp-hr. Similar to observations in results presented in section 5.2.4.1, these two events were generated during the initial warm-up phase. In-depth evaluation of these two events showed that T_{SCR IN} was between 230 and 250 °C, while the T_{SCR OUT} was below 200 °C. Therefore, indicative of insufficient thermal energy for efficient SCR activity.

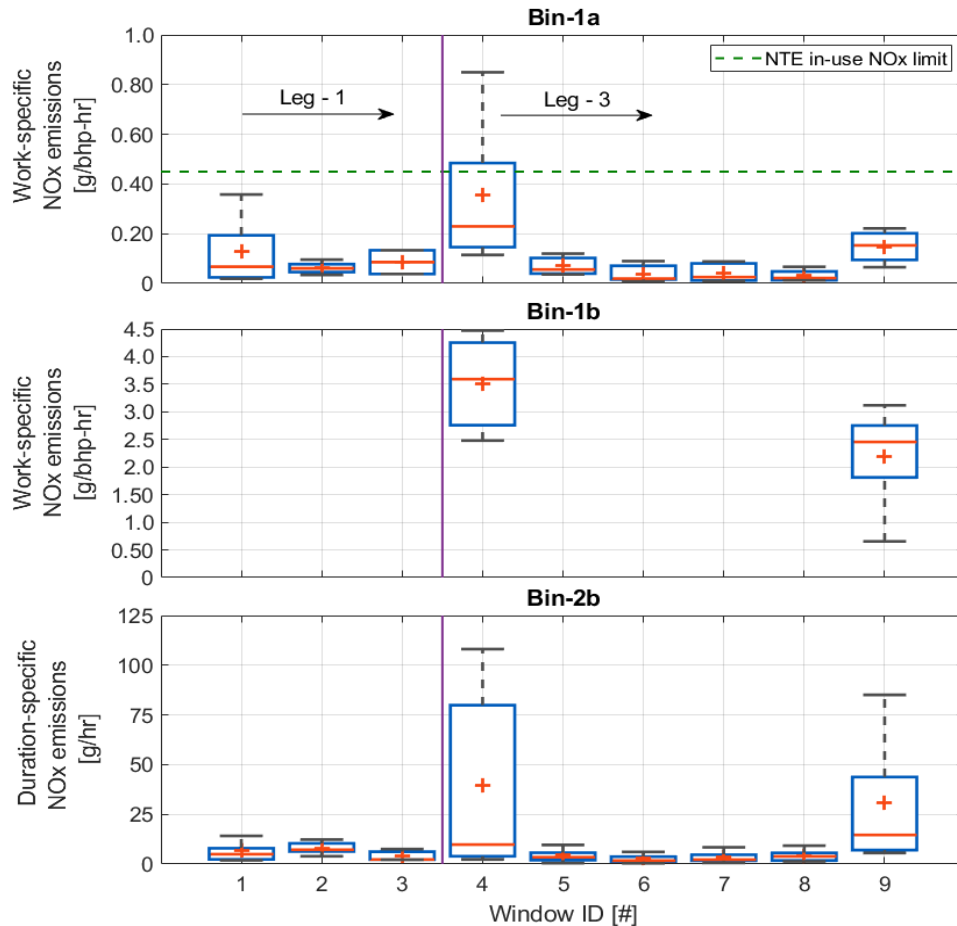


Figure 63: ABW bin-based summary of NO_x emissions for vehicle-D operated on route-3

Out of the nine events generated in bin-1b, three events comprising of a total of duration of 2.69% of the test were generated during the initial onset of leg-3 from the port harbour. Therefore, resulting in bsNO_x emissions levels of 3.51 ± 0.99 g/bhp-hr. During the final phase of the test route after the highway segment, the vehicle experienced low-vehicle speed operation with stop-and-go activity, therefore,

resulting in cool-down of the EATS. Six events were generated during this phase of test activity in bin-1b, therefore resulting in an average bsNO_x emissions of 2.19 g/bhp-hr for these events. Specific to the vehicle operation described above, 10 and 11 events were generated in ABW-4 and 9, respectively (i.e., in bin-2b). Among the 21 events, the event averaged T_{SCR IN} of 10 events was below 250 °C. The events generated comprising of low-load engine operation with frequent stop-and-go activity resulting in cool down of the SCR system. The resultant tsNO_x emissions of these ten events were 68.72 ± 42.38 g/hr. Remaining low-power events generated in other ABW's comprise of activity generated during rural/highway driving conditions. The average tsNO_x emissions of events in bin-2b reduced from 11.17 g/hr (i.e., an average of all events generated) to 5.30 g/hr upon excluding the ten events (i.e., discussed above) generated from ABW-4 and 9.

Table 24 overall time-weight data and NO_x mass distribution of the entire test route. On average, 92.92% of entire data acquired and 81.22% of NO_x mass emitted in leg-1 and 3 of the test was used for emissions assessment. There was 9.82% of the data acquired in leg-1 of the route that was not excluded from emissions evaluation due to cold engine operating conditions (i.e., ECT). This specific mode of engine operation resulted in 37.56% of total NO_x mass emitted in leg-1 of the test route.

Table 24: Comparison of data membership and NOx mass distribution within each event category of route-3 operated on vehicle-D

Dataset Membership Distribution [%]		
	Leg-1	Leg-3
Bin-1a	68.40	57.95
Bin-1b		5.92
Bin-2a		
Bin-2b	19.60	33.96
NOx Mass Distribution [%]		
	Leg-1	Leg-3
Bin-1a	57.59	29.67
Bin-1b		51.16
Bin-2a		
Bin-2b	4.85	19.17

Similar to the analysis presented earlier in this subsection of the results, test activity collected from vehicle-C operated on route-3 was evaluated using ABW binning approach. Figure 64 presents an overall NOx emissions summary for ABW binning evaluated on test activity acquired from the port-route.

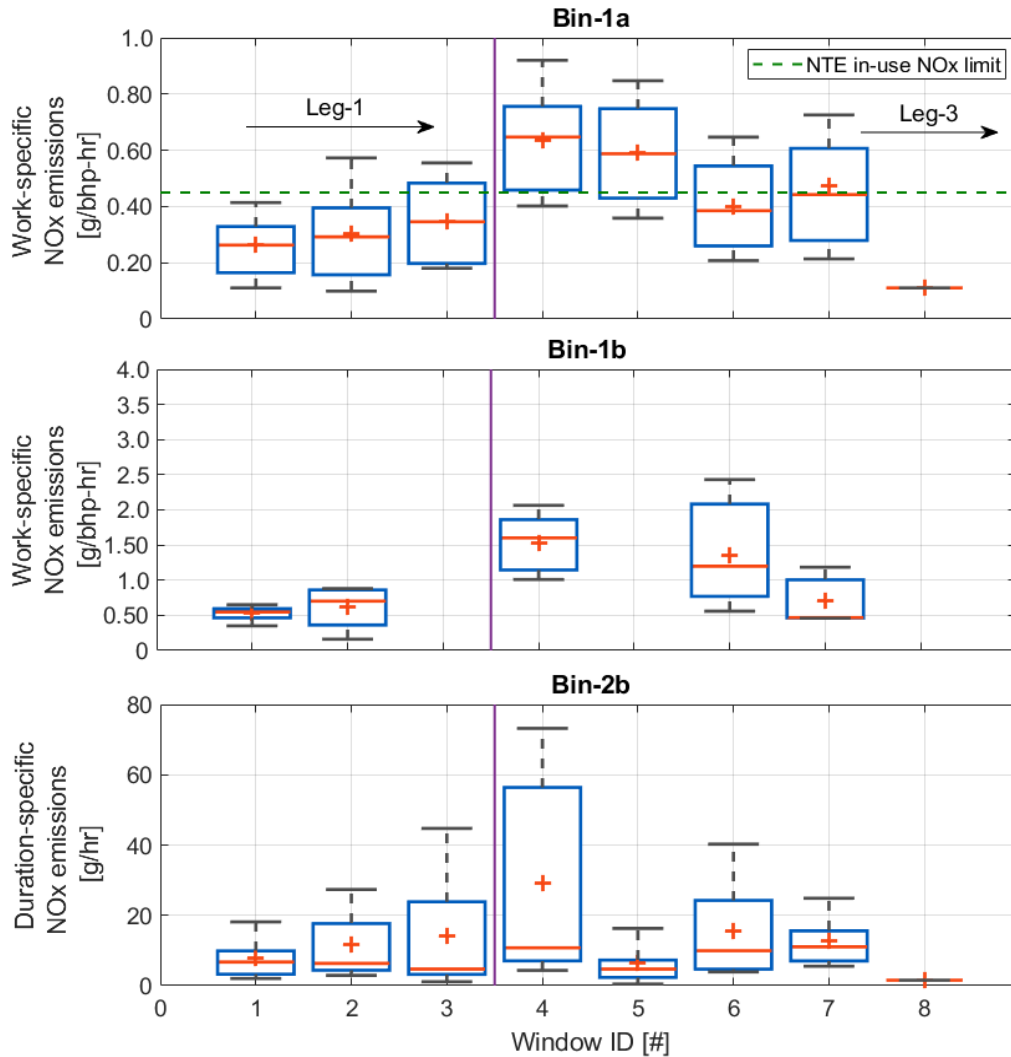


Figure 64: Summary of ABW binning for NO_x emissions for vehicle-C operated on route-3

Figure 65 illustrates a comparison of bsNO_x emissions for events generated in bin-1a and 1b, respectively. The results show that 36.44% of events generated in bin-1a comprise of event-averaged bsNO_x emissions to be above 0.45 g/bhp-hr. Similar to the analysis presented in section 5.2.4.1, the data-driven analysis is inconclusive of the observed deviations (i.e., bin-1a data presented in quadrant-1). The bsNO_x emissions of all events generated in bin-1a was 0.41 ± 0.21 g/bhp-hr.

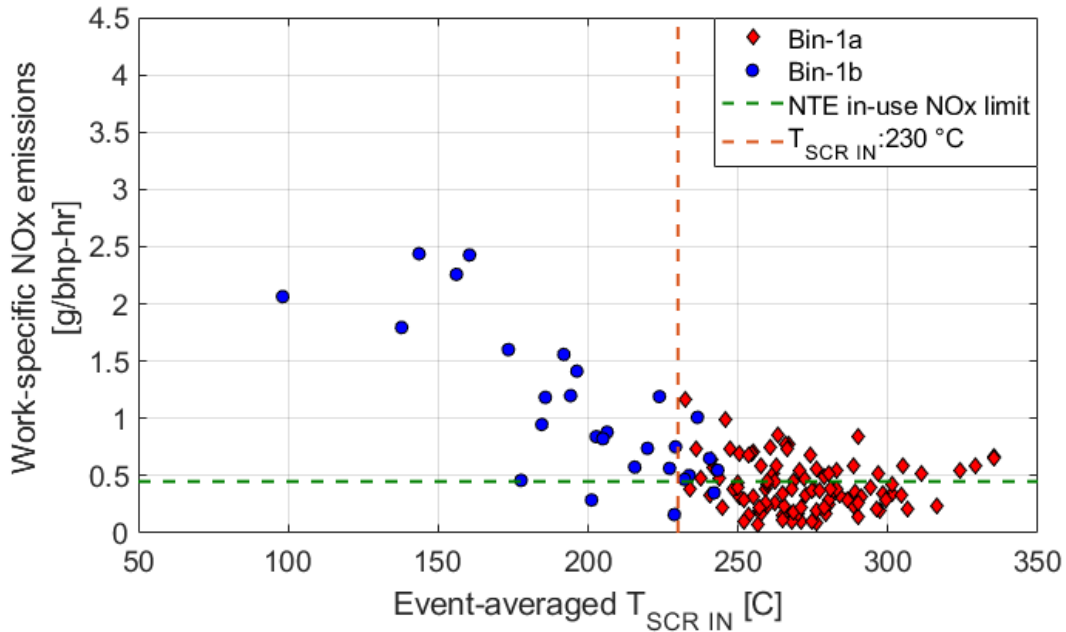


Figure 65: Comparison of event averaged $T_{SCR IN}$ and bsNOx emissions of all events generated in bin-1a and 1b for vehicle-C operated on route-3

A total of 28 events were captured in bin-1b, and the event-averaged bsNOx emissions rates were 1.06 ± 0.65 g/bhp-hr. The average tsNOx emissions of all events generated in bin-2b are 13.54 g/hr. There were 12 out of 131 events (i.e., four events captured in ABW-4 and eight events captured in ABW-6) comprised of event-average $T_{SCR IN}$ to be below 230 °C. An in-depth evaluation of these events exhibited vehicle activity comprising of a combination of low-vehicle speed operation and low-load engine operation. Therefore, resulting in tsNOx emissions of 48.83 ± 26.26 g/hr. On average, 95.72% and 91.14% of the entire dataset and NOx mass emitted in leg-1 and leg-3 of the test route, respectively, was used for emissions assessment using the ABW approach.

Table 25: Comparison of data membership and NO_x mass distribution within each event category of route-3 operated on vehicle-C

Dataset Membership Distribution [%]		
	Leg-1	Leg-3
Bin-1a	57.86	45.62
Bin-1b	10.12	10.02
Bin-2a		
Bin-2b	24	43.83
NO _x Mass Distribution [%]		
	Leg-1	Leg-3
Bin-1a	53.09	55.65
Bin-1b	20.86	25.45
Bin-2a		
Bin-2b	8.32	18.90

As discussed at the beginning of this section, leg-2 of route-3 (i.e., simulation of port-draysage activity) did not generate any ABW's. The simulation of activity experienced in the port harbour was depicted by extended engine idle operation followed by a short duration of creep operation. The extended engine idle operation in conjunction with a short segment of creep operation results in the cool-down of the SCR system. The 30-minute soak duration (i.e., engine key-off activity) between the end of leg-1 and onset of leg-2 resulted in a cool-down of SCR inlet temperature from 255.70 to 144.21 °C for vehicle-D and from 228.21 to 150.78 °C for vehicle-C. It is known from literature that such modes of in-use operation are one of the challenging modes of NO_x control from modern HD trucks (Boriboonsomsin et al., 2018; Quiros et al., 2016; Thiruvengadam et al., 2015). Figure 66 depicts the vehicle speed, engine work and SCR inlet temperature profile of leg-2 of the port route collected from vehicle-D.

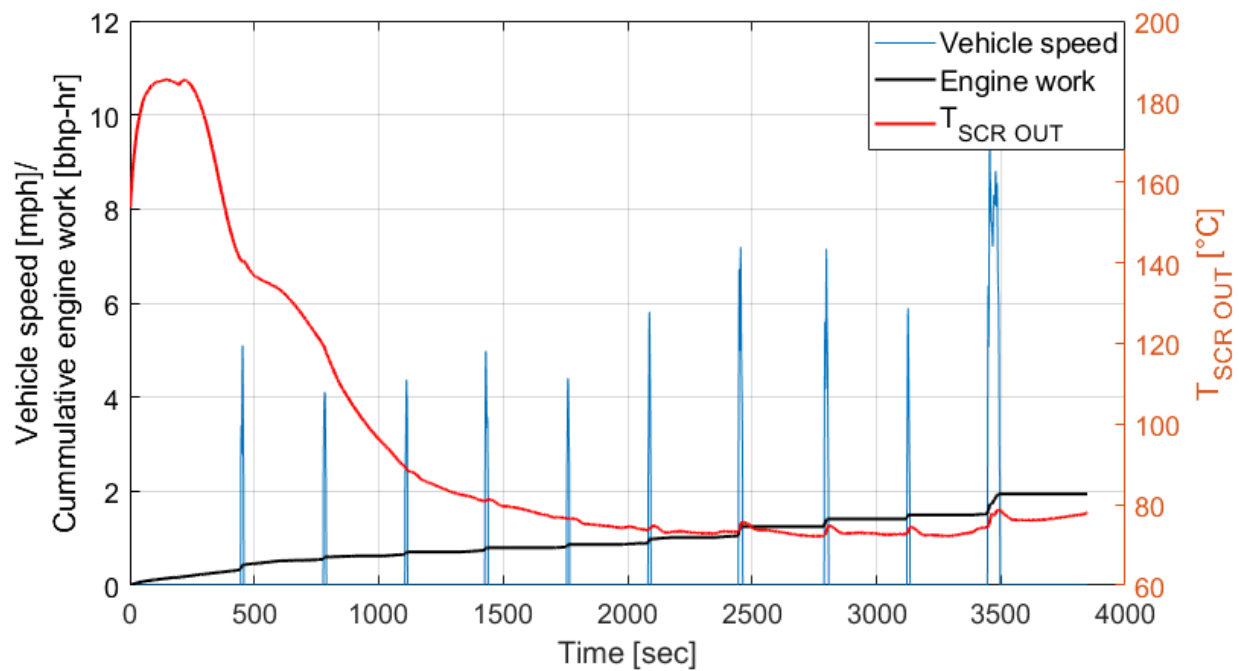


Figure 66: Comparison of vehicle speed, engine work, and T_{SCR IN} of vehicle-3 operated on leg-2 of route-3

The integrated tsNO_x emissions for the entire segment of activity acquired in leg-2 of route-3 was 19.18 and 35.16 g/hr for vehicle-C and D, respectively. The differences in tsNO_x emissions rates are attributed to different in-cylinder combustion control strategies used by engine manufacturer C and D for extended engine idle operation.

5.2.4.3. Summary of Phase-1 ABW Analysis

Figure 67 shows a cumulative empirical distribution of bsNO_x emissions of all events generated in bin-1a for the four vehicle datasets (i.e., irrespective of test routes and engine operating conditions) collected in section 3.2. For reference and comparison purposes, the certification standard and NTE in-use standard for NO_x emissions are indicated by the red and green dashed line, respectively.

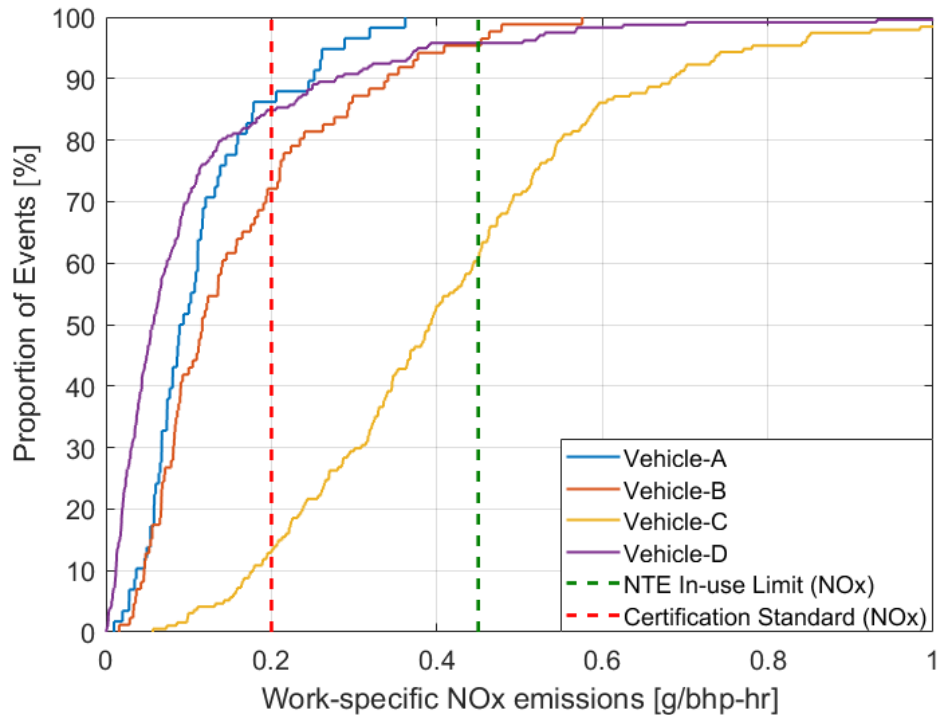


Figure 67: Cumulative frequency distribution of bsNO_x emissions of all events generated in ABW-bin-1a

While, SCR technology is the primary driving force for the reduction in tailpipe NO_x emissions of the four HD vehicles, the cumulative NO_x emissions trends presented in Figure 67 provides the ability to track deviations in NO_x emissions performance under modes of operating conditions favorable for SCR catalysis. Interestingly, bin boundary thresholds of engine power and $T_{SCR\ IN}$ evaluated for bin-1a exhibit a robust assessment of the metric-based results to comply with the current NTE in-use threshold for NO_x emissions. Except for test activity acquired from vehicle-C, nearly more than 90% of events generated in bin-1a demonstrate bsNO_x emissions levels to be below 0.45 g/bhp-hr. Additionally, a comparison with respect to the certification

standard shows that proportion of events that lie within the boundary of 0.20 g/bhp-hr for NO_x emissions ranged from approximately 71% for vehicle-B to an average of 85% for vehicle-A and D, respectively. The trends illustrated in Figure 67 highlight that independent of test route and vocational activity, a substantial amount of events generated in this bin category were within the thresholds for the certification standard and NTE in-use limit for NO_x emissions. The details mentioned above highlight the significance of SCR activity that supports efficient tailpipe NO_x reduction under favourable exhaust gas thermal conditions. Additionally, a 95% confidence interval (CI) (i.e., with a $z_{critical}:1.96$) was computed from NO_x emissions results acquired from all events generated in bin-1a. The lower and upper boundary of CI around the mean was 0.20 and 0.24 g/bhp-hr, respectively. The proportion of events that lie within these bounds ranged from approximately 72% at lower bound of CI (i.e., from vehicle-B) to 87% at the upper bound of CI (i.e., from vehicle-A and D). Conversely, only 21% of overall events generated from vehicle-C were below the upper bound of quantified CI. It is to be emphasized again that engines equipped in vehicle-A, B and D were within the useful compliance life.

With respect to test activity acquired from vehicle-C, approximately 40% of events generated in bin-1a emitted relatively higher bsNO_x emissions (i.e., above 0.45 g/bhp-hr). The cumulative distribution chart shows a significant offset in the overall trend of bsNO_x emissions for this specific vehicle compared to the remaining three-vehicle datasets. Results from ABW binning approach are inconclusive of the primary reason for the deviations in bsNO_x emissions mentioned above (i.e., specifically from vehicle-C), but aids in explicitly identifying test activity that demonstrates unanticipated results (i.e., specific to bin-1a) under modes of operating conditions that are typically favourable for SCR activity. It is highlighted in literature that there exist several factors that affect SCR performance such as real-world thermal aging, catalyst poisoning (i.e., sulfur or phosphorous) and formation of solid urea deposits on the catalyst substrate (Kwak et al., 2012; Yuan et al., 2015).

The four vehicles were equipped with HD engines certified to U.S.EPA 2010 certification standard for NO_x emissions. However, the FTP certification values for the four vehicle datasets ranged from 0.06 to 0.17 g/bhp-hr for NO_x emissions. While vehicle-D was certified for the lowest certification value, cumulative bsNO_x emissions trends presented in Figure 67 (comprising of different engine operational conditions), depict similar trends to that of vehicle-A and B (i.e., which were certified to a relatively higher NO_x emissions value), under modes of operating conditions favorable for SCR catalytic performance. Although the four HD engines were certified to 0.20 g/bhp-hr standard, depending on engine calibration and technological feasibility in terms of meeting engine performance, power demand and emissions targets of regulated pollutants over the FTP cycle, HD engine manufacturers often target to exhibit NO_x emissions value to be below than the certification standard. This is primarily attributed to account for a range of factors such as variability in fuel composition, thermal degradation, deterioration of the aftertreatment catalyst and emissions control technologies that the engine may experience under a range of real-world ambient and driving conditions throughout the useful life of the engine.

Table 26 provides a comparison of the overall duration and NO_x mass distribution of test activity within each of the bin categories. Except for test activity acquired from vehicle-C, the results show a notable decrease in the overall NO_x mass emitted in comparison with the fraction of test duration, i.e., specifically in bin-1a. The substantial reduction is primarily due to active and efficient SCR operation, which results in an overall reduction in the NO_x mass fraction. Approximately a third of operation acquired in bin-1b for test activity from vehicle-A and B results in accumulation of approximately 60% of total NO_x mass emitted. A broader comparison of activity in bin-1a and 1b highlights the necessity for technological solutions needed for NO_x reduction in-line with activity acquired from modes of operation captured in bin-1b. It is interesting also to compare the amount of time spent in bin-1a for vehicle-C and D. The two vehicles were operated on a near similar test route, and the time-weighted activity profile (i.e., data presented in Figure 49) for the two test routes (i.e., route-3 and 4) did not showcase a substantial difference. Also, the two vehicles were

equipped with engines of a near similar rated power, but different torque rating and the difference in vehicle weight during the testing phase was within 1000 lbs. However, a comparison of $T_{SCR IN}$ (i.e., data presented in Figure 50) highlights a notable difference in the thermal profile distribution, especially for test activity acquired above 180 °C. Therefore, indicative of the significant differences in engine control strategies by the two engine manufacturers.

Table 26: Global comparison of time spent and NOx mass distribution within each ABW bin categories

Parameter	ABW Bin	Vehicle [-]			
		A	B	C	D
Duration [%]	Bin-1a	26.3	31.7	41.8	54.3
	Bin-1b	32.2	34.4	13.5	5.8
	Bin-2a		1.6	0.7	1.4
	Bin-2b	34.6	30.2	39.8	33.6
NOx Mass [%]	Bin-1a	18.6	27.6	46	36.4
	Bin-1b	62.6	58.5	31.5	35.2
	Bin-2a		1	0.1	0.10
	Bin-2b	13.4	6.6	17	19

Figure 68 shows a cumulative comparison of bsNOx emissions for events generated in bin-1b. From a global comparison perspective of the four vehicle datasets, vehicle-B emitted the lowest NOx emissions rates. Events that exhibited bsNOx emissions levels to be above 1 g/bhp-hr ranged from approximately 40% for vehicle-C and A to 60% for vehicle-B. Although NOx emissions under this mode of operating conditions are not regulated during in-use operation as per the NTE protocol, the trends observed in Figure 68 correspond to different in-cylinder combustion control strategies used to limit tailpipe NOx emissions under modes of activity captured in bin-1b. The engine control parameters play a substantial role in reducing in-cylinder NOx formation without a significant impact on engine performance under various engine speed and load operating conditions beneath the maximum torque curve of the engine. Some of the strategies typically used under such modes of in-use operation

include optimized control of turbocharger and EGR, and fuel injection strategies to reduce in-cylinder peak temperature.

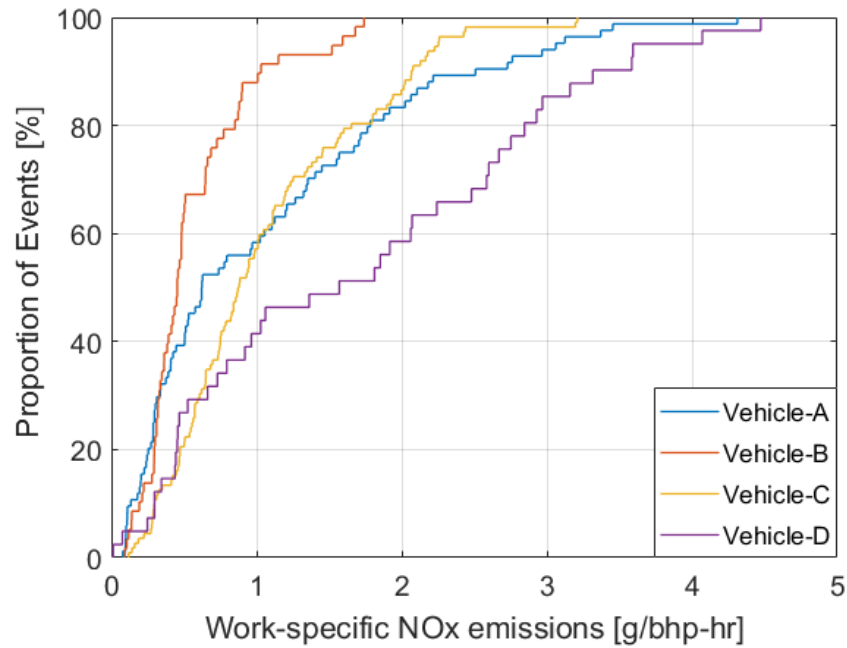


Figure 68: Cumulative frequency distribution of bsNOx emissions of all events generated in ABW bin 1b

Figure 69 shows a box and whisker distribution of bsNOx and CO₂-specific NOx emissions (i.e., top and bottom graph respectively) of all events generated in each of the four vehicle datasets for tractive work producing events (i.e., bin-1a and bin-1b) of the ABW binning approach. The results (i.e., top charts of Figure 69) indicate that the grouped average for bsNOx emissions acquired from each of the box and whisker distribution in bin-1a and bin-1b are 0.20 and 1.08 g/bhp-hr. It is to be noted that bin-1b is primarily a remainder bin for tractive work-producing events that do not comprise of entire event activity above the ABW T_{SCR IN} threshold (i.e., 230 °C). Therefore, events acquired in this category are representative of (i) Events that demonstrate minimal to no SCR activity (i.e., for example, bin-1b events captured in quadrant-2 in Figure 59 and Figure 60), and (ii) Events that showcase a combination of both active and non-active SCR operation (i.e., for example, bin-1b events captured in quadrant-1, 3 and 4 in Figure 59 and Figure 60). However, the catalyst de-NOx efficiency for test activity acquired is greatly dependent on the thermal hysteresis,

SCR control strategies, and the amount of time spent during active SCR operation. The overall 86% decrease in average bsNOx emissions between the two bin categories (i.e., bin-1a and bin-1b) is primarily attributed to the SCR aftertreatment system that reduces NOx emissions under favorable thermal conditions (i.e., dependent on the real-world duty cycle and thermal management strategies).

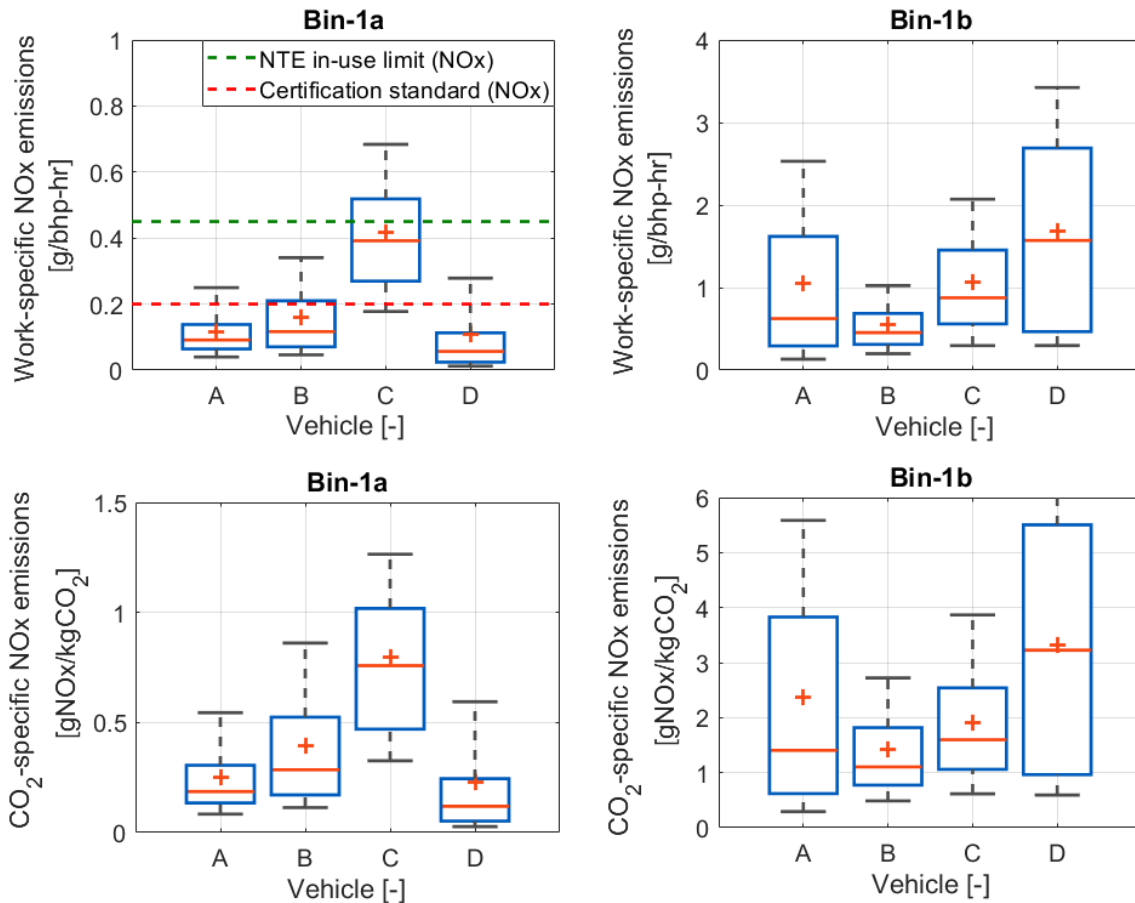


Figure 69: Comparison of work-specific and CO₂-specific NOx emissions of all events generated in bin-1a and 1b of each vehicle dataset

In comparison, CO₂-specific NOx emissions rates (i.e., bottom charts of Figure 68) highlights the CO₂ requirements needed for NOx reduction specifically for activity acquired in bin-1a. Since modern diesel engines are greatly dependent on EATS to demonstrate reductions in real-world tailpipe emissions (i.e., specifically of NOx and PM emissions). The results obtained from test activity captured in bin-1a are indicative of the associated engine control strategies (i.e., such as optimization of fuel injection timing, fuel quantity, air mass management using intake throttling and

turbocharger etc.) used to increase and maintain exhaust gas thermal conditions favourable for SCR operation. Additionally, once the EATS has achieved catalyst conductive thermal conditions for SCR operation, HD engine manufacturers typically use control strategies achieve simultaneous CO₂ reductions without drastically impacting exhaust gas energy, therefore also leading to fuel consumption benefits under such modes of in-use operation.

Table 27: Comparison of group average CO₂-specific NO_x emissions of all events generated in bin-1a and 1b

Statistical Parameter	NO _x Emissions [gNO _x /kgCO ₂]	
	Bin-1a	Bin-1b
Average	0.42	2.25
90 th percentile	0.80	4.64

The arithmetic mean of individual average and 90th percentile (i.e., each vehicle) of CO₂-specific events is outlined in Table 27. The CO₂-specific NO_x emissions indicate an average reduction of 81.3% and 82.7% (i.e., average and 90th percentile) for activity captured in bin-1a. The quantitative comparison of operation captured from each of the vehicle datasets highlights the difference (i.e., NO_x versus CO₂ trade-off) in results obtained between bin-1a and 1b, respectively. As discussed earlier, NO_x emissions from vehicle-C were observed to be relatively higher (i.e., specifically for activity in bin-1a), excluding data from vehicle-C results in the group arithmetic mean to be 0.29 and 2.37 gNO_x/kgCO₂ for bin-1a and 1b, respectively.

Although the binning metric does not use temperature-based segregation of activity captured in bin-2, a temperature threshold (i.e., T_{SCR IN}: 230 °C) was used to highlight the differences in event-averaged NO_x emissions rates under low-power operation. The comparative analysis shows the real-world NO_x reduction (i.e., left chart in Figure 70) achieved during low-power engine operation while the thermal conditions are favourable for SCR activity. The group arithmetic mean tsNO_x emissions for events presented in Figure 70 is 7.70 and 30 g/hr for events that include an average T_{SCR IN}, i.e., above and below 230 °C, respectively. The relatively lower tsNO_x

emissions observed in the left graph of Figure 70 exhibits events generated from an operation where the conductive catalyst temperature in conjunction with stored NH_3 and low space velocity were favorable for NO_x reduction

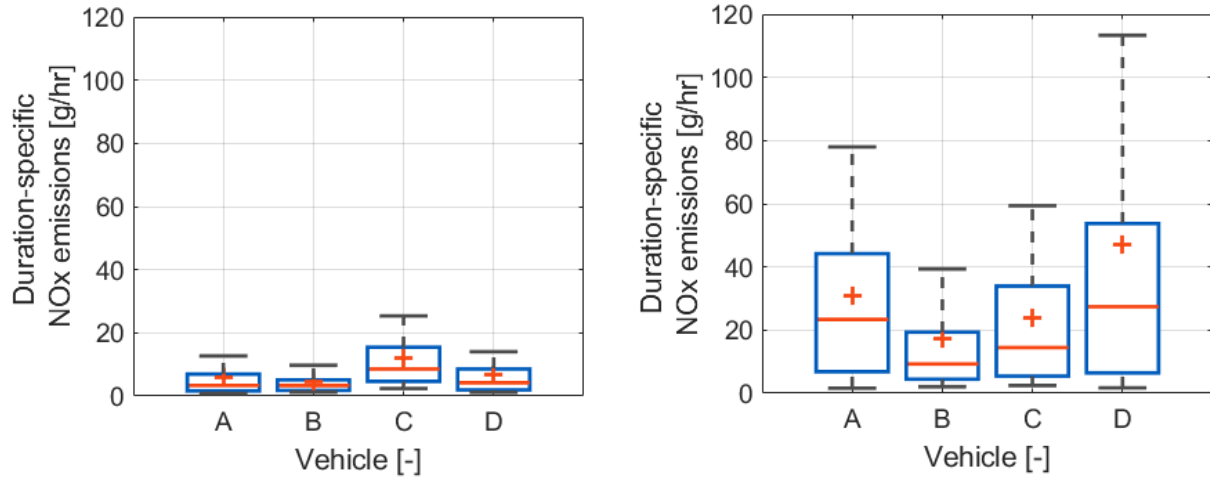


Figure 70: Comparison of duration-specific NO_x emissions for events generated in bin-2b divided into two categories: (a) Event-averaged $T_{SCR IN}$ greater than $230\text{ }^\circ\text{C}$; (b) Event-averaged $T_{SCR IN}$ less than $230\text{ }^\circ\text{C}$

The quantitative difference in NO_x emissions results observed specifically at low-power engine operating conditions demonstrates the potential of the SCR system to reduce NO_x emissions even during low-load operating conditions. The above highlights show the necessity of alternate technological solution to suffice thermal mass/energy requirements needed to unleash the potential of SCR activity for NO_x reduction even at low-load operating conditions.

In summary, ABW binning performed on test activity acquired in phase-1 of the study resulted in average utilization of 95.56% and 93.71% of data acquired and NO_x mass emitted for emissions assessment from all trips that generated at least 1 ABW. There were 22 trips out of 24 trips captured that generated at least 1 ABW. As discussed, earlier leg-2 of route-3 did not generate any ABW, since the activity captured in the entire trip did not meet the minimum W_{Ref} requirements.

5.3. Evaluation of ABW - Phase 2

With an actively growing regulatory interest in monitoring NO_x emissions from actual in-fleet operation, CARB implemented OBD regulatory requirements for tracking and reporting of OB data stream (i.e., NO_x emissions, engine and vehicle operational parameters) starting from engine MY 2022 (CFR/13/1971.1; Ellis, 2017; Montes, 2018). The tracking approach evaluates NO_x emissions as a function of real-time instantaneous binning of test activity into 14 discrete bins (i.e., based on vehicle speed and engine power). Three additional bins are also incorporated to evaluate test activity for (i) NTE operation, (ii) Active DPF regeneration, and (iii) OBD Malfunction.

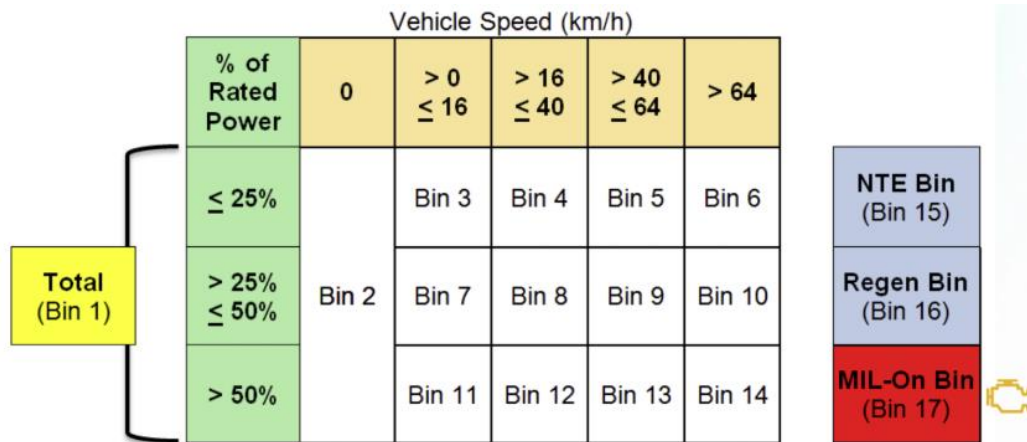


Figure 71: CARB HD-OBD NO_x binning approach (Henderick, 2019)

Although the approach (i.e., presented in Figure 71) provides a unique opportunity of real-time performance evaluation of emissions control devices over a wide range of vehicle and engine operating conditions, 1 Hz data instantaneous binning approach requires a robust evaluation to account for errors associated with real-time signal alignment and dispersion. Additionally, it is important to keep in mind that on-board NO_x sensors are only operational above a certain dew-point temperature of exhaust gas (i.e., typically between 150 and 200 °C). Therefore, the overall bin-population will primarily be biased dependent on vocational application and operation. Note that data analysis related to the aforementioned on-board NO_x tracking approach is not discussed in this work.

This section demonstrates the application of the ABW approach on test activity collected from actual in-fleet vocational operation. To acquire in-use NOx emissions data from a wide range of real-world operating conditions, NOx sensors instrumented on fleet operational trucks were configured to bypass the minimum dew-point temperature requirement. Literature discussed in section 2.9 highlights the cross-sensitive interference of exhaust gas products on NOx sensor measurements, and due to the absence of a real-time correction factor, test activity acquired from the NOx sensor was not subjected to any corrective factors to account for the cross-sensitive behavior. In order to provide a general understanding of the associated deviations in measurements, section 5.4 discusses the measurement thresholds associated with NOx sensor measurements compared to a PEMS during real-world operation.

Equation 5.2 was used to quantify NOx mass emissions rates using exhaust gas mass flow rate broadcasted by the ECU. The correction factor presented in equation 5.2 converts exhaust flow rate from kg/hr (i.e., in standard conditions) to mol/sec and concentration of NOx emissions from ppm to mol/mol (Montes, 2018). In the current study, for vehicle datasets that did not broadcast exhaust gas mass flow rate (i.e., SPN ID: 3236) the summation of ECU signal broadcast for engine air intake mass flow rate (i.e., accounted for EGR mass flow rate) and fuel flow rate converted from volumetric flow rate to mass flow rate (i.e., assuming diesel fuel density of 0.830 kg/L) was used as a predicted (or) estimated exhaust flow rate. An error propagation comparison of the derived exhaust flow rate versus ECU broadcasted exhaust flow rate is presented in Appendix D.

$$\text{NOx} \left[\frac{\text{g}}{\text{sec}} \right] = 0.001588 \cdot \text{Exh Flow} \cdot \text{NOx} \cdot \frac{1}{3600} \quad \text{Equation 5.2}$$

Where:

Exh Flow is the exhaust flow rate broadcasted by the ECU (SPN ID: 3236) in kg/hr corrected for standard pressure and temperature

NOx is the concentration of NOx emissions broadcasted by the sensor in ppm

5.3.1. Vehicle Activity Characteristics

This section illustrates a detailed overview of the diverse vocational in-fleet operational vehicle activity profiles collected from 18 trucks (i.e., 10 HD and 8 MD) operating in southern California. Table 28 presents an aggregate summary of total engine work, fuel consumption, distance travelled, and average speed categorized based on vehicle vocation. As expected, the global average vehicle speed of line-haul trucks used for long-haul application is the highest at 40.7 mph compared to trucks operating in other vocations such as urban delivery goods distribution, drayage application. The average vehicle speed of trucks recruited in Category-C (i.e., used for construction equipment such as cement mixers) is approximately 9.9 mph. Vehicles sampled in this specific category spent approximately 61.79% of the operational time while the engine was producing non-tractive engine work. This is primarily due to the vocational demand that involves the use of power take-off (PTO).

Table 28: Summary of vocation-specific vehicle/engine operational parameters

Parameter	Vocational Category					
Category [-]	A	B	C	D	E	F
Vehicle ID [-]	1,2,3	4,5,6	7,8,9	10,11,12	13,14,15	16,17,18
Duration [hr]	897	800	1133	174	197	267
Engine Work [bhp-hr]	90,539	38,898	65,334	7387	7843	9901
Fuel Consumption [L]	16,359	8742	12,890	1529	1675	2156
Distance [miles]	36,117	12,605	11,209	2992	1859	3431
Average Vehicle Speed [mph]	40.7	16.2	9.9	15.1	9.6	13.9

Table 29: Summary of vocational vehicle class, engine MY, and time-weighted fraction of active OBD MIL and DPF regeneration

Vocational Category	Vehicle ID	Vehicle Class	Engine MY	OBD MIL ¹	DPF Regeneration ²
[-]	[#]	[-]	[#]	[%]	[%]
A	1	HD	2016	0	0.80
	2	HD	2018	0	0.86
	3	HD	2018	0	3.40
B	4	HD	2016	0	29.58
	5	HD	2015	0	39.00
	6	HD	2016	92.21	24.85
C	7	HD	2015	0	1.21
	8	HD	2015	0	1.88
	9	HD	2014	0	1.05
D	10	MD	2017	0	3.76
	11	MD	2015	0	2.13
	12	MD	2018	0	5.56
E	13	MD	2015	0	1.86
	14	MD	2015	0	2.53
	15	MD	2016	0	2.11
F	16	HD	2017	0	18.11
	17	MD	2015	0	1.22
	18	MD	2016	0	1.12

1) OBD malfunction (SPN ID:5086) status bit 1

2) Combination of DPF active regeneration (SPN ID:3700) status bit 1 and 2

Trucks sampled in this study were segregated into MD and HD vehicle class category based on GVWR (i.e., MD vehicles comprising of GVWR between 19,501 and 33,000 lbs, and HD vehicles comprising of GVWR above 33,000 lbs). Table 29 outlines the individual categorization of vehicle class and time-weighted percentage of operational activity that resulted during an active OBD malfunction, and DPF regeneration. It was observed that OBD MIL was active for approximately 92.21% of operational time

for test activity acquired from vehicle 6. Therefore, a significant amount of test activity acquired from this vehicle was not evaluated using the ABW binning approach. HD delivery trucks that experienced a significant amount of operation during stationary idle operation (or) low vehicle speed operation (i.e., urban driving operation) exhibit relatively higher (i.e., on average 28%) operational time during DPF regeneration activity.

Figure 72 presents a time-weighted overview of vehicle-speed based distribution for each of the individual test vehicle datasets, and Table 30 summarizes the distribution of time-weighted vehicle speed and engine power for each of the vocational vehicle categories. Bin thresholds discussed in section 5.2.1. were used for vehicle activity characterization in the herein presented section.

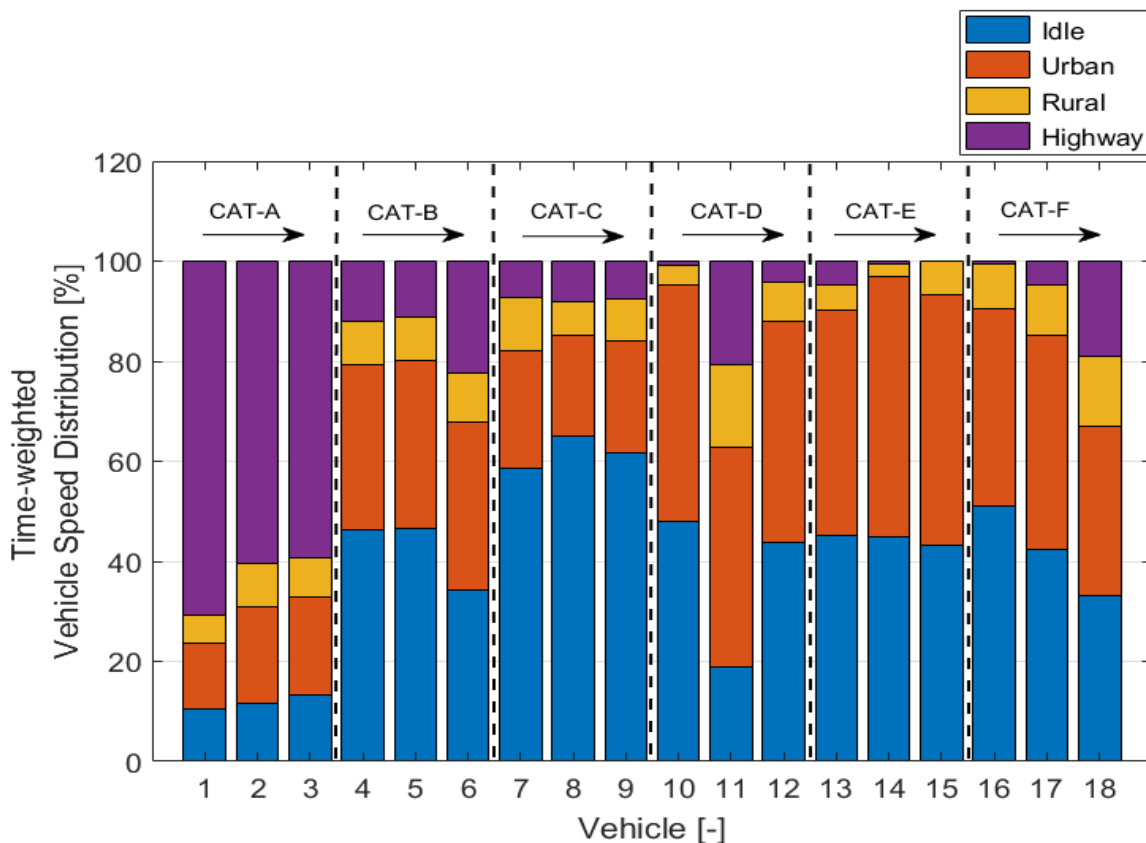


Figure 72: Time-weighted vehicle speed distribution of all in-use datasets sampled in section 3.3; (CAT-Vocational category)

Table 30: Time-weighted vehicle speed and engine power distribution segregated by vocational category

Vehicle Speed distribution [%]						
Vocational Category	A	B	C	D	E	F
Idle	11.72	42.38	61.79	36.88	44.46	42.15
Urban	17.48	33.41	22.02	45.14	49.04	38.79
Rural	7.21	9.04	8.51	9.40	4.67	11.02
Highway	63.59	15.17	7.68	8.58	1.83	8.04
Engine Power Distribution [%]						
Vocational Category	A	B	C	D	E	F
Low	63.69	83.99	80.38	80.89	87.27	84.42
Medium	24.59	10.54	12.51	13.36	10.43	10.31
High	11.72	5.47	7.11	5.75	2.31	5.27

The majority of in-use operation occurs during stationary idle, low-vehicle speed and power operation for all vocational application except for category A. Trucks recruited in category-A were typically used for distribution of grocery products in and between the northern and southern corridor of California. Therefore, representative of a significant amount of highway/freeway driving conditions. Specific to drayage truck application (i.e., category B), these vehicles on average spent 42.38% and 33.41% of the operational time during stationary idle and low vehicle speed operation, respectively. This is because of test activity acquired in LA traffic and at the port harbour. Trucks recruited in category-D and E were used for short-haul pick-up and delivery of beverage across local warehouses in LA. Except for vehicle-11 (i.e., used for beverage distribution outside the metropolitan area of LA), on average more than 90% of test activity collected from beverage distribution vehicles experienced low-vehicle speed operation. Most of the beverage distribution trucks sampled in this study operated in the inner metropolitan area of LA that experience congested traffic operation. There was 83.09% of soak time events (i.e., between a key-off event and the following key-on event) for the above-mentioned beverage distribution trucks that were less than 30 minutes. All vehicles recruited in category-F (i.e., short-haul

delivery application) were used to deliver industrial, medical, and speciality gas bottles across LA. Vehicle-16 and 17 were typically used for short-haul delivery while the typical delivery route of vehicle-18 included relatively longer transport distance that experienced highway driving operating conditions.

Figure 73 shows the time-weighted distribution of $T_{SCR\ IN}$ (i.e., divided into five different temperature bins) of the entire test activity collected for each vehicle dataset. The integrated work-specific NO_x emissions for each vehicle dataset is indicated by (◆). Test activity comprising of active OBD MIL and DPF regeneration was excluded from the computation of work-specific NO_x emissions presented in Figure 73. Integrated bsNO_x emissions evaluated from all valid test activity was the highest from Vehicle-12 and 5. It is interesting to compare the time-weighted vehicle speed and $T_{SCR\ IN}$ distribution of vehicle-12 and 17. The vehicle speed-based distribution was observed to be near similar with a maximum difference of 2.5% across the different vehicle speed bins. Depending on the vocational demand, while both vehicle-12 and 17 were equipped with the same engine, it was observed that vehicle-17 which was used for delivery of speciality bottles spent the majority of the operational time (i.e., ~52.53%) under test conditions that exhibited $T_{SCR\ IN}$ to be greater than 250 °C, compared to vehicle-12 which spent approximately 33% of operating time above 250 °C.

Table 31 shows the time-weighted distribution of $T_{SCR\ IN}$ based on the vocational vehicle category. The $T_{SCR\ IN}$ distribution is significantly dependent on engine displacement, payload, vocational real-world duty cycle, thermal inertia, engine control and thermal management strategies. Except for port-drage trucks, a dominant fraction (i.e., greater than 60%) of real-world operation for trucks recruited in other vocational categories was captured while $T_{SCR\ IN}$ was between 180 and 400 °C (i.e., ranging from 65.21% to 80.12%). For port-drage application, approximately 44.32% of test activity was captured while $T_{SCR\ IN}$ was below 180 °C. Due to limitations associated with solid urea deposit formation, the current urea-SCR systems cannot be used at system temperature below 180 °C (Johnson and Joshi, 2018). Although

entirely dependent on the SCR thermal management strategies, the discussion presented earlier with regards to port-drayage application shows that these trucks experience extended engine idle operation and frequent stop-and-go activity at the port harbour, therefore resulting in cooldown of the EATS.

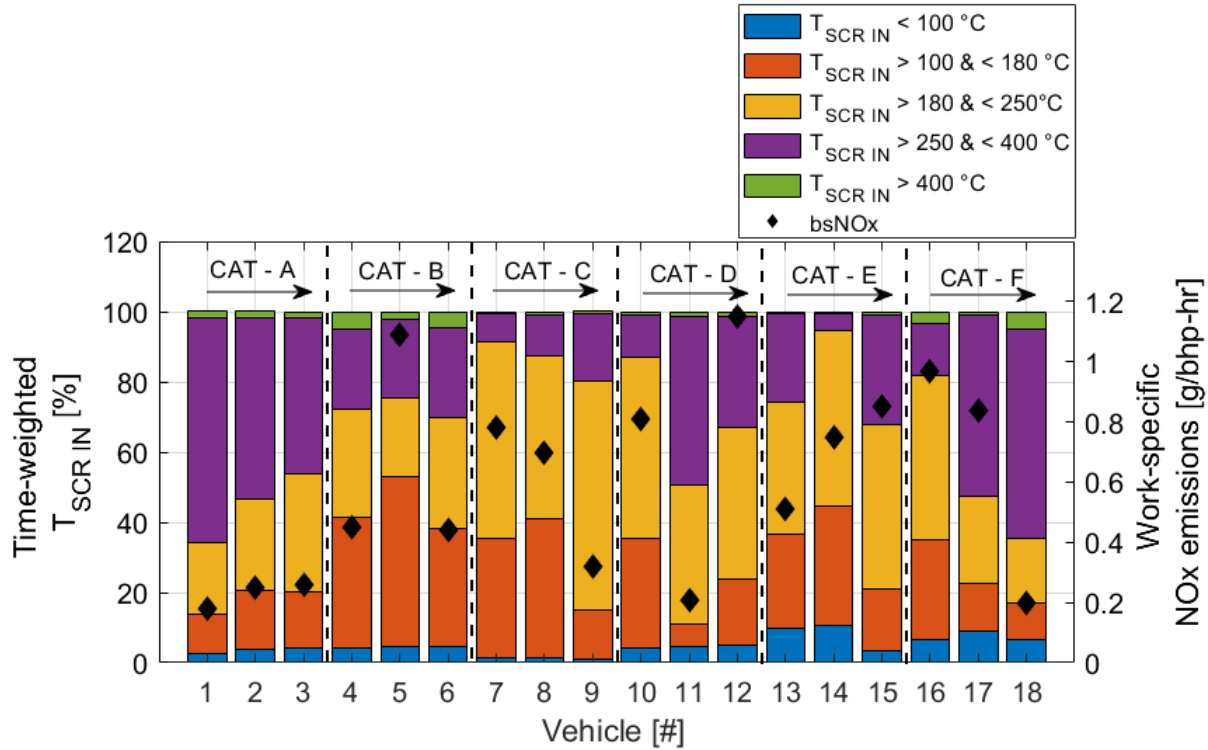


Figure 73: Time-weighted $T_{SCR IN}$ distribution of all in-use datasets sampled in section 3.3; (CAT-Vocational category)

Table 31: $T_{SCR IN}$ distribution as a function of three different temperature bandwidths

Vocational Category [-]	Time-weighted $T_{SCR IN}$ Distribution [%]		
	$T_{SCR IN} \leq 180 \text{ } ^\circ\text{C}$	$180 \text{ } ^\circ\text{C} < T_{SCR IN} \leq 400 \text{ } ^\circ\text{C}$	$T_{SCR IN} > 400 \text{ } ^\circ\text{C}$
A	18.16	80.12	1.72
B	44.32	51.67	4.01
C	30.55	68.73	0.72
D	23.50	75.31	1.19
E	34.09	65.21	0.70
F	24.75	72.11	3.14

5.3.2. Application of ABW Approach

The ABW binning approach was performed on test activity acquired from fleet-based vehicle activity for each trip (i.e., key-on to key-off). Due to unavailability of the full-load torque curves from the engine manufacturers, the ECU broadcasted six-point torque curve was used for seven out of 18 vehicle datasets to compute W_{Ref} (i.e., minimum engine work required for the generation of an ABW). The simulated W_{Ref} for FTP test cycle of the 18 vehicle datasets ranged from ~ 15 to 35 bhp-hr. Figure 74 shows a comparison of the number count of all trips acquired and valid trips (i.e., named as valid ABW trips) that were used by the ABW binning approach for each of the vehicle dataset. The significant difference between the total and valid trip count is because a majority of trips acquired did not meet the minimum W_{Ref} criteria of the ABW approach. Additionally, the total percentage of data utilization from valid ABW trips is presented on the right y-axis of Figure 74 and is indicated by the red diamond symbol.

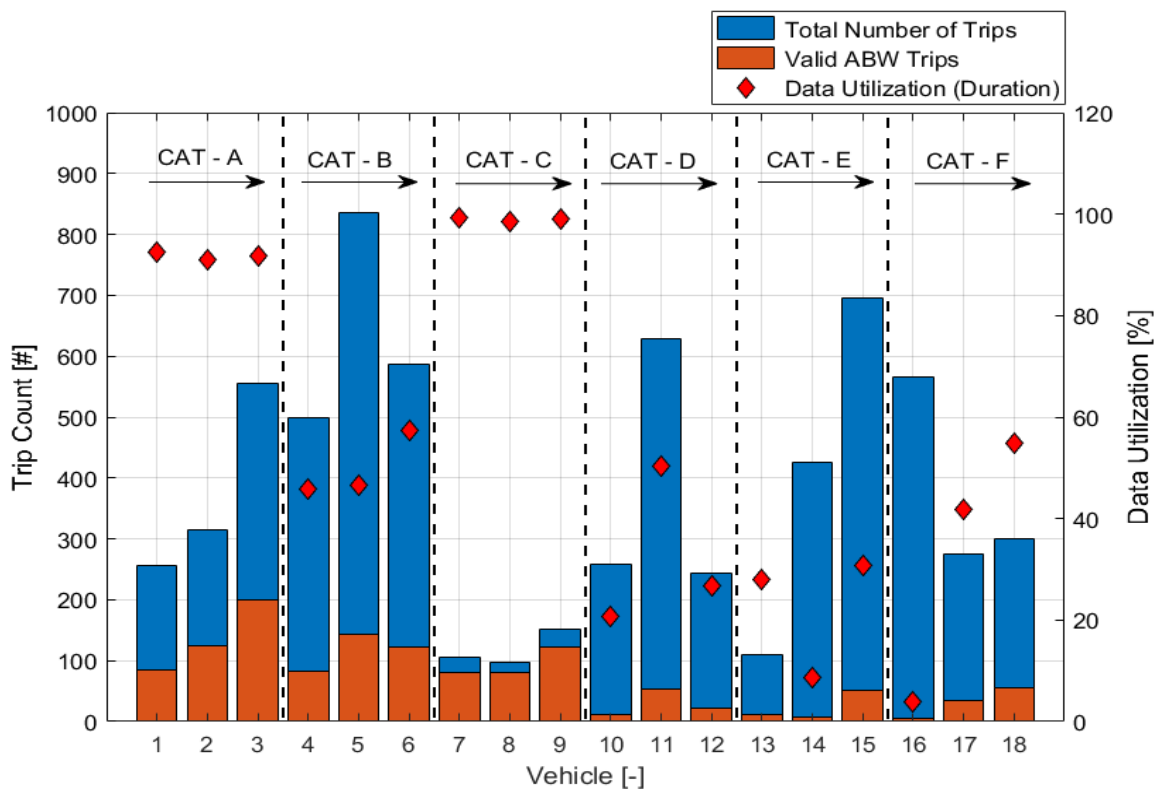


Figure 74: Comparison of trip count and overall data utilization for ABW binning; (CAT-Vocational category)

Figure 75 presents an overview of trip-based engine work distribution as a function of total engine work produced over the FTP cycle for each of the 18 vehicle datasets. On average, only 26.40% of trips acquired from the 18 vehicle datasets were used for emissions assessment by the ABW binning approach. Therefore, resulting in a time-weighted data utilization of 54.88% of entire vehicle activity collected. In-fleet activity shows that the majority of trips generated (i.e., on average, 53.68%) demonstrated the total trip engine work to be less than $0.25 \times \text{FTP}_{\text{Work}}$. Evaluation of actual in-fleet vocational activity indicates that the threshold selected as a minimum test requirement for window generation plays a critical role in determining the fraction of test activity utilized for emissions assessment using the ABW binning approach.

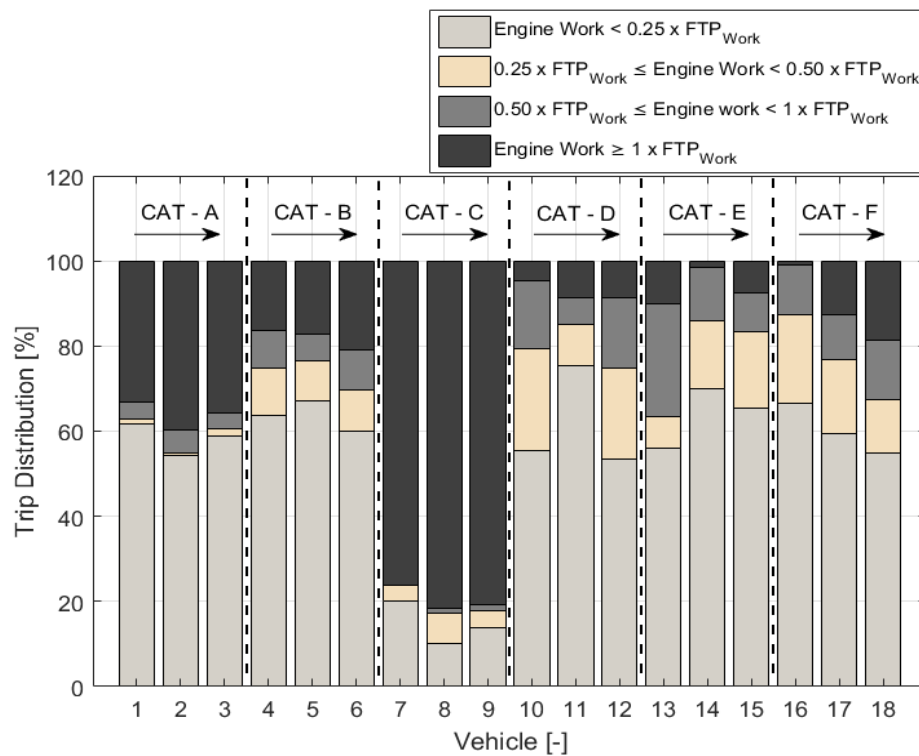


Figure 75: Trip-based distribution of engine work

Figure 76 and Figure 77 illustrate the box and whisker distribution of bsNOx emissions of all events generated within each ABW in bin-1a and 1b, respectively, and event-averaged $T_{\text{SCR IN}}$ for events generated in bin-1a. The comparison of the spread of event-averaged bsNOx emissions (i.e., in Figure 76) and $T_{\text{SCR IN}}$ (i.e., in

Figure 77) provides a general understanding of the overall distribution of event-activity captured in bin-1a for each vocational vehicle category. Although a measurement allowance protocol (or) an in-use threshold is not yet set forth for measurements obtained from NO_x sensors, NTE in-use limit and certification standard for NO_x emissions are used as a reference for the following discussion. In-line with results presented in Figure 76,

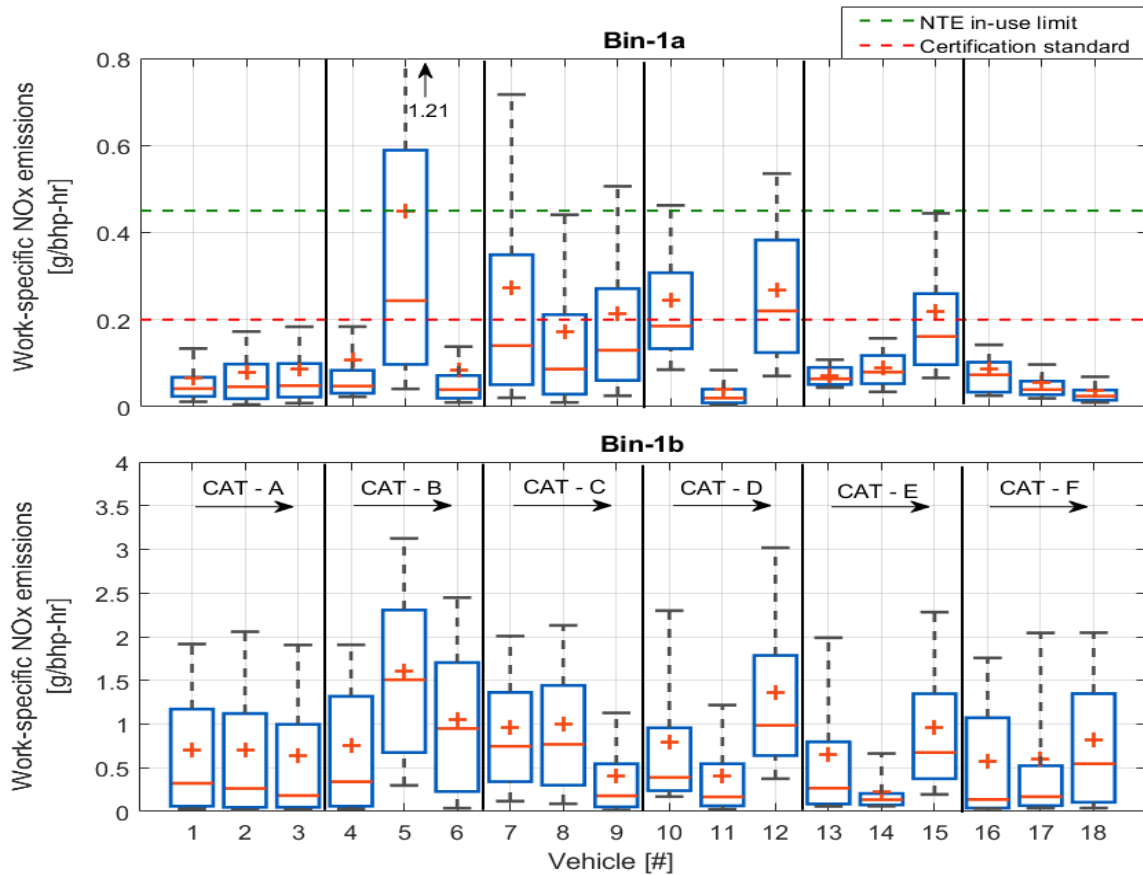


Figure 76: Comparison of work-specific NO_x emissions of (a) Top graph: All events generated within each ABW in bin-1a, and (b) Bottom graph: All events generated within each ABW in bin-1b for each of the 18 vehicle datasets

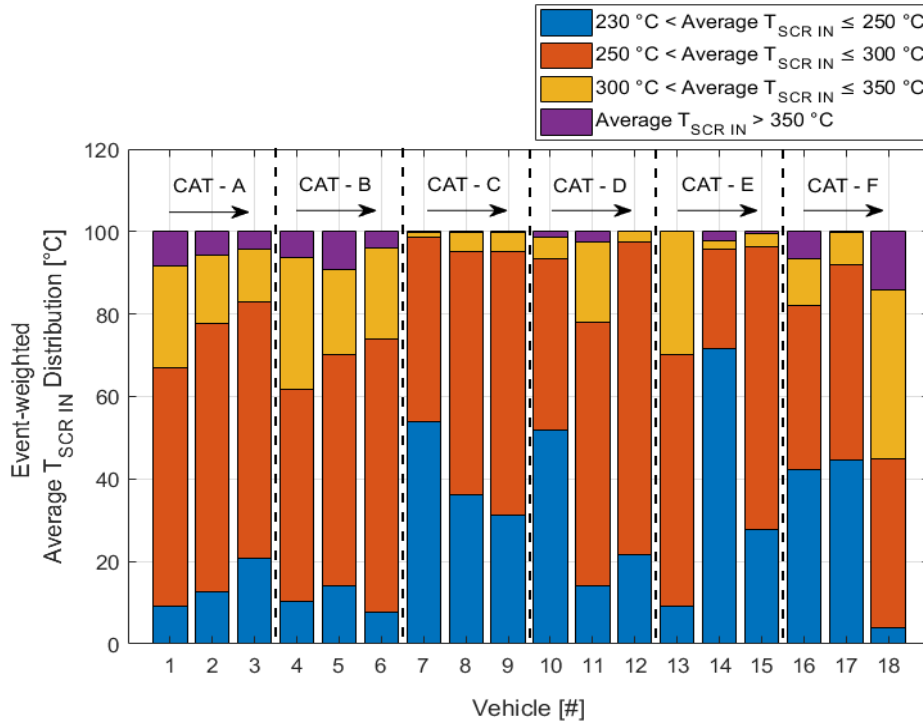


Figure 77: Distribution of event-averaged $T_{SCR IN}$ of bin-1a events

Comparing the 90th percentile of total events generated in bin-1a, results indicate that independent of vocational duty cycle characteristics, 11 and 13 out of 18 vehicle datasets exhibit bsNOx emissions levels below the certification standard (i.e., 0.20 g/bhp-hr for NOx emissions) and NTE in-use limit for NOx emissions, respectively. The average bsNOx emissions of all events from each of the 18 vehicle datasets were 0.15 and 0.78 g/bhp-hr for bin-1a and 1b, respectively.

The five-vehicle datasets that generated a significant proportion (i.e., above 10%) of events above the current NTE in-use limit are vehicle-5, 7, 9, 10, and 12. Approximately, 19.46% of events generated in the five-vehicle datasets demonstrated bsNOx emissions levels to be above the 0.45 g/bhp-hr threshold. These relatively high NOx events captured in bin-1a accounted for an average of 18.39% of time-weighted event duration. A comparative analysis of bsNOx emissions captured in bin-1a (i.e., from data presented in Figure 76 and Table 32) indicated vehicle-5 as an outlier (i.e., due to relatively higher bsNOx emissions under favourable SCR operating conditions). The results show that approximately 31.79% of events captured in bin-

1a demonstrate relatively higher bsNO_x emissions (i.e., above 0.45 g/bhp-hr). An in-depth evaluation of test activity showed that exhaust gas thermal conditions of these events (i.e., average T_{SCR IN} of 303 °C for these specific events) were favorable for SCR operation. The OBD MIL lamp command was 0 (i.e., OBD Lamp: Off) for the entire data logging phase and fault code SPN ID: 3719 (i.e., Soot level very high) was active for nearly 10% of these above-mentioned high NO_x events captured. Due to the absence of instrumentation of NH₃ sensor on this vehicle dataset, the analysis is inconclusive of the primary cause of the observed deviations.

Table 32 presents an overview of the fraction of events that exhibit bsNO_x emissions levels to be above and below the NTE in-use limit for NO_x emissions for bin-1a and 1b, respectively.

Table 32: Proportion of event count and duration for events generated above and below the NTE in-use limit for NO_x emissions for bin-1a and 1b

Vocational Category	Vehicle ID	Bin-1a		Bin-1b		
		bsNO _x Emissions Above NTE In-use NO _x Limit		bsNO _x Emissions Below NTE In-use NO _x Limit		
		Event count	Duration	Event count	Duration	Average T _{SCR IN}
[-]	[#]	[%]	[%]	[%]	[%]	[°C]
A	1	1.4	0.74	55.46	70.94	229.42
	2	1.58	0.78	57.58	76.12	226.96
	3	1.91	0.93	62.6	77.64	224.54
B	4	3.83	2.74	53.37	65.95	221.69
	5	31.79	22.16	16.73	27.7	225.69
	6	2.6	2.47	39.19	65.87	223.67
C	7	18.96	14.23	32.04	36.02	216.71
	8	9.68	6.3	34.17	42.62	221.54
	9	12.83	14.58	70.78	71.67	215.04
D	10	14.67	28.72	53	57.09	225.98
	11	0.45	0.41	70.7	84.05	230.14
	12	19.05	12.29	11.82	25.42	242.89
E	13	0	0	62	72.47	220.04
	14	1.79	0.77	83.58	79.09	227.01
	15	9.34	8.45	33.33	37.72	232.82
F	16	2.22	1.6	62.5	60.33	222.99
	17	5.09	2.71	42.52	55.28	239.01
	18	0.57	0.26	46.59	57.88	245.54

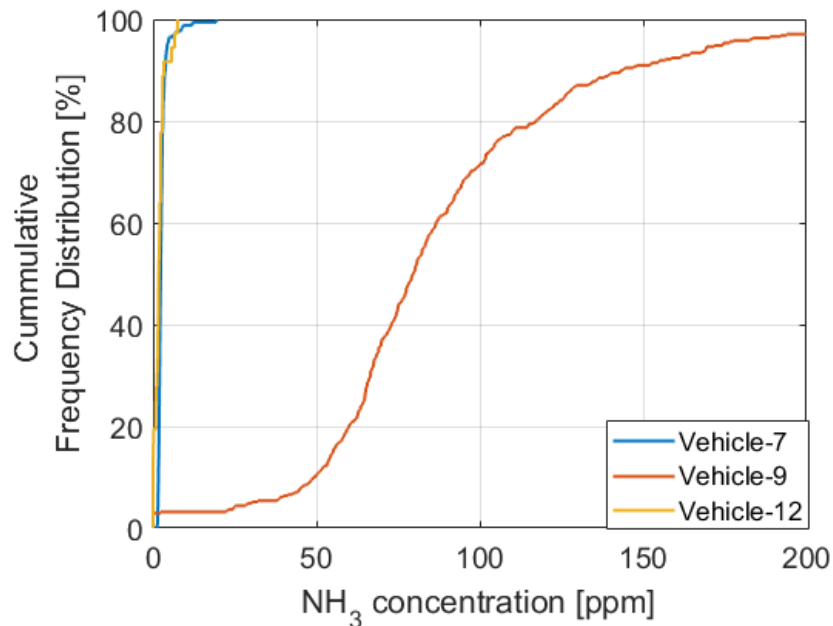


Figure 78: Cumulative frequency distribution of event averaged NH₃ concentration in bin-1a

Specific to vehicles whose 90th percentile of bin-1a bsNO_x emissions was above 0.45 g/bhp-hr, Figure 78 shows the event-averaged cumulative frequency distribution of NH₃ concentration. Among the five vehicle datasets (i.e., vehicle-5, 7, 9, 10 and 12), the NH₃ sensor was instrumented in only vehicle-7, 9 and 12. The frequency distribution of these events shows that the event-averaged NH₃ concentration was below ten ppm for 100% and 98% of these relatively high NO_x events for vehicle-9 and 12, respectively. The averaged NH₃ concentration ranges from 22.36 ppm for ~3% of the events to approximately 152 ppm for 90% of these relatively high NO_x events. It is well established in the literature that NO_x sensor measurements are impacted due to the presence of NH₃ gas (Demirgok et al., 2019; Frobert et al., 2013). The trend indicates that the NO_x sensor measurements acquired from vehicle-9 might have been impacted due to the notable presence of NH₃ gas. The impact of NH₃ interference on sensor reported measurements is discussed in section 5.4. Due to the absence of NH₃ sensor instrumentation in vehicle-5 and 10, it is therefore difficult to rule out the possibility of NH₃ gas interference to be the primary cause for the deviations observed.

Figure 79 shows the percentage contribution of bin-1a events whose average $T_{SCR IN}$ was below the ABW $T_{SCR IN}$ limit (i.e., indicative of insufficient thermal energy across the control volume of the SCR catalyst). The distribution is specific to events in bin-1a whose bsNOx emissions was above 0.45 g/bhp-hr for the five vehicle datasets whose 90th percentile of event-averaged bin distribution demonstrated bsNOx emissions levels to be above the NTE in-use limit for NOx emissions. Among the five specific datasets, bin-1a events generated from vehicle-12 had the highest fraction of events where $T_{SCR OUT}$ was below 230 °C.

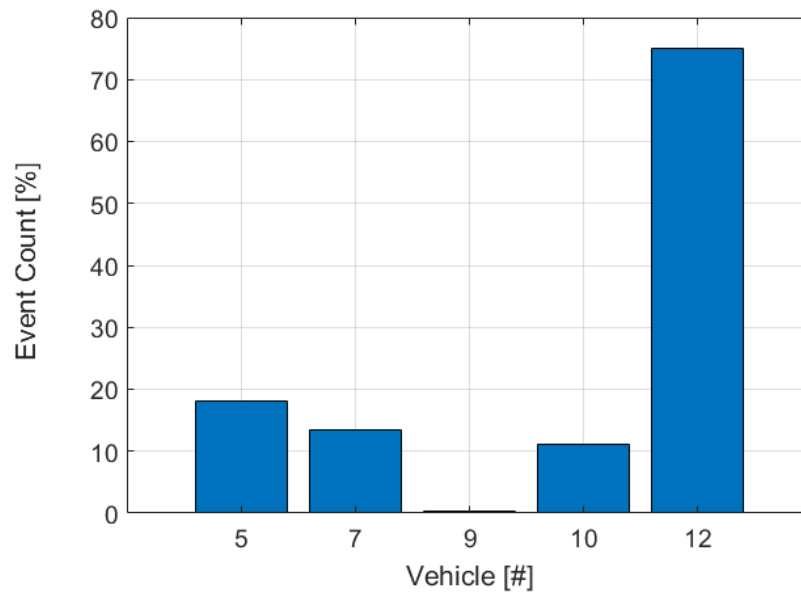


Figure 79: Proportion of event count for bin-1a ($T_{SCR IN} < 230^{\circ}C$)

Specific to events generated in bin-1b, on average 51.16% (i.e., data presented in Table 32 column 5) of total events generated exhibit bsNOx emissions levels below the current NTE in-use limit for NOx emissions. Therefore, resulting in an average time-weighted data distribution of 59.10%. This is because bin-1b acts as a remainder bin for events that do not meet bin-1a requirements, therefore, in this specific bin there exist engine work-producing events that exhibit a certain event-based time fraction operating below the ABW $T_{SCR IN}$ threshold. The results demonstrate that utilizing a traditional approach of a single thermal boundary threshold to separate events between bin-1a and 1b indicates inefficiency in the segregation of active versus

non-active SCR operational binning modes (i.e., specifically under critical SCR operating conditions). From a quantitative comparison basis, excluding these low NOx events from bin-1b resulted in an average increase in bsNOx emissions from 0.78 to 1.41 g/bhp-hr.

Figure 80 shows the distribution of events generated in bin-1b as a function of NOx emissions levels. Events generated in bin-1b are classified into four different categories (i) NOx level-1 comprises of events whose bsNOx emissions were below 0.45 g/bhp-hr, (ii) NOx level-2 comprises of events whose bsNOx emissions were between 0.45 and 1.5 g/bhp-hr, (iii) NOx level-3 comprises of events whose bsNOx emissions were between 1.5 and 3.0 g/bhp-hr, and (iv) NOx level-4 comprises of events whose bsNOx emissions were above 3.0 g/bhp-hr.

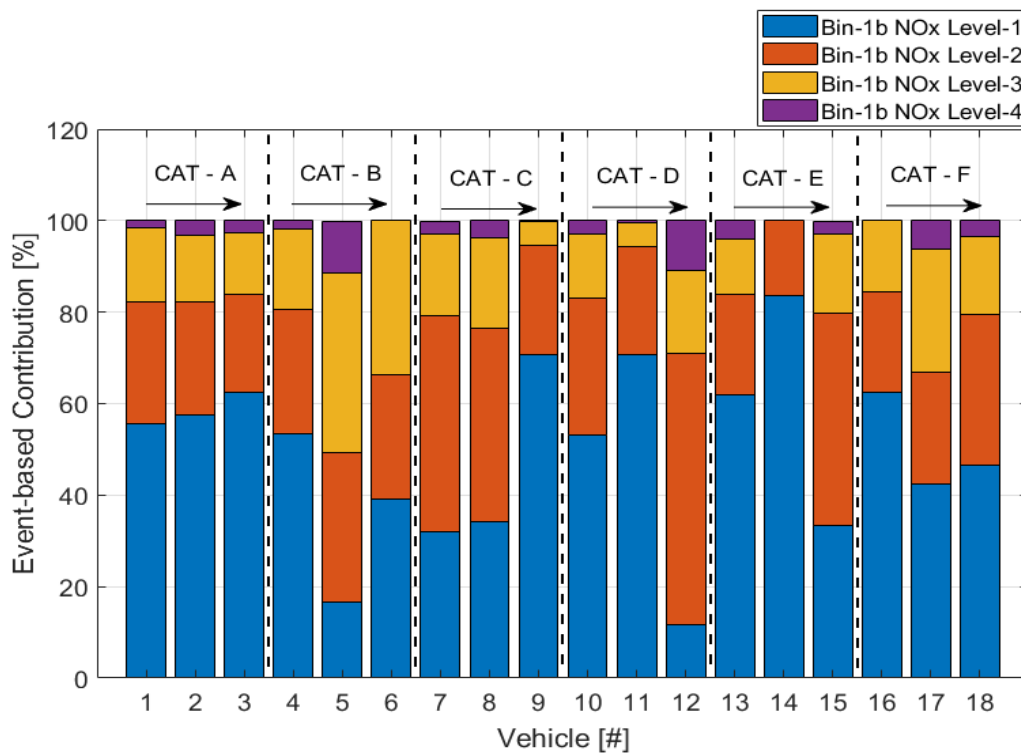


Figure 80: Distribution of NOx emissions for bin-1b events

Events generated in NOx level-1 of bin-1b are primarily of those whose $T_{SCR IN}$ dropped below the ABW $T_{SCR IN}$ threshold for a certain time fraction of test activity. Therefore, demonstrating relatively lower bsNOx emissions (i.e., in bin-1b category).

Events generated in NOx level-2, 3 and 4 are significantly dependent on the vocational operation and the different in-cylinder combustion control strategies used to limit in-use NOx formation without drastically impacting engine performance and durability. Since the NTE protocol is primarily tailored to evaluate in-use emissions only during SCR activity, modes of in-use operation often characterized by relatively high NOx events (i.e., those captured in the above-mentioned NOx levels) are exempt from evaluation during real-world operation. On average, approximately 47.4% of events generated in bin-1b emit NOx emissions in the range of 0.45 g/bhp-hr and 3.0 g/bhp-hr.

Evaluation of CO₂-specific NOx emissions rates provides the advantage of eliminating measurement uncertainty associated with ECU torque reporting and exhaust flow rate estimation or measurement. An estimate of CO₂ emissions was derived from the ECU broadcasted fuel rate. Since test activity evaluated in this phase of the study comprised of actual in-fleet operation, and due to the unavailability of actual fuel composition information, CO₂ emissions were derived based on the assumption of a constant fuel density (i.e., from API gravity), hydrogen to carbon ratio and complete combustion (CFR/40/1065/703). A comparison of ECU fuel rate versus PEMS measured CO₂ emissions is presented in the Appendix. Limited real-world test data presented in the appendix indicated that the average bin error is within ± 10% for CO₂ mass rates above 15 g/sec.

$$\dot{m}_{\text{CO}_2} = \dot{V}_{\text{fuel}} \left[\frac{\text{L}}{\text{hr}} \right] \cdot \rho_{\text{fuel}} \left[\frac{\text{kg}}{\text{L}} \right] \cdot \frac{M_{\text{CO}_2}}{(\alpha \cdot M_{\text{H}} + M_{\text{C}})} \quad \text{Equation 5.3}$$

Where,

\dot{m}_{CO_2} is the estimated mass rate of CO₂ emissions

\dot{V}_{fuel} is the volumetric fuel flow rate broadcasted from the ECU (SPN ID: 183)

ρ_{fuel} is the assumed density of fuel (i.e., 0.830 kg/L)

M_{CO_2} , M_{H} , and M_{C} are the molar mass of CO₂, hydrogen and carbon respectively

α is the hydrogen to carbon ratio for diesel fuels (1.85) (CFR/40/1065/1005)

Figure 81 shows a comparison of CO₂-specific NOx emissions rates of all events generated in bin-1a and 1b, respectively. Table 33 presents a comparative analysis of

the arithmetic mean of the average and 90th percentile (i.e., individual vehicle dataset) of CO₂-specific NOx emissions rates for events generated in bin-1a and 1b.

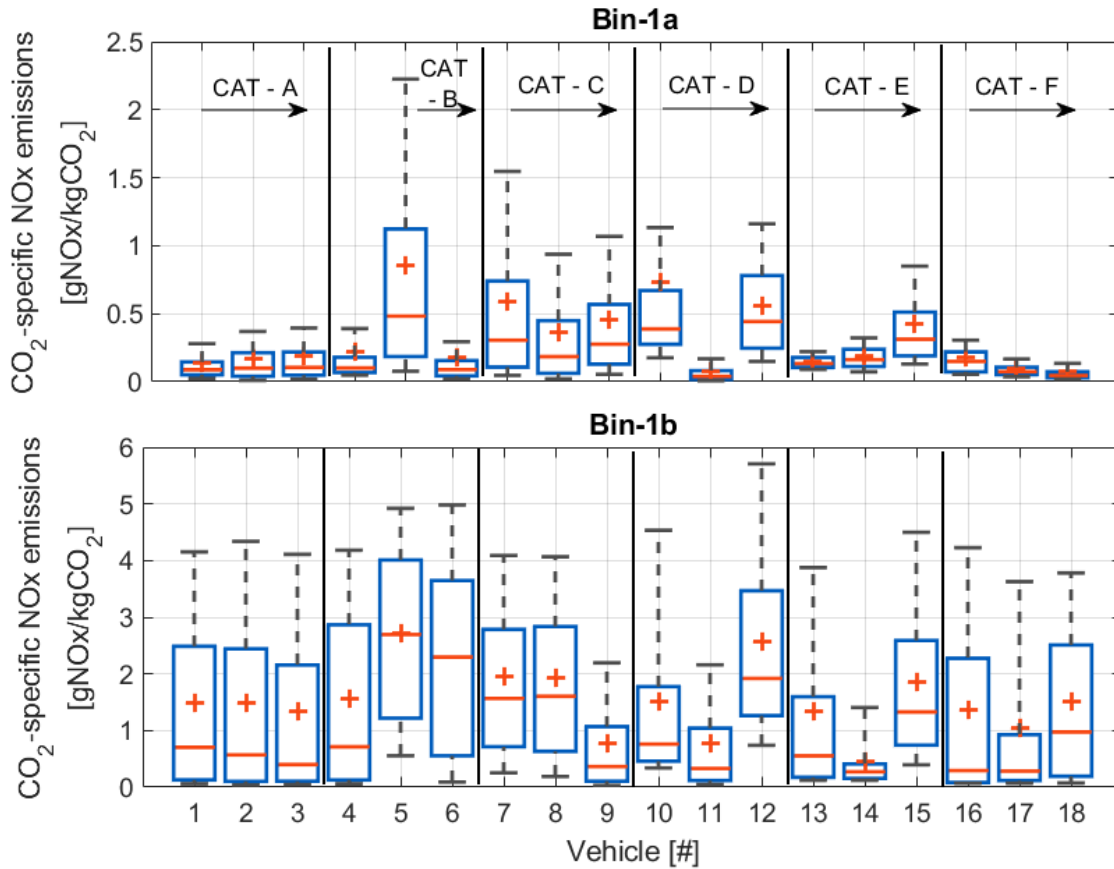


Figure 81: Comparison of CO₂-specific NOx emissions of (a) Top graph: All events generated within each ABW in bin-1a, and (b) Bottom graph: All events generated within each ABW in bin-1b for each of the 18 vehicle datasets

Table 33: Comparison of group mean CO₂-specific NOx emissions of all events generated in bin-1a and 1b

Statistical Parameter	NOx emissions [gNOx/kgCO ₂]	
	Bin-1a	Bin-1b
Average	0.31	1.55
90 th percentile	0.67	3.90

A comparison of NOx emissions indicates an average reduction of 80% and 82.82% for group-average and 90th percentile, respectively. As discussed earlier, the proportion of events generated in bin-1b includes events (i.e., on average, 51.16%)

that exhibit relatively lower bsNO_x emissions. This is due to the fact if the event experienced a certain time fraction of test activity below the $T_{SCR\ IN}$, then the event is assigned to bin-1b. To provide a quantitative comparison, these low NO_x events (i.e., events generated in bin-1b that exhibit bsNO_x emissions of less than 0.45 g/bhp-hr) were shifted into bin-1a (i.e., based on the assumption that these events experienced catalytic conducive thermal conditions). This resulted in an arithmetic mean of 0.31 versus 2.80 gNO_x/kgCO₂ (i.e., a reduction of 89%) for events in bin-1a and 1b (i.e., group mean of individual vehicle dataset), respectively. Since current-day modern diesel engines are significantly dependent on aftertreatment technology for NO_x reduction, the above-mentioned results demonstrate the impact on CO₂ emissions that is needed to maintain catalytic conducive thermal energy that is favorable for the SCR system for NO_x reduction under real-world driving conditions. It is to be highlighted that the estimated CO₂ emissions are significantly dependent on the reported fuel flow measurements and a range of assumptions, as described in equation 5.3.

Figure 82 (a) shows the distribution of duration-specific NO_x emissions rates and the right y-axis of the chart depicts the average engine power fraction for test activity captured in bin-2b during real-world operation from the 18 vehicle datasets. Additionally, Table 34 illustrates a distribution of events captured in bin-2b that are separated based on the event-averaged $T_{SCR\ IN}$. The results (i.e., presented in Figure 82 (b)) show an average NO_x emissions rates of 34.31 and 17.82 g/hr for events that experienced an average $T_{SCR\ IN}$ of less than 190 and 230 °C (i.e., corresponding to 13.80% and 36.70% of average events captured), respectively. The two thermal boundary conditions were selected (i.e., based on the thresholds from ABW DOE analysis) to highlight the differences in NO_x emissions rates under critical SCR operating conditions. The results show that a dominant fraction of events captured in bin-2b corresponds to a relatively higher average $T_{SCR\ IN}$ for all vehicle datasets. Therefore, indicative of aftertreatment activity (i.e. dependent on thermal hysteresis, NH₃ buffer and active thermal management strategies) is a primary driving force in limit/reducing NO_x emissions even at low-power engine operation. Specific to events

generated from vehicle-5 and 6, the long tail of whisker are characterized specifically from low-power operation resulting from frequent stop-and-go activity, therefore resulting in the cooldown of the SCR system.

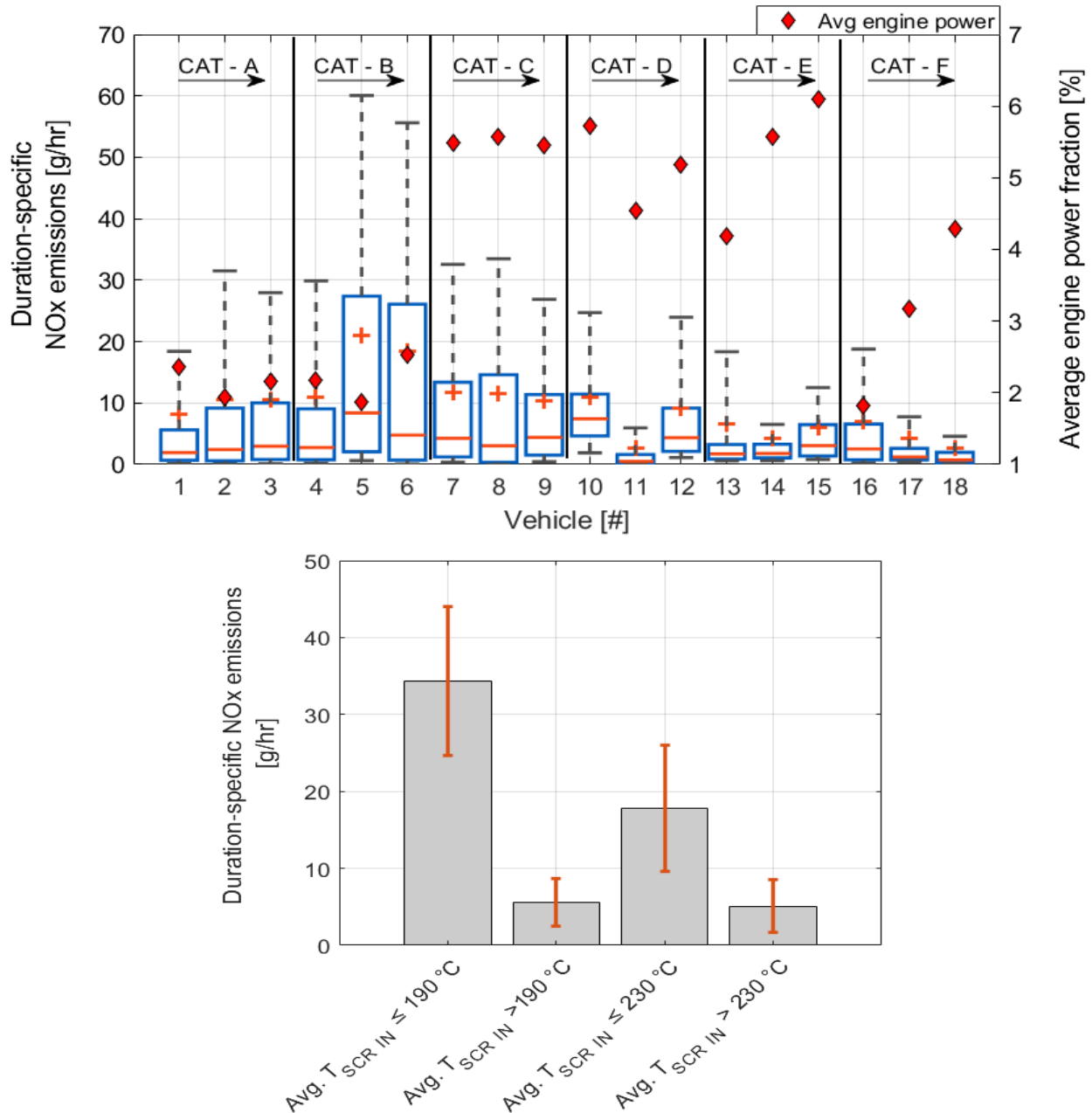


Figure 82: (a) Top graph: Box and whisker distribution of events generated in bin-2b; (b) Bottom graph: Comparison of average and standard deviation of NOx emissions rates as a function of average T_{SCR IN}; (Avg: Average)

Table 34: Distribution of bin-2b events separated as a function of event averaged $T_{SCR IN}$

Vocational Category	Vehicle ID	Average $T_{SCR IN}$			
		Less than 190 °C	Greater than 190 °C	Less than 230 °C	Greater than 230 °C
[-]	[#]	[%]	[%]	[%]	[%]
A	1	9.88	90.12	21.45	78.55
	2	17.73	82.27	35.48	64.52
	3	17.25	82.75	38.50	61.50
B	4	17.74	82.26	35.14	64.86
	5	24.22	75.78	39.88	60.12
	6	31.29	68.71	44.90	55.10
C	7	28.19	71.81	73.03	26.97
	8	27.65	72.35	62.43	37.57
	9	13.28	86.72	47.51	52.49
D	10	9.78	90.22	46.74	53.26
	11	4.64	95.36	17.60	82.40
	12	5.64	94.36	23.82	76.18
E	13	12.41	87.59	31.03	68.97
	14	5.22	94.78	50.43	49.57
	15	2.42	97.58	10.40	89.60
F	16	8.86	91.14	36.71	63.29
	17	9.51	90.49	37.04	62.96
	18	2.83	97.17	8.62	91.38

Table 35 shows the distribution of test activity as a function of different ABW bins. It is evident from data presented in Table 35 that with the exception of vocational category-A (i.e., long haul application), on average ~44.83% of real-world activity is captured from operation bin-2b (i.e., test activity that includes low power transient engine operation and a combination of engine idle and low power transient operation). Specific to MD trucks used for delivery application (i.e., category-D, E and F), on average ~51.44% of test activity was captured in bin-2b. Bin-2a includes low-power operational events (i.e., stationary engine idle) and the results show that this specific bin captures the least amount of test activity. This is because bin-2b acquires

segments of test activity that exhibit a combination of engine idle and low-power transient operation. All events generated in bin-2a exhibited tsNO_x emissions to be below 30 g/hr. Specific to test activity acquired from vehicle-6, the OBD MIL command was active for approximately 92.21% of the entire test activity evaluated. Therefore, resulting in evaluating only 6.15% of the duration of valid ABW trips.

Table 35: Event-duration based data distribution for each of the ABW bins

Vocational Category [-]	Vehicle ID [-]	ABW Data Utilization [%]				
		Bin-1a	Bin-1b	Bin-2a	Bin-2b	Σ Bin-1 + Σ Bin-2
A	1	54.29	15.85	0.00	27.43	97.58
	2	40.04	25.47	0.04	31.21	96.76
	3	36.38	28.51	0.04	27.20	92.14
B	4	22.97	10.62	0.04	31.30	64.92
	5	18.01	9.47	0.04	29.31	56.82
	6	2.53	1.49	0.00	2.13	6.15
C	7	4.62	28.86	3.13	56.18	92.80
	8	7.15	22.02	5.38	57.41	91.96
	9	13.99	23.07	6.67	45.64	89.36
D	10	11.27	12.84	0.00	63.84	87.94
	11	43.33	13.61	0.17	33.32	90.43
	12	27.28	13.99	0.20	54.06	95.53
E	13	24.19	16.45	3.27	51.31	95.22
	14	19.23	18.75	0.00	55.91	93.89
	15	27.58	6.60	0.19	54.51	88.87
F	16	9.79	8.29	0.00	38.92	57.01
	17	31.28	4.74	0.06	59.66	95.74
	18	50.89	3.99	0.46	38.96	94.29

Additionally, HD trucks that experience significant time fraction of operational time during DPF regeneration activity (i.e., Vehicle-4, 5, 6, and 16) exhibited relatively lower operational activity usage for the ABW binning analysis. The remainder of events generated were excluded from emissions assessment due to one or more of the following exclusion criteria, i.e., ECT, DPF regeneration, in-valid NO_x sensor data due to the sensor not reporting stable measurements and OBD MIL.

5.3.3. Compliance Factor Determination

The goal of the study was not to develop a criterion to determine if a given test passes or fails for the ABW binning method. Since the ABW approach assesses in-use emissions over a wide range of engine and aftertreatment operating modes, the results of the study could be used perhaps to develop a protocol (i.e., a function of events generated within each ABW) that evaluates test pass/failure. The study suggests generating a compliance score for events generated within each ABW and bin category and utilizes the score of all ABW's generated to generate global composite weighting criteria to determine the test pass/fail criterion.

$$ABW_{\text{Window compliance score}} = \frac{\sum \text{Duration of valid events}}{\sum \text{Duration of all events}} \quad \text{Equation 5.4}$$

Equation 5.4 depicts a pass ratio classification for each ABW, where the numerator represents the total duration of events within each ABW that meet the applicable threshold for each bin category, and the denominator represents the total duration of all events generated within the ABW for the respective bin category. Such a robust assessment metric will aid in ensuring compliance with the desired thresholds across various operational modes of in-service operation. Additional exclusion criterion such as barometric pressure, ambient temperature, and altitude need to be evaluated and incorporated to avoid emissions evaluation during critical modes of engine operating conditions.

5.4. Measurement Variability of On-board NO_x Sensors

This section of the results presents an overview of the accuracy and variability in NO_x measurements reported by the sensor compared to a laboratory-grade NDUV analyzer during real-world operating conditions. Results presented in the aforementioned section demonstrates the application of ABW binning approach using measurements acquired from tailpipe Zr-O₂ NO_x sensor. Additionally, from a regulatory perspective CARB introduced a pilot program, i.e., REAL (effective from MY 2022) to monitor and bin real-world NO_x emissions rates using data broadcasted by on-board NO_x sensors. It is therefore essential to understand the variability and selectivity associated with the sensor-based measurement technology. NO_x sensors are known to be highly selective in detecting NO_x emissions but are also sensitive to detect a proportion of NH₃ gas. Therefore, demonstrating cross-sensitive behavior.

Test activity acquired from vehicle-A (i.e., on-board NO_x sensor) and vehicle-D (i.e., instrumented tailpipe NO_x sensor) were used to examine the measurement accuracy of NO_x sensors. It is crucial to keep in mind while interpreting the results that the NO_x sensor was sampling directly from the exhaust transfer line and has a very small control volume for sample detection, as compared to a conventional PEMS measurement that includes a pre-conditioned heated sampling line that transfers the exhaust gas sample to the analyzer. Therefore, resulting in signal dispersion and delay.

Figure 83 shows the error propagation of the tailpipe NO_x sensor signal compared to measurements acquired from a PEMS (i.e., NO + NO₂ measurements) for test activity acquired from vehicle-D and A, respectively. The evaluation range presented for NO_x concentration is from 0 to 200ppm. This is because approximately 99% and 95% of test activity acquired was less than 200 ppm for vehicle-A and D, respectively. Test activity acquired was binned as a function of NO_x concentration (i.e., bin width of 5ppm) measurements acquired from the NDUV analyzer. Average bin NH₃ gas concentration is indicated on the right y-axis of the chart.

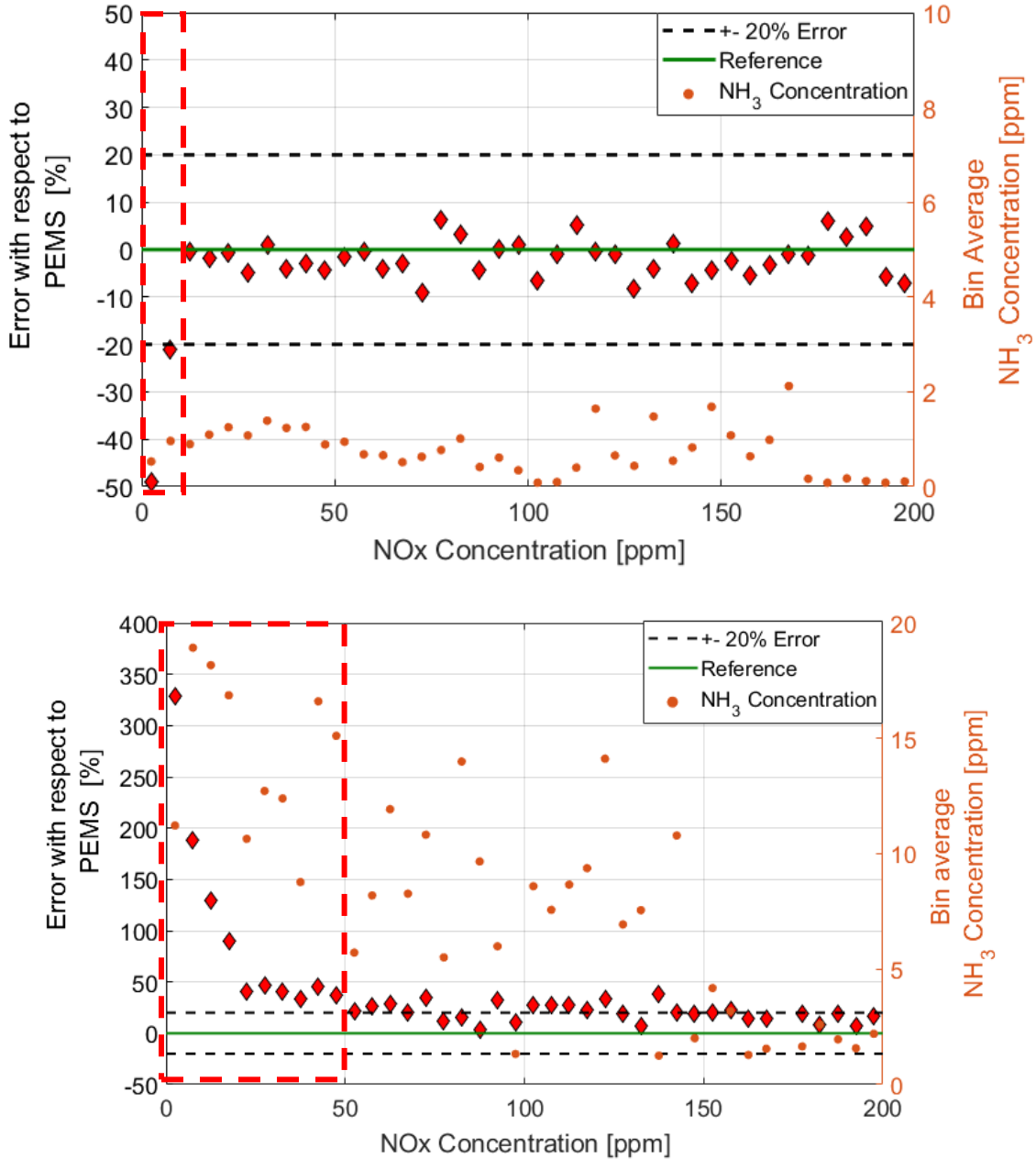


Figure 83: Comparison of error propagation (Tailpipe measurements) of NOx sensor with respect to PEMS measured under real-world operating conditions: (a) Top graph: Vehicle-D, and (b) Bottom graph: Vehicle-A

Results of the analysis presented in Figure 83 (i.e., top graph) shows that the average measurement error of the NOx sensor is within $\pm 10\%$ for NOx concentration levels between 10 ppm and 200 ppm. The measured NH₃ gas concentrations were less than 5ppm for approximately 98% for the test activity collected from vehicle-D. Therefore, indicative of minimum interference due to NH₃ gas. The error propagation presented

in the bottom chart of Figure 83 shows significant deviations which may be attributed to the presence of NH_3 gas (i.e., due to NH_3 slip from the catalyst). The error propagation indicates that approximately 80% of bins at concentration levels below 100ppm show that the deviations in sensor measurements are greater than 20%. Figure 84 shows the cumulative frequency distribution of NH_3 gas concentrations (i.e., measurements acquired from FTIR) for the two-vehicle datasets.

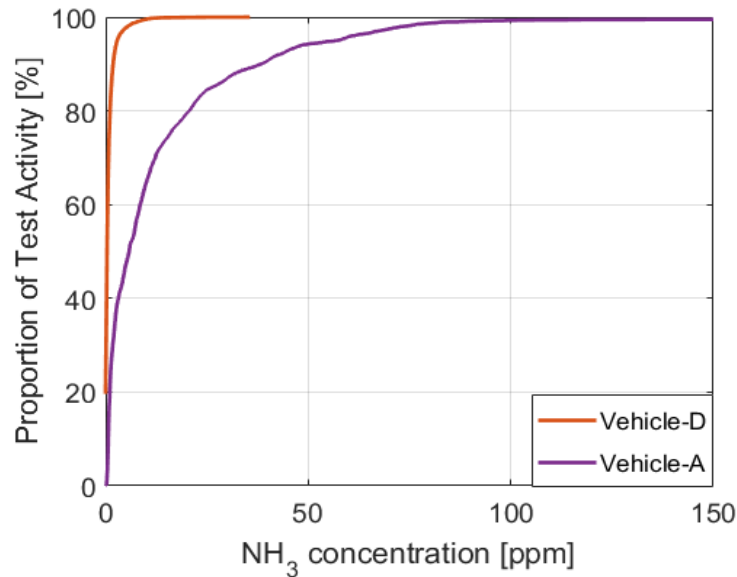


Figure 84: Cumulative frequency distribution of NH_3 gas concentration

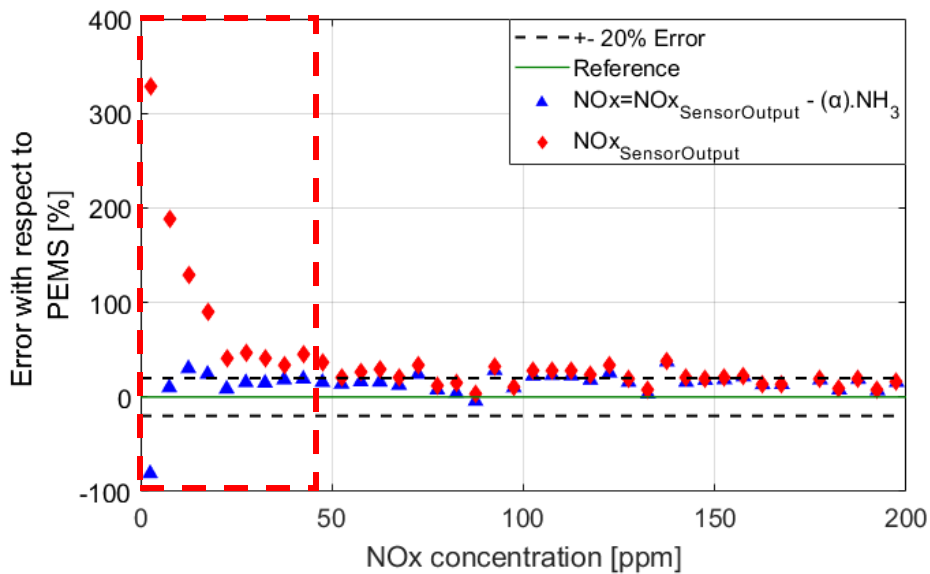


Figure 85: Comparison of measurement accuracy of reported NO_x sensor signal versus NH_3 corrected ($\alpha=0.67$) NO_x signal for data acquired from vehicle A

For NO_x concentration levels below 100 ppm, implementing an NH₃ correction factor of 0.67 (i.e., obtained from Frobert et al., 2013) resulted in the measurement accuracy to be within 20% of error margin for ~65% of bins at concentration levels below 100 ppm. The cross-interference factor was obtained from a synthetic gas blend (i.e., bench-scale evaluation), while there may exist other factors influencing the sensor signal output during real-world operating conditions.

Demirgok et al. performed a controlled environment bench scale evaluation of NO_x sensors to evaluate the NH₃ gas sensitivity. Figure 86 shows a comparison of the NO_x sensor response to NH₃ gas, where the supply gas was varied from 0 to 120 ppm. The experimental evaluation was performed at ambient test conditions, and the results demonstrated a cross-interference factor of ~ 0.678. Similar results were obtained by (Frobert et al., 2013).

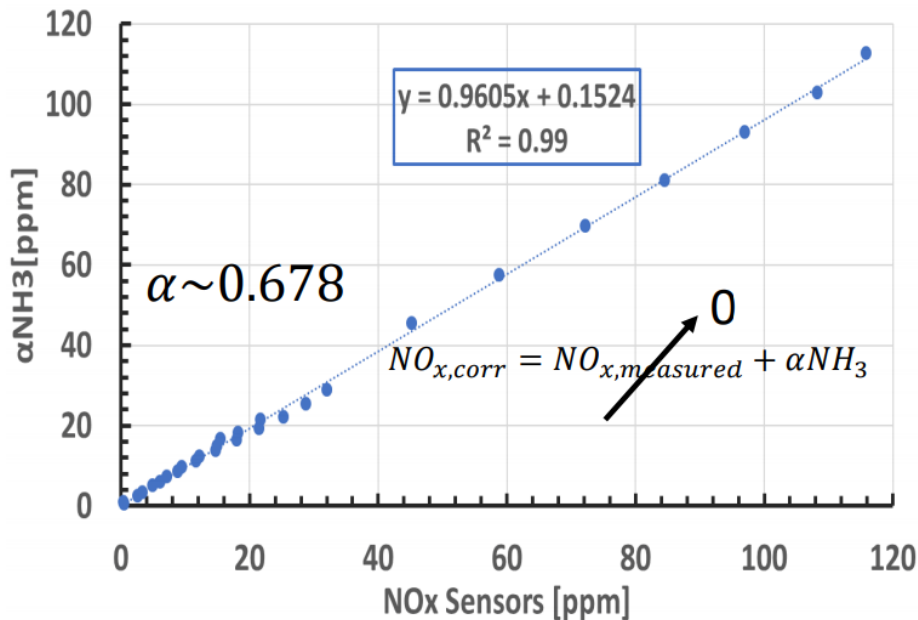


Figure 86: Bench-scale cross-interference evaluation of NH₃ gas on NO_x sensor measurement (Demirgok et al., 2019)

Figure 87 presents a comparison of the continuous-time trace of measurements obtained from NDUV analyzer and Zr-O₂ sensor for tailpipe NO_x emissions, FTIR spectroscopy measurement for tailpipe NH₃ gas, and ECU broadcasted vehicle speed and SCR outlet temperature. The data presented in the figure is an excerpt from real-

world operation acquired from vehicle-A operated on route-2. The average concentration levels for this section of test activity presented in Figure 87 was 9.21, 152.28, and 134.91 ppm for tailpipe PEMS NO_x, FTIR NH₃, and NO_x sensor reported measurements, respectively. The results show that under such test conditions, the NO_x sensor reported measurements consistently follow the trace of NH₃ gas, i.e., measured by FTIR device.

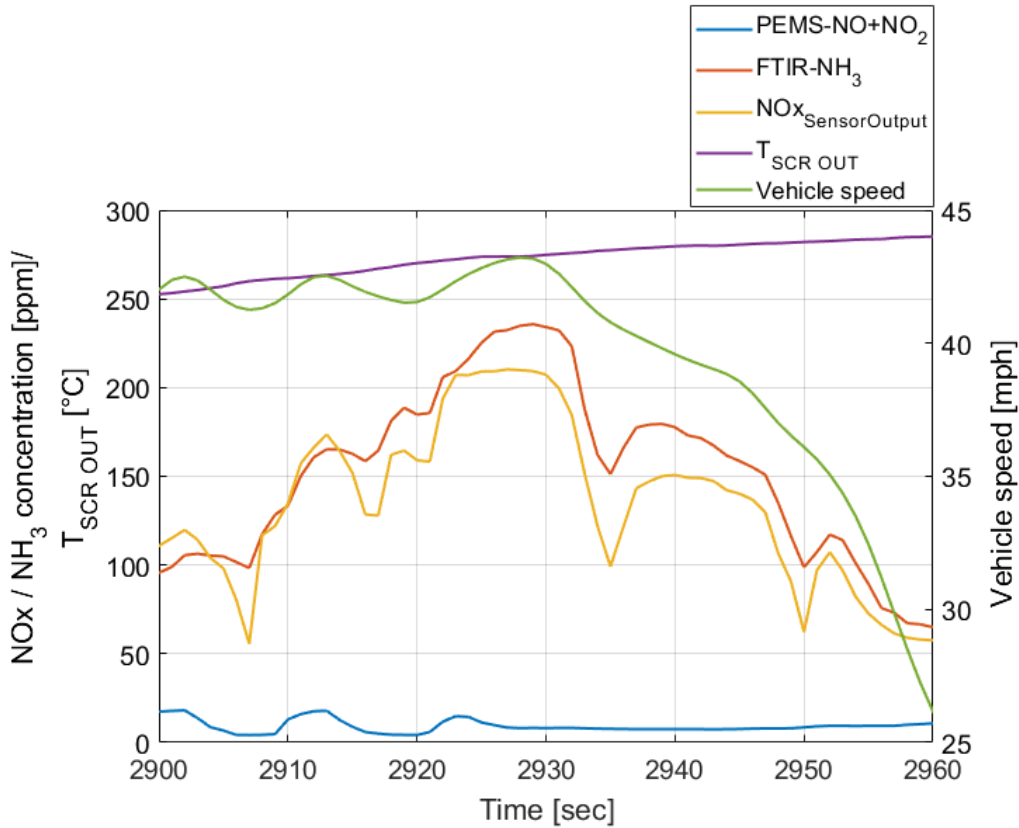


Figure 87: Influence of NH₃ slip on tailpipe NO_x sensor response

$$\alpha_{\text{NH}_3} = \frac{\text{NOx}_{\text{Sensor}} - \text{NOx}}{\text{NH}_3} \quad \text{Equation 5.56}$$

Equation 5.5 (Frobert et al., 2013) quantifies the signal disturbance factor of NH₃ gas on sensor measurements. The average cross-interference factor (α_{NH_3}) for NH₃ is approximately 0.825 for the segment of the test activity presented in Figure 87. While α_{NH_3} is less than 1, it can be inferred (i.e., as per discussion presented in Frobert et al., 2013), the primary cause of interference for the segment of test activity is due to

the presence of NH_3 . The average tsNO_x for the data presented in the chart above was 11.87 and 174.30 g/hr for measurements reported by PEMS and NO_x sensor, respectively. Therefore, indicative of causing a potential offset while determining in-use NO_x emissions rates and OBD compliance evaluation for measurements reported by NO_x sensor during the presence of NH_3 gas in the exhaust stream. Tailpipe NH_3 slip is dependent on the distribution of injected urea in the exhaust gas stream, SCR control strategies, catalyst degradation, or over injection of urea. Additionally, a defective NH_3 dosing system or SCR catalyst can also lead to relatively higher tailpipe levels of NH_3 gas.

While only a specific portion of an in-use test was presented in the above example to highlight the offset in sensor response in the presence of NH_3 gas, it is, therefore, important to understand the frequency (or) percentage of occurrence of test conditions where NO_x sensor measurements exhibit deviations with respect to measurements procured using a PEMS. Evaluation of the entire in-use test presented in Figure 87 indicated that tailpipe NH_3 concentration was above 10ppm for approximately 30% of the test duration. Based on the above-mentioned modes of operating conditions, the quantified α_{NH_3} was below 1 for approximately 74% of test activity. Therefore, indicative of NH_3 interference to be the primary cause for deviations in measurements observed. However, at NH_3 concentration levels below 10ppm, it was observed that α_{NH_3} was above one from approximately 40% of test time. Under such modes of in-use operating conditions, the analysis indicates that the NO_x sensor response may be impacted due to other species in the exhaust gas stream.

To better understand measurement errors at low-level concentrations (i.e., presented in the top graph of Figure 83), statistical PCA analysis (i.e., based on variance-correlation) using JMP software was performed on test activity collected from vehicle-D to examine the influence of other exhaust gas species that exhibit correlating trends. A research study performed by (Frobert et al., 2013) showed that exhaust gas species such as N_2O , HC's (such as propene (C_3H_6) and propane (C_3H_8)) show a negligible impact on NO_x sensor measurements. The study shows that the presence

of HNCO and NH₃ can potentially act as a disturbance factor for NO_x sensor measurements. To identify a first list (i.e., iteration 1) of correlating variables, PCA analysis was initially performed on NO_x concentration measurements (NDUV) less than 100 ppm. Exhaust gas species such as methane (CH₄), HCNO, NH₃, and rate of change of H₂O (dH₂O/dt) sampled using an FTIR device were evaluated. The acquired concentrations for HNCO and CH₄ were less than 15 and 5 ppm for approximately 95% and 99% of test activity acquired.

Figure 88 illustrates the projected z-score or loading matrix (i.e., a function of eigenvector and eigenvalue) of each parameter of interest onto PC-1 and 2. Therefore, representing how each of the variables contributes to the two PC's. Specific to identifying set of correlating variables, the quantified parameters of loading matrix for PC-1 represent a positive trend, i.e., 0.66, 0.44 and 0.56 for measurements obtained from NO_x sensor, dH₂O/dt, and NH₃, respectively. Other exhaust gas parameters of interest such as HNCO and CH₄ showcase a negative impact, i.e., -0.35 and -0.53, respectively.

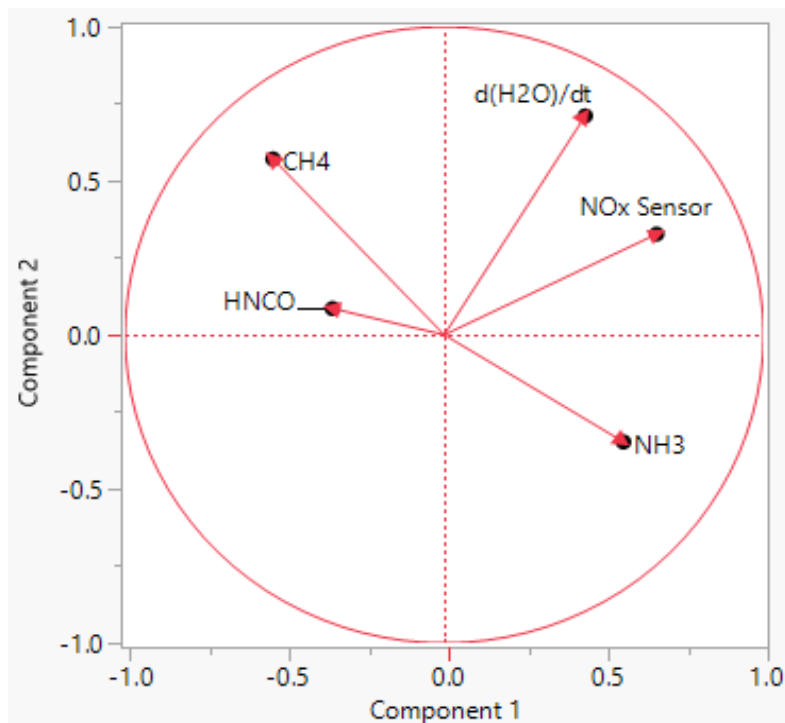


Figure 88: Biplot for PCA analysis: Iteration-1

The second iteration of PCA analysis was explicitly performed on $\text{dH}_2\text{O}/\text{dt}$ and NH_3 to identify the corresponding impact on NO_x sensor measurements. The analysis was performed on test conditions for tailpipe NO_x concentration below ten ppm (i.e., based on measurements from NDUV analyzer). The boundary conditions were primarily aimed to identify the impact of highly transient rapid fluctuations. Figure 89 represents the direction and length of the projected scores onto PC-1 and 2. Data acquired in PC- 1 and 2 correspond to approximately 76.2% of the variance in the entire input dataset. The eigenvalues for the first two PC's were 1.36 and 0.92 respectively. All three variables are projected on the right half of the chart for PC-1 (i.e., represented on the horizontal x-axis), therefore representing positive coefficients. In contrast, only NH_3 measurements are projected on the positive segment of PC-2 (i.e., y-axis), while measurements obtained from the NO_x sensor and $\text{dH}_2\text{O}/\text{dt}$ indicate negative coefficients. Table 36 presents the quantified loading scores of each parameter of interest that is projected on PC 1 and 2, respectively.

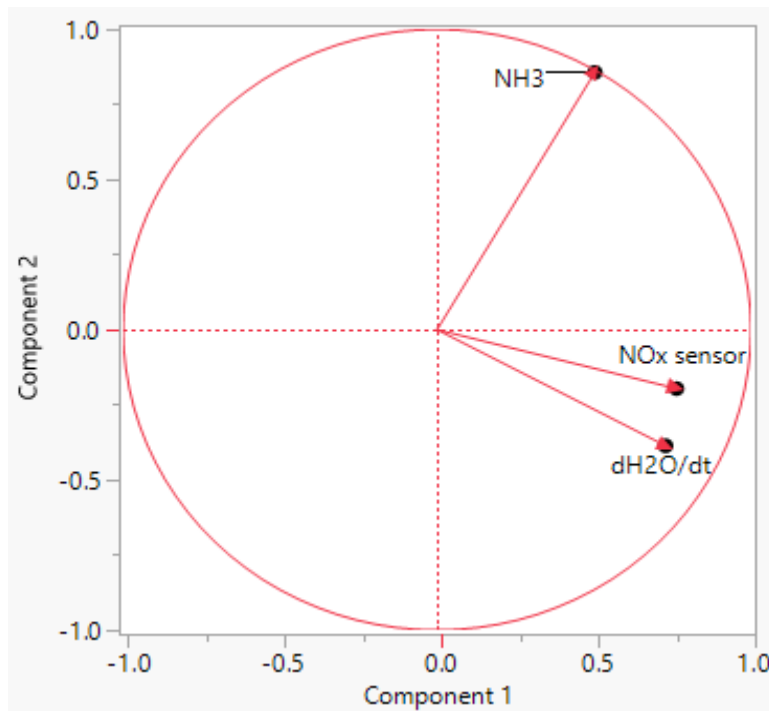


Figure 89: Biplot for PCA analysis: Iteration-2

Table 36: Loading matrix for PC 1 and 2

Parameter	Principal Component	
	1	2
NOx sensor	0.76	-0.19
$\frac{d(H_2O)}{dt}$	0.73	-0.39
NH ₃	0.50	0.86

$$\text{Individual Contribution for PC}_j = \left(\frac{(\text{Score}_i)^2}{((\text{Score}_i)^2 + \dots + (\text{Score}_n)^2)} \right) \cdot 100 \quad \text{Equation 5.57}$$

Where,

j represents the principal component (or) column

i represents the parameter of interest (or) row

n represents the total number of variables (or) rows

Table 37: Percentage contribution of individual variables

Parameter	Principal Component	
	1	2
NOx sensor	42.66	4.17
$\frac{d(H_2O)}{dt}$	38.82	16.17
NH ₃	18.51	79.65

It is evident from data presented in Table 37 that NOx sensor signal output and dH₂O/dt contribute to approximately 81.48% of data variables represented by PC-1 (i.e., corresponding to the variables that attribute to the highest amount of variance in the dataset), while PC-2, i.e., dominantly represented by NH₃ corresponds to 79.65%. Comparing the two measurement signals (i.e., NOx sensor output and dH₂O/dt) resulted in a correlation coefficient of 0.28. Overall, results from the analysis presented in this section show that sensor voltage output corresponding to NOx measurement may be impacted due to rapid changes in dH₂O/dt. The

observations of variability in sensor reported measurements is evident at low levels of NO_x concentrations.

Figure 90 presents an overview of the continuous-time trace of NO_x concentration measured from PEMS (i.e., NO+NO₂), SCR outlet temperature (i.e., left y-axis) and dH₂O/dt concentrations (i.e., right y-axis) for measurement acquired from vehicle-D operated on leg-3 of route-3. An excerpt of test activity is presented in the bottom figure that shows that the magnitude of sensor response correlates with the response obtained from the rate of change of H₂O. Therefore, resulting in under and overestimation of the reported measurements. Real-world test activity is inconclusive of the phenomena causing the rapid changes in sensor output. Similar observations corresponding to rapid changes in dH₂O/dt were shown by Soltis et al., (2006). Additional bench-scale controlled environment testing is required to be performed to evaluate the hypothesis of the influence of rapid rate of change of dH₂O/dt on reported NO_x sensor measurements.

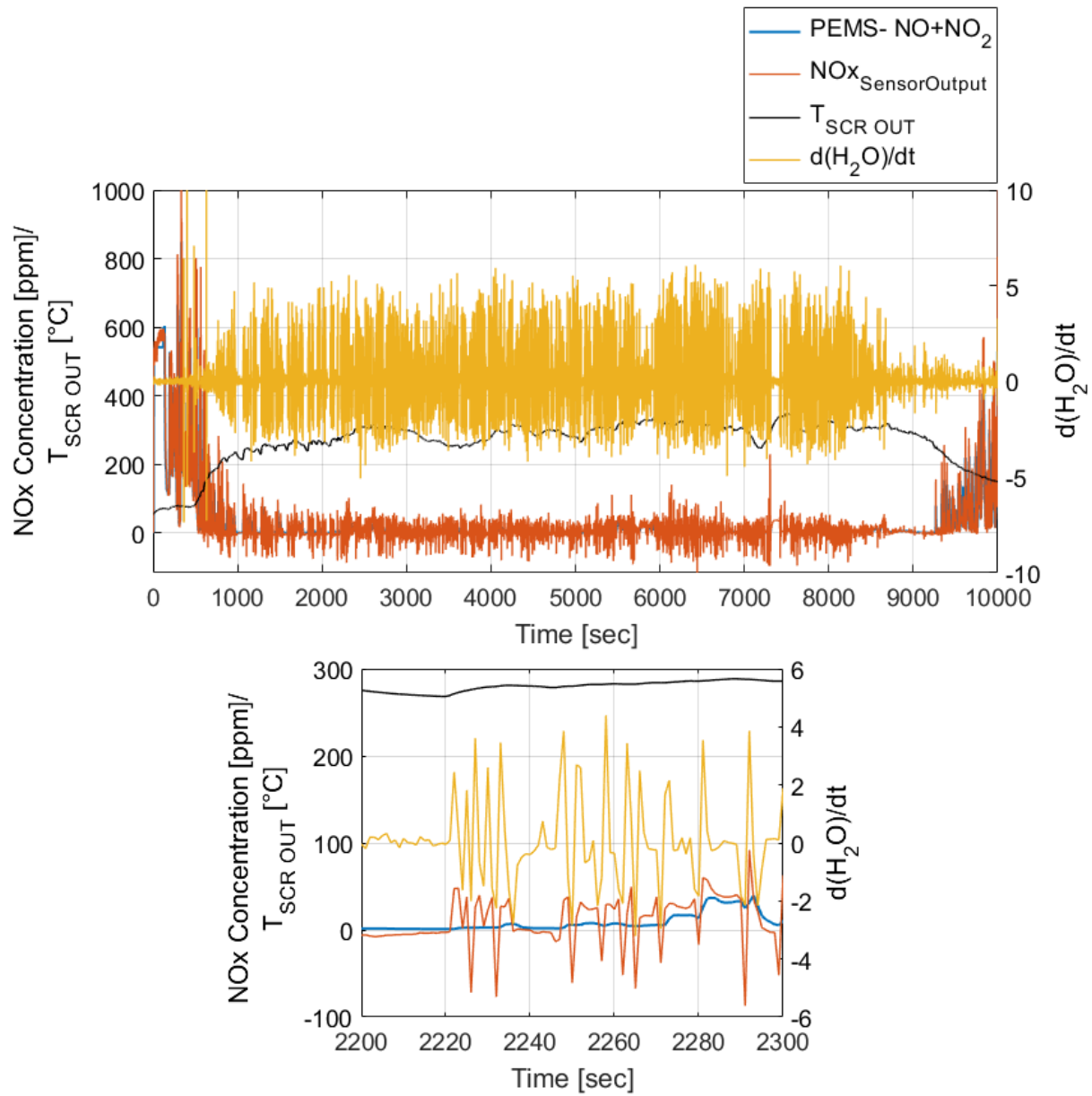


Figure 90: Comparison of (a) NO_x measurements acquired from a PEMS and sensor, (b) T_{SCR OUT}, and (c) Rate of change of H₂O concentration

6. Summary, Conclusions and Recommendations

Regulatory agencies such as U.S.EPA and CARB have emphasized increased scrutiny in assessment of RDE to ensure emissions compliance throughout the useful life of HD engines. Furthermore, the NTE method has come under scrutiny by both the regulatory agencies and the HD engine manufacturers for evaluation of real-world emissions compliance only under specific modes of vocational in-fleet activity. As a result, regulatory agencies are evaluating the prospects of developing an alternative emissions assessment metric, i.e., intended to be implemented in conjunction with the next phase of emissions regulations. Additionally, while PEMS serves as the state-of-the-art laboratory-grade portable analyzer, increased research and regulatory efforts have been employed to evaluate the response characteristics of NOx sensor technology to be implemented as a cost-effective alternative for monitoring of in-use NOx emissions rates.

The study presents the development and evaluation of an alternative analytical technique to characterize mode-specific NOx emissions from modern MD and HD diesel trucks. Furthermore, in view of utilizing NOx sensors as a potential cost-effective measurement tool for monitoring and screening of NOx emissions from in-fleet operation, the study also examines the performance of NOx sensors under real-world operating conditions. The following sections summarize the findings of the study, provides recommendations to further improve the work accomplished and describes the studies contributions to relevant areas of interest.

6.1. Summary: In-use Emissions Evaluation Metrics

The key aims of the study were to examine the current in-use emissions quantification protocols and to develop an alternative analytical platform to characterize NOx emissions during real-world fleet operation.

Figure 91 and Table 38 depicts a global comparison of NTE, WBW and ABW emissions quantification methods that were presented in section 5.1, 5.2, and 5.3. The top chart presented in Figure 91 shows a comparison of the 90th percentile of the

individual method-based results for each vehicle dataset and the total time-weighted data utilization.

Table 38: Summary of reference to the discussion of in-use emissions quantification methods

Method	Thresholds	Sample Size	Results Section
NTE	Table 10	75	5.1.2
WBW	Table 11	75	5.1.3
ABW	Table 20	4, 18	5.2, 5.3

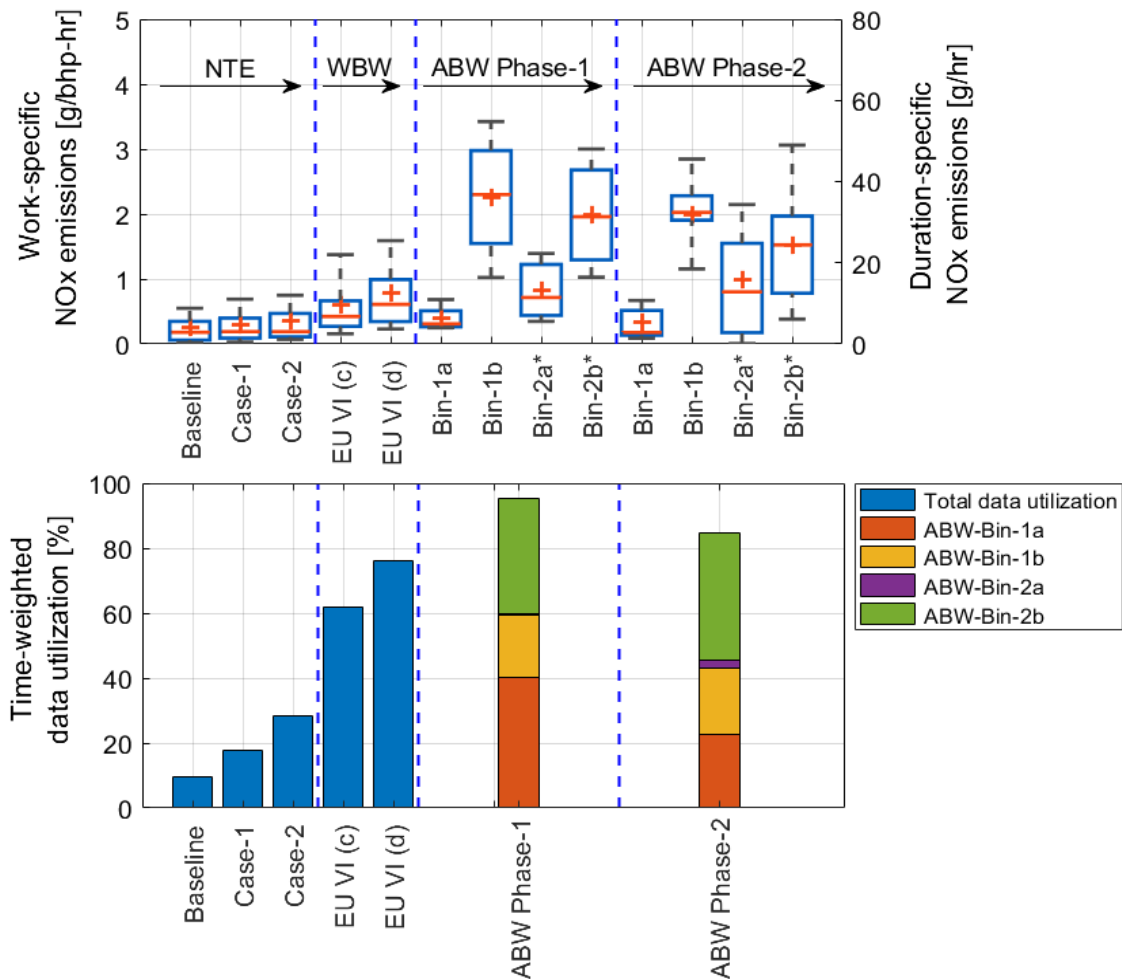


Figure 91: Comparison of (a): Top Chart: 90th percentile distribution of bsNOx emissions of each vehicle dataset, and (b) Bottom Chart: Total time-weighted data utilization for NTE, WBW and ABW approach; *: Duration-specific NOx emissions rates (Right y-axis)

One of the primary limitations associated with the NTE approach was the utilization of a sparse amount of test activity in-use emissions compliance assessment. Modification of NTE boundary parameters demonstrated an increase in total data utilization from 9% to 28%, i.e., for NTE baseline and case 2, respectively. For the above-mentioned case scenario, it was observed that on average, the 90th percentile of bsNO_x emissions increased from 0.25 g/bhp-hr to 0.35 g/bhp-hr. The relatively lower NO_x emissions rates are primarily attributed to the evaluation of in-use emissions only under exhaust gas thermal boundary conditions favorable for SCR catalytic activity.

On the contrary, implementation of the WBW approach on the same vehicle datasets resulted in utilization of a relatively higher total time fraction of test activity (i.e., on average 62% and 76% for EU VI (c) and (d) boundary thresholds) in comparison with the current NTE in-use emissions evaluation approach (i.e., 9%). However, the method-based evaluation criteria as per EU regulations (i.e., 90th percentile of valid window results) exhibited variability in emissions results for in-fleet vocational activity (i.e., ranging from 0.15 to 1.30 g/bhp-hr, and 0.22 to 1.58 for EU VI (c) and (d) boundary thresholds, respectively). Therefore, highlighting an inability to be compared to a fixed in-use emissions standard (i.e., like the NTE approach used in the U.S. (or) the WBW approach used in Europe). It is important to mention that EU regulations evaluate for in-service conformity over a pre-defined route-based threshold (i.e., a characteristic function of vehicle speed and total engine work). Evaluation of a Class 8 HD truck (certified for U.S.EPA 2010 emissions standards) over a pre-defined test route as per EU VI (c) regulations demonstrated the 90th percentile of valid WBW results to be below the current NTE in-use limit for NO_x emissions.

Due to differences in NO_x emissions characteristics during real-world operating conditions from modern MD and HD diesel trucks, and limitations associated with the NTE in-use emissions evaluation approach, the study introduced an alternative approach (i.e., ABW approach) to assess mode-specific characteristics of NO_x

emissions. The approach segregates consecutive segments of test activity (i.e., based on a minimum time-period) as a function of engine power fraction and thermal boundary threshold (i.e., a function of inlet temperature of NO_x reduction aftertreatment system). Results from the evaluation of experimental test activity from phase-1 and 2 of the ABW approach shows that NO_x emissions trends for test activity captured in bin-1a were comparable to current NTE in-use emissions limit. The average bsNO_x emissions rates of the 90th percentile of the distribution of each of the vehicle datasets were 0.39 and 0.32 g/bhp-hr for phase-1 and phase-2, respectively. Test conditions acquired in bin-1b and 2b exhibited modes of operating conditions that are not regulated as per the current NTE in-use boundary conditions and therefore demonstrate variability in results depending on test conditions and different engine control strategies used to reduce NO_x emissions. The experimental findings resulted in an average bsNO_x and tsNO_x emissions rates of the 90th percentile of the distribution of each vehicle dataset (i.e., based on test activity acquired in phase-1 and 2 of the study) to be 2.26 and 2.0 g/bhp-hr, and 31.8 and 24.4 g/hr for bin-1b and 2b, respectively. The magnitude of difference in NO_x emissions rates between bin-1a and 1b can be attributed to aftertreatment thermal state-based bin boundary thresholds selected for bin-1a; therefore, exhibiting near favorable conditions of SCR catalytic activity for NO_x abatement.

In summary, the ABW approach outlines a data integration and evaluation platform that characterizes NO_x emissions performance and characteristics under various modes of real-world operating conditions. While, SCR technology plays a key role in limiting tailpipe NO_x emissions for test activity captured in bin-1a, alternative and innovative technological developments associated with engine and aftertreatment technology are primarily needed to reduce the magnitude of difference in tailpipe NO_x emissions rates explicitly for test activity captured under challenging NO_x control modes of operating conditions (i.e., activity acquired in bin-1b and 2b, respectively) in comparison with bin-1a. With upcoming ultra-low NO_x rule making, results from bin-1a emphasize that even under active SCR operating condition, additional technological improvements are required in terms of aftertreatment

design and packaging to ensure compliance with stringent forthcoming in-use NOx standards (under modes of operating conditions favorable for NOx reduction aftertreatment system).

Results from both Figure 70 (Phase-1) and Figure 82(b) (Phase-2) of the study highlights that SCR catalytic reactions also reduces tailpipe NOx emissions under favorable exhaust gas thermal conditions for catalyst activity (i.e., primarily attributed to low space velocity, stored NH₃, and most importantly due to activity occurring after sustained medium/high load operation). In terms of data utilization, the ABW approach provides the ability to evaluate a relatively higher fraction of in-use test activity captured from valid ABW trips (i.e., total trip work of at least 1 x W_{Ref}) compared to the current NTE approach (i.e., resulting in less than 10% of overall time-weighted data utilization). Phase-1 and 2 of the study resulted in the utilization of more than 80% of time-weighted data utilization from valid ABW trips.

While the above discussion presented a global summary of the results, Table 39 shows a summary of learnings (i.e., merits and demerits) of the three different in-use emissions evaluation approaches presented in this study.

Table 39: Comparison of metric characteristics for NTE, WBW and ABW approach

Metric Characteristics	NTE	WBW	ABW
Implementation of minimum datapoint exclusions/ Covers a broader range of engine operating conditions			
Attempts to separate diverse in-use operating conditions			
Evaluation of emissions only under favorable boundary conditions for aftertreatment catalytic activity			
Predictability in repeatable emissions performance		+	*
Reduces risk of false-positive and false-negative results		o	

+ For predefined route-based characteristics (like EU regulations)

* Only for bin-1a (For current modern MD and HD diesel trucks certified as per NTE regulations)

o Results in section 5.1.3 highlight variability in NOx emissions for actual in-fleet vocational activity. Single dataset WBW evaluation as per EU VI (c) predefined route-based characteristics exhibits results comparable to a fixed standard

Due to limitations associated with the current NTE in-use protocol in terms of limited data utilization and evaluation of emissions only under favorable exhaust gas thermal conditions for catalytic activity, the study highlights upon the necessity of development of an alternative metric that is deemed necessary to evaluate NO_x emissions performance over a wide range of engine operating conditions. In addition to utilization of a relatively higher data utilization compared to the NTE approach, data presented in Figure 91 emphasizes on one of the salient features of the ABW approach i.e., providing the ability to characterize NO_x emissions rates from different modes of operating conditions. Therefore, establishing a platform for OEM's as a viable tool to identify challenging real-world engine and aftertreatment operational regimes (i.e., depicted in Figure 91 based on the variability (or) spread in NO_x emissions results for ABW bin-1b and 2b). Some of the proposed future technologies that are currently being examined such as cylinder deactivation (CDA), closed-coupled SCR aftertreatment are primarily being evaluated to enhance/utilize the benefit associated with exhaust gas thermal energy to unleash the potential of SCR technology for NO_x abatement. A bin-based categorization would therefore provide a pathway to evaluate the feasibility of implementation of NO_x abatement technologies and its associated impact/change in terms of mode-specific/bin-based NO_x emissions rates and its impact on bin-based CO₂ emission rates. On the other hand, mode-specific characterization of NO_x emissions also provides an opportunity for the regulatory agencies to utilize a platform that would therefore potentially assess NO_x emissions compliance with feasible standards across multiple modes of real-world operating conditions.

Although the ABW approach presents a metric that caters to segregation of modes of in-use operating conditions to characterize operational-specific NO_x emissions rates, the approach is primarily tailored to boundary conditions (i.e., explicitly for bin-1a) that is technology dependent (i.e., SCR technology in the current study). However, to be implemented as an in-use compliance evaluation, an emissions assessment metric requires to be technology independent. The WBW approach (i.e., for example) depicts

as a robust emissions assessment approach, i.e., independent of emissions control technology, however, the implementation of predefined route-based characteristics and sequence of vehicle activity patterns by the EU regulations indirectly acts as a thermal boundary shield (i.e., explicitly for HD engines equipped with aftertreatment technology for NO_x reduction).

With the implementation of the next phase of emissions reductions in certification standards, there exists a need for a paradigm shift in the evaluation of in-use emissions compliance over a wide range of real-world operating conditions. Therefore, ensuring emissions compliance across multiple modes of real-world engine operating conditions. For example, while the current regulatory standards over the FTP certification test cycle is 0.20 g/bhp-hr for NO_x emissions, data presented in Figure 91 highlights upon deviations in NO_x emissions during tractive work-producing activity (i.e., for example ABW bin-1b) that lies outside the boundaries of SCR activity. It is to be acknowledged that the primary driving force for technological developments associated with a reduction in tailpipe emissions can be attributed to performance over the FTP test cycle. However, evaluation of current product performance under vocational and in-fleet operation highlights that an aggressive stringency on the certification standard may not necessarily translate in compliance with certification standard across all modes of in-use operating conditions. While, HD engine manufacturers earn emissions credits based on demonstrating product performance (i.e., for example, ultra-low NO_x requirements) over custom controlled environment based testing, a paradigm shift in terms of incentivizing based on evaluation of in-use emissions performance within (or) towards the end of useful emissions compliance life of the engine, would, therefore, tailor an aggressive control on tailpipe emissions across a wide range of operating conditions and also act as a primary driving force to ensure technical developments associated with NO_x control during real-world driving conditions.

6.2. Conclusions

Measurement and evaluation of RDE plays a vital role in monitoring the performance of emissions control devices, while the vehicle is operating on its vocational in-fleet duty cycle. The study examined in-use emissions quantification protocols based on test activity acquired from a range of diverse MD and HD engines (i.e., in terms of engine displacement, power rating) deployed in a wide range of vocational applications.

A comparison of both NTE and WBW protocols indicate that the WBW metric exhibits superiority in the evaluation of RDE (i.e., in terms of data utilization) over an extended range of engine and aftertreatment operating conditions compared to the NTE protocol. HDIUT datasets evaluated in this study (maximum altitude of 2844.8 ft) showed that the IMT exclusion criteria of the NTE approach are the most influential contributor towards invalidation of NTE events. It is to be emphasized that the current NTE approach is primarily driven by $T_{AT\ OUT}$ exclusion to determine the validity of an NTE event and the findings of this study suggest the elimination of IMT threshold since the exclusion was introduced for engine technology without aftertreatment systems. Outcomes of the sensitivity analysis of NTE boundary parameters highlight that expansion of NTE control area and eliminating/altering the boundary parameter thresholds still yields to evaluation of a limited amount of in-use test activity (i.e., on average less than 30% of the entire in-use test). The requirement of continuous consecutive engine operation within the NTE zone is one of the primary challenges pertaining to acquiring a wide range of test activity for compliance evaluation using the NTE protocol.

Characterization of WBW approach (i.e., explicitly for HDIUT datasets) yielded substantial variability in the spread of the 90th percentile of valid window bsNO_x emissions (i.e., evaluation criterion used by EU regulations for in-service conformity). Therefore, leading to non-attainment of predictable emissions factors to be compared to a fixed in-use pollutant limit. The primary factors (or) phenomena for non-attainment of repeatable results are stated as follows:

- (i) Non-uniform distribution of emissions activity across multiple MAW's
- (ii) The dependency of duty-cycle characteristics on SCR performance

In light of limitations associated with the above-mentioned metrics for a robust assessment of in-fleet operation, the study developed an alternate NO_x emissions evaluation metric which includes a combination of windowing and event-based bifurcation features to characterize in-use operational mode-specific NO_x emissions rates. Introduction of windowing was primarily attributed to isolate and evaluate individual segments of test activity and to incorporate a linkage between the certification test cycle and real-world operation.

The analytical model/approach demonstrated the ability to characterize in-use NO_x emissions rates from four distinctive modes of real-world operating conditions. This was possible due to event-based categorization of test activity as a function of engine power produced and exhaust gas thermal conditions. Characterization of events generated in bin-1a showed that independent of the vocational duty-cycle more than 90% of events generated in phase-1 of the ABW evaluation (i.e., explicitly of trucks within useful emissions compliance life) exhibited in-use NO_x emissions levels to be below the current NTE in-use limit. Similar bsNO_x emissions results were observed from 90th percentile of bin-1a distribution for 13 out of 18 trucks in phase-2 of the study. Findings of the study indicate a predictable behavior of bsNO_x emissions generated in bin-1a, therefore, providing the ability to track and compare in-use bsNO_x emissions captured in this bin to the certification and NTE in-use standard for NO_x emissions. The desirability of achieving relatively lower NO_x emissions reductions can be attributed to the potential of active SCR operation (i.e., under exhaust gas thermal conditions favorable for catalytic activity). Since the approach only uses event-based T_{SCR IN} distribution as a simple-analytical criterion to separate SCR activity, this could, however, explain some of the differences observed in NO_x emissions trends under critical SCR operating conditions (i.e., due to a range of factors associated with the SCR de-NO_x conversion efficiency).

Evaluation of events generated in bin-1b and 2b exhibits variability in NO_x emissions rates. This is because current-day product performance under such modes of operating conditions are dependent on the transient operational mode and different in-cylinder combustion control strategies used by the engine manufacturers to limit NO_x formation (i.e., under modes of operating conditions where SCR is not functional). With the implementation of next phase of emissions reduction on the FTP test cycle and implementation of a new engine dynamometer test cycle, i.e., specifically focused on low load engine power, it is anticipated that technological developments will be aimed to provide a more aggressive and robust control of NO_x emissions from modes of in-use operating conditions captured in ABW bin-1b, and 2b. Therefore, providing an ability to also ensure real-world NO_x reductions under some of the identified and challenging NO_x control modes of in-use operation.

Results from ABW analysis emphasizes the importance of binning (i.e., to categorize diverse real-world operating conditions) and assessment of bin-based NO_x emissions rates across multiple modes of in-use operating conditions. In this regard, while there exist challenges pertaining characterization of RDE, two of the key features of the ABW approach aid as an effective and alternative means (i.e., independent of the duty cycle) of evaluating in-use NO_x emissions, while attempting to overcome limitations of the NTE and WBW method.

- (a) Segregating the influence of diverse real-world engine and aftertreatment operating conditions which therefore translates to the operational mode-specific characterization of NO_x emissions
- (b) Evaluation of a wide range of real-world engine operating conditions

One of the critical aspects of the current NTE in-use metric was the utilization of a relatively lower percentage of operational test time for in-use emissions assessment. Evaluation of ABW approach resulted in utilization of 95% and 83 (i.e., individual dataset average) of test activity acquired from valid ABW trips in phase-1 and 2, respectively. The findings of the study clearly show that compared to the NTE

approach, the ABW approach provides a unique opportunity for evaluation of in-use activity across a wide range of engine and aftertreatment operating conditions.

In comparison with NTE and WBW approach, the ABW approach demonstrates superiority in characterizing and evaluating bin-specific in-use NO_x emission rates. However, the metric evaluation highlighted that the minimum W_{Ref} requirements (i.e., minimum test requirement) for the generation of a valid ABW is one of the primary limitations associated with regards to overall data utilization. Analysis of in-fleet vocational activity (i.e., Phase-2) showed that on average only 26.40% of trips generated (i.e., resulting in the utilization of ~55% of test activity) demonstrated total trip engine work to be above $1 \times \text{FTP}_{\text{Work}}$.

Finally, the utilization of PEMS serves as a robust technique to evaluate RDE but yields as an expensive tool for real-world data acquisition. Once the study has established an alternative data-driven platform for evaluating of in-use NO_x emissions, the study investigated measurement thresholds of NO_x sensor reported measurements (i.e., evaluation of an alternative cost-effective measurement pathway) during real-world operation. While the cross-sensitive nature of sensor measurements in the presence of NH₃ is well established, bin-average comparison of real-world NO_x measurements acquired from Zr-O₂ sensor technology and PEMS (i.e., NDUV analyzer) reported that in the absence of the substantial amount of tailpipe NH₃ levels, the error deviations were within $\pm 10\%$ (i.e., for tailpipe NO_x concentration between 10 and 200 ppm). An in-depth statistical investigation (i.e., based on PCA analysis) at NO_x concentrations below ten ppm established a hypothetical relation between the rapid changes in H₂O concentration and sensor reported measurements. Under these conditions, the results show that the sensor measurements may exhibit sensitivity associated with rapid fluctuations in H₂O concentrations in the exhaust gas. To be implemented as a cost-effective alternative for monitoring of NO_x emissions, further research and associated developments are required to mitigate cross-sensitive behavior and to improve the accuracy bandwidth of the reported sensor-based measurements.

6.3. Recommendations

The ABW binning approach can be used as an alternative method to verify in-use emissions compliance. Some of the recommendations to improve the approach are as follows:

- Further improvements can be made to explicitly characterize bin-1b events that experience a combination of test activity above and below the $T_{SCR IN}$ threshold. Instead of using a fixed thermal boundary threshold for bin-1a, a composite weighting of emissions can be derived for test activity that experiences test conditions as mentioned above. The weighting function, for example, can be determined based on the thermal profile of SCR activity over the certification test cycle.

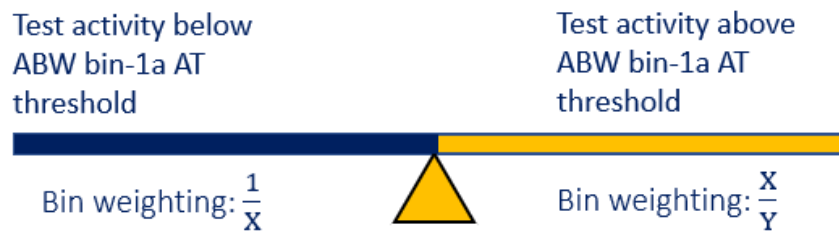


Figure 92: Thermal-based weighting scheme for bin-1a

- Evaluation of various parameters and thresholds such as exhaust energy and distance travelled can be assessed to define minimum trip-based requirements (i.e., key-on to key-off activity). Additionally, future work could also include the development of an evaluation metric to assess emissions compliance across multiple ABW bins to determine a vehicle pass/fail criterion.
- To perform uncertainty/perturbation analysis of ABW engine operational and thermal boundary thresholds to assess the impact on method-based results.
- Quantification of measurement uncertainty as a function of pollutant concentrations acquired from a PEMS, flow rate acquired from EFM, and J1939 reported engine speed and torque.

- Lastly, the proposed ABW approach is explicitly designed for emissions assessment of on-highway modern diesel trucks. Since MD and HD engines are dependent on aftertreatment technology are used in a wide range of applications, the ABW based thermal boundary approach can be fine-tuned to evaluate applications such as marine engines, non-road engines and also on-highway stoichiometric natural gas engines equipped with a three-way catalyst (TWC).

6.4. Contributions

This research contributes to the area of HD in-use testing and emissions assessment. The U.S.EPA and CARB have initiated the rule-making process for ultra-low NO_x standards, and it is, therefore, essential to implement a versatile and robust protocol to ensure that NO_x reductions are also achieved under the current identified challenging modes of NO_x control in-use operation. The findings of the study lay the foundation of the necessity to improve in-use emissions assessment and evaluation protocols used in the U.S. Results from the evaluation of the existing in-use compliance metrics provides answers to the impact modified boundary parameters would have for a robust assessment for in-use emissions. The primary contribution of this work is the demonstration of an alternative approach (i.e., independent of the in-use duty cycle) to evaluate in-use emissions, and the findings of the study presented herein provide essential insights to both the regulatory agencies and engine manufacturers of the current product performance of emissions control systems across different modes of in-use operation.

References

- Abdi, H., Williams, L.J., 2010. Principal component analysis. *WIREs Computational Statistics* 2, 433–459. <https://doi.org/10.1002/wics.101>
- Akard, M., Nakamura, H., Aoki, S., Kihara, N., and Adachi, M., 2005. Performance Results and Design Considerations for a New In-Use Testing Instrument. Presented at the SAE Commercial Vehicle Engineering Conference. <https://doi.org/10.4271/2005-01-3606>
- Ardanese, M., 2008. Simple strategy-based technique to reduce emissions from SCR-equipped heavy-duty diesel engine over different engine-out calibrations (Ph.D.). West Virginia University. <https://doi.org/10.33915/etd.2856>
- AVL, 2010. M.O.V.E Gas PEMS 493: Product Description.
- Badshah, H., Posada, F., and Muncrief, R., 2019. Current state of NO_x emissions from in-use heavy-duty diesel vehicles in the United States. The International Council on Clean Transportation.
- Besch, M.C., 2016. In-line, Real-time Particulate Matter Sensors for OBD and Exhaust After-treatment System Control Applications (Ph.D.). West Virginia University. <https://doi.org/10.33915/etd.5197>
- Besch, M.C., Chalagalla, S.H., and Carder, D.K., 2017. On-Road and Chassis Dynamometer Testing of Light-duty Diesel Passenger Cars. West Virginia University.
- Besch, M.C., Pondicherry, R., Thiruvengadam, A., and Carder, D.K., 2018. Real-world emissions from Heavy-duty In-use Testing program: NTE vs Work-based window, Sensitivity and Limitations of these methods. Presented at the 8th Annual PEMS Conference, Riverside, California.
- Bishop, G., Schuchmann, B., Stedman, D., 2013. Heavy-Duty Truck Emissions in the South Coast Air Basin of California. *Environmental Science & Technology* 47, 9523–9529. <https://doi.org/10.1021/es401487b>
- Blanco-Rodriguez, D., 2013. Modelling and Observation of Exhaust Gas Concentrations for Diesel Engine Control (Ph.D.). Universitat Politècnica de València.
- Bonfils, A., Creff, Y., Lepreux, O., and Petit, N., 2012. Closed-loop control of a SCR system using a NO_x sensor cross-sensitive to NH₃. *IFAC Proceedings Volumes* 45, 738–743. <https://doi.org/10.3182/20120710-4-SG-2026.00088>
- Bonnel, P., Kubelt, J., and Provenza, A., 2011. Heavy-Duty Engines Conformity testing based on PEMS (No. EUR 24921 EN-2011). JRC European Commission.
- Boriboonsomsin, K., Durbin, T., Scora, G., Johnson, K., Sandez, D., Vu, A., Jiang, Y., Burnette, A., Yoon, S., Collins, J., Dai, Z., Fulper, C., Kishan, S., Sabisch, M.,

- and Jackson, D., 2018. Real-world exhaust temperature profiles of on-road heavy-duty diesel vehicles equipped with selective catalytic reduction. *Science of The Total Environment* 634, 909–921. <https://doi.org/10.1016/j.scitotenv.2018.03.362>
- Brook, R.D., Rajagopalan, S., Pope, C.A., Brook, J.R., Bhatnagar, A., Diez-Roux, A.V., Holguin, F., Hong, Y., Luepker, R.V., Mittleman, M.A., Peters, A., Siscovick, D., Smith, S.C., Whitsel, L., and Kaufman, J.D., American Heart Association Council on Epidemiology and Prevention, Council on the Kidney in Cardiovascular Disease, and Council on Nutrition, Physical Activity and Metabolism, 2010. Particulate matter air pollution and cardiovascular disease: An update to the scientific statement from the American Heart Association. *Circulation* 121, 2331–2378. <https://doi.org/10.1161/CIR.0b013e3181dbee1>
- Buckingham, J.P., Mason, R.L., and Spears, M.W., 2009. Determination of PEMS Measurement Allowances for Gaseous Emissions Regulated Under the Heavy-Duty Diesel Engine In-Use Testing Program: Part 2 – Statistical Modeling and Simulation Approach. *SAE International Journal of Fuels and Lubricants* 2, 422–434. <https://doi.org/10.4271/2009-01-0939>
- Burch, R., Millington, P.J., and Walker, A.P., 1994. Mechanism of the selective reduction of nitrogen monoxide on platinum-based catalysts in the presence of excess oxygen. *Applied Catalysis B: Environmental* 4, 65–94. [https://doi.org/10.1016/0926-3373\(94\)00014-X](https://doi.org/10.1016/0926-3373(94)00014-X)
- Cai, H., Burnham, A., Wang, M., Hang, W., and Vyas, A., 2015. The GREET Model Expansion for Well-to-Wheels Analysis of Heavy-Duty Vehicles. <https://doi.org/10.2172/1212730>
- CARB, 2019. Staff Current Assessment of the Technical Feasibility of Lower NOx Standards and Associated Test Procedures for 2022 and Subsequent Model Year Medium-Duty and Heavy-Duty Diesel Engines.
- Carder, D.K., Ryskamp, R., Besch, M.C., and Thiruvengadam, A., 2017. Emissions Control Challenges for Compression Ignition Engines. *Procedia IUTAM*, 24th International Congress of Theoretical and Applied Mechanics 20, 103–111. <https://doi.org/10.1016/j.piutam.2017.03.015>
- Cavataio, G., Girard, J., Patterson, J.E., Montreuil, C., Cheng, Y., and Lambert, C.K., 2007. Laboratory Testing of Urea-SCR Formulations to Meet Tier 2 Bin 5 Emissions. Presented at the SAE World Congress & Exhibition. <https://doi.org/10.4271/2007-01-1575>
- Chih-Cheng, C., Chia-Jui, C., Yu-Hsuan, S., and Yong-Yuan, K., 2014. Identification of Cross-Sensitivity of Smart NOx Sensors to Ammonia in Urea-Selective Catalyst Reduction Systems via Fast Fourier Transform. *Sensors and Materials* 313. <https://doi.org/10.18494/SAM.2014.986>
- Code of Federal Regulations, 2018. Title 13, Section 1971.1, On-Board Diagnostic System Requirements.

- Code of Federal Regulations. Title 40 Protection of Environment: Part 86.1370 - Not-To-Exceed test procedures., 2016.
- Code of Federal Regulations. Title 40 Protection of Environment: Part 86.1912 - How do I determine whether an engine meets the vehicle-pass criteria?, 2016.
- Code of Federal Regulations. Title 40 Protection of Environment: Part 1065 - Engine Testing Procedures, 2016.
- Code of Federal Regulations. Title 40 Protection of Environment: Part 1065 Subpart J - Field Testing and Portable Emission Measurement Systems, 2011.
- Code of Federal Regulations. Title 40 Protection of Environment: Part 1065.307 - Linearity Verification, 2014.
- Code of Federal Regulations. Title 40 Protection of Environment: Part 1065.610 - Duty cycle generation, 2014.
- Code of Federal Regulations. Title 40 Protection of Environment: Part 1065.703 - Distillate diesel fuel, 2014.
- Code of Federal Regulations. Title 40 Protection of Environment: Part 1065.1005- Symbols, abbreviations, acronyms, and units of measure, 2016.
- ControlTec, 2014. Overview of ControlTec-CT 1000.
- Cozzolini, A., Besch, M.C., Ardanese, M., Ardanese, R., Gautam, M., Oshinuga, A., and Miyasato, M., 2012. Determination of Optimal Engine Parameters for Exhaust Emissions Reduction Using the Taguchi Method. Presented at the ASME 2011 Internal Combustion Engine Division Fall Technical Conference, American Society of Mechanical Engineers Digital Collection. <https://doi.org/10.1115/ICEF2011-60134>
- Dahlmann, K., Grewe, V., Ponater, M., and Matthes, S., 2011. Quantifying the contributions of individual NO_x sources to the trend in ozone radiative forcing. *Atmospheric Environment* 45, 2860–2868. <https://doi.org/10.1016/j.atmosenv.2011.02.071>
- Dallmann, T.R., and Harley, R.A., 2010. Evaluation of mobile source emission trends in the United States. *Journal of Geophysical Research: Atmospheres* 115. <https://doi.org/10.1029/2010JD013862>
- Demirgok, B., 2018. Development of an Emissions Monitoring Methodology Using On-Board NO_x Sensors and Revision to Current In-Use Emissions Regulatory Protocols. West Virginia University.
- Demirgok, B., Besch, M.C., Ryskamp, R., Pondicherry, R., Selimi, B., Thiruvengadam, A., and Carder, D., 2019. Evaluation of On-Board NO_x and NH₃ sensors for collecting real-world emissions data. Presented at the 29th CRC Real-world emissions workshop, California.

- Dixit, P., Miller, J.W., Cocker, D.R., Oshinuga, A., Jiang, Y., Durbin, T.D., and Johnson, K.C., 2017. Differences between emissions measured in urban driving and certification testing of heavy-duty diesel engines. *Atmospheric Environment* 166, 276–285. <https://doi.org/10.1016/j.atmosenv.2017.06.037>
- DOJ, U.S. EPA, 1998. DOJ Announce One Billion Dollar settlement with diesel engine industry for clean air violation.
- Eijnden, E. v.d., Cloudt, R., Willems, F., and Heijden, P. v.d., 2009. Automated Model Fit Tool for SCR Control and OBD Development. Presented at the SAE World Congress & Exhibition. <https://doi.org/10.4271/2009-01-1285>
- Ellis, J., 2017. CARB: Heavy Duty OBD Program Update. Presented at the SAE On-Board Diagnostic Symposium, California.
- Englund, M.S., 1982. Field Compatible NO_x Emission Measurement Technique. Presented at the 33rd Annual Earthmoving Industry Conference. <https://doi.org/10.4271/820647>
- Environmental Policy Division, 1975. Environmental Protection Affairs of the Ninety-Third Congress (No. 94–2).
- Feist, M.D., Sharp, C.A., and Spears, M.W., 2009. Determination of PEMS Measurement Allowances for Gaseous Emissions Regulated Under the Heavy-Duty Diesel Engine In-Use Testing Program: Part 1 – Project Overview and PEMS Evaluation Procedures. *SAE Int. J. Fuels Lubr.* 2, 435–454. <https://doi.org/10.4271/2009-01-0938>
- Fontaras, G., Zacharof, N.-G., and Ciuffo, B., 2017. Fuel consumption and CO₂ emissions from passenger cars in Europe – Laboratory versus real-world emissions. *Progress in Energy and Combustion Science* 60, 97–131. <https://doi.org/10.1016/j.pecs.2016.12.004>
- Frobert, A., Raux, S., Creff, Y., and Jeudy, E., 2013. About Cross-Sensitivities of NO_x Sensors in SCR Operation. Presented at the SAE World Congress & Exhibition, pp. 2013-01–1512. <https://doi.org/10.4271/2013-01-1512>
- Gautam, M., Thompson, G.J., Carder, D.K., and Clark, N.N., Shade, B.C., Riddle, W.C., Lyons, D.W., 2001. Measurement of In-Use, On-Board Emissions from Heavy-Duty Diesel Vehicles: Mobile Emissions Measurement System. Presented at the SAE International Fall Fuels & Lubricants Meeting & Exhibition. <https://doi.org/10.4271/2001-01-3643>.
- Giechaskiel, B., Clairottee, M., Valverde, V., and Bonnel, P., 2018. Real driving emissions: 2017 assessment of Portable Emissions Measurement Systems (PEMS) measurement uncertainty (No. EUR 29138 EN). JRC European Commission.
- Gierczak, C.A., Korniski, T.J., Wallington, T.J., and Butler, J.W., 2006. Laboratory Evaluation of the SEMTECH-G® Portable Emissions Measurement System

- (PEMS) For Gasoline Fueled Vehicles. Presented at the SAE World Congress & Exhibition. <https://doi.org/10.4271/2006-01-1081>
- Girard, J.W., Montreuil, C., Kim, J., Cavataio, G., and Lambert, C., 2008. Technical Advantages of Vanadium SCR Systems for Diesel NO_x Control in Emerging Markets. *SAE Int. J. Fuels Lubr.* 1, 488–494. <https://doi.org/10.4271/2008-01-1029>
- Glarborg, P., Miller, J.A., Ruscic, B., and Klippenstein, S.J., 2018. Modeling nitrogen chemistry in combustion. *Progress in Energy and Combustion Science* 67. <https://doi.org/10.1016/j.pecs.2018.01.002>
- Hausberger, S., and Lipp, S., 2014. Evaluation Methods for Real Drive Emission Tests of LDV for a Future Legislation. Presented at the 8th Internationales Forum Abgas- und Partikelemissionen, Wiesbaden.
- He, H., and Jin, L., 2017. A historical review of the U.S. vehicle emission compliance program and emission recall cases. *The International Council on Clean Transportation*.
- Henderick, P., 2019. California's Real Emissions Assessment Logging (REAL) Initiative: On-Road Vehicles Will Track Their Own NO_x and GHG Emissions.
- Heywood, J.B., 1988. *Internal combustion engine fundamentals*. McGraw-Hill.
- Hofmann, L., Rusch, K., Fischer, S., and Lemire, B., 2004. Onboard Emissions Monitoring on a HD Truck with an SCR System Using Nox Sensors. *SAE Journal of Fuels and Lubricants* 113, 559–572. <https://doi.org/10.4271/2004-01-1290>
- Horiba, 2014. On-Board Emissions Measurement System: OBS-ONE: Product Description.
- Idicheria, C.A., and Pickett, L.M., 2005. Soot Formation in Diesel Combustion under High-EGR Conditions. Presented at the SAE World Congress & Exhibition. <https://doi.org/10.4271/2005-01-3834>
- Ishida, M., Yamamoto, S., Ueki, H., and Sakaguchi, D., 2010. Remarkable improvement of NO_x–PM trade-off in a diesel engine by means of bioethanol and EGR. *Energy* 35, 4572–4581. <https://doi.org/10.1016/j.energy.2010.03.039>
- Iverach, D., Basden, K.S., and Kirov, N.Y., 1973. Formation of nitric oxide in fuel-lean and fuel-rich flames. *Symposium (International) on Combustion* 14, 767–775. [https://doi.org/10.1016/S0082-0784\(73\)80071-2](https://doi.org/10.1016/S0082-0784(73)80071-2)
- Jacobs, T., Assanis, D., and Filipi, Z., 2003. The Impact of Exhaust Gas Recirculation on Performance and Emissions of a Heavy-Duty Diesel Engine. Presented at the SAE World Congress & Exhibition. <https://doi.org/10.4271/2003-01-1068>
- Jiang, Z., McDonald, B.C., Worden, H., Worden, J.R., Miyazaki, K., Qu, Z., Henze, D.K., Jones, D.B.A., Arellano, A.F., Fischer, E.V., Zhu, L., and Boersma, K.F.,

2018. Unexpected slowdown of US pollutant emission reduction in the past decade 115, 5099–5104. <https://doi.org/10.1073/pnas.1801191115>
- JMP, 2018. Design of Experiments Guide.
- Johnson, J.A., 2012. Measuring Conventional and Alternative Exhaust Emissions from a Gas Turbine Engine (M.Sc). University of Kansas.
- Johnson, T., 2008. Diesel Engine Emissions and Their Control. *Platinum Metals Rev.* 52, 23–37. <https://doi.org/10.1595/147106708x248750>
- Johnson, T.V., and Joshi, A., 2018. Chapter 1 Review of deNO_x Technology for Mobile Applications 1–35. <https://doi.org/10.1039/9781788013239-00001>
- Jolliffe, I.T., 2002. Principal Component Analysis. Springer.
- JRC European Union, Commission Regulation EU 582/2011, 2011.
- Kamasamudram, K., Currier, N., Szailer, T., and Yezerets, A., 2010. Why Cu- and Fe-Zeolite SCR Catalysts Behave Differently At Low Temperatures. *SAE Int. J. Fuels Lubr.* 3, 664–672. <https://doi.org/10.4271/2010-01-1182>
- Kamimoto, T., and Bae, M., 1988. High Combustion Temperature for the Reduction of Particulate in Diesel Engines. Presented at the SAE International Congress and Exposition. <https://doi.org/10.4271/880423>
- Kang, C.-S., You, Y.-J., Kim, K.-J., Kim, T., Ahn, S.-J., Chung, K.-H., Park, N.-C., Kimura, S., and Ahn, H.-G., 2006. Selective catalytic reduction of NO_x with propene over double wash-coat monolith catalysts. *Catalysis Today, Advances in Catalysis and Catalytic Materials for Energy and Environmental Protection* 111, 229–235. <https://doi.org/10.1016/j.cattod.2005.10.031>
- Kappanna, H.K., 2015. Development of a Reference Dataset to Evaluate PEMS Post-Processing Software (Ph.D.). West Virginia University.
- Keuper, A., Unger, H.-M.I., Huang, J., Bressler, H., and Albrecht, W., 2011. Investigations to Achieve Highest Efficiencies in Exhaust Gas After-Treatment for Commercial Vehicles using an SCR System. *SAE Int. J. Commer. Veh.* 4, 145–154. <https://doi.org/10.4271/2011-01-2201>
- Kihara, N., Tsukamoto, T., Matsumoto, K., Ishida, K., Kon, M., and Murase, T., 2000. Real-Time On-Board Measurement of Mass Emission of NO_x, Fuel Consumption, Road Load, and Engine Output for Diesel Vehicles. Presented at the SAE World Congress. <https://doi.org/10.4271/2000-01-1141>
- Kittelson, D.B., 1998. Engines and nanoparticles: A review. *J Aerosol Sci* 29, 575–588. [https://doi.org/10.1016/S0021-8502\(97\)10037-4](https://doi.org/10.1016/S0021-8502(97)10037-4)
- Kröcher, O., 2007. Chapter 9 Aspects of catalyst development for mobile urea-SCR systems — From Vanadia-Titania catalysts to metal-exchanged zeolites. *Studies in Surface Science and Catalysis* 171, 261–289. [https://doi.org/10.1016/S0167-2991\(07\)80210-2](https://doi.org/10.1016/S0167-2991(07)80210-2)

- Kwak, J.H., Tran, D., Burton, S.D., Szanyi, J., Lee, J.H., and Peden, C.H.F., 2012. Effects of hydrothermal aging on NH₃-SCR reaction over Cu/zeolites. *Journal of Catalysis* 287, 203–209. <https://doi.org/10.1016/j.jcat.2011.12.025>
- Liati, A., Schreiber, D., Dimopoulos Eggenschwiler, P., and Arroyo Rojas Dasilva, Y., 2013. Metal Particle Emissions in the Exhaust Stream of Diesel Engines: An Electron Microscope Study. *Environ. Sci. Technol.* 47, 14495–14501. <https://doi.org/10.1021/es403121y>
- MECA, 2007. Emission Control Technologies for Diesel-Powered Vehicles. Manufacturers of Emission Controls Association.
- Mendoza-Villafuerte, P., Suarez-Bertoa, R., Giechaskiel, B., Riccobono, F., Bulgheroni, C., Astorga, C., and Perujo, A., 2017. NO_x, NH₃, N₂O and PN real driving emissions from a Euro VI heavy-duty vehicle. Impact of regulatory on-road test conditions on emissions. *Science of The Total Environment* 609, 546–555. <https://doi.org/10.1016/j.scitotenv.2017.07.168>
- Misra, C., Collins, J.F., Herner, J.D., Sax, T., Krishnamurthy, M., Sobieralski, W., Burntizki, M., and Chernich, D., 2013. In-Use NO_x Emissions from Model Year 2010 and 2011 Heavy-Duty Diesel Engines Equipped with Aftertreatment Devices. *Environ. Sci. Technol.* 47, 7892–7898. <https://doi.org/10.1021/es4006288>
- Montes, T., 2018. CARB: Heavy Duty OBD Program Update. Presented at the SAE On-Board Diagnostics Symposium, Barcelona, Spain.
- Moos, R., 2009. Recent Developments in Automotive Exhaust Gas Sensing. *Proceedings SENSOR 1*, 227–231. <http://dx.doi.org/10.5162/sensor09/v1/b5.1>
- Moos, R., 2005. A Brief Overview on Automotive Exhaust Gas Sensors Based on Electroceramics. *International Journal of Applied Ceramic Technology* 2, 401–413. <https://doi.org/10.1111/j.1744-7402.2005.02041.x>
- Murray, E.P., Kharashi, K., and Adedeji, K., 2017. Managing H₂O Cross-Sensitivity Using Composite Electrolyte NO_x Sensors. *Electrochemical Sensors Technology*. <https://doi.org/10.5772/67827>
- Nakamura, H., Akard, M., Porter, S., Kihara, N., Adachi, M., and Khalek, I.A., 2007. Performance Test Results of a New On Board Emission Measurement System Conformed with CFR Part 1065. Presented at the SAE World Congress. <https://doi.org/10.4271/2007-01-1326>
- Nova, I., and Tronconi, E. (Eds.), 2014. Urea-SCR technology for deNO_x after treatment of diesel exhausts, Fundamental and applied catalysis. Springer.
- O'Connor, J., and Musculus, M., 2013. Post Injections for Soot Reduction in Diesel Engines: A Review of Current Understanding. *SAE Int. J. Engines* 6, 400–421. <https://doi.org/10.4271/2013-01-0917>
- Oestergaard, K., Akard, M., Porter, S., and Carder, D., 2004. Further Investigation into the Performance of Two Different On-Board Emissions Measurement

- System Compared to Laboratory Measurements. Presented at the SAE Brasil Congress and Exhibit. <https://doi.org/10.4271/2004-01-3480>.
- Olsson, L., and Fridell, E., 2002. The Influence of Pt Oxide Formation and Pt Dispersion on the Reactions $\text{NO}_2 \rightleftharpoons \text{NO} + 1/2 \text{O}_2$ over Pt/Al₂O₃ and Pt/BaO/Al₂O₃. *Journal of Catalysis* 210, 340–353. <https://doi.org/10.1006/jcat.2002.3698>
- Perujo Mateos del Parque, A., and Mendoza Villafuerte, P., 2015. PEMS Emissions testing of Heavy Duty Vehicles/Engines: Assesment of PEMS procedures in fulfilment of Article 14(3) to regulation EU 582/2011 (No. EUR 27251 EN). JRC European Commission.
- Pondicherry, R., 2017. Effects of Boundary Parameters on the Work-Based Window (WBW) and Not-to-Exceed (NTE) In-Use Emissions Quantification Methods (M.Sc). West Virginia University.
- Pondicherry, R., Besch, M.C., Thiruvengadam, A., and Carder, D., 2018. Investigation of Boundary Parameter Effects on In-Use Emissions Quantification Methods. Presented at the 37th FISITA World Automotive Congress, India.
- Pondicherry, R., Demirgok, B., Selimi, B., Besch, M.C., Thiruvengadam, A., and Carder, D.K., 2019. In-Use Activity and NO_x Emissions from On-highway vehicles using Tail-pipe NO_x sensor. Presented at the 29th CRC Real-world Emissions Workshop, California.
- Quiros, D.C., Thiruvengadam, A., Pradhan, S., Besch, M.C., Thiruvengadam, P., Demirgok, B., Carder, D.K., Oshinuga, A., Huai, T., and Hu, S., 2016. Real-World Emissions from Modern Heavy-Duty Diesel, Natural Gas, and Hybrid Diesel Trucks Operating Along Major California Freight Corridors. *Emiss. Control Sci. Technol.* 2, 156–172. <https://doi.org/10.1007/s40825-016-0044-0>
- Ramadhas, A.S., Xu, H., Liu, D., and Tian, J., 2017. Reducing Cold Start Emissions from Automotive Diesel Engine at Cold Ambient Temperatures. *Aerosol Air Qual. Res.* 16, 3330–3337. <https://doi.org/10.4209/aaqr.2015.11.0616>
- Ravichettu, S., Gaddale, A.P.R., and Kotha, M.M., 2017. Effective reduction of NO_x emissions from diesel engine using split injections. *Alexandria Engineering Journal* 57, 1379–1392. <https://doi.org/10.1016/j.aej.2017.06.009>
- Riegel, J., Neumann, H., and Wiedenmann, H.-M., 2002. Exhaust gas sensors for automotive emission control. *Solid State Ionics, Proceedings of International Conference on Solid State Ionics* 152–153, 783–800. [https://doi.org/10.1016/S0167-2738\(02\)00329-6](https://doi.org/10.1016/S0167-2738(02)00329-6)
- Rohrer, R.A., Luck, J.D., Pitla, S.K., and Hoy, R., 2018. Evaluation of the Accuracy of Machine Reported CAN Data for Engine Torque and Speed. *Transactions of the ASABE* 61, 1547–1557. <https://doi.org/10.13031/trans.12754>
- Sakai, N., Yamaji, K., Horita, T., Xiong, Y.P., Kishimoto, H., and Yokokawa, H., 2003. Effect of Water on Oxygen Transport Properties on Electrolyte Surface in SOFCs: I. Surface Reaction Mechanism of Oxygen Isotope Exchange on Solid

Oxide Electrolytes. *J. Electrochem. Soc.* 150, A689.
<https://doi.org/10.1149/1.1568938>

- Sanchonx, 2017. Schematic diagram of a Michelson interferometer, configured for FTIR.
- Sandhu, G.S., Frey, H.C., Bartelt-Hunt, S., and Jones, E., 2016. Real-world activity, fuel use, and emissions of diesel side-loader refuse trucks. *Atmospheric Environment* 129, 98–104. <https://doi.org/10.1016/j.atmosenv.2016.01.014>
- Scora, G., Boriboonsomsin, K., Durbin, T.D., Johnson, K., Yoon, S., Collins, J., and Dai, Z., 2019. Variability in Real-World Activity Patterns of Heavy-Duty Vehicles by Vocation. *Transportation Research Record* 2673, 51–61. <https://doi.org/10.1177/0361198119844247>
- Sensors, 2011. On Board Vehicle Emissions Analyzer User Manual.
- Shade, B.C., 2006. A work-based window method for calculating in-use brake-specific oxides of nitrogen emissions of heavy -duty diesel engines (Ph.D.). West Virginia University.
- Shade, B.C., Carder, D.K., Thompson, G.J., and Gautam, M., 2008. A Work-Based Window Method for Calculating In-Use Brake-Specific NO_x Emissions of Heavy-Duty Diesel Engines. *SAE Int. J. Engines* 1, 778–793. <https://doi.org/10.4271/2008-01-1301>
- Sharp, C.A., Feist, M.D., Laroo, C.A., and Spears, M.W., 2009. Determination of PEMS Measurement Allowances for Gaseous Emissions Regulated Under the Heavy-Duty Diesel Engine In-Use Testing Program Part 3 – Results and Validation. *SAE Int. J. Fuels Lubr.* 2, 407–421. <https://doi.org/10.4271/2009-01-0938>
- Smith, H., Lauer, T., Mayer, M., and Pierson, S., 2014. Optical and Numerical Investigations on the Mechanisms of Deposit Formation in SCR Systems. *SAE Int. J. Fuels Lubr.* 7, 525–542. <https://doi.org/10.4271/2014-01-1563>
- Smith, M., 1978. Heavy-duty Vehicle Cycle Development (No. EPA 460/3-78-008).
- Soltis, R., Ding, Y., Kubinski, D.J., and Visser, J.H., 2006. Influence of H₂O on NO_x Sensors. *ECS Trans.* 3, 173–178. <https://doi.org/10.1149/1.2357257>
- Spears, M.W., 2019. Assessment of a Candidate Metric for a New Paradigm of In-Use NO_x Emissions Compliance for Heavy-duty On-Highway Engines. Presented at the 29th CRC Real-world emissions workshop, California.
- Stanton, D., Charlton, S., and Vajapeyazula, P., 2013. Diesel Engine Technologies Enabling Powertrain Optimization to Meet U.S. Greenhouse Gas Emissions. *SAE Int. J. Engines* 6, 1757–1770. <https://doi.org/10.4271/2013-24-0094>
- Stanton, D.W., 2013. Systematic Development of Highly Efficient and Clean Engines to Meet Future Commercial Vehicle Greenhouse Gas Regulations. *SAE Int. J. Engines* 6, 1395–1480. <https://doi.org/10.4271/2013-01-2421>

- Tan, Y., Henderick, P., Yoon, S., Herner, J., Montes, T., Boriboonsomsin, K., Johnson, K., Scora, G., Sandez, D., and Durbin, T.D., 2019. On-Board Sensor-Based NO_x Emissions from Heavy-Duty Diesel Vehicles. *Environ. Sci. Technol.* 53, 5504–5511. <https://doi.org/10.1021/acs.est.8b07048>
- Thiruvengadam, A., Besch, M.C., Thiruvengadam, P., Pradhan, S., Carder, D.K., Kappanna, H., Gautam, M., Oshinuga, A., Hogo, H., and Miyasato, M., 2015. Emission rates of regulated pollutants from current technology heavy-duty diesel and natural gas goods movement vehicles. *Environ. Sci. Technol.* 49, 5236–5244. <https://doi.org/10.1021/acs.est.5b00943>
- Thiruvengadam, P., 2017. Dual-layered Multi-Objective Genetic Algorithms (D-MOGA): A Robust Solution for Modern Engine Development and Calibrations (PhD). West Virginia University.
- Todo, Y., Ichikawa, H., Yotou, H., Aoki, K., and Kawai, M., 2018. Development of High Accuracy and Quick Light-off NO_x Sensor. Presented at the SAE World Congress, pp. 2018-01–0334. <https://doi.org/10.4271/2018-01-0334>
- Ura, J.A., Girard, J., Cavataio, G., Montreuil, C., and Lambert, C., 2009. Cold Start Performance and Enhanced Thermal Durability of Vanadium SCR Catalysts. Presented at the SAE World Congress & Exhibition, pp. 2009-01–0625. <https://doi.org/10.4271/2009-01-0625>
- U.S. EPA, 2016a. Emission Standards for Heavy-Duty Highway Engines and Vehicles.
- U.S. EPA, 2016b. Regulations for Greenhouse Gas Emissions from Commercial Trucks & Buses.
- U.S. EPA, 2005. On-Road Heavy-Duty Diesel Engine In-Use Compliance Program.
- U.S. EPA, 2002. Selective Catalytic Reduction (Review Draft).
- Vojtisek-Lom, and M., Cobb, J.T., 1998. On-Road Light-Duty Vehicle Emission Measurements Using a Novel Inexpensive On-Board Portable System. Presented at the 8th CRC On-road vehicle emissions workshop, California.
- Wang, Y.-Y., Zhang, H., and Wang, J., 2016. NO_x Sensor Reading Correction in Diesel Engine Selective Catalytic Reduction System Applications. *IEEE/ASME Transactions on Mechatronics* 21, 460–471. <https://doi.org/10.1109/TMECH.2015.2434846>
- Warey, A., Long, D., Balestrino, S., Szymkowicz, P., and Bika, A.S., 2013. Visualization and Analysis of Condensation in Exhaust Gas Recirculation Coolers. Presented at the SAE World Congress & Exhibition. <https://doi.org/10.4271/2013-01-0540>.
- Woo, L.Y., and Glass, R.S., 2012. NO_x Sensor Development (No. LLNL-TR-599052). Lawrence Livermore National Lab. <https://doi.org/10.2172/1055836>

- Wu, Y., 2010. Laboratory and Real-World Measurement of Diesel Particulate Matter (Ph.D.). West Virginia University. <https://doi.org/10.33915/etd.3013>
- Yong-Wha, K., and Van Nieuwstadt, M., 2006. Threshold Monitoring of Urea SCR Systems. Presented at the SAE Commercial Vehicle Engineering Congress & Exhibition. <https://doi.org/10.4271/2006-01-3548>
- Yuan, X., Liu, H., and Gao, Y., 2015. Diesel Engine SCR Control: Current Development and Future Challenges. *Emiss. Control Sci. Technol.* 1, 121–133. <https://doi.org/10.1007/s40825-015-0013-z>
- Zelenka, P., Kriegler, W., Herzog, P.L., and Cartellieri, W.P., 1990. Ways Toward the Clean Heavy-Duty Diesel. *SAE Journal of Engines* 99, 1279–1291. <https://doi.org/10.4271/900602>.

Appendix

A. Semtech-DS Analyzer Specifications

This section of the appendix contains the specifications of the analyzer used for on-road measurements acquired using Semtech-DS (i.e., a 40 CFR §1065 compliant PEMS). Table 40 list the specifications of the individual gas detection NDIR analyzer used for measurement of CO, CO₂, and HC emissions.

Table 40: Specifications of Semtech-DS NDIR analyzer (Sensors, 2011)

Gas	CO	CO ₂	HC
Range of measurement	0 – 8 % lowest span value 1000ppm	0 – 20 % lowest span value 6%	0 – 2,000 ppm hexane 0 – 4,000 ppm propane
Accuracy	±3 % of reading or 50 ppm, whichever is greater	±3 % of reading or ±0.1%, whichever is greater	±3 % of reading or 4.0 ppmC6, whichever is greater
Resolution	10 ppm	0.01%	1 ppmC6
Linearity	0.990 ≤Slope ≤1.01 SEE ≤1.0 % of FS r ² ≥0.998		
Linearity intercept	0.5% of span value down to 3000ppm; 1% of span value below 3000ppm	0.5% of span value down to 6%	0.5% of span value
Repeatability	±2 % of reading or 20 ppm, whichever is greater	±2 % of reading or ±0.05 %, whichever is greater	±2 % of reading or 2.0 ppmC6, whichever is greater
Noise	≤20 ppm	≤0.02%	≤1 ppmC6
Span drift (over 8 hours)	≤2 % of span or 20 ppm, whichever is greater ¹	≤2 % of span or 0.1 %, whichever is greater ¹	≤% of reading or 2.0 ppmC6, whichever is greater ¹
Zero drift (over 1 hour)	≤0.005 % (50 ppm) ¹	≤0.1 % ¹	≤4 ppmC6 ¹
Response time	T90 ≤ 3 seconds ²	T90 ≤ 3 seconds ²	T90 ≤ 3 seconds ²
Data rate	0.833 Hz	0.833 Hz	0.833 Hz
Flow rate (nominal)	3 lpm	3 lpm	3 lpm

1. Assumes stable ambient temperature.
2. At nominal flowrate.

Table 41 list the specifications of the individual gas detection NDUV analyzer used for measurement of NO and NO₂ emissions.

Table 41: Specifications of bench-scale evaluation for Semtech-DS NDUV analyzer (Sensors, 2011)

Gas	NO	NO ₂
Range of measurement	0 to 3,000 ppm 0 to 900 ppm 0 to 300 ppm	0 to 500 ppm 0 to 300 ppm 0 to 100 ppm
Accuracy	±2 % of rdg or ±1 % FS ¹	±2 % of rdg or ±1% of FS ¹
Resolution	0.1 ppm	0.1 ppm
Linearity	Intercept ≤0.5 % FS all ranges 0.990 ≤Slope ≤1.01 SEE ≤1.0 % of FS r ² ≥0.998	Intercept ≤0.5% of FS (1% for lowest range) 0.990 ≤Slope ≤1.01 SEE ≤1.0 % of FS r ² ≥0.998
Repeatability	±1 % of reading or ±1 ppm ¹	±1 % of reading or ±1 FS ¹
Noise	≤1 ppm	≤1 ppm
Span drift (over 8 hours)	≤2 % of FS or 10 ppm ^{1,2}	≤2 % of FS or 5 ppm ^{1,2}
Zero drift (over 1 hour)	≤ 4 ppm ²	≤ 4 ppm ²
Response time	T90 ≤ 3 seconds ³	T90 ≤ 3 seconds ³
Data rate	Up to 4 Hz	Up to 4 Hz
Flow rate (nominal)	3 lpm	3 lpm

¹ Whichever is greater

² Assumes stable ambient temperature. FID requires 24 hour burn-in if unused for more than a week for optimal stability.

³ At nominal flow rate.

B. Schematic Representation of the ABW approach

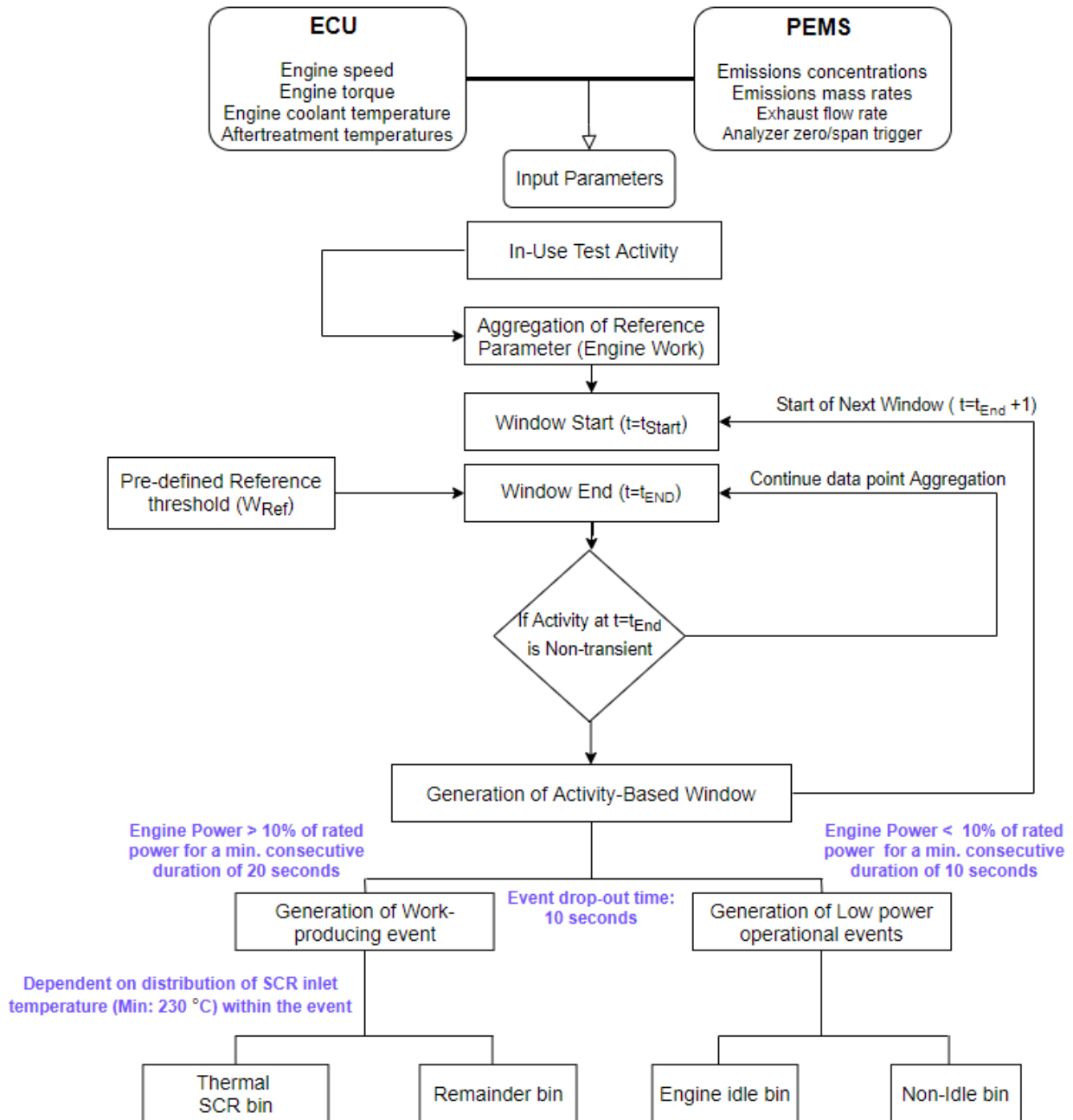


Figure 93: Flow chart-based description of ABW approach

C. Supplemental ABW Analysis

Figure 94 presents a comparative analysis of bsNO_x and bsCO₂ emissions for events generated from test activity collected on route-3 and 4 from vehicle-C and D for ABW bin category 1a. With respect to the discussion presented in section 5.2.4.1 and 5.2.4.3, the data presented in the figure depicts the various control strategies used in bin-1a that depict three different operation modes. (i) Low-NO_x and high-CO₂ emissions: Event-averaged emissions rates that are below 0.20 and 0.45 g/bhp-hr for NO_x and above 475 g/bhp-hr for CO₂, (ii) Low-NO_x and low-CO₂ emissions: Event-averaged emissions rates that are below 0.20 and 0.45 g/bhp-hr for NO_x and below 475 g/bhp-hr for CO₂, and (iii) High-NO_x and low/high CO₂: Event-averaged emissions rates that are above 0.45 g/bhp-hr for NO_x and above 475 g/bhp-hr for CO₂. Events generated in (iii) are representative of test conditions that are indicative of either insufficient thermal energy to support catalyst reactions (or) a possible failure/defect in the EATS.

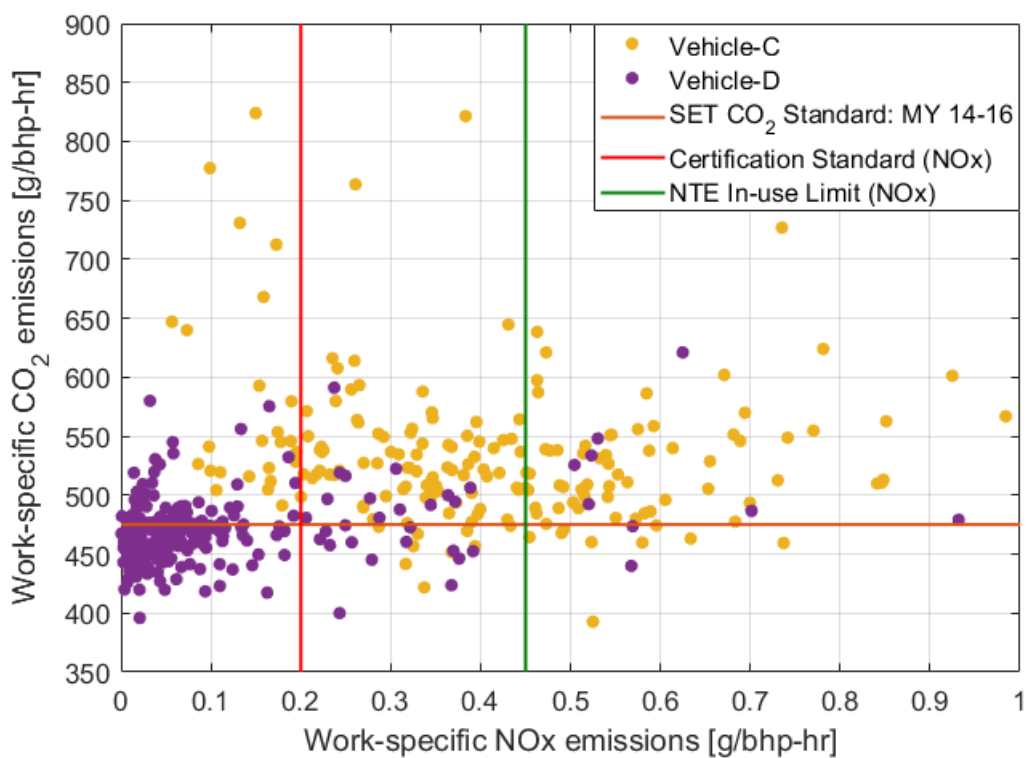


Figure 94: Comparison of NO_x versus CO₂ emissions

D. Evaluation of ECU derived Exhaust Flow Rate

Phase-2 of the ABW approach comprised of an evaluation of test activity collected from the actual in-fleet operation. Vehicle-7, 11, 13, 14 and 18 did not broadcast ECU parameter for exhaust gas mass flow rate. Specific for these vehicle datasets, the exhaust flow rate was derived by summation of ECU broadcast of intake gas mass flow rate and fuel mass flow rate. J1939 CAN protocol broadcasts volumetric fuel flow rate. The parameter was quantified to mass flow rate based on the assumption of a constant density for ULSD (i.e., 0.830 kg/L). In order to provide an understanding of the errors associated with the predicted exhaust gas flow rate, Figure 95 presents an example scenario with respect to the comparison of error propagation between ECU derived and broadcasted exhaust flow rate. Data presented in the figure was acquired from vehicle-10 and binned as a function of ECU broadcasted exhaust flow rate (i.e., bin width: 100 kg/hr). The comparative analysis shows that the error bandwidth is within $\pm 10\%$ for exhaust flow rates below 1000 kg/hr.

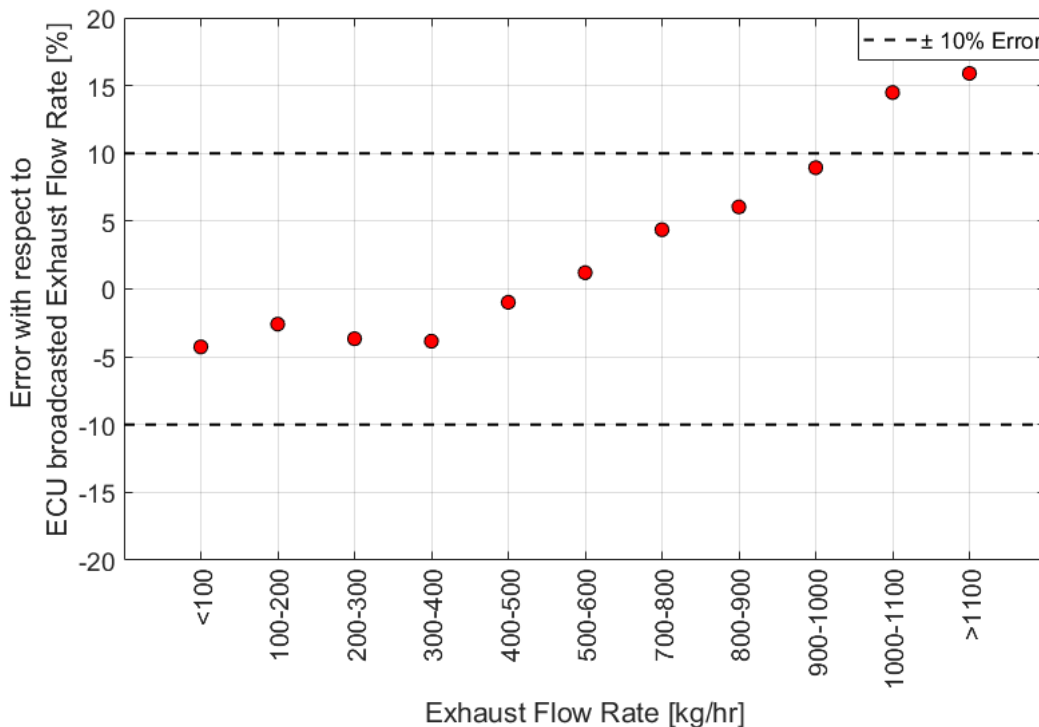


Figure 95: Error propagation of ECU derived exhaust flow rate

E. Evaluation of ECU derived CO₂ Emissions

Phase-2 of the ABW approach demonstrated a comparison of NO_x versus CO₂ emissions for test activity acquired in bin-1a and 1b. Since test activity was acquired from J1939 ECU broadcasted parameters, CO₂ emissions were derived from ECU broadcasted fuel flow rate based on the assumption of constant fuel density and complete combustion. Figure 96 presents an example scenario of comparison of errors associated with ECU derived CO₂ emissions versus CO₂ emissions quantified from measurements acquired using an NDUV analyzer. Test activity acquired from vehicle-D operated on leg-3 of route-3 is presented in the figure. The data were binned as a function of PEMS quantified CO₂ mass rate (i.e., bin width: 5 g/sec). The analysis shows that for the vehicle and test dataset mentioned above, the error propagation was within $\pm 10\%$ for CO₂ mass flow rate above 15 g/sec. An in-depth evaluation of data acquired from multiple engine manufacturers and engine platforms (i.e., comprising of a large sample size) is required to provide an effective and efficient correction factor in order to minimize the deviations between ECU derived, and PEMS reported CO₂ emissions.

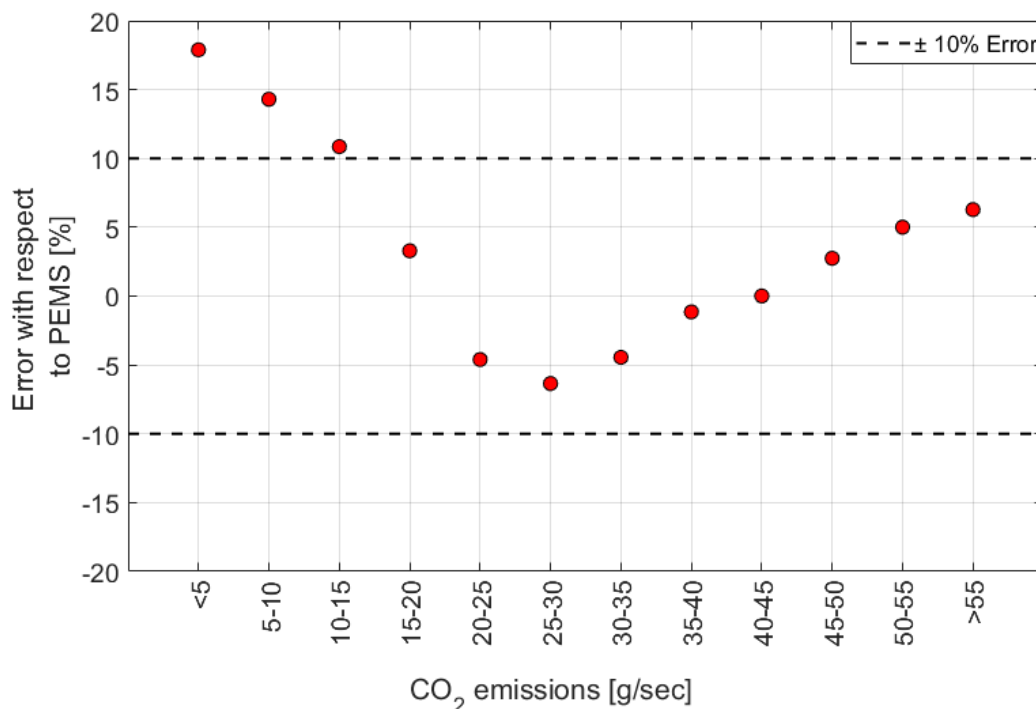


Figure 96: Error propagation of ECU derived CO₂ emissions

F. Exhaust Thermal Profile of In-fleet Activity

Figure 97 presents a histogram-based $T_{SCR IN}$ distribution of entire test activity acquired from fleet-based vehicle vocational operation. In-use activity collected from trucks sampled in section 3.3 is presented in the following figure.

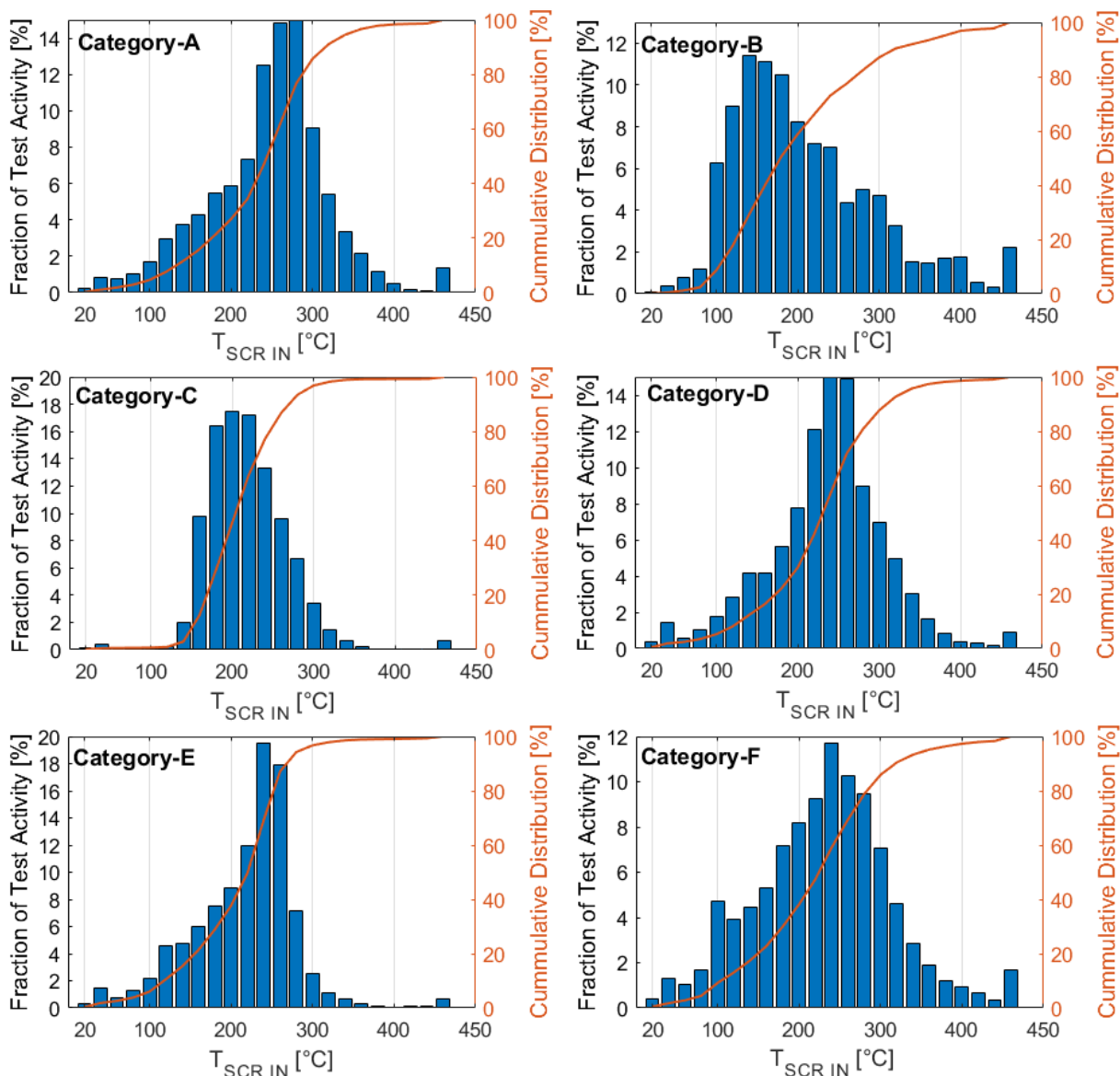


Figure 97: Distribution of $T_{SCR IN}$ for in-fleet vocational activity